VOLUME: 16 NO: 3 YEAR: 2019

ISSN: 1304-530X

TURKISH JOURNAL OF PHARMACEUTICAL SCIENCES

An Official Journal of the Turkish Pharmacists' Association, Academy of Pharmacy

TURKISH
JOURNAL OF PHARMACEUTICAL SCIENCES

TÜRK ECZACILIK BİLİMLERİ DERGİSİ

TURKISH JOURNAL OF PHARMACEUTICAL SCIENCES

AIMS AND SCOPE

The Turkish Journal of Pharmaceutical Sciences is the only scientific periodical publication of the Turkish Pharmacists' Association and has been published since April 2004.

Turkish Journal of Pharmaceutical Sciences is an independent international open access periodical journal based on double-blind peer-review principles. The journal is regularly published 3 times a year and the publication language is English. The issuing body of the journal is Galenos Yayinevi/Publishing House.

The aim of Turkish Journal of Pharmaceutical Sciences is to publish original research papers of the highest scientific and clinical value at an international level.

The target audience includes specialists and physicians in all fields of pharmaceutical sciences.

The editorial policies are based on the "Recommendations for the Conduct, Reporting, Editing, and Publication of Scholarly Work in Medical Journals (ICMJE Recommendations)" by the International Committee of Medical Journal Editors (2016, archived at http://www.icmje.org/) rules.

Editorial Independence

Turkish Journal of Pharmaceutical Sciences is an independent journal with independent editors and principles and has no commerical relationship with the commercial product, drug or pharmaceutical company regarding decisions and review processes upon articles.

ABSTRACTED/INDEXED IN

Web of Science-Emerging Sources Citation Index (ESCI)
SCOPUS SJR
Directory of Open Access Journals (DOAJ)
ProQuest
Chemical Abstracts Service (CAS)
EBSCO
EMBASE
Analytical Abstracts
International Pharmaceutical Abstracts (IPA)
Medicinal & Aromatic Plants Abstracts (MAPA)
TÜBİTAK/ULAKBİM TR Dizin
Türkiye Atıf Dizini
UDL-EDGE

OPEN ACCESS POLICY

This journal provides immediate open access to its content on the principle that making research freely available to the public supports a greater global exchange of knowledge.

Open Access Policy is based on the rules of the Budapest Open Access Initiative (BOAI) http://www.budapestopenaccessinitiative.org/. By "open access" to peer-reviewed research literature, we mean its free availability on the public internet, permitting any users to read, download, copy, distribute, print, search, or link to the full texts of these articles, crawl them for indexing, pass them as data to software, or use them for any other lawful purpose, without financial, legal, or technical barriers other than those inseparable from gaining access to the internet itself. The only constraint on reproduction and distribution, and the only role for copyright in this domain, should be to give authors control over the integrity of their work and the right to be properly acknowledged and cited.

CORRESPONDENCE ADDRESS

Editor-in-Chief, Feyyaz ONUR, Prof.Dr.
Address: Lokman Hekim University, Faculty of Pharmacy, Department of Analytical Chemistry, 06100 Tandoğan-Ankara, TURKEY
E-mail: onur@pharmacy.ankara.edu.tr

PERMISSION

Requests for permission to reproduce published material should be sent to the editorial office. Editor-in-Chief, Prof. Dr. Feyyaz ONUR

ISSUING BODY CORRESPONDING ADDRESS

Issuing Body : Galenos Yayınevi
Address: Molla Gürani Mah. Kaçamak Sk. No: 21/1, 34093 İstanbul, TURKEY
Phone: +90 212 621 99 25 Fax: +90 212 621 99 27
E-mail: info@galenos.com.tr

INSTRUCTIONS FOR AUTHORS

Instructions for authors are published in the journal and on the website http://turkjps.org

MATERIAL DISCLAIMER

The author(s) is (are) responsible for the articles published in the JOURNAL.

The editor, editorial board and publisher do not accept any responsibility for the articles.

Publisher Contact
Address: Molla Gürani Mah. Kaçamak Sk. No: 21/1
34093 İstanbul, Turkey
Phone: +90 (212) 621 99 25 **Fax:** +90 (212) 621 99 27
E-mail: info@galenos.com.tr/yayin@galenos.com.tr
Web: www.galenos.com.tr | Publisher Certificate Number: 14521
Printing at: Üniform Basım San. ve Turizm Ltd. Şti.
Matbaacılar Sanayi Sitesi 1. Cad. No: 114 34204 Bağcılar, İstanbul, Turkey
Phone: +90 (212) 429 10 00 | Certificate Number: 42419
Printing Date: June 2019
ISSN: 1304-530X
International scientific journal published quarterly.

TURKISH
JOURNAL OF PHARMACEUTICAL SCIENCES

INSTRUCTIONS TO AUTHORS

Turkish Journal of Pharmaceutical Sciences is the official double peer-reviewed publication of The Turkish Pharmacists' Association. This journal is published every 4 months (3 issues per year; April, August, December) and publishes the following articles:

• Research articles

• Reviews (only upon the request or consent of the Editorial Board)

• Preliminary results/Short communications/Technical notes/Letters to the Editor in every field or pharmaceutical sciences.

The publication language of the journal is English.

The Turkish Journal of Pharmaceutical Sciences does not charge any article submission or processing charges.

A manuscript will be considered only with the understanding that it is an original contribution that has not been published elsewhere.

The Journal should be abbreviated as "Turk J Pharm Sci" when referenced.

The scientific and ethical liability of the manuscripts belongs to the authors and the copyright of the manuscripts belongs to the Journal. Authors are responsible for the contents of the manuscript and accuracy of the references. All manuscripts submitted for publication must be accompanied by the Copyright Transfer Form [copyright transfer]. Once this form, signed by all the authors, has been submitted, it is understood that neither the manuscript nor the data it contains have been submitted elsewhere or previously published and authors declare the statement of scientific contributions and responsibilities of all authors.

Experimental, clinical and drug studies requiring approval by an ethics committee must be submitted to the JOURNAL with an ethics committee approval report including approval number confirming that the study was conducted in accordance with international agreements and the Declaration of Helsinki (revised 2013) (http://www.wma.net/en/30publications/10policies/b3/). The approval of the ethics committee and the fact that informed consent was given by the patients should be indicated in the Materials and Methods section. In experimental animal studies, the authors should indicate that the procedures followed were in accordance with animal rights as per the Guide for the Care and Use of Laboratory Animals (http://oacu.od.nih.gov/regs/guide/guide.pdf) and they should obtain animal ethics committee approval.

Authors must provide disclosure/acknowledgment of financial or material support, if any was received, for the current study.

If the article includes any direct or indirect commercial links or if any institution provided material support to the study, authors must state in the cover letter that they have no relationship with the commercial product, drug, pharmaceutical company, etc. concerned; or specify the type of relationship (consultant, other agreements), if any.

Authors must provide a statement on the absence of conflicts of interest among the authors and provide authorship contributions.

All manuscripts submitted to the journal are screened for plagiarism using the 'iThenticate' software. Results indicating plagiarism may result in manuscripts being returned or rejected.

The Review Process

This is an independent international journal based on double-blind peer-review principles. The manuscript is assigned to the Editor-in-Chief, who reviews the manuscript and makes an initial decision based on manuscript quality and editorial priorities. Manuscripts that pass initial evaluation are sent for external peer review, and the Editor-in-Chief assigns an Associate Editor. The Associate Editor sends the manuscript to at least two reviewers (internal and/or external reviewers). The reviewers must review the manuscript within 21 days. The Associate Editor recommends a decision based on the reviewers' recommendations and returns the manuscript to the Editor-in-Chief. The Editor-in-Chief makes a final decision based on editorial priorities, manuscript quality, and reviewer recommendations. If there are any conflicting recommendations from reviewers, the Editor-in-Chief can assign a new reviewer.

The scientific board guiding the selection of the papers to be published in the Journal consists of elected experts of the Journal and if necessary, selected from national and international authorities. The Editor-in-Chief, Associate Editors may make minor corrections to accepted manuscripts that do not change the main text of the paper.

In case of any suspicion or claim regarding scientific shortcomings or ethical infringement, the Journal reserves the right to submit the manuscript to the supporting institutions or other authorities for investigation. The Journal accepts the responsibility of initiating action but does not undertake any responsibility for an actual investigation or any power of decision.

The Editorial Policies and General Guidelines for manuscript preparation specified below are based on "Recommendations for the Conduct, Reporting, Editing, and Publication of Scholarly Work in Medical Journals (ICMJE Recommendations)" by the International Committee of Medical Journal Editors (2016, archived at http://www.icmje.org/).

Preparation of research articles, systematic reviews and meta-analyses must comply with study design guidelines:

CONSORT statement for randomized controlled trials (Moher D, Schultz KF, Altman D, for the CONSORT Group. The CONSORT statement revised recommendations for improving the quality of reports of parallel group randomized trials. JAMA 2001; 285: 1987-91) (http://www.consort-statement.org/);

PRISMA statement of preferred reporting items for systematic reviews and meta-analyses (Moher D, Liberati A, Tetzlaff J, Altman DG, The PRISMA Group. Preferred Reporting Items for Systematic Reviews and Meta-Analyses: The PRISMA Statement. PLoS Med 2009; 6(7): e1000097.) (http://www.prisma-statement.org/);

STARD checklist for the reporting of studies of diagnostic accuracy (Bossuyt PM, Reitsma JB, Bruns DE, Gatsonis CA, Glasziou PP, Irwig LM, et al., for the STARD Group. Towards complete and accurate reporting of studies of diagnostic accuracy: the STARD initiative. Ann Intern Med 2003;138:40-4.) (http://www.stard-statement.org/);

STROBE statement, a checklist of items that should be included in reports of observational studies (http://www.strobe-statement.org/);

MOOSE guidelines for meta-analysis and systemic reviews of observational studies (Stroup DF, Berlin JA, Morton SC, et al. Meta-analysis of observational studies in epidemiology: a proposal for reporting Meta-analysis of observational Studies in Epidemiology (MOOSE) group. JAMA 2000; 283: 2008-12).

Authorship

Each author should have participated sufficiently in the work to assume public responsibility for the content. Any portion of a manuscript that

TURKISH
JOURNAL OF PHARMACEUTICAL SCIENCES

INSTRUCTIONS TO AUTHORS

is critical to its main conclusions must be the responsibility of at least 1 author.

GENERAL GUIDELINES

Manuscripts can only be submitted electronically through the Journal Agent website (http://journalagent.com/tjps/) after creating an account. This system allows online submission and review.

The manuscripts are archived according to ICMJE, Web of Science-Emerging Sources Citation Index (ESCI), SCOPUS, Chemical Abstracts, EBSCO, EMBASE, Analytical Abstracts, International Pharmaceutical Abstracts, MAPA(Medicinal & Aromatic Plants Abstracts), Tübitak/ Ulakbim Turkish Medical Database, Türkiye Citation Index Rules.

Format: Manuscripts should be prepared using Microsoft Word, size A4 with 2.5 cm margins on all sides, 12 pt Arial font and 1.5 line spacing.

Abbreviations: Abbreviations should be defined at first mention and used consistently thereafter. Internationally accepted abbreviations should be used; refer to scientific writing guides as necessary.

Cover letter: The cover letter should include statements about manuscript type, single-Journal submission affirmation, conflict of interest statement, sources of outside funding, equipment (if applicable), for original research articles.

The ORCID (Open Researcher and Contributor ID) number of the all authors should be provided while sending the manuscript. A free registration can be done at http://orcid.org.

REFERENCES

Authors are solely responsible for the accuracy of all references.

In-text citations: References should be indicated as a superscript immediately after the period/full stop of the relevant sentence. If the author(s) of a reference is/are indicated at the beginning of the sentence, this reference should be written as a superscript immediately after the author's name. If relevant research has been conducted in Turkey or by Turkish investigators, these studies should be given priority while citing the literature.

Presentations presented in congresses, unpublished manuscripts, theses, Internet addresses, and personal interviews or experiences should not be indicated as references. If such references are used, they should be indicated in parentheses at the end of the relevant sentence in the text, without reference number and written in full, in order to clarify their nature.

References section: References should be numbered consecutively in the order in which they are first mentioned in the text. All authors should be listed regardless of number. The titles of Journals should be abbreviated according to the style used in the Index Medicus.

Reference Format

Journal: Last name(s) of the author(s) and initials, article title, publication title and its original abbreviation, publication date, volume, the inclusive page numbers. Example: Collin JR, Rathbun JE. Involutional entropion: a review with evaluation of a procedure. Arch Ophthalmol. 1978;96:1058-1064.

Book: Last name(s) of the author(s) and initials, book title, edition, place of publication, date of publication and inclusive page numbers of the extract cited. Example: Herbert L. The Infectious Diseases (1st ed). Philadelphia; Mosby Harcourt; 1999:11;1-8.

Book Chapter: Last name(s) of the author(s) and initials, chapter title, book editors, book title, edition, place of publication, date of publication and inclusive page numbers of the cited piece.

Example: O'Brien TP, Green WR. Periocular Infections. In: Feigin RD, Cherry JD, eds. Textbook of Pediatric Infectious Diseases (4th ed). Philadelphia; W.B. Saunders Company;1998:1273-1278.

Books in which the editor and author are the same person: Last name(s) of the author(s) and initials, chapter title, book editors, book title, edition, place of publication, date of publication and inclusive page numbers of the cited piece. Example: Solcia E, Capella C, Kloppel G. Tumors of the exocrine pancreas. In: Solcia E, Capella C, Kloppel G, eds. Tumors of the Pancreas. 2nd ed. Washington: Armed Forces Institute of Pathology; 1997:145-210.

TABLES, GRAPHICS, FIGURES, AND IMAGES

All visual materials together with their legends should be located on separate pages that follow the main text.

Images: Images (pictures) should be numbered and include a brief title. Permission to reproduce pictures that were published elsewhere must be included. All pictures should be of the highest quality possible, in

JPEG format, and at a minimum resolution of 300 dpi.

Tables, Graphics, Figures: All tables, graphics or figures should be enumerated according to their sequence within the text and a brief descriptive caption should be written. Any abbreviations used should be defined in the accompanying legend. Tables in particular should be explanatory and facilitate readers' understanding of the manuscript, and should not repeat data presented in the main text.

MANUSCRIPT TYPES

Original Articles

Clinical research should comprise clinical observation, new techniques or laboratories studies. Original research articles should include title, structured abstract, key words relevant to the content of the article, introduction, materials and methods, results, discussion, study limitations, conclusion references, tables/figures/images and acknowledgement sections. Title, abstract and key words should be written in both Turkish and English. The manuscript should be formatted in accordance with the above-mentioned guidelines and should not exceed 16 A4 pages.

Title Page: This page should include the title of the manuscript, short title, name(s) of the authors and author information. The following descriptions should be stated in the given order:

1. Title of the manuscript (Turkish and English), as concise and explanatory as possible, including no abbreviations, up to 135 characters

2. Short title (Turkish and English), up to 60 characters

3. Name(s) and surname(s) of the author(s) (without abbreviations and academic titles) and affiliations

4. Name, address, e-mail, phone and fax number of the corresponding author

5. The place and date of scientific meeting in which the manuscript was presented and its abstract published in the abstract book, if applicable

TURKISH
JOURNAL OF PHARMACEUTICAL SCIENCES

INSTRUCTIONS TO AUTHORS

Abstract: A summary of the manuscript should be written in both Turkish and English. References should not be cited in the abstract. Use of abbreviations should be avoided as much as possible; if any abbreviations are used, they must be taken into consideration independently of the abbreviations used in the text. For original articles, the structured abstract should include the following sub-headings:

Objectives: The aim of the study should be clearly stated.

Materials and Methods: The study and standard criteria used should be defined; it should also be indicated whether the study is randomized or not, whether it is retrospective or prospective, and the statistical methods applied should be indicated, if applicable.

Results: The detailed results of the study should be given and the statistical significance level should be indicated.

Conclusion: Should summarize the results of the study, the clinical applicability of the results should be defined, and the favorable and unfavorable aspects should be declared.

Keywords: A list of minimum 3, but no more than 5 key words must follow the abstract. Key words in English should be consistent with "Medical Subject Headings (MESH)" (www.nlm.nih.gov/mesh/MBrowser.html). Turkish key words should be direct translations of the terms in MESH.

Original research articles should have the following sections:

Introduction: Should consist of a brief explanation of the topic and indicate the objective of the study, supported by information from the literature.

Materials and Methods: The study plan should be clearly described, indicating whether the study is randomized or not, whether it is retrospective or prospective, the number of trials, the characteristics, and the statistical methods used.

Results: The results of the study should be stated, with tables/figures given in numerical order; the results should be evaluated according to the statistical analysis methods applied. See General Guidelines for details about the preparation of visual material.

Discussion: The study results should be discussed in terms of their favorable and unfavorable aspects and they should be compared with the literature. The conclusion of the study should be highlighted.

Study Limitations: Limitations of the study should be discussed. In addition, an evaluation of the implications of the obtained findings/results for future research should be outlined.

Conclusion: The conclusion of the study should be highlighted.

Acknowledgements: Any technical or financial support or editorial contributions (statistical analysis, English/Turkish evaluation) towards the study should appear at the end of the article.

References: Authors are responsible for the accuracy of the references. See General Guidelines for details about the usage and formatting required.

Review Articles

Review articles can address any aspect of clinical or laboratory pharmaceuticals. Review articles must provide critical analyses of contemporary evidence and provide directions of or future research. Most review articles are commissioned, but other review submissions are also welcome. Before sending a review, discussion with the editor is recommended.

Reviews articles analyze topics in depth, independently and objectively. The first chapter should include the title in Turkish and English, an unstructured summary and key words. Source of all citations should be indicated. The entire text should not exceed 25 pages (A4, formatted as specified above).

CORRESPONDENCE

All correspondence should be directed to the Turkish Journal of Pharmaceutical Sciences editorial board;

Post: Turkish Pharmacists' Association

Address: Willy Brandt Sok. No: 9 06690 Ankara, TURKEY

Phone: +90 312 409 8136

Fax: +90 312 409 8132

Web Page: http://turkjps.org/home/

E-mail: onur@pharmacy.ankara.edu.tr

TURKISH
JOURNAL OF PHARMACEUTICAL SCIENCES

CONTENTS

TURKISH
JOURNAL OF PHARMACEUTICAL SCIENCES

CONTENTS

PUBLICATION NAME	Turkish Journal of Pharmaceutical Sciences
TYPE OF PUBLICATION	Vernacular Publication
PERIOD AND LANGUAGE	Quarterly- English
OWNER	Erdoğan ÇOLAK on behalf of the Turkish Pharmacists' Association
EDITOR-IN-CHIEF	Feyyaz ONUR
ADDRESS OF PUBLICATION	Cinnah Mah. Willy Brandt Sok. No: 9 Çankaya-Ankara/TURKEY

TURKISH
JOURNAL OF PHARMACEUTICAL
SCIENCES

Volume: 16, No: 3, Year: 2019

CONTENTS

Original articles

Review

Turk J Pharm Sci 2019;16(3):252-260
DOI: 10.4274/tjps.galenos.2018.92408

ORIGINAL ARTICLE

Synthesis and Swelling Behavior of Sodium Alginate/Poly(vinyl alcohol) Hydrogels

Sodyum Aljinat/Poli(vinil alkol) Hidrojellerinin Sentezi ve Şişme Davranışları

Lachakkal Rudrappa SHIVAKUMARA, Thippaiah DEMAPPA*

University of Mysore, Sir. M. Visvesvaraya Post-Graduate Center, Department of Post Graduate Studies and Research in Polymer Science, Tubinakere, Mandya, Karnataka, India

ABSTRACT

Objectives: Hydrogels are macromolecular networks able to absorb and release water/biological fluids in a reverse-phase manner, in response to specific environmental stimuli. Such stimuli-sensitive behavior makes hydrogels interesting for the design of smart devices applicable to a variety of technological fields. They are able to absorb and retain 10-20% and up to 1000 times the water or biological fluids than their dry weight can. The aim of this study was to extend the work on drug delivery in the stomach at pH 2-2.2.

Materials and Methods: The authors synthesized sodium alginate (SA)/poly(vinyl alcohol) (PVA) hydrogels. These hydrogels were characterized by fourier transform infrared spectroscopy and scanning electron microscopy, and the swelling properties of the hydrogels were examined at different pH values, in different salts, at different temperatures, and in different acids and bases.

Results: The authors studied and reported the swelling effects or variations such as the effects of salts, acids, bases, temperature, and pH. The results for the crosslinking agent glutaraldehyde showed that 8 mL of glutaraldehyde had a higher swelling rate compared to that of 10 mL and 12 mL.

Conclusion: In this work the authors studied the swelling degree in different acids and bases. It is concluded that the degree of swelling decreases with increases in the concentration of glutaraldehyde and also depending on the concentrations of the acids. The swelling degrees of PVA/SA hydrogels gradually increase with increases in the concentrations of acids (low pH). The swelling of hydrogels decreases with increases in pH (>7) or at high alkaline. Based on the results for salt solutions the swelling behavior was found to be in the order: $K^+ > Na^+ > Ca^{2+} > Mg^{2+}$.

Key words: Swelling, pH, crosslinking agent, buffer solution, sodium alginate, PVA

ÖZ

Amaç: Hidrojeller, belirli çevresel uyaranlara yanıt olarak su/biyolojik sıvıları ters fazda emebilen ve serbest bırakabilen makromoleküler ağlardır. Bu tür uyaranlara duyarlı davranış, çeşitli teknolojik alanlara uygulanabilen akıllı cihazların tasarımı için hidrojelleri ilginç kılar. Kuru ağırlığından %10-20 ve 1000 veya daha fazla su veya biyolojik sıvıları emebilir ve tutabilirler. Bu çalışmanın amacı, midede ilaç dağıtım çalışmalarını pH 2-2.2'sinde genişletmektir.

Gereç ve Yöntemler: Yazarlar sentezlenmiş sodyum aljinat (SA)/poli(vinil alkol) (PVA) hidrojellerdir. Bu hidrojeller fourier dönüşümü kızılötesi spektroskopisi, taramalı elektron mikroskobu, farklı pH'larda hidrojellerin şişme özellikleri, tuzlar, farklı sıcaklık, farklı asitler ve bazlar ile karakterize edilir.

Bulgular: Yazarlar, tuzların, asitlerin, bazların, sıcaklığın ve pH'ın etkisi gibi şişme etkilerini veya varyasyonlarını incelediler ve rapor ettiler. Çapraz bağlama maddesi glutaraldehitin etkisi, 8 mL glutaraldehidin, 10 mL ve 12 mL'ninkiyle karşılaştırıldığında en yüksek şişme oranına sahip olduğunu göstermektedir.

Sonuç: Bu çalışmada yazarlar farklı asit ve bazlarda şişme derecesini incelemişlerdir. Glutaraldehit konsantrasyonundaki artışla ve aynı zamanda asit konsantrasyonuna bağlı olarak şişlik derecesinin azaldığı sonucuna varılmıştır. PVA/SA hidrojellerinin şişme derecesi, asit konsantrasyonundaki artışla (düşük pH) kademeli olarak artmaktadır. Hidrojellerin şişmesi pH'ın (>7) artmasıyla veya yüksek alkali ile azalır. Tuz çözeltilerinin etkisinde şişme davranışının sırasıyla: $K^+ > Na^+ > Ca^{2+} > Mg^{2+}$ olduğu bulunmuştur.

Anahtar kelimeler: Şişme, pH, çapraz bağlama maddesi, tampon çözelti, sodyum aljinat, PVA

***Correspondence: E-mail:** tdemappa2003@yahoo.co.in - shivu9686178586@gmail.com, **Phone:** 9686178586
Received: 24.11.2017, **Accepted:** 09.05.2018

INTRODUCTION

Hydrogels have been used in various chemical and biomedical applications in ophthalmology as contact lenses and surgical sutures, as well as in numerous other areas like agricultural applications.

Sodium alginate (SA) is an anionic copolymer composed of 1,4-linked β-D-mannuronic acid (M-blocks) and α-L-guluronic acid (G-blocks), interspersed with regions of alternating structure. Gel formation and three-dimensional network structures occur when divalent ions (Ca^{2+}, Ba^{2+}, Fe^{2+}, Si^{2+}, etc.) or trivalent ions (Al^{3+}, etc.) crosslink with G-blocks in the polymer chain. Such binding zones between G-blocks are often referred to as "egg boxes". These crosslinked ions stabilize alginate chains, forming a gel structure, with more freely movable chains that bind and entrap large quantities of water or biological fluids. The gel formation (gelification) process is characterized by the eviction of water.[1] The softer, more fragile, and lower porosity gels are made of M-rich alginate groups. This is due to the lower binding strength between the polymer chains and to the higher flexibilities of the molecules. The gel formation process is highly dependent on diffusion of gel formation ions into the polymer network. Visco-elasticity and transmittance of alginate structures are highly affected by the M/G ratio. Alginic acid and its salts of sodium and calcium are used in the medical, pharmaceutical, cosmetic, and food industries because of its nontoxicity and biocompatibility.[2] The main advantage of hydrogels is that they possess a degree of flexibility very similar to that of natural tissues, due to their significant water content. Their stimuli-sensitive behavior makes hydrogels interesting for the design of smart devices applicable to a variety of technological fields.

Hydrogels are, in general, materials composed of three-dimensional hydrophilic polymer networks and water that fills the free spaces inside this network. Hydrogels are able to absorb and retain 10-20% up to 1000 times the water or biological fluids than their dry weight can. Hydrogels respond reversibly to slight changes in the properties of surrounding media; hence they are called "intelligent materials". This ability means hydrogels have found many applications in industry and in pharmaceuticals, for example as controlled drug delivery systems.[3] The swelling and dehydration behavior is one of the most important properties of hydrogels.[4] Applications of hydrogels include drug delivery systems (slow drug release), wound dressings, dental applications, transdermal implants, injectable polymers, contact lenses, superabsorbents, and environmentally sensitive hydrogels.[5-9] Hydrogels interact with aqueous solutions and swell to a certain equilibrium and retain a significant proportion of water within their structure.[10] SA is a hydrophilic polysaccharide, a natural polymer, composed of a mannuronic acid unit. This compound has been used for a long time in various industries, such as agriculture, food, medicine, textile, cosmetics, and printing. SA is also used as a thickener, stabilizer, and emulsifier and for microencapsulation, as well as in slow release drug delivery systems and fertilizers.[11] SA has a molecular structure similar to collagen; therefore it can make the skin smooth and elastic and can accelerate wound healing, and it can be used as a natural alternative product for health care and cosmetics.[12-14] SA is of biological origin and has good characteristics, such as biocompatibility, biodegradability, and gel-forming ability. Poly(vinyl alcohol) (PVA) is a hydrophilic polymer and is of great interest for use as a biomaterial because of its good biocompatible properties. It has chemical stability, high durability, and a high degree of swelling in water or biological fluids. PVA is nontoxic to viable cells, noncarcinogenic, has high biocompatibility, and has a consistency similar to soft tissue, film forming with high mechanical strength, and long-term temperature stability. Its three-dimensional network enables diffusional exchange of nutrients and waste products with the surrounding environment, and it is used in various biomedical, pharmaceutical, biotechnological, and other industrial fields.[15-20] However, even though PVA is a biomaterial it is brittle in nature; therefore, it needs to be blended with other polymers or by copolymerization, e.g., with SA, to obtain a better property that can be used to encapsulate or entrap or to immobilize an enzyme or drug in micron or submicron (nano) size, to keep the constancy of its activity, or to prevent activity decreases drastically. Hence it works more effectively and efficiently compared to when it is in free condition.[6,21,22] The crosslinked alginate hydrogels have been used as a controlled release medium for drugs,[23-27] pesticides,[28] superabsorbent filament fibers,[29] and flocculants.[30]

In the presence of an aqueous solution, the polymer chains absorb water and the association, dissociation, and binding of various ions to polymer chains cause the hydrogel to swell. The shrinking and swelling properties of hydrogels are currently being exploited in a number of applications including the control of microfluidic flow,[31] muscle-like actuators,[32,33] filtration/separation,[34] and drug delivery.[35,36] The structure and properties of hydrogels are similar to those of many biological tissues such as cartilage and the corneal stroma in the eye.[37,38] Hydrogels are accomplished through large reversible deformation in response to changes in several environmental factors.[39] For example, hydrogel size is sensitive to pH, temperature, concentration of salts, and electric fields.

EXPERIMENT

MATERIALS AND METHODS

Materials

SA, PVA molecular weight 125.000, and glutaraldehyde (25%) were purchased from S.D. Fine Chem Limited, Mumbai, India. Hydrochloric acid, perchloric acid, sodium hydroxide, and acetic acid were purchased from Reachem Laboratory Chemicals Private Ltd, Chennai, India. Calcium chloride, magnesium chloride, sodium chloride, and potassium chloride were purchased from E-Merck Limited, Mumbai, India, and double distilled water was used throughout the experiment.

Methods

Preparation of SA/PVA hydrogels

First 7 g of SA was dissolved in 100 mL of water with constant stirring. Then 9 g of PVA was dissolved in the same solution with stirring for about 3 h at 80°C to 85°C, 12 mL of glutaraldehyde

(25%) was added to the same solution, and this solution was kept at 80°C for 3 h. After 3 h the obtained hydrogel was washed with distilled water and ethanol to remove the excess monomer and crosslinking agent. After washing 2-3 times the hydrogel was dried at 40°C in an oven. Likewise the different SA/PVA hydrogels synthesized with varying volume of glutaraldehyde (10 and 8 mL) were used for swelling studies.

CHARACTERIZATION

Fourier-transform infrared spectroscopy

The FTIR spectra of the SA, PVA, and the crosslinked hydrogel samples were recorded in the range of 4000 to 500 cm^{-1} to provide the proof of hydrogels (Figure 1).

Surface morphology of hydrogels

The surface morphology of the SA, PVA, and glutaraldehyde crosslinking hydrogels were investigated using scanning electron microscopy (SEM) (SEM Zeiss, LS15) (Figure 2).

Swelling behavior of hydrogels

For the swelling behavior of hydrogels, the swelling ratio of the hydrogel samples was measured at different temperatures in different solvents by gravimetric method. Pre-weighed dry hydrogel samples were immersed in excessive different solutions and left undisturbed for 24 h, 48 h, and 72 h at different temperatures like room temperature, 30°C, 37°C, and 40°C until constant values were obtained. Degree of swelling rate can be calculated by the following equation:

$$\% DS = (W_2 - W_1) / W_1 \times 100 \quad \text{..... (Equation 1)}$$

% DS is the degree of swelling expressed in a percentage and W_1 and W_2 are the masses of sample before and after swelling, respectively (Figures 3 to 5) (Table 1).

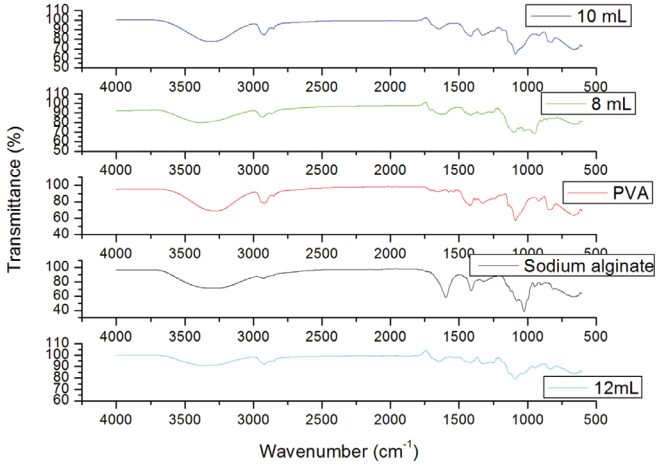

Figure 1. FTIR spectra of pure SA, PVA, 12% glutaraldehyde crosslinked, 10% glutaraldehyde crosslinked, and 8% glutaraldehyde crosslinked hydrogels

FTIR: Fourier transform infrared spectroscopy, SA: Sodium alginate, PVA: Poly(vinyl alcohol)

Swelling at various pHs

The solution was adjusted to acidic, basic, and neutral pH by diluting with phosphate buffer (pH 3.2, pH 7, pH 2, and pH 10) solutions at room temperature, 30°C, 37°C, and 40°C. The pH values were checked by pH meter. The dried hydrogel samples were used for the swelling measurement according to Equation (1) (Figure 6).

Swelling in salt solutions

The swelling capacity of hydrogels was determined in different salt solutions (KCl, NaCl, $CaCl_2$, and $MgCl_2$) and also with various concentrations like 0.4, 0.6, 0.8, 1, and 1.2 N according to the above method (Figure 7).

RESULTS

The authors reported the swelling effects on hydrogels of different salts, acids, bases, temperatures, and pH values. A higher swelling rate was shown by 8 mL of glutaraldehyde compared to 10 mL and 12 mL. Figure 1 shows the FTIR spectra of the molecular interaction between SA and PVA. The surface morphology of the hydrogels was studied using SEM (SEM Zeiss, LS15) as shown in Figure 2; Figures 3 to 5 and Table 1 represent the swelling behavior of the hydrogels at different temperatures, i.e. 30°C, 37°C, 40°C, and room temperature, with different salts. Figure 6 shows the behavior of the hydrogels at different pH values.

DISCUSSION

Fourier transformed infrared spectral analysis

Figure 1 represents the FTIR spectra, characterizing the molecular interaction of SA and PVA hydrogels. The FTIR spectra of SA show the characteristic absorption peak at 3270.47 cm^{-1} is for the hydroxyl (-OH) group. The asymmetric and symmetric stretching vibration of the carboxylic (COO-) group is found to be at 1597.36 and 1412 cm^{-1}, respectively.[40,41] The peak at 2925.38 cm^{-1} represents the C-H alkyl stretching bond.[42] An absorption peak around 2919.05 cm^{-1} shows the characteristic spectra of PVA. This peak arises from the C-H stretching at 1570 to 1420 cm^{-1} is assigned for CH_2 (vinyl group), while the sharp absorption peak at 1150-1050 cm^{-1} is used for indication of PVA.[43] In addition, it was found that the peak at 1549-1453 cm^{-1} is a stretching band for the CH_2 group. This band is also found in pure PVA and crosslinked SA/PVA hydrogels. The decrease in wave number of the carbonyl peak from 1652.14 to 1635.24 cm^{-1} is for the crosslinking of SA/PVA hydrogels. Crosslinking of glutaraldehyde takes place at 2863 to 2750 cm^{-1}.

SEM images

SEM describes the surface morphology of SA/PVA hydrogels in Figure 2. According to the SEM images (Figure 2a), the pure SA shows a very smooth surface nearly devoid of any surface feature.[43] In Figure 2b the SEM images of pure PVA show a very smooth, uniform, and nonporous surface structure, which may be attributed to the crystallization of PVA.[44] However, the addition of SA to PVA hydrogel in different portions provides very tiny pores at the surface and these pores decrease with an increase in glutaraldehyde concentration (Figures 2c to 2e).

Effect of pH on the swelling of hydrogels

The sensitivity of the hydrogels was measured from pH 2 to pH 10. No additional ions (through buffer solutions) were added to the medium for setting pH because the absorbency of an absorbent is strongly affected by ionic strength. Therefore, stock HCl (pH 1.0) and NaOH (pH 10.0) solutions were diluted with distilled water to achieve the preferred acidic or basic pH values, respectively. In Table 2 and Figure 6, the swelling capacity of hydrogel at pH 2 can be accredited to the high repulsion of anion–anion COO- groups. At basic conditions (pH ≥7), most of the carboxylate groups are protonated and the low swelling values of hydrogels can be attributed to the presence of nonionic hydrophilic -OH and -COOH groups in the PVA and alginate backbones, respectively. The swelling capacity is decreased with further increase in pH (pH 10 or pH >7). Again

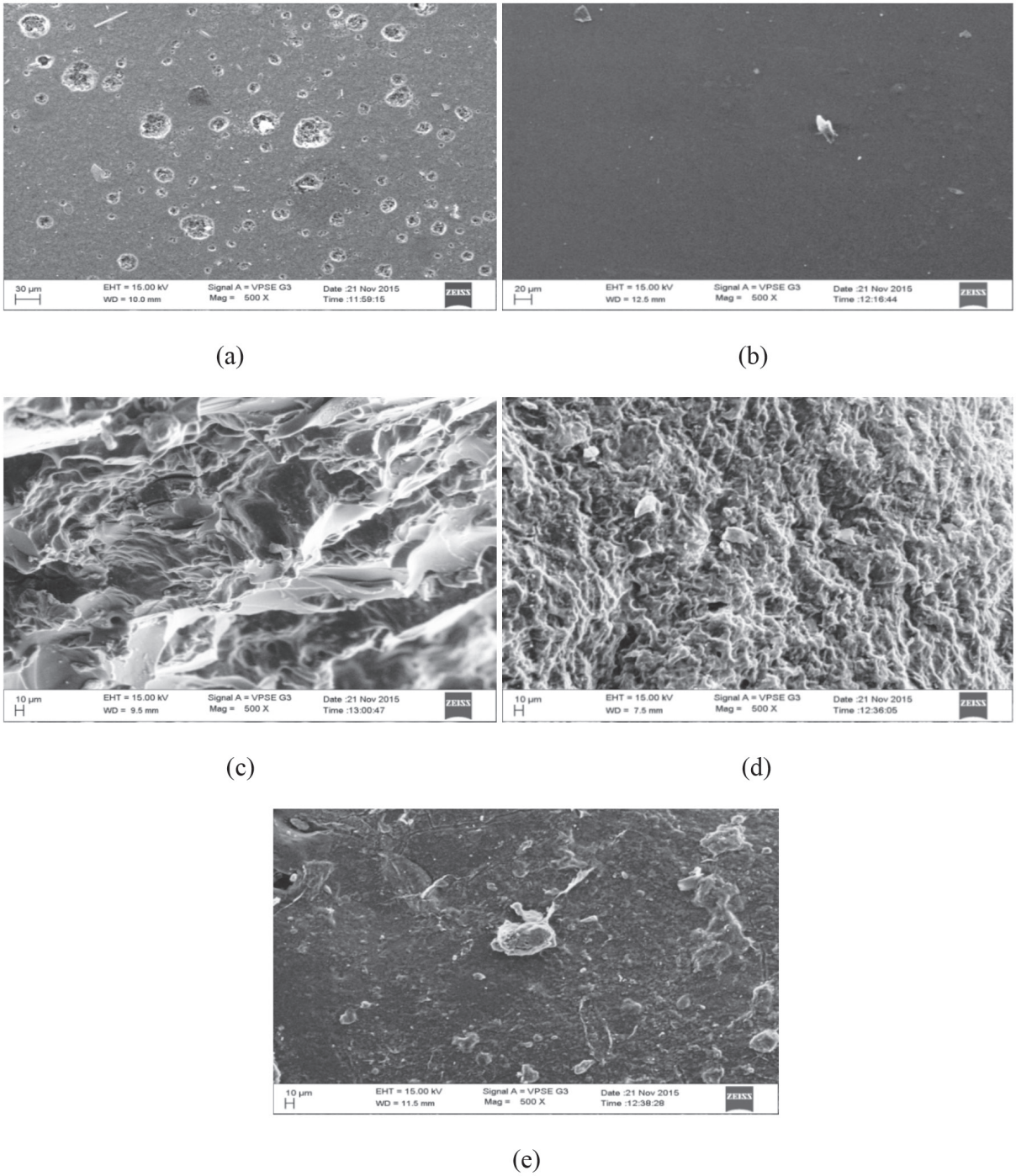

Figure 2. SEM images of (a) pure sodium alginate, (b) pure PVA, (c) 8 mL glutaraldehyde crosslinked SA/PVA hydrogel, (d) 10 mL glutaraldehyde crosslinked SA/PVA hydrogels, (e) 12 mL glutaraldehyde crosslinked SA/PVA hydrogels

SEM: Scanning electron microscopy, SA: Sodium alginate, PVA: Poly(vinyl alcohol)

the swelling loss is due to the counter ions, i.e. Na^+, that shield the charge of the carboxylate anions and prevent efficient anion–anion repulsion. As a result, a remarkable decrease in equilibrium swelling is observed.

pH Dependence of the swelling rate of water

The swelling rate decreased with increasing pH from 2 to 10; it was evident from the data given. The negatively charged ionic backbones of PVA and SA are more expanded because the protonation of COO- groups is negatively charged. This expanded form makes for easy diffusion of water molecules into the hydrogel network. On the other hand, the -OH groups are mostly in the protonated form and show less polar character at pH ≥7. Therefore, this results in a polymer with lower affinity to water. Thus, hydrogels are less expanded at pH ≥7. The increases in swelling ratio are responsible for the theory of electrostatic repulsion between COO- ions in the polymer chains and ionic present in the pH solution and the ionic osmotic pressure generated from mobile counter ions to charged ions in the network. Thus, the charge density of the hydrogel is diluted, because PVA is not ionic in character (Table 2). Figure 6 shows the swelling studies of phosphate buffered pH solutions. The glutaraldehyde crosslinked PVA/SA samples show a gradual increase (in swelling degree at pH 2 and 3.2) followed by a decrease in swelling degree at pH 7 and 10 at different temperatures (25°C, 30°C, 37°C). In these studies the 8% glutaraldehyde crosslinked hydrogel has a high swelling degree compared to the 10% and 12% glutaraldehyde crosslinked hydrogels.

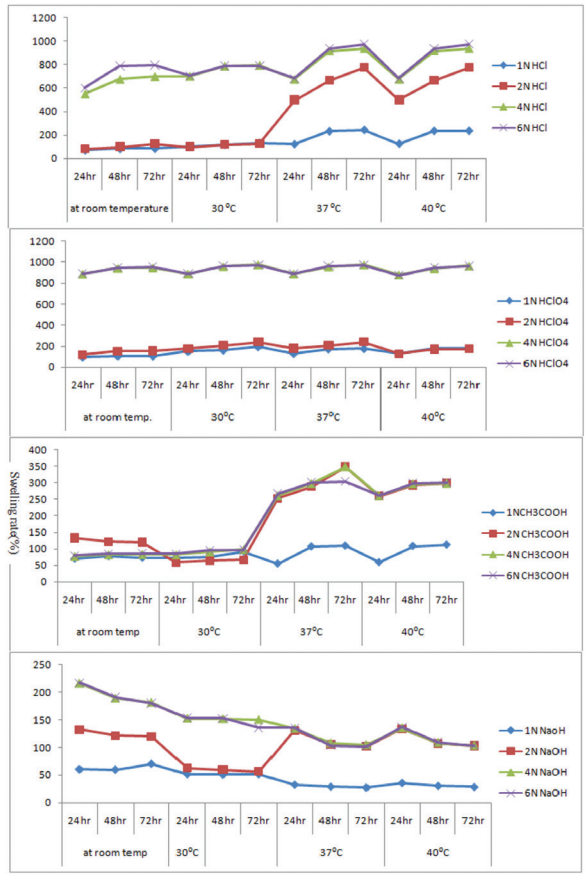

Figure 3. Swelling rate of 8 mL glutaraldehyde crosslinked hydrogels

Table 1. Data of swelling rate of 8 mL glutaraldehyde, 10 mL glutaraldehyde, and 12 mL glutaraldehyde crosslinked hydrogels at 37°C

Conc.	8 mL glutaraldehyde			10 mL glutaraldehyde			12 mL glutaraldehyde		
	24 h	48 h	72 h	24 h	48 h	72 h	24 h	48 h	72 h
1N CH_3COOH	54.46	107.56	109.85	45.78	63.39	66.32	14.02	32.15	33.85
2N CH_3COOH	252.3	288.74	348.05	51.23	69.34	70.15	14.71	32.79	34.21
4N CH_3COOH	260.74	297.36	348.05	60.19	72.43	74.12	14.97	33.56	34.69
6N CH_3COOH	266.08	300.42	303.35	63.48	74.12	77.06	15.09	33.81	34.8
1N HCl	70.16	229.4	240.17	61.19	67.93	71.72	12.43	23.79	25.77
2N HCl	495.5	662.89	771.3	88.49	112.83	115.98	19.19	28.07	32.08
4N HCl	673.93	918.08	938.37	126.25	133.29	137.58	28.18	35.93	40.34
6N HCl	679.83	937.44	973.77	129.18	133.7	139.0	55.44	69.88	71.86
1N $HClO_4$	124.47	169.92	173.65	132.12	133.5	137.56	11.09	10.69	11.79
2N $HClO_4$	179.23	209.78	239.01	166.09	207.7	209.05	17.74	22.18	27.19
4N $HClO_4$	890.19	957.01	976.08	260.01	268.59	277.18	19.21	23.29	31.07
6N $HClO_4$	892.27	968.14	973.0	263.72	268.72	278.29	23.41	32.17	34.02
1N NaOH	47.26	47.02	46.24	32.87	29 April	27.64	34.97	22.83	19.31
2N NaOH	50.75	50.13	49.08	130.31	105.43	101.92	35.21	29.01	29.09
4N NaOH	53.24	53.02	52.86	134.04	107.47	104.36	39.93	38.14	36.69
6N NaOH	55.23	54.71	53.01	135.6	104.25	102.1	41.74	37.25	36.07

Effect of temperature on the swelling of hydrogels

It is obvious from Figure 6 that the temperature leading to hydrogels with the highest absorbency is around 37°C. The swelling capacity of hydrogels decreased with increasing temperature above 37°C. The increase in swelling rates is dependent on the kinetic energy of the polysaccharide chains, which led to lower soluble content of the hydrogel as well as increasing concentration of glutaraldehyde diffusion rate of SA and PVA backbones. The higher reaction temperature proves the results from higher reactant movement and effective collision. At temperatures about 37°C, the possible "thermal crosslinking" reaction to polysaccharide backbones may play a major role in the creation of low-swelling hydrogels. In addition, the swelling loss may be related to the increase in crosslinked bond formation of completion of the ester and ether formations by further reaction to the possible mono-ester species with another polysaccharides chain (Scheme 1).

Effect of salt solution on hydrogels

Hydrogels are considered polyelectrolytes, suggesting that their porosity should decrease as ionic strength increases. SA/PVA hydrogels with various chloride salt solutions are appreciably

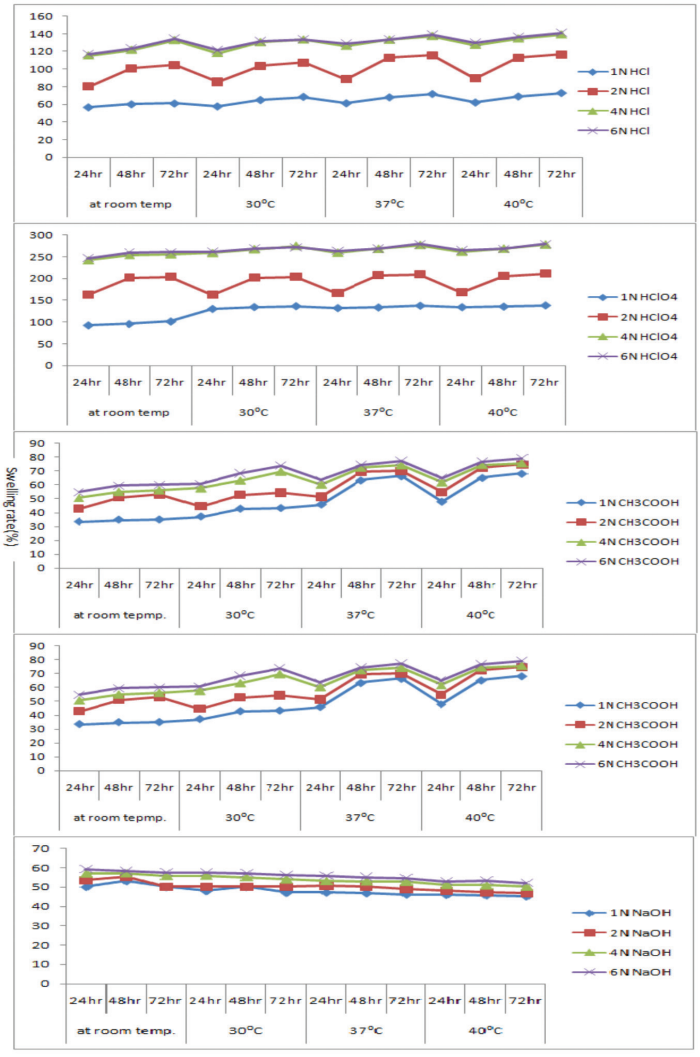

Figure 4. Swelling rate of 10 mL glutaraldehyde crosslinked hydrogels

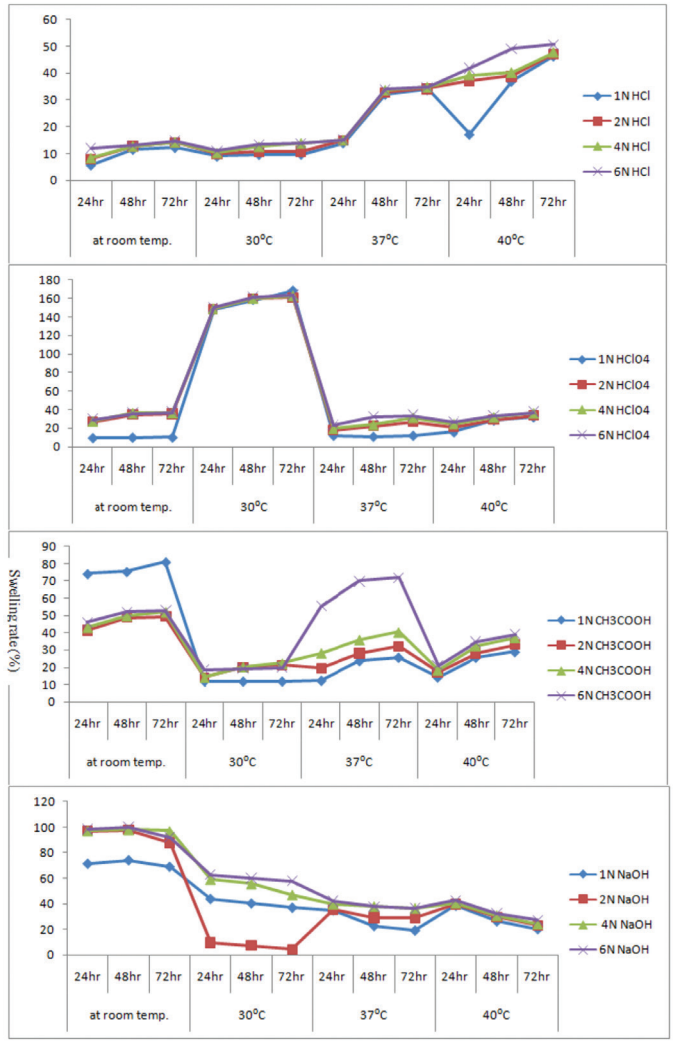

Figure 5. Swelling rate of 12 mL glutaraldehyde crosslinked hydrogels

Table 2. Data of swelling studies of hydrogels in different pH solutions at 37°C

	8 mL glutaraldehyde			10 mL glutaraldehyde			12 mL glutaraldehyde		
	24 h	48 h	72 h	24 h	48 h	72 h	24 h	48 h	72 h
pH 2	120.2	121.56	122.01	75.65	76.92	77.15	75.19	76.08	77.33
pH 3.2	109.2	113.2	116.07	72.01	74.1	76.12	73.24	74.19	75.28
pH 7	70.37	77.78	83.34	67.92	68.12	69.12	66.27	67.19	68.92
pH 10	69.24	71.34	73.45	65.26	66.74	67.05	65.48	66.47	67.19

reduced in swelling compared to those measured in deionized water. This results from a charge screening effect of the additional cations causing anion–anion electrostatic repulsion, which leads to a decreased osmotic pressure difference between the polymer network and the external solution. At a given ionic strength, Mg^{2+} and Ca^{2+} contribute more charge than monovalent cations like Na^{+} and K^{+} and induce a bigger drop in intermolecular repulsion and increased interaction between molecules, which, in turn, cause to a large extent the hydrogel collapse. In addition, Mg^{2+} and Ca^{2+} can chelate COO- groups, leading to a compact network and causing further shrinking from the hydrogel; on the other hand, we also find that the smaller the radius of atoms of some valent monoatomic cations, the more the water absorption capacity if different cations were K^{+}>Na^{+}>Ca^{2+}>Mg^{2+} (Table 3 and Figure 7).[45]

CONCLUSIONS

In this work the authors studied the swelling degree in different acids and bases. It is concluded that the degree of swelling decreases with an increase in the concentration of the glutaraldehyde and also depending on the concentration of the acids. Here the swelling degree of PVA/SA hydrogels gradually increases with increases in the concentrations of acids. The aldehyde groups are covalently bonded with the COO- and OH- groups of PVA/SA and consequently the swelling degree is significantly reduced. In different concentrations of different salts the swelling rates decreased with increasing concentrations of salts. The swelling rate is in the order of K^{+}>Na^{+}>Ca^{2+}>Mg^{2+}.

Further extension of the work

This swelling study is to be extended for biomedical and agricultural applications such as drug delivery and controlled release fertilizers.[45]

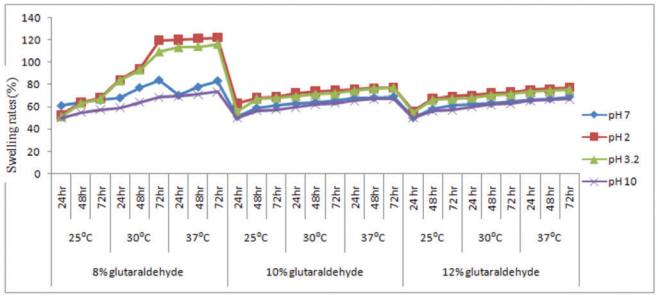

Figure 6. Swelling studies of hydrogels at different pH values of phosphate buffer solutions

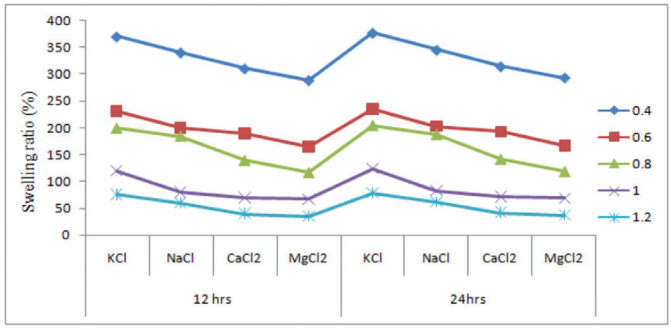

Figure 7. Swelling studies of different concentrated salt solutions at different times

ACKNOWLEDGEMENTS

The authors are grateful to the Institution of Excellence for the FTIR and SEM analysis help.

Conflict of Interest: No conflict of interest was declared by the authors.

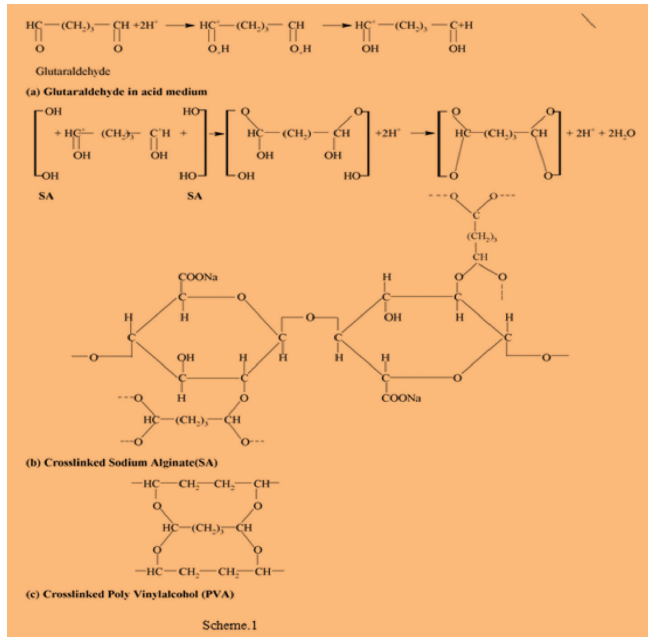

Scheme 1. (a) Glutaraldehyde in acid medium, (b) crosslinked sodium alginate, (c) crosslinked poly(vinly alcohol)

Table 3. Data of swelling studies of hydrogels in different salt solutions

Conc.	12 h				24 h			
	KCl	NaCl	$CaCl_2$	$MgCl_2$	KCl	NaCl	$CaCl_2$	$MgCl_2$
0.4	370.42	340.16	310.72	288.02	377.72	345.45	314.7	293.6
0.6	230.17	200.36	190.64	165	235.46	203.8	193.4	167.9
0.8	200.23	185.34	140.39	117.79	205.0	188.1	142.9	119.2
1.0	120.14	80.08	70.06	67.58	124.19	82.5	72.01	69.1
1.2	75.09	60.63	40.46	35.96	78.20	62.04	42.02	37.4

REFERENCES

1. Serp D, Mueller M, Von Stockar U, Marison IW. Low-temperature electron microscopy for the study of polysaccharide ultrastructures in hydrogels. II. Effect of temperature on the structure of Ca^{2+}-alginate beads. Biotechnol Bioeng. 2002;79:253-259.
2. Wee S, Gombotz WR. Protein release from alginate matrices. Adv Drug Deliv Rev. 1998;31:267-285.
3. Dumitriu S. Polymeric Biomaterials, Revised and Expanded. Boca Raton; CRC Press; 2001:1-62.
4. Gemienhart RA, Guo C. Fast swelling hydrogel systems. In: Yui N, Mrsny RJ, Park K, eds. Reflexive Polymers and Hydrogels. New York; CRC Press; 2004:245-258.
5. Rosiak JM, Yoshii F. Hydrogels and medical applications. Nucl Instr Meth Phys Rev. 1999;151:56-64.
6. Silva GS, Fernadez LRV, Higa OZ, Vitolo M, De Queiroz ASA. Alginate-Poly (vinyl alcohol) core-shell microspheres for lipase - immobilization. Cebecimat, XVI congreso Brasileiro de Engenhariae Ciencia dos Materials. Porto Alegre – RS de 28 de novembroa 02 de dezembro de; 2004:15.
7. Abbas AA, Lee SY, Selvaratnam L, Yusof N, Kamaru T. Porous PVA-chitosan based hydrogels as an extracellular matrix scaffold for cartilage regeneration. European Cells and materials. 2008;16(Suppl 2):50.
8. Ustundag GC, Karaca E, Ozbek S, Cavusoglu I. *In vivo* evaluation of electrospun Poly (vinyl alcohol) / sodium alginate nanofibrous mat a wound Dressing. Tekstil ve Konveksiyon. 2010;4:290-298.
9. Sariri R. Physicochemical characteristics and Biomedical applications of hydrogel. A review. J Phys Theor Chem IAU Iran. 2011;8:217-231.
10. Tombs MP, Harding SE. An Introduction to Polysaccharide Biotechnology. Taylor and Francis UK; 1999:183.
11. Cunha AG, Gandini A. Turning polysaccharides into hydrophobic materials: a critical review. Part 2. Hemicellulose, chitin/chitosan, starch, pectin and alginates. Cellulose. 2001;17:1045-1065.
12. Cha DS, Choi JH, Chinnan MS, Park HJ. Antimicrobial film based on Na-alginate and K- carrageenan. Lebensmittel Wissenschaft und Technologie. 2002;35:715- 719.
13. Boninsegna S, Dal Toso RD, Monte RD, Carturan G. Alginate microspheres loaded with animal cells and coated by a siliceous layer. Journal of Sol-Gel Science and Technology. 2003;26:1151-1157.
14. Lee KY. Mooney DJ. Hydrogels for tissue engineering. Chem Rev. 2001;101:1869-1879.
15. Hoffman AS. Hydrogels for biomedical applications. Adv Drug Deliv Rev. 2002;43:3-12.
16. Bahrami SB, Kordestani SS, Mirzadeh H, Mansoori P. Poly (vinyl alcohol) - Chitosan blends: preparation, mechanical and physical properties. Iranian Polymer Journal. 2003;12:139-146.
17. Nam SY, Nho YC, Hong SH, Chae GT, Jang HS, Suh TS, Ahn WS, Ryu KE, Chun HJ. Evaluations of poly (vinyl alcohol)/alginate hydrogels cross-linked by γ-ray irradiation technique. Macromolecular Research. 2004;12:219-224.
18. Mishra S, Bajpai R, Katare R, Bajpai AK. Radiation induced cross linking effect on semi -interpenetrating polymer networks of poly (vinyl alcohol). Express Polymer Letters. 2007;1:407-415.
19. Zain NAM, Suhaimi MS, Idris A. Development and modification of PVA - alginate as suitable immobilization matrix. Process Biochemistry. 2011;46:2122-2129.
20. Wu KY, Wisecarver KD. Cell immobilization using PVA crosslinked with boric acid. Biotechnol Bioeng. 1992;39:447-449.
21. Dave R, Madamwar D. Polymer of poly (vinyl alcohol)- boric acid for esterification in organic media. Indian Journal of Biotechnology. 2006;5(Suppl):368-372.
22. Kulkarni AR, Soppimath KS, Aminabhavi TM. Controlled release of diclofenac sodium from sodium alginate beads crosslinked with glutaraldehyde. Pharm Acta Helv. 1999;74:29-36.
23. Ostberg T, Vesterhus L, Graffner C. Calcium alginate matrices for oral multiple unit administration. Part 2. Effect of process and formulation factors on matrix properties. Int J Pharm. 1993;97:183-193.
24. Pillay V, Dangor DM, Govender T, Moopanar KR, Hurbans N. Drug release modulation from cross-linked calcium alginate microdiscs, 2: swelling, compression, and stability of the hydrodynamically-sensitive calcium alginate matrix and the associated drug release mechanisms. Drug Delivery. 1998;5:35-46.
25. Pillay V, Dangor CM, Govender T, Moopanar KR, Hurbans N. Ionotropic gelation: encapsulation of indomethacin in calcium alginate gel discs. J Microencapsul. 1998;15:215-226.
26. Pillay R, Fassihi R. *In vitro* release modulation from crosslinked pellets for site-specific drug delivery to the gastrointestinal tract. I. Comparison of pH-responsive drug release and associated kinetics. J Controlled Release. 1999;59:229-242.
27. Kulkarni AR, Soppimath KS, Aminabhavi TM, Dave AM, Mehta MH. Glutaraldehyde crosslinked sodium alginate beads containing liquid pesticide for soil application. J Control Release. 2000;63:97-105.
28. Kim YJ, Yoon KJ, Ko SW. J Appl Polym Sci. 2000;78:1797-1804.
29. Tripathy T, Pandey SR, Karmakar NC, Bhagat RP, Singh RP. Eur Polym J. 1999;35:2057-2072.
30. Beebe DJ, Moore JS, Bauer JM, Liu Q, Yu RH, Devadoss C, Jo BH. Functional hydrogel structures for autonomous flaw control inside micro- fluidic channels. Nature. 2000;404:588-590.
31. Shahinpoor M. J. Micro-elecctro - mechanics of ionic polymer gels as electrically controllable artificial muscles. Intell Mater Syst Struct. 1995;6:307-314.
32. Brock D, Lee WJ. A dynamic model of a linear actuator based on polymer Hydrogels. Intel Mater System Struct. 1994;5:764-771.
33. Helfferich F. Ion exchange. New York: McGraw-Hill, 1962:5.
34. Grodzinsky AJ, Grinshaw PE. Elctrically and chemically controlled hydrogels, for drug delivery. Pulsed and Self-Regulated Drug Delivery. 1990:47-64.
35. Peppas NA, Brannon - Peppas L. Solute and Penetrant diffusion in swellable polymers. IX. The mechanism of drug release from pH – sensitive swelling –controlled systems. J Control Release. 1989:267-274.
36. Eisenberg SR. The kinetics of chemically induced non equilibrium swelling of articular cartilage and corneal stroma. J Biomed Eng. 1987;109:79-89.
37. Myers ER, Lai WM, Mow VC. A continuum theory and an experiment for the ion-induced swelling behavior of articular cartilage. J Biomech Eng. 1984;106:151- 158.

38. Okano K, Bac YH, Kim SW. "Temperature responsive controlled drug delivery." Pulsed and self- regulated drug delivery pulsed and self-regulated Drug Delivery. 1990:17-46.

39. Kim JO, Park JK, Kim JH, Jin SG, Yonga CS, Li Dx, Choi HG. Development of Poly (vinyl alcohol) - sodium alginate gel-matrix –based wound dressing system Containing Nitrofurazone. Int J Pharm. 2008;359:79-86.

40. Chhatri A, Bajpai AK, Shandhu SS, Jain N, Biswas, J. Cryogenic fabrication of salvon loaded macroporous blends of alginate and Poly(vinyl alcohol) (PVA). Swelling, deswelling and antibacterial behaviors. Cabohydr Polym. 2011;83:876-882.

41. Mansur HS, Orefice RL, Mansur AAP. Characterization of Poly (vinyl alcohol)/ Poly (ethylene glycol) hydrogels and PVA – derived hybrids by small –angle x-Ray Scattering and FTIR spectroscopy. Polymer 2004;45:7193-7202.

42. Sonali K, Udayabhanu MJ, Karthik KT, Rebecca G, David KM. Permance evalution of nanoclay enriched anti-microbial hydrogels for biomedical application. Heliyon. 2016;2:e00072.

43. Kamouna EA, Kenawy ERS, Tamer TM, Meligy MAE, Eldin MSM. Poly (vinyl alcohol)-alginate physically crosslinked hydrogel membranes for wound dressing applications: Characterization and bio-evaluation. Arabian Journal of Chemistry. 2015;8:38-47.

44. Zho Y, Su H, Fang L, Tan T. Superabsorbent hydrogels from poly(aspartic acid) with salt-, temperature- and pH-responsiveness properties. Polymer. 2005;46:5368-5376.

45. Raafat AI, Eid M, El-Arnaouty MB. Radiation synthesis of superabsorbent CMC based hydrogels for agriculture applications. Nuclear Instrument and Methods in Physics Research Section B Beam Interactions with Materials and Atoms. 2012;283:71-76.

Turk J Pharm Sci 2019;16(3):261-264
DOI: 10.4274/tjps.galenos.2018.65487

ORIGINAL ARTICLE

Evaluation of the Antidiabetic Activity of *Alchemilla persica* Rothm. in Mice with Diabetes Induced by Alloxan

Alloksanla İndüklenen Farelerde *Alchemilla persica* Rothm.'nın Antidiyabetik Etkisinin Değerlendirilmesi

Serkan ÖZBİLGİN[1], Hanefi ÖZBEK[2], Neriman İpek KIRMIZI[3], Burçin ERGENE ÖZ[1]*, Ekin KURTUL[1], Bade Cevriye ÖZRENK[3], Gülçin SALTAN İŞCAN[1], Özlem BAHADIR ACIKARA[1]

[1]Ankara University, Faculty of Pharmacy, Department of Pharmacognosy, Ankara, Turkey
[2]İstanbul Medipol University, Faculty of Medicine, Department of Pharmacology, İstanbul, Turkey
[3]İstanbul Medipol University, Faculty of Medicine, Department of Vocational School of Health Services, İstanbul, Turkey

ABSTRACT

Objectives: *Alchemilla* species are used in Turkish folk medicine for the treatment of many diseases together with diabetes. *Alchemilla persica*, belonging to this genus, is widely distributed in Eastern Anatolia as well as in Caucasia, northern and northeastern Iran, and northern Iraq.

Materials and Methods: Methanolic-water extracts of the aerial parts and roots of *A. persica* were evaluated for their hypoglycemic activities in mice with alloxan-induced diabetes in order to verify its usage in folk medicine.

Results: None of the tested extracts exhibited a significant lowering effect on blood glucose levels. However, the aerial parts notably increased blood glucose levels at doses of 100 mg/kg and 200 mg/kg.

Conclusion: *A. persica* usage as an antidiabetic is not confirmed in the present study.

Key words: *Alchemilla persica*, alloxan, antidiabetic activity, diabetes, hypoglycemic activity

ÖZ

Amaç: *Alchemilla* türleri Türk halk tıbbında diyabetin yanında birçok hastalığın da tedavisinde kullanılmaktadır. Bu cinse ait olan *Alchemilla persica*; Doğu Anadolu, Kafkasya, Kuzey ve Kuzeydoğu İran ile Kuzey Irak'ta yetişmektedir.

Gereç ve Yöntemler: Bu çalışmada *Alchemilla persica*'nın halk arasındaki kullanımını doğrulamak amacıyla; toprak üstü kısım ve köklerinin sulu-metanollü ekstrelerinin alloksan indüklü diyabetik fareler üzerindeki hipoglisemik etkileri test edilmiştir.

Bulgular: Test edilen ekstrelerden hiçbiri kan glukoz düzeyini kayda değer biçimde düşürmezken, *A. persica* toprak üstü kısımları kan glukoz düzeyini 100 mg/kg ve 200 mg/kg dozlarda önemli ölçüde artırmıştır.

Sonuç: Bu çalışma *A. persica*'nın antidiyabetik olarak kullanımını doğrulamamıştır.

Anahtar kelimeler: *Alchemilla persica*, alloksan, antidiyabetik aktivite, diyabet, hipoglisemik aktivite

*Correspondence: **E-mail:** ergene@pharmacy.ankara.edu.tr, **Phone:** +90 542 688 62 26 **ORCID-ID:** orcid.org/0000-0001-6927-6652
Received: 09.02.2018, **Accepted:** 16.05.2018

INTRODUCTION

The genus *Alchemilla* L. (Rosaceae), with more than 1000 species, is distributed mainly in western Eurasia as well as in southern and eastern Africa, Madagascar, southern India, Sri Lanka, and Java.[1,2] In Turkey 50 species of the genus *Alchemilla*, which are mainly distributed in Northeast Anatolia, were recorded and this number has reached 74 with new records.[1] *Alchemilla persica* Rothm., belonging to this genus, grows naturally in Eastern Anatolia, Caucasia, northern and northeastern Iran, and northern Iraq.[3]

Alchemilla vulgaris L. (lady's mantle, bear's foot, lion's foot) is the best known species from the genus *Alchemilla* and is mainly used for treating women's illnesses, wounds, and skin disorders in Europe.[4-6] Its usage for nonspecific diarrhea is approved by Commission E.[7] Additionally, ESCOP Monographs described this plant's usage for nonspecific diarrhea, gastrointestinal disorders, and dysmenorrhea based on clinical studies and long-term use.[8] *Alchemilla* species are used for their wound healing, sedative,[9-12] antidiareic, tonic, and diuretic activities,[13-15] and in treatment for menstruation disorders,[16] gynecological problems,[17,18] liver inflammation,[17] asthma, bronchitis, cough,[19] and diabetes, as well as kidney, intestinal, and gastric disorders[20-21] and skin diseases.[10]

Previous studies have revealed that the aerial parts and roots of *A. persica* showed antioxidant activity by DPPH radical scavenging (IC_{50} 0.055 M and 0.151 M, respectively) and reducing MDA levels (5.9 nmol/mL and 19.08 nmol/mL respectively).[22] Extract of the aerial parts of *A. persica* exhibited a reduction in the endometrioma. However, no significant reduction in the levels of cytokine, tumor necrosis factor-α, vascular endothelial growth factor, or interleukin-6 were recorded.[23] *A. persica* displayed significant wound healing activity with tensile strength values of 33.3% and contraction values of 43.5% in linear incision and circular excision wound models, respectively. Hydroxyproline estimation and histopathological analysis also confirmed the results. *A. persica* showed significant anti-inflammatory activity with a value of 26.6%.[24] Phenolic constituents, namely caffeic acid esters with sugars, flavonoid glycosides, catechin and epicatechin, condensed tannins related to gallic acid, such as pedunculatin/pedunculagin, agrimoniin, casuarictin, castalagin/vescalagin, and sanguiin H-10 isomers, were identified by HR-MS Q-TOF in the aerial parts of *A. persica* and its essential oil consisted of diterpenoids (19.6%) and sesquiterpenoids (17.2%) mainly.[25]

The current study was designed to evaluate the hypoglycemic activities of the roots and aerial parts of *A. persica* using an alloxan-induced diabetic mice test model to test its traditional usage for treatment of diabetes in Turkish folk medicine.

MATERIALS AND METHODS

Plant material

Plant material was collected from the Kop Pass, Erzurum, Turkey. The taxonomic identification of these plants was confirmed by H. Duman, at the Department of Biological Sciences, Faculty of Arts and Sciences, Gazi University. Voucher specimens were deposited in the herbarium of the Faculty of Pharmacy at Ankara University (AEF 25896).

Extraction

Aerial parts and roots of *A. persica* were extracted with a methanol:water (80:20) solvent system for 8 h at room temperature by stirring and then filtered. The methanol was evaporated under vacuum at 35-40°C and then the remaining water was lyophilized to obtain crude extracts.

Animals

Balb/C mice (22-30 g) were used for testing antidiabetic activity. The study protocol (30/09/2015-69) was approved by the Ethical Committee of İstanbul Medipol University. The animals were housed in standard cages (48 cm×35 cm×22 cm) at room temperature (22±2°C), with artificial light from 7.00 am to 7.00 pm, and provided with pelleted food and water *ad libitum*. The procedures followed were in accordance with animal rights as per the Guide for the Care and Use of Laboratory Animals.

Chemicals

Alloxan was purchased from Sigma (Steinheim, Germany). The alloxan and *A. persica* extracts were dissolved in distilled water (w/v).

Antidiabetic activity

Diabetes was induced by injecting 150 mg/kg of alloxan solution in isotonic saline solution (ISS) i.p. into the mice after fasting for 18 h. This procedure was repeated three times at 48 h intervals. After 7 days of treatment, the mice's blood glucose levels were measured. The mice with 200 mg/dL or over were included in the study as diabetic mice. The diabetic animals were randomly divided into five groups of six animals each. Group I mice received 0.1 mL of ISS i.p. The animals in groups II and III were treated with 100 mg/kg body weight of extracts of the aerial parts of *A. persica* at 100 mg/kg and 200 mg/kg doses, while those in groups IV and V were treated with 100 mg/kg and 200 mg/kg root extract of *A. persica*, respectively. The animals were treated with ISS and *A. persica* extracts in a single dose at the beginning of the procedure. Blood was taken from the tail vein by scalpel blade and blood glucose levels were determined before treatment and 1, 2, and 4 h after treatment by applying the glucose oxidase peroxidase method using an Accu-Check® device (Abbott, United Kingdom).

Statistical analysis

The statistics were analyzed using SPSS 18.0. The results are reported as mean ± standard error of mean and as percentages (%). One-way analysis of variance (*post-hoc* least significant difference test) was used for the statistical analysis. Probability levels of less than 0.05 ($p<0.05$) were considered significant.

RESULTS

In order to investigate the hypoglycemic activities of extracts of the aerial parts and roots of *A. persica* on alloxan-induced diabetes in mice blood glucose levels were measured before and 1, 2, and 4 h after treatment. Table displays the effect of the *A. persica* extracts on blood sugar levels. The current study's

Table. Blood sugar levels of mice with alloxan-induced diabetes

Groups	Blood sugar levels (mg/dL)			
	Before treatment with *Alchemilla persica*	After treatment with *Alchemilla persica*		
		1 h (0-1)	2 h (0-2)	4 h (0-4)
Control (ISS)	470.00±23.62	471.00±13.78 (0.74±3.99)	493.80±15.55 (5.54±3.73)	494.20±27.32 (4.97±2.18)
Alchemilla persica (AE) 100 mg/kg	306.67±36.13	501.67±27.97 (70.97±15.01)*	484.67±22.12 (67.15±17.39)*	387.66±20.77 (36.35±17.91)
Alchemilla persica (AE) 200 mg/kg	297.40±38.09	410.00±25.37 (42.81±10.85)*	354.20±33.90 (22.50±12.27)	290.60±59.97 (1.36±26.06)
Alchemilla persica (R) 100 mg/kg	337.00±27.28	379.83±52.56 (14.45±15.87)	425.33±52.26 (29.80±17.04)	355.83±61.67 (8.87±18.78)
Alchemilla persica (R) 200 mg/kg	405.17±24.40	445.00±44.83 (9.01±7.30)	427.83±50.04 (4.64±9.13)	305.80±63.67 (-23.73±13.49)

Mean ± standard error of mean; Results of *post-hoc* LSD test; *: Comparison with SF group ($p<0.05$)
AE: Aerial parts, R: Roots, LSD: Least significant difference, ISS: Isotonic saline solution

results revealed that none of the extracts induced significant reductions in the levels of blood sugar ($p>0.05$). On the other hand, notable increases in blood glucose levels were observed 1 h and 2 h after treatment with the aerial parts of *A. perisca* at 100 mg/kg dosage and 1 h after treatment with 200 mg/kg dosage. A decrease in blood glucose level was detected only with treatment of *A. persica* roots at 200 mg/kg dosage 4 h after treatment. However, the results were not significant.

DISCUSSION

In Turkish folk medicine, the use of *Alchemilla compactilis* Juz., *Alchemilla speciosa* Buser, and other *Alchemilla* species for the treatment of diabetes is recorded.[20,21] The present study did not confirm the usage of *A. persica* in folk medicine for the treatment of diabetes. A previous study related to the hypoglycemic effect of *Alchemilla xanthochlora* (*A. vulgaris*) also reported that decoction of the leaves was not active on streptozotocin-induced diabetic mice.[8] The aerial parts and roots of *Acanthus mollis* were also tested for their antidiabetic activities and results similar to those for *A. persica* were obtained.[26] All study results indicated that the *Alchemilla* species *A. mollis*, *A. vulgaris*, and *A. persica* had no lowering effect on blood glucose levels. In contrast, the aerial parts of *A. mollis* and *A. persica* increased blood glucose levels at 100 mg/kg and 200 mg/kg dosages 4 h after treatment.

CONCLUSIONS

Based on the current study results, the aerial parts and roots of *A. persica* are not useful for decreasing blood sugar levels in short-term treatment. Furthermore, *A. persica* is not suitable in phytotherapy for other medicinal purposes in diabetic patients.

Conflict of Interest: No conflict of interest was declared by the authors.

REFERENCES

1. Hayırlıoğlu-Ayaz S, Inceer H. Three new Alchemilla L. (Rosaceae) records from Turkey. Pak J Bot. 2009;41:2093-2096.
2. Faghir MB, Attar F, Shavvon RS, Mehrmanesh A. Pollen morphology of the genus Alchemilla L. (Rosaceae) in Iran. Turk J Bot. 2015;39:267-279.
3. Davis PH. Flora of Turkey and the East Aegean Islands. Edinburgh University Press; 1982:99.
4. PDR for Herbal Medicines. (2nd ed.). Montvale, NJ; Thomson Medical Economics; 2000.
5. Said O, Khalil K, Fulder S, Azaizeh H. Ethnopharmacological survey of medicinal herbs in Israel, the Golan Heights and the West Bank region. J Ethnopharmacol. 2002;83:251-265.
6. Tasic S. Ethnobotany in SEE-WB countries; Traditional Uses of Indigenous Plants. Lek Sirov. 2012;32:71-81.
7. Blumenthal M, Werner RB. The Complete German Commission E Monographs: Therapeutic Guide to Herbal Medicines. (1st ed). Austin, Texas; American Botanical Council, Lippincott Williams & Wilkins; 1998:158.
8. Mills MS, Hutchins R. European Scientefic Cooperative on Phytotherapy (ESCOP) Monographs Online Series, Alchemilla herba-Alchemilla/Lady's Mantle. United Kingdom; ESCOP Notaries House; 2013.
9. Saraç DU, Ozkan ZC, Akbulut S. Ethnobotanic features of Rize/Turkey province. Biological Diversity and Conservation. 2013;6:57-66.
10. Kaval I, Behçet L, Cakilcioglu U. Ethnobotanical study on medicinal plants in Geçitli and its surrounding (Hakkari-Turkey). J Ethnopharmacol. 2014;155:171-184.
11. Güzel Y, Güzelşemme M, Miski M. Ethnobotany of medicinal plants used in Antakya: A multicultural district in Hatay Province of Turkey. J Ethnopharmacol. 2015;174:118-152.
12. Mükemre M, Behçet L, Çakılcıoğlu U. Ethnobotanical study on medicinal plants in villages of Çatak (Van-Turkey). J Ethnopharmacol. 2015;166:361-374.
13. Baytop T. Türkiye'de Bitkiler ile Tedavi. İstanbul; Nobel Tıp Kitabevleri Ltd Şti; 1999.
14. Altundağ E, Ozturk M. Ethnomedicinal studies on the plant resources of east Anatolia, Turkey. Procedia Social and Behavioral Sciences. 2011;19:756-777.
15. Akbulut S, Bayramoğlu MM. The trade and use of some medical and aromatic herbs in Turkey. Ethno Med. 2013;7:67-77.

16. Polat R, Satıl F, Cakılcıoğlu U. Medicinal plants and their use properties of sold market in Bingöl (Turkey) district. Biological Diversity and Conservation. 2011;4:25-35.

17. Sağıroğlu M, Arslanturk A, Akdemir ZK, Turna M. An ethnobotanical survey from Hayrat (Trabzon) and Kalkandere (Rize/Turkey). Biological Diversity and Conservation. 2012;5:31-43.

18. Kalankan G, Ozkan ZC, Akbulut S. Medicinal and aromatic wild plants and traditional usage of them in Mount Ida (Balıkesir/Turkey). JABS. 2015;9:25-33.

19. Polat R, Çakılcıoğlu U, Kaltalıoğlu K, Ulusan MD, Türkmen Z. An ethnobotanical study on medicinal plants in Espiye and its surrounding (Giresun-Turkey). J Ethnopharmacol. 2015;163:1-11.

20. Akbulut S, Bayramoğlu MM. Reflections of socio-economic and demographic structure of urban and rural on the use of medicinal and aromatic plants: the sample of Trabzon Province. Ethno Med. 2014;8:89-100.

21. Akbulut S, Ozkan ZC. Traditional usage of some wild plants in Trabzon region (Turkey). Kastamonu Univ. Journal of Forestry Faculty. 2014;14:135-145.

22. Ergene B, Bahadır Acıkara Ö, Bakar F, Saltan G, Nebioğlu S. Antioxidant Activity and Phytochemical Analysis of *Alchemilla persica* Rothm. J Fac Pharm. 2010;39:145-154.

23. Küpeli Akkol E, Demirel MA, Bahadır Acıkara Ö, Süntar I, Ergene B, Ilhan M, Ozbilgin S, Saltan G, Keleş H, Tekin M. Phytochemical analyses and effects of Alchemilla mollis (Buser) Rothm. and *Alchemilla persica* Rothm. in rat endometriosis model. Arch Gynecol Obstet. 2015;292:619-628.

24. Ergene Öz B, Ilhan M, Özbilgin S, Küpeli Akkol E, Bahadır Acıkara Ö, Saltan G, Keleş H, Süntar I. Effects of *Alchemilla mollis* and *Alchemilla persica* on the wound healing process. Bangladesh Journal of Pharmacology. 2016;11:577-584.

25. Heshmati Afshar F, Maggi F, Ferrari S, Peron G, Dall'Acqua S. Secondary Metabolites of *Alchemilla persica* Growing in Iran (East Azarbaijan). Natural Product Communications. 2015;4:1-10.

26. Özbek H, Bahadır Acıkara Ö, Keskin I, Kırmızı NI, Özbilgin S, Ergene Öz B, Kurtul E, Özrenk BC, Tekin M, Saltan G. Evaluation of hepatoprotective and antidiabetic activity of *Alchemilla mollis*. Biomed Pharmacother. 2017;86:172-176.

Turk J Pharm Sci 2019;16(3):265-272
DOI: 10.4274/tjps.galenos.2018.20082

ORIGINAL ARTICLE

Palmitic Acid–Pluronic F127–Palmitic Acid Pentablock Copolymer as a Novel Nanocarrier for Oral Delivery of Glipizide

Glipizidin Oral Uygulanması için Yeni Bir Nanotaşıyıcısı Olarak Palmitik Asit – Pluronic F127 – Palmitik Asit Pentablok Kopolimeri

Vipan Kumar KAMBOJ, Prabhakar Kumar VERMA*

Maharshi Dayanand University, Department of Pharmaceutical Sciences, Rohtak, India

ABSTRACT

Objectives: The aim of the present study was to develop nanotechnology-based oral formulations of glipizide to enhance the bioavailability and eliminate the frequent oral administration of the conventional dosage form. Glipizide is an antidiabetic drug with a short biological half-life and limited oral bioavailability. Novel palmitic acid–pluronic F127–palmitic acid (PA-F127) pentablock copolymer-based prolonged release glipizide nanoparticles (GNs) were prepared and screened for *in vitro* and *in vivo* studies.

Materials and Methods: GNs were prepared using a novel PA-F127 pentablock copolymer by solvent evaporation technique. The prepared nanoparticles were evaluated for particle size, polydispersity index (PDI), zeta potential, entrapment efficiency, percentage yield, and drug excipient compatibility using fourier transform infrared spectroscopy (FTIR) and differential scanning calorimeter (DSC) analysis, X-ray diffraction, scanning electron microscopy, *in vitro* drug release studies, stability studies, and *in vivo* pharmacokinetic studies.

Results: The results of FTIR and DSC analysis revealed the absence of drug–excipient interactions. The optimized GN1 had particle size 242.60±4.20 nm, PDI 0.171±0.014, and zeta potential -21.41±0.462 mV. The prepared nanoparticles were spherical and showed semi-amorphous characteristics. The *in vitro* release studies showed 34.43±4.8% drug was released in the first 8 h and 56.11±4.12% glipizide was released further over 24 h. The GN1 was found to be stable at 5±3˚C for up to 3 months. Pharmacokinetic studies showed that the orally administered GN1 was superior with C_{max} 2.35-fold, t_{max} 1.6-fold, area under the curve ($AUC_{0\rightarrow\infty}$) 3.3-fold, and mean residence time 1.2-fold as compared to pure glipizide ($p<0.05$).

Conclusion: The bioavailability of the newly developed GN1 was successfully increased and the problem of frequent oral administration with the conventional dosage form can be overcome for diabetes treatment.

Key words: Glipizide, nanoparticles, palmitic acid, pluronics, bioavailability

ÖZ

Amaç: Bu çalışmanın amacı, glipizidin biyoyararlanımı arttırmak ve geleneksel dozaj formunun oral yoldan sık sık verilmesini elimine etmek için nanoteknoloji bazlı oral formülasyonlarını geliştirmektir. Glipizide, biyolojik olarak kısa yarı ömrü ve sınırlı oral biyoyararlanımı olan antidiyabetik bir ilaçtır. Yeni palmitik asit-pluronik F127-palmitik asit (PA-F127) pentablok kopolimer bazlı uzun süreli salım yapan glipizid nanopartikülleri (GNs) *in vitro* ve *in vivo* çalışmalar için hazırlanmış ve taranmıştır.

Gereç ve Yöntemler: GN'ler yeni PA-F127 pentablok kopolimer kullanılarak solvent buharlaştırma yöntemi ile hazırlanmıştır. Hazırlanan nanopartiküller, partikül büyüklüğü, polidispersite indeksi (PDI), zeta potansiyeli, yükleme etkinliği, yüzde verimi ve fourier transform kızılötesi spektroskopisi (FTIR) ve diferansiyel tarama kalorimetresi (DSC) analizi, X-ışını kırınımı kullanılarak etken madde ile eksipiyan geçimliliği, taramalı elektron mikroskobu, *in vitro* etken madde salım çalışmaları, stabilite çalışmaları ve *in vivo* farmakokinetik çalışmalar değerlendirildi.

Bulgular: FTIR ve DSC analizlerinin sonuçları, etken madde-eksipiyan etkileşimlerinin olmadığını göstermiştir. Optimize edilmiş GN1'in, partikül büyüklüğü 242.60±4.20 nm, PDI 0.171±0.014 ve zeta potansiyeli -21.41±0.462 mV idi. Hazırlanan nanopartiküller küreseldi ve yarı amorf özellikler göstermiştir. *İn vitro* salım çalışmaları, ilk 8 saatte %34.43±4.8 etken madde salındığını ve 24 saat içinde 56.11±%4.12 glipizid salındığını göstermiştir. GN1'in 5±3˚C'de 3 aya kadar stabil olduğu bulunmuştur. Farmakokinetik çalışmalar, oral yoldan verilen GN1'in, saf glipizide göre 2.35 kat C_{max}, 1.6 kat t_{max}, 3.3 kat eğri altındaki alan ($AUC_{0\rightarrow\infty}$) ve 1.2 kat ortalama kalış süresi ile daha üstün olduğunu göstermiştir ($p<0.05$).

Sonuç: Yeni geliştirilen GN1'in biyoyararlanımı başarılı bir şekilde arttırılmıştır ve diyabet tedavisi için ticari dozaj formu ile sık sık oral uygulama sorunu aşılabilmiştir.

Anahtar kelimeler: Glipizid, nanopartiküller, palmitik asit, pluronikler, biyoyararlanım

*Correspondence: E-mail: vermapk422@rediffmail.com, Phone: +919992581437 ORCID-ID: orcid.org/0000-0002-1769-6484
Received: 09.03.2018, Accepted: 16.05.2018

INTRODUCTION

Glipizide is a potential second-generation sulfonylurea derivative belonging to Biopharmaceutical Classification System Class-II drugs. It is commonly utilized as an oral hypoglycemic agent for the treatment of type II diabetes mellitus.[1,2] Glipizide is the most effective insulin secretagogue and presents fewer side effects compared to the first-generation drugs.[3] It is a weak acid with a pka value of 5.9 and is better absorbed from acidic medium. Due to the very low pH level of glipizide, its aqueous solubility is negligible, which causes discrepancies in bioavailability.[4] After absorption from the gastrointestinal tract, glipizide reduces the blood glucose levels in 30 min and peak concentration of the drug is reached within 1-3 h.[3] It is rapidly eliminated from the body due to its small biological half-life (3.4±0.7 h) and hence the drug needs frequent oral administration in 2 or 3 doses of 2.5 to 10 mg per day.[5] Due to the poor solubility of glipizide, researchers have investigated several drug delivery systems including a solid self-nanoemulsifying drug delivery system,[2] microspheres,[5] poly(lactic-co-glycolic acid), Eudragit nanoparticles,[6] cyclodextrin complex,[7,8] chitosan and xanthan beads,[9] and nanosuspension[10] to increase the solubility and bioavailability of glipizide. Nanotechnology-based drug delivery systems with the use of biodegradable polymers seem to be most convenient for the delivery of any drug due to negligible chances of toxicity and overall improved therapeutic properties.[11]

Pluronics are A-B-A type triblock nonionic, biodegradability copolymers listed in the British and US Pharmacopoeia as excipients and extensively used in drug delivery systems.[10,12] Due to the amphiphilic nature of Pluronics, they are self-assembled into micelles above the critical micelle concentration in an aqueous solvent.[13] The critical micelle concentration (CMC) value of Pluronic F127 was observed in the range 0.26-0.8 wt %. The high CMC value indicates the dissociation of nanoparticles occurs before the target site is reached. This problem can be overcome using mixed polymers. The modified block copolymers like stearic acid-coupled F127 nanoparticles of doxorubicin[12] and Pluronic/poly(lactic acid) vesicles for oral insulin delivery[14] have been investigated. These studies inspired us to go further to explore the application of Pluronics in a nanotechnology-based oral drug delivery system for glipizide.

In the present study, we aimed to develop glipizide nanoparticles (GNs) with better bioavailability that overcome the problem of frequent dose administration. We prepared orally active GNs using PA-F127 copolymer that were optimized for physicochemical properties and evaluated their pharmacokinetic parameters in rats. We also analyzed the stability of the GNs at 5±3°C and 25°C over 3 months.

MATERIALS AND METHODS

Materials

Pharmaceutical grade glipizide was purchased from Swapnroop Drugs and Pharmaceuticals, Aurangabad, India. Palmitic acid (PA), Pluronic F127, and polyvinyl alcohol (PVA) were procured from Sigma-Aldrich, India. The other chemicals and solvents used were of analytical grade and were purchased from Molychem, Mumbai.

Synthesis of PA-F127 pentablock copolymer

PA (15 g) and 15 g of Pluronic F127 (15 g) were added to a 100 mL round bottom flask and the mixture was heated with constant stirring to yield a well-mixed molten phase and it was reacted at 160°C for 6 h. The PA-F127 copolymer was recovered by mixing the resulting solution into an ethyl acetate/petroleum ether 1:1 (v/v) solution to eliminate the unreacted PA by filtration. The PA-F127 copolymer was obtained by evaporating the organic solvent at room temperature and dried at 25°C under vacuum for 24 h. The synthesized copolymer structure was confirmed by the spectrum of fourier transform infrared spectroscopy (FTIR) (Bruker 1-206-0280, KBr pellets) and ^{1}H NMR (Bruker Model Advance II 400; 400 MHz) spectroscopy.

Preparation of glipizide loaded PA-F127 nanoparticles

GNs were fabricated by solvent evaporation technique using PA-F127 and PVA polymeric systems. A mixture of chloroform and methylene chloride (1:1 v/v) was prepared and glipizide was dissolved in it. The PA-F127 copolymer was dissolved in chloroform. The copolymer solution was added to glipizide solution drop by drop with continuous stirring. Next 1.0 mL of the aqueous phase of PVA (2%) was added dropwise to the organic mixture of drug and copolymer with continuous homogenization (12000 rpm; IKA T25 ultra homogenizer) followed by stirring (700 rpm) for 3 h and the nanosuspension obtained was stored in vacuum desiccators overnight at room temperature in order to remove the remaining organic solvents. The un-incorporated glipizide aggregates were removed through filtration using Whatman paper no. 1. The filtrate was centrifuged (14000 rpm; Remi, India) and sediment containing nanoparticles was separated and dried by lyophilization.[12,15]

Characterization of prepared GNs

Particle size, polydispersity index, and zeta potential

The average particle size, polydispersity index (PDI), and zeta potential of the GNs were evaluated using a Zetasizer Nano-ZS (Malvern Instruments, UK). Then 0.5 mg/mL suspension was prepared in Milli-Q water and analyzed to determine these parameters. The results were described as mean ± standard deviation for three replicates.[16]

Entrapment efficiency and percentage yield

Accurately weighed GNs were dissolved in methylene chloride (20 mL). This solution was added to 100 mL of freshly prepared phosphate buffer (pH 7.4) and continuously stirred to extract the glipizide in it. The methylene chloride evaporates during the stirring process.[17] The undissolved content was removed by centrifugation at 10000 rpm (Remi, India), the supernatant was filtered, and the amount of glipizide was assessed using a ultraviolet-Vis spectrophotometer (Lab India 3000^{+}) at 225 nm. Drug entrapment efficiency (%) and percentage yield were calculated using Equation 1 and 2, respectively.

$$\text{Entrapment efficiency}\ (\%) = \frac{\text{Amount of glipizide in nanoparticles}}{\text{Amount of glipizide used in formulation}} \times 100 \quad \textbf{Equation 1}$$

$$\text{Percentage yield} = \frac{\text{Total nanoparticles weght}}{\text{Total solid weight}} \times 100 \quad \textbf{Equation 2}$$

FTIR studies

The interactions between glipizide and excipients were analyzed using FTIR. FTIR spectra of the PA-F127 copolymer, PVA, pure glipizide, physical mixture, and GN1 were taken in KBr pellets using a Bruker (1-206-0280 with software: OPUS-7.2.139.1294) spectrometer and the values of λ max were reported in cm^{-1} (range: 400-4000).

Differential scanning calorimetric analysis

The samples used for FTIR studies were selected for the analysis of thermal properties by using DSC Q10 V9.9, US. The instrument was calibrated using indium as standard. The samples were sealed in aluminum pans with lids and heated at a rate of 10°C/min under a nitrogen environment (60 L/min). The empty aluminum pan was used as a reference. The heat flow was recorded from 35 to 280°C.

X-ray diffraction analysis

X-ray diffraction (XRD) analysis of selected samples was carried out using a Rigaku Miniflex-600 diffractometer. A Cu Kα source operation (40 kV, 15 mA) was used. The diffraction pattern of samples was recorded over a 2θ angular range of 10-70.

Surface morphological studies

The surface morphology of the physical mixture and best-optimized batch was examined by field emission scanning electron microscopy (FE-SEM; JEOL-JSM-7600F, Japan). The samples were dispersed on metallic stubs and then gold coating was done using an ion-sputtering machine. These samples were vacuum dried before the examination.

In vitro dissolution studies

In vitro dissolution studies were performed for the optimized GN1 batch and pure glipizide by modified dialysis sac method.[18] Accurately weighed GN1 suspension (equivalent to 5 mg of glipizide) and pure glipizide suspension (5 mg) were placed in dialysis membrane bags (12-14 kDa cut-off, HiMedia, India) and tied with dialysis clips. The dialysis bags were immersed in separate conical flasks containing 150 mL of 0.1 M phosphate buffer solution (pH 7.4). The conical flasks were stirred at 100 rpm with temperature 37.0±0.5°C. At fixed time intervals, an aliquot of 1 mL was withdrawn from the conical flask and replenished with 1 mL of fresh phosphate buffer and the assay was performed using a UV-Vis spectrophotometer (Lab India 3000+) at 225 nm.

Stability studies

It is important to have an insight into the stability of prepared nanoparticles. The GN1 suspension was kept in a colored glass bottle at 5±3°C and 25°C for short-term stability studies. An aliquot of GN1 samples was taken after 1 and 3 months. These samples were analyzed for any possible change in particle size, PDI, zeta potential, entrapment efficiency, and color of suspension.

Animals

In vivo studies were accomplished in female Wistar albino rats weighing between 250 and 300 g. The rats were procured from the Lala Lajpat Rai University of Veterinary and Animal Sciences, Hisar, India. The rats were kept in polypropylene cages and housed in the central animal house of Maharshi Dayanand University, Rohtak, under standard environmental conditions (23.0±1°C, 55±5% humidity, and 12 h/12 h light/dark cycle). The animals had *ad libitum* access to standard animal diet and water. The protocols of the animal studies were permitted by the Institutional Animal Ethical Committee (IAEC 151/57 dated 30/03/2015) and the experiments were performed according to CPCSEA guidelines.

Pharmacokinetic evaluation in Wistar albino rats

The overnight fasted rats (n=6) were treated with a single oral dose of freshly prepared GN1 carrying 1.5 mg of drug (group I) and pure glipizide suspension was given in group II (1.5 mg/kg b.w.). The blood samples were withdrawn at different time intervals (0, 0.5, 1, 2, 3, 4, 6, 9, 12, and 24 h) through the tail vein using heparinized tubes. The plasma was separated by centrifugation (Plasto Crafts, India) and stored at -20°C until further examination. A rat plasma sample of 0.1 mL and 0.1 mL of 0.1 N HCl were vortexed for 3 min and then 3 mL of benzene was added for the precipitation of plasma proteins. The mixture was smoothly shaken using a cyclo-mixer for 5 min followed by centrifugation for 10 min at 6000 rpm and the precipitates were removed by syringe filter (0.22 µm). The organic phase was evaporated under a nitrogen environment and the residue was thawed in 0.1 mL of mobile phase by vortex mixing. An aliquot of 20 µL was injected into the column of the reverse phase-high performance liquid chromatographic (HPLC) by auto-sampler.

Glipizide in the rat blood plasma was estimated by HPLC using an earlier reported bioanalytical method.[19] The pharmacokinetic studies were performed on a Dionex UHPLC ultimate 3000 RS containing a pump, auto-sampler, column compartment (column: Agilent; 250 mm×4.6 mm; particle size 5 µm), and diode array detector. The data acquisition was achieved through Chromoleon 6.8 software. The monobasic potassium dihydrogen orthophosphate buffer (20 mM; pH 3.5) and acetonitrile were used as mobile phase (65:35 v/v). The mobile phase was filtered through a membrane filter (0.22 µm) and sonicated. The flow rate was kept at 1 mL/min and the total run time of the method was set at 15 min. The effluent was monitored at 225 nm.

Statistical analysis

The pharmacokinetic data were compared by Student's paired t-test using GraphPad Prism 7 software. P values <0.05 were considered significant.

RESULTS AND DISCUSSION

Characterization of PA-F127 pentablock copolymer

The carboxylic group of PA was esterified with the hydroxyl groups of Pluronic F127 (Scheme 1). The structure of PA-F127 copolymer was determined by ^{1}H NMR spectroscopy in $CDCl_3$ and the δ (ppm) values of different groups are shown in Table 1. The FTIR spectra of the synthesized copolymer having an ester band (C=O stretching vibration) at 1700.77 cm^{-1} were observed, which confirmed the reaction between PA and F127.

Preparation of glipizide loaded polymeric nanoparticles

The GNs were fabricated by the solvent evaporation method with different glipizide to copolymer ratios (glipizide:PA-F127; 1:1, 1:2, 1:3, and 2:1 w/w) and a fixed concentration of PVA. By this technique, nanoparticles are easily prepared compared to the other methods. A mixture of PA-F127 copolymer and glipizide in organic solvent forms the organic phase. Aqueous phase comprising PVA was added drop by drop to the organic phase. The organic solvents used in these nanoparticles quickly partitioned into the exterior aqueous phase and PVA precipitated around copolymer encapsulated glipizide particles. Evaporation of the entrapped organic solvents leads to the formation of glipizide loaded polymeric nanoparticles.[15]

Optimization parameters of prepared GNs

The GNs were optimized on the basis of morphological properties (in terms of particle size and surface characteristics), entrapment efficiency, and percentage yield. Particle size analysis used to characterize the nanoparticles and it helps us to understand the dispersion and aggregation.[20] With the reduction in particle size, enhancement of surface area and attractive forces between the particles generate the possibility of aggregation. To overcome such aggregation problems, the use of a surfactant in the nanoparticle preparation becomes essential. PVA can encapsulate the nanoparticles and also work as a surfactant by reducing the aggregation of nanoparticles, which keeps them suspended in solution after formation, and also re-suspension of lyophilized nanoparticles becomes easy.[15,21] The zeta potential of the particles is a significant characteristic that can demonstrate particle stability. The higher the magnitude of zeta potential, irrespective of the charge type (positive or negative), the higher stability is anticipated.[20,22]

Entrapment efficiency and percentage yield are the targets of modern nanotechnology-based drug development. Generally, those excipients are selected that can entrap the maximum amount of drug and give the best yield along with other significant parameters. Higher drug entrapment leads to a reduction in drug loss during the manufacturing process.[22,23]

The glipizide to PA-F127 copolymer ratios critically affect particle size as well as other studied parameters. The optimization data of the GNs (Table 2) exhibited that the nanoparticles produced were of submicron size ranging from 242.6 to 891.2 nm. The zeta potential and PDI values varied between 0.171 and 0.556 and between -8.03 and -21.41 mV, respectively. The ranges of entrapment efficiency and percentage yield were 35.42% to 81.13% and 23.2% to 76.4%, respectively.

Based on the morphological properties, entrapment efficiency, and percentage yield, among the five batches, 1:1 ratio (GN1) was chosen as the optimized one. The above parameters in the other four batches (GN2, 3, 4, and 5) were less valuable and hence were not selected for further studies. In batch GN5, a slight improvement in particle size, entrapment efficiency, and percentage yield was observed over batches GN2, 3, and 4. This happened due to the change in the ratio of drug to copolymer. These preparation trials were performed three times, for reproducibility and uniformity of the results. The

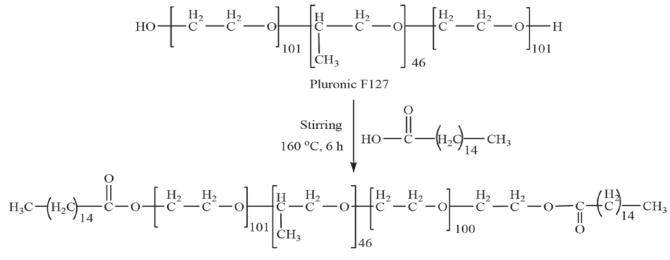

Scheme 1. Preparation of PA-F127 copolymer

Table 1. Major features of 1H NMR spectra of the PA-F127 copolymer in $CDCl_3$

δ (ppm)	Assigned
CH_2-O in PEO	3.68-3.66
CH_2CH_2-O in PEO	2.37-2.34
$CH_2CH(CH_3)$-O in PEO	1.66-1.62
$CH_2CH(CH_3)$-O in PEO	1.31-1.27
CH_2 in PA	1.17-1.14

PEO: Polyethylene oxide, PA: Palmitic acid

Table 2. Evaluation parameters of prepared GNs

Batch	Glipizide:PA-F127 (w/w)	Particle size (nm)	PDI	Zeta potential (mV)	Entrapment efficiency (%)	Yield (%)
GN1	1:1	242.60±4.20	0.171±0.0143	-21.41±0.462	81.13±3.12	76.40±2.23
GN2	1:2	630.46±4.05	0.556±0.0362	-16.33±0.153	60.41±4.41	59.31±4.22
GN3	1:3	721.30±6.77	0.328±0.0238	-10.23±0.513	50.30±3.34	49.84±3.41
GN4	1:4	891.20±7.80	0.471±0.0264	-8.03±0.737	35.42±1.94	23.20±3.45
GN5	2:1	540.24±3.51	0.391±0.0211	-11.5±0.561	70.60±2.51	66.34±4.14

n=3, mean values ± standard deviation, PDI: Polydispersity index, GN: Glipizide nanoparticles

particle size and zeta potential analysis of the optimized batch GN1 are shown in Figure 1.

FTIR analysis

The FTIR spectra provide a distinct idea about the interaction(s) between diverse functional groups existing in drugs and excipients.[24,25] The possible interactions between PA-F127, PVA, glipizide, physical mixture, and optimized GN1 were investigated by comparing the FTIR peaks (Figure 2).

The IR spectra of pure glipizide exhibited peaks at 3250.44 cm^{-1} (-NH stretching), 2941.02 cm^{-1} (C-H stretching), 1690.44 cm^{-1} (C=O stretching), 1649.88 cm^{-1} (-CONH- stretching), 1591.28 cm^{-1} (C=C aromatic stretching), 1461 cm^{-1} (C-H aromatic bending), and 1337.27 and 1160.14 cm^{-1} (O=S=O), which are also detected in the physical mixture and GN1. No significant shift in peaks were detected in the physical mixture or optimized GN1 as compared to the spectra of PA-F127, PVA, and pure glipizide. This indicates that the glipizide and excipients used were compatible and suitable for the current investigation.

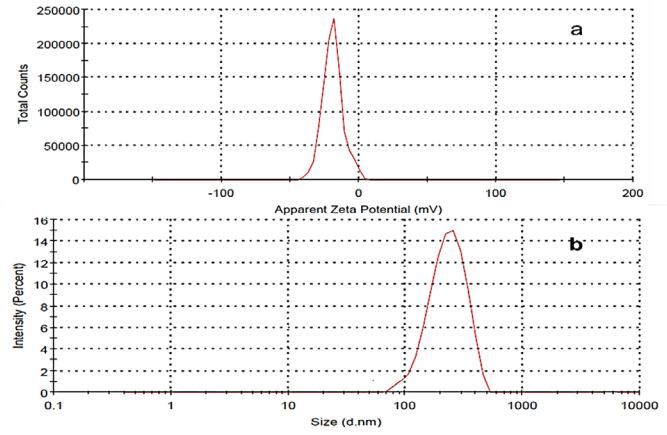

Figure 1. (a) Zeta potential and (b) particle size analysis of GN1

GN: Glipizide nanoparticles

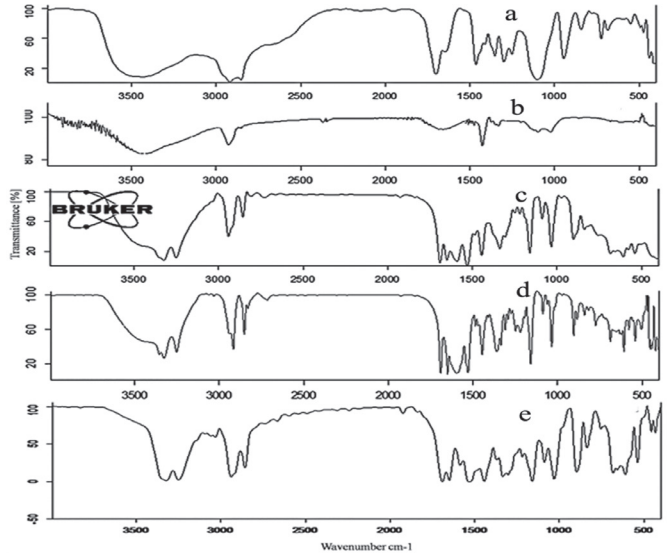

Figure 2. FTIR spectra of (a) PA-F127, (b) PVA, (c) pure glipizide, (d) physical mixture, and (e) GN1

FTIR: Fourier transform infrared spectroscopy, PVA: Polyvinyl alcohol,

GN: Glipizide nanoparticles

DSC analysis

It was found to be useful in the examination of the thermal properties of the nanoparticles, providing quantitative and qualitative information about the physicochemical state of the drug inside the nanoparticles as well as drug–polymer interactions.[26]

A characteristic sharp endothermic peak at 212.18°C was observed for pure glipizide (Figure 3c) that was absent in PA-F127 (Figure 3a) copolymer. PVA (Figure 3b) showed an endothermic peak at 215.31°C that overlapped with the glipizide peak in the physical mixture (Figure 3d) and GN1 (Figure 3e). A close look at the overlay in Figure 3 suggests that no significant shift in endothermic peaks was detected. Hence, there was no interaction between glipizide and polymeric excipients. The selection of excipients was done on the basis of the results of FTIR and DSC analysis and further studies were extended.

XRD studies

The XRD patterns of the PA-F127 copolymer (Figure 4a) and PVA (Figure 4b) showed a diffused spectrum having fewer peaks and suggested a semi-amorphous nature. The XRD patterns of glipizide showed several sharp peaks (Figure 4c) that were found to be in line with a previous report.[27] The characteristic sharp diffraction peaks due to pure glipizide and the diffused peaks of PA-F127 copolymer and PVA can be seen in the physical mixture (Figure 5d). After being formulated into nanoparticles, the XRD pattern of GN1 showed less sharp peaks (Figure 5e) with reduced intensity and had a partially amorphous nature. This decreased intensity shows the reduced crystalline properties of the drug.[28]

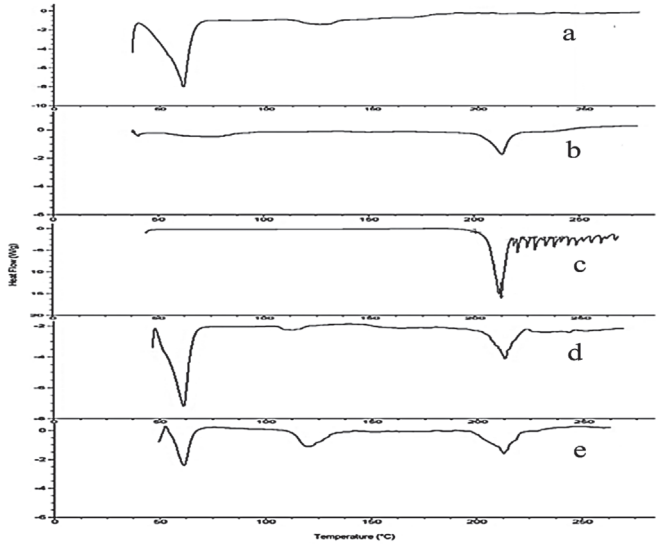

Figure 3. DSC thermograms of (a) PA-F127, (b) PVA, (c) pure glipizide, (d) physical mixture, and (e) GN1

DSC: Differential scanning calorimeter, PVA: Polyvinyl alcohol, GN: Glipizide nanoparticles

Surface morphology by SEM

Smooth surfaced rectangular crystals of glipizide in the physical mixture (Figure 5a) can be seen clearly, which were not visible in optimized GN1 (Figure 5b). The GN1 showed smooth and spherical nanoparticles, indicating that the glipizide becomes encapsulated in the polymeric matrix. This smooth surface property of nanoparticles demonstrated the complete removal of solvents from the GNs and was a sign of good quality.[29]

In vitro studies

The *in vitro* release of the glipizide from GN1 first showed burst release followed by sustained release (Figure 6). The release of glipizide from GN1 at 8 and 24 h was 34.43±4.8% and 56.11±4.64%, respectively, whereas in the same time interval 53.1±4.6 and 92.1±4.12% drug was released from pure glipizide. The initial burst release of glipizide from GN1 may have been due to the loosely associated drug on the interface of the polymeric matrix. The drug incorporated into the inner core compartment stayed firmly inside the nanoparticles, showing a sustained drug release pattern.[12]

Stability studies

Three-month stability studies were performed for GN1 at two temperatures (4 and 25˚C) and the results are shown in Table 3. The nanosuspension stored at both temperatures carried nanosized particles (<250 nm), whereas a slight increase in PDI and a reduction in zeta potential and entrapment efficiency were observed. During the storage time, no visual color change was noted. The reduction in entrapment efficiency and increase in particle size might be attributed to the semi-amorphous character of the amphiphilic PA-F127 copolymer in GN1. When the lipophilic part of a copolymer is exposed to kinetic energy (temperature or light), the semi-amorphous state changes into the more stable amorphous state, which leads to an increase in particle size and expulsion of drug from the polymeric matrix with the reduction in entrapment efficiency.[30] The results of the stability studies were statistically nonsignificant. The nanoparticles stored at 5±3˚C showed nonsignificant variation in the studied parameters, which indicates that the above temperature was the optimum storage temperature.

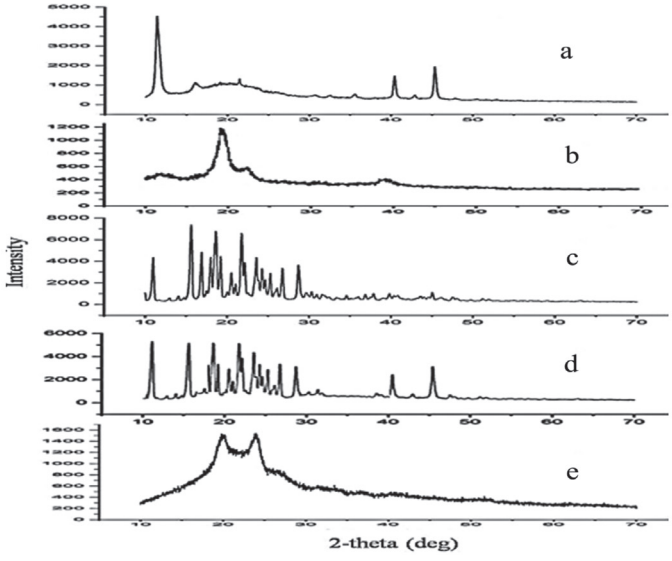

Figure 4. XRD patterns of (a) PA-F127, (b) PVA, (c) pure glipizide, (d) physical mixture, and (e) GN1

PVA: Polyvinyl alcohol, GN: Glipizide nanoporticles

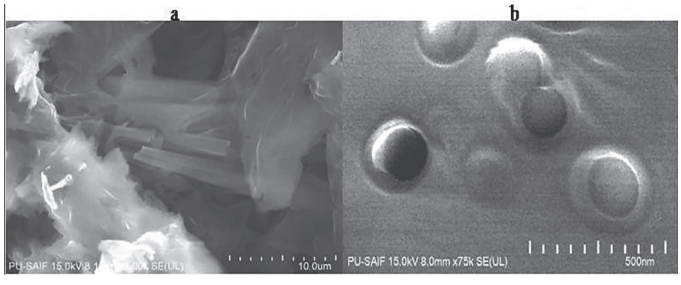

Figure 5. SEM images of (a) physical mixture (drug + excipients), (b) GN1

SEM: Scanning electron microscopy, GN: Glipizide nanoporticles

Pharmacokinetic studies

The mean plasma concentrations of glipizide vs. time profile adopting a single oral dose of GN1 (1.5 mg/kg) and glipizide suspension (1.5 mg/kg) in six rats is presented in Table 4 and Figure 7. The value of peak plasma concentration (C_{max}) of GN1 was 2.35-fold higher than that of the glipizide suspension ($p<0.05$). The time required to reach the maximum plasma concentration (t_{max}) after oral administration of GN1 and glipizide suspension was 6.0 and 4.0, respectively. The elimination half-life ($t_{1/2}$) of GN1 was 1.5-fold ameliorated than the glipizide suspension ($p<0.05$). The area under the curve ($AUC_{0\rightarrow\infty}$) of

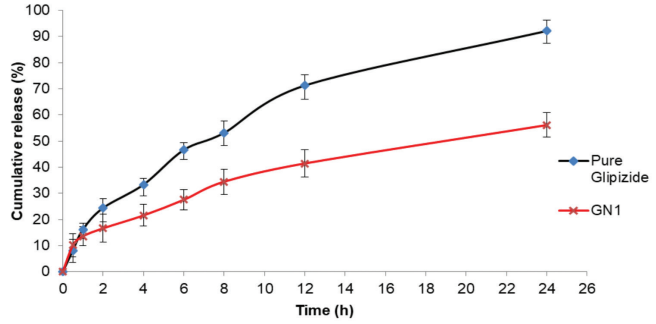

Figure 6. *In vitro* release profiles of GN1 and pure glipizide

GN: Glipizide nanoporticles

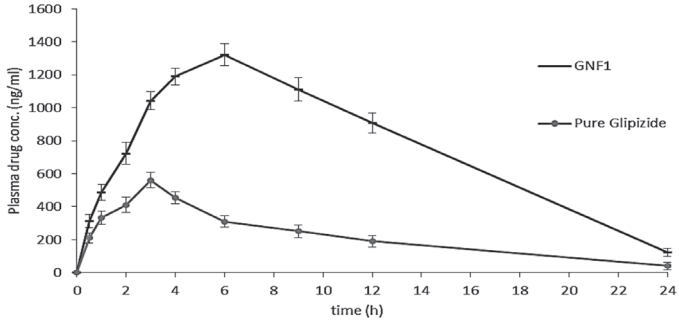

Figure 7. Mean plasma concentrations of glipizide vs time graph after single oral administration of GN1

GN: Glipizide nanoporticles

Table 3. Stability studies of GN1

Storage condition	Particle size (nm)	PDI	Zeta potential (mV)	Entrapment efficiency (%)	Visual observation
Fresh GN1	242.6±4.20	0.171±0.01	-21.41±0.462	81.13±3.1	Clear suspension
1 month (5±3˚C)	244.2±4.04	0.171±0.02	-21.20±0.472	80.43±2.5	Clear suspension
3 month (5±3˚C)	246.0±3.42	0.184±0.03	-21.01±0.522	79.25±4.5	Clear suspension
1 month (25˚C)	246.3±4.70	0.182±0.02	-20.84±0.341	78.64±4.2	Clear suspension
3 month (25˚C)	249.5±5.43	0.196±0.03	-20.35±0.52	77.25±3.5	Clear suspension

n=3, mean values ± standard deviation, PDI: Polydispersity index, GN: Glipizide nanoporticles

Table 4. Pharmacokinetic parameters of GN1 and pure glipizide suspension

Sample	C_{max} (ng/mL)	t_{max} (h)	$t_{1/2}$ (h)	$AUC_{0\rightarrow\infty}$ (ng.h/mL)	MRT (h)
GN1	1321±110	6.0	10.51±0.2	18574±96	11.06±0.4
Glipizide suspension	561±86	4.0	7.04±0.1	5688±102	9.25±0.3

mean ± standard deviation, n=6, AUC: *Area under the curve,* MRT: Mean residence time GN: Glipizide nanoporticles

GN1 was 3.3-fold higher compared to the glipizide suspension ($p<0.05$). Finally, an improvement (1.2-fold) in the mean residence time of GN1 over pure glipizide suspension ($p<0.05$) was recorded. Overall, the oral bioavailability and circulation time of GN1 were improved significantly.

CONCLUSIONS

In the present investigation, GNs were prepared using the newly synthesized PA-F127 copolymer. The drug and excipients were compatible with each other. The optimized nanoparticles batch (GN1) can be best stored at 5±3˚C without losing its properties. The ameliorated pharmacokinetic parameters of GN1 confirmed the improved bioavailability and circulation time. The therapeutic plasma concentration of drug with a single oral dose of GN1 was maintained up to 24 h and the problem of frequent oral dose administration (2 or 3 times a day) with the conventional dosage form can be overcome by the use of GN1. The reported PA-F127 pentablock copolymer could be a suitable carrier for nanotechnology-based oral glipizide.

ACKNOWLEDGEMENTS

The authors are grateful to the University Grant Commission (UGC), New Delhi, for providing a fellowship under Major Research Project (MRP) Reference No: FN/42/703/2013/SR. The authors are also grateful to the Secretary-cum-Scientific Director, Indian Pharmacopoeia Commission, Ghaziabad, for providing chromatographic facilities at the ARD Lab.

Conflict of Interest: No conflict of interest was declared by the authors.

REFERENCES

1. Lahoti SR, Puranik PK, Heda AA, Navale RB. Development and validation of RP-HPLC method for analysis of glipizide in guinea pig plasma and its application to pharmacokinetic study. Int J PharmTech Res. 2010;2:1649-1654.
2. Dash RN, Mohammed H, Humaira T, Ramesh D. Design, optimization and evaluation of glipizide solid self-nanoemulsifying drug delivery for enhanced solubility and dissolution. Saudi Pharm J. 2015;23:528-540.
3. Emami J, Boushehri MSS, Varshosaz J. Preparation, characterization and optimization of glipizide controlled-release nanoparticles. Res Pharm Sci. 2014;9:301-314.
4. Ammar HO, Salama HA, Ghorab M, El-Nahhas SA, Elmotasem H. A transdermal delivery system for glipizide. Curr Drug Deliv. 2006;3:333-341.
5. Patel JK, Patel RP, Amin AF, Patel MM. Formulation and evaluation of mucoadhesive glipizide microspheres. AAPS PharmSciTech. 2005;6:49-55.
6. Naha P, Byrne HJ, Panda AK. Role of polymeric excipients on controlled release profile of glipizide from PLGA and Eudragit RS 100 nanoparticles. J Nanopharm Drug Deliv. 2013;1:74-81.
7. Huang H, Wu Z, Qi X, Zhang H, Chen Q, Xing J, Chen H, Rui Y. Compression-coated tablets of glipizide using hydroxypropylcellulose for zero-order release: *In vitro* and *in vivo* evaluation. Int J Pharm. 2013;446:211-218.
8. Nie S, Zhang S, Pan W, Liu Y. *In vitro* and *in vivo* studies on the complexes of glipizide with water-soluble beta-cyclodextrin-epichlorohydrin polymers. Drug Dev Ind Pharm. 2011;37:606-612.
9. Kulkarni N, Wakte P, Naik J. Development of floating chitosanxanthan beads for oral controlled release of glipizide. Int J Pharm Investig. 2015;5:73-80.
10. Mahesh KV, Singh SK, Gulati M. A comparative study of top-down and bottom-up approaches for the preparation of nanosuspensions of glipizide. Powder Technol. 2014;256:436-449.
11. Soppimath KS, Aminabhavi TM, Kulkarni AR, Rudzinski WE. Biodegradable polymeric nanoparticles as drug delivery devices. J Control Release. 2001;70:1-20.
12. Gao Q, Liang Q, Yu F, Xu J, Zhao Q, Sun B. Synthesis and characterization of novel amphiphilic copolymer stearic acid-coupled F127 nanoparticles for nano-technology based drug delivery system. Colloids Surf B Biointerfaces. 2011;88:741-748.
13. Kamboj VK, Verma PK. Poloxamers based nanocarriers for drug delivery system. Der Pharm Lett. 2015;7:264-269.
14. Xiong XY, Li YP, Li ZL, Zhou CL, Tam KC, Liu ZY, Xie GX. Vesicles from Pluronic/poly(lactic acid) block copolymers as new carriers for oral

insulin delivery. J Control Release. 2007;120:11-17.

15. Dhanalekshmi UM, Poovi G, Kishore N, Reddy PN. *In vitro* characterization and *in vivo* toxicity study of repaglinide loaded poly (methyl methacrylate) nanoparticles. Int J Pharm. 2010;396:194-203.
16. Patil P, Bhoskar M. Optimization and evaluation of spray dried chitosan nanoparticles containing doxorubicin. Int J Curr Pharma Res. 2014;6:7-15.
17. Lokhande A, Mishra S, Kulkarni R, Naik J. Formulation and evaluation of glipizide loaded nanoparticles. Int J Pharm Pharm Sci. 2013;5:147-151.
18. Rani R, Dahiya S, Dhingra D, Dilbaghi N, Kim KH, Kumar S. Evaluation of antidiabetic activity of glycyrrhizin-loaded nanoparticles in nicotinamide-streptozotocin induced diabetic rats. Eur J Pharm Sci. 2017;106:220-230.
19. Mutalik S, Udupa N, Kumar S, Agarwal S, Subramanian G, Ranjith AK. Glipizide matrix transdermal systems for diabetes mellitus: Preparation, *in vitro* and preclinical studies. Life Sci. 2006;79:1568-1577.
20. Duarah S, Pujari K, Ghosh J, Unnikrishnan D. Formulation and evaluation of metformin engineered polymeric nanoparticles for biomedical purpose. Res J Pharm Biol Chem Sci. 2015;6:1005-1019.
21. Birnbaum DT, Kosmala JD, Brannon-Peppas L. Optimization of preparation techniques for poly(lactic acid-co-glycolic acid) nanoparticles. J Nanopart Res. 2002;1:173-181.
22. Jain S, Saraf S. Influence of processing variables and *in vitro* characterization of glipizide loaded biodegradable nanoparticles. Diabetes Metab Syndr Clin Res Rev. 2009;3:113-117.
23. Kusum VD, Bhosale UV. Formulation and optimization of polymeric nano drug delivery system of acyclovir using 32 full factorial design. Int J PharmTech Res. 2009;1:644-653.
24. Mukherjee B, Mahapatra S, Gupta R, Patra B, Tiwari A, Arora P. A comparison between povidone-ethylcellulose and povidone-eudragit transdermal dexamethasone matrix patches based on *in vitro* skin permeation. Eur J Pharm Biopharm. 2005;59:475-483.
25. Mukherjee B, Santra K, Pattnaik G, Ghosh S. Preparation, characterization and *in vitro* evaluation of sustained release protein-loaded nanoparticles based on biodegradable polymers. Int J Nanomed. 2008;3:487-496.
26. Ramazani A, Keramati M, Malvandi H, Danafar H, Kheiri Manjili H. Preparation and *in vivo* evaluation of anti-plasmodial properties of artemisinin-loaded PCL-PEG-PCL nanoparticles. Pharm Dev Technol. 2018;23:911-920.
27. Dash RN, Mohammed H, Humaira T, Reddy AV. Solid supersaturatable self-nanoemulsifying drug delivery systems for improved dissolution, absorption and pharmacodynamic effects of glipizide. J Drug Deliv Sci Technol. 2015;28:28-36.
28. Mokale V, Rajput R, Patil J, Yadava S, Naik J. Formulation of metformin hydrochloride nanoparticles by using spray drying technique and *in vitro* evaluation of sustained release with 32-level factorial design approach. Dry Technol. 2016;34:1455-1461.
29. Lekshmi UM, Kishore N, Reddy PN. Subacute toxicity assessment of glipizide engineered polymeric nanoparticles. J Biomed Nanotechnol. 2011;7:578-589.
30. Elbahwy IA, Ibrahim HM, Ismael HR, Kasem AA. Enhancing bioavailability and controlling the release of glibenclamide from optimized solid lipid nanoparticles. J Drug Deliv Sci Technol. 2017;38:78-89.

Turk J Pharm Sci 2019;16(3):273-281
DOI: 10.4274/tjps.galenos.2018.27146

ORIGINAL ARTICLE

The Anticancer and Anti-inflammatory Effects of *Centaurea solstitialis* Extract on Human Cancer Cell Lines

İnsan Kanser Hücre Hatları Üzerinde *Centaurea solstitialis* Özütünün Anti-Kanser ve Anti-İnflamatuar Etkileri

Mehlika ALPER[1], Hatice GÜNEŞ[2]*

[1]Muğla Sıtkı Koçman University, Department of Molecular Biology and Genetics, Muğla, Turkey
[2]Muğla Sıtkı Koçman University, Department of Biology, Division of Molecular Biology and Biotechnology, Muğla, Turkey

ABSTRACT

Objectives: Natural products originating from plants have been used for many years in the treatment of various diseases, including cancer. *Centaurea solstitialis* subsp. *solstitialis* is used in Turkish folk medicine. This study was the first to determine the *in vitro* biological effects of ethanolic extract from the flowering parts of *C. solstitialis* L. subsp. *solstitialis* collected from Muğla Province.

Materials and Methods: The cytotoxic effect was evaluated against Daudi, A549, and HeLa cancer cells and one normal BEAS-2B cell line using the MTT (3-(4,5-dimethylthiazol-2-yl)-2,5- dipenyltetrazolium bromide) assay. Flow cytometric analysis and the caspase-3 activity assay were performed to detect apoptotic cell death. Angiogenic factor [vascular endothelial growth factor (VEGF)] secretion and the release of interleukin (IL)-1α, IL-6, and tumor necrosis factor (TNF)-α by cells treated with the extract were measured using enzyme-linked immunosorbent assay.

Results: The extract exhibited cytotoxic effects against all the cancer cell lines used but HeLa and Daudi were the most sensitive cells, with IC_{50} values of 63.18 µg/mL and 69.27 µg/mL, respectively. Selective cytotoxicity was observed between the HeLa and normal BEAS-2B cell lines. The extract arrested the cell cycle at the S and G2 phases. In addition, apoptotic cell death was detected in HeLa and A549 cells. Moreover, the plant extract caused a significant decrease in VEGF secretion in A549 cells and a fluctuation in IL-1α, IL-6, and TNF-α secretion in A549 and Daudi cells.

Conclusion: These observations suggest that the flowering parts of *C. solstitialis* may be a potential source in the development of natural drugs for the treatment of cancer and modulation of cytokine secretion.

Key words: *Centaurea solstitialis*, cancer cell lines, anti-cancer, anti-inflammatory

ÖZ

Amaç: Bitkilerden elde edilen doğal ürünler, kanser dahil çeşitli hastalıkların tedavisinde uzun yıllardır kullanılmaktadır. *Centaurea solstitialis* subsp. *solstitialis*'in Türk geleneksel tıbbında yeri olduğu bilinmektedir. Bu araştırma, Muğla ilinden toplanan *C. solstitialis*'in çiçekli kısımlarından elde edilen etanolik özütün *in vitro* biyolojik etkilerini belirleyen ilk çalışmadır.

Gereç ve Yöntemler: Özütün Daudi, A549 ve HeLa kanser hücrelerine ve normal BEAS-2B hücre hattına karşı sitotoksik etkisi MTT (3-(4,5-dimetiltiyazol-2-il)-2,5-dipeniltetrazolyum bromür) testi ile belirlendi. Apoptotik hücre ölümü akış sitometri analizi ve kaspaz-3 aktivite deneyleriyle araştırıldı. Özüt ile muamele edilen hücreler tarafından üretilen anjiyojenik faktör [vasküler endotel büyüme faktörü (VEGF)] salınımı ve sitokinlerden interlökin (IL)-lα, IL-6 ve tümör nekroz faktör (TNF)-α'nın salınımı enzim bağlı immünosorbent deneyi testleriyle ölçüldü.

Bulgular: Bitki özütü kullanılan tüm kanser hücre hatlarına karşı sitotoksik etki gösterirken, özüte karşı en duyarlı hücrelerin 63.18 µg/mL and 69.27 µg/mL olan IC_{50} değerleri ile sırasıyla HeLa ve Daudi hücreleri olduğu gözlendi. Seçici sitotoksisite HeLa ve normal BEAS-2B hücre hatları arasında tespit edildi. Bitki özütü S ve G2 fazlarında hücre döngüsü arrestine yol açtı. Buna ilave olarak, HeLa ve A549 hücrelerinde apoptotik hücre ölümü kaydedildi. Ayrıca bitki özütü A549 hücrelerinin VEGF salgılamasında anlamlı bir düşüşe yol açarken, A549 ile Daudi hücrelerinin IL-lα, IL-6 ve TNF-α salgılamasında önemli değişime neden oldu.

Sonuç: Bu bulgular kanser tedavisi ve sitokin salgısının modülasyonunda gerekli olan doğal ilaçların geliştirilmesi için *C. solstitialis*'in çiçekli kısımlarının potansiyel bir kaynak olabileceğini göstermektedir.

Anahtar kelimeler: *Centaurea solstitialis*, kanser hücre hatları, anti-kanser, anti-inflamatuar

Part of this study was presented at the "5th International Molecular Biology and Biotechnology Congress, Tetova" on August 25-29, 2016, and published as an abstract in the abstract book pp 60.

*Correspondence: E-mail: haticegunes@mu.edu.tr, Phone: +90 534 282 11 33 ORCID-ID: orcid.org/0000-0001-5191-365X
Received: 04.05.2018, Accepted: 24.05.2018

INTRODUCTION

Cancer is one of the most common diseases in both developed and developing countries. Plant products have been used throughout history to treat and prevent diseases because of their large number of different phytochemicals with different biological activities.[1] In fact, the compounds derived from plants play an important role in the development of anticancer agents to be used in clinical practice.[2] Since substantial evidence has proved that plant secondary metabolites are a potential source of anticancer compounds and cancer cells may develop resistance to existing drugs, today extensive research is being carried out all over the world to discover new plant species with anticancer properties.

Cancer is a multistage disease. Angiogenesis, defined as the formation of new blood vessels, is an essential process in tumor development and prevention of tumor vasculation is a crucial strategy in cancer treatment.[3,4] Even though there are a variety of angiogenic factors, vascular endothelial growth factor (VEGF) is a key regulator of angiogenesis. Increased VEGF secretion promotes invasion and metastasis and so targeting of VEGF is pivotal in the prevention of tumor metastasis. Therefore, the discovery of a new plant extract with anti-angiogenic activity is necessary to serve as an alternative to toxic chemotherapeutics.

Inflammation is a common cause of many diseases and alone it is not sufficient to cause cancer, but epigenetic events and mutations caused by environmental exposure or immune modulation contribute significantly to the cancer process.[5] In addition, the cytokine release-mediated inflammatory mechanisms were reported to facilitate cancer metastasis.[6] Various plants or their bioactive compounds can inhibit or stimulate different enzymes associated with inflammatory and immune response regulating pathways.[7] Because anti-inflammatory drugs may be effective in cancer therapy or prevention,[8] it is important to evaluate the anti-inflammatory potential of plant extracts as well.

The genus *Centaurea* L., belonging to the family *Asteraceae*, is the third largest genus in Turkey.[9] Some *Centaurea* species are used as remedies against various diseases in Turkish folk medicine.[10] *Centaurea solstitialis* is known in Turkish as "gelin dikeni" and it has been used to treat hemorrhoids, peptic ulcers, common colds,[11,12] malaria,[13] and herpes infections around the lips of children.[14] Previous studies examined the pharmacological and biological properties of *Centaurea* species and some *Centaurea* species exhibited cytotoxic effects against some cancer cell lines.[15] The major constituents of *Centaurea* species were reported to be sesquiterpene lactones, flavonoids, and fatty acids.[16,17] Nevertheless, to the best of our knowledge, there were no adequate reports about the anticancer or anti-inflammatory effects of *C. solstitialis*. Therefore, the present study has scientific importance for the anticancer and anti-inflammatory potential of ethanolic extract from the flowering parts of *C. solstitialis* collected from Muğla.

MATERIALS AND METHODS

Plant material

The plant *C. solstitialis* was collected during the flowering period from June to July 2015 from Muğla, in the southwest of Turkey. The plant species was identified in the Herbarium Laboratory, Department of Biology, Muğla Sıtkı Koçman University.

Plant extraction

The flowering parts of *C. solstitialis* were washed with distilled water and air-dried under shade for about 15 days. Air-dried flowers were ground into powder in a porcelain mill. The powder (10 g) was soaked in absolute ethanol (96°, Merck, USA) and placed in a Soxhlet apparatus for 10 h to obtain ethanolic extract. After filtration of the extract using Whatman filter paper no. 1, the ethanol was removed using a rotary evaporator (IKA, RV 10, USA). The solvent was evaporated by keeping the extracts at 37°C for 7 days. The powdered crude extract was stored at 4°C in an air-tight container until used. The extract was dissolved in 10% dimethyl sulfoxide (DMSO) as stock solution and further diluted to obtain working solutions. DMSO in the final concentrations of the extract was less than 1% and showed no effect on the examined parameters.

Cell lines and culture conditions

Daudi (Burkitt's lymphoma, CCL-213), A549 (lung carcinoma), HeLa (cervix adenocarcinoma), and BEAS-2B (normal bronchial epithelium) cell lines were originally obtained from ATCC. The cells were maintained in RPMI 1640 medium premixed with stable L-glutamine (Biochrom, Germany) and supplemented with 10% heat inactivated fetal bovine serum (Biochrom, Germany), penicillin (100 U/mL), and streptomycin sulfate (100 mg/mL) (Biochrom, Germany). All cell lines were incubated in a humidified atmosphere of 5% CO_2 and 95% air at 37°C.

In vitro cytotoxicity assay

The cytotoxic effects of ethanolic extracts from the flowering parts of *C. solstitialis* on Daudi, A549, HeLa, and Beas-2B were determined by MTT (3-(4,5-dimethylthiazol-2-yl)-2,5-dipenyltetrazolium bromide) assay. In this assay, the reduction of yellow soluble MTT to insoluble blue formazan crystals by mitochondrial dehydrogenase reflects cell viability.[18] A total of 4×10^3 cells/well were seeded in 96-well plates (Greiner, Germany) in triplicate and incubated for 24 h. Plant extracts were added to the wells at 7 different final concentrations between 1000 µg/mL and 15.625 µg/mL followed by incubation for 72 h. Then 10 µL of 5 mg/mL MTT reagent (Applichem, USA) in phosphate-buffered saline (PBS) was added to each well. After 4 h of incubation, the medium was gently discarded and 100 µL of pure DMSO was added to each well to dissolve the formazan blue crystals formed in the cells. The absorbance of reduced MTT in each well was measured at 540 nm using a microplate reader (Thermo Scientific, Multiskan FC, USA). The cytotoxic effects of the extracts were determined by comparing the optical density of treated cells against that of untreated cells.

Cell cycle analysis

Cells at 5×10^5/well were seeded in 6-well plates and treated with plant extracts at 500 µg/mL and 200 µg/mL for 24 h. After treatment, the cells were washed with ice-cold PBS, fixed in 4 mL of absolute ethanol, and stored at -20˚C for 48 h. After that, the cells were centrifuged at 1200 rpm for 10 min at 4˚C and the cell pellets were washed in ice-cold PBS. The cells were resuspended in 1 mL of PBS containing 0.1% (v/v) Triton X-100 (Amresco, USA) and then 100 µL of RNase A (200 µg/mL) (Applichem, USA) was added to each of the cell suspensions. After incubation for 30 min at 37˚C, 100 µL of propidium iodide (PI) (1 mg/mL in ddH_20) was added to each cell suspension and the cells were incubated in the dark for 15 min at room temperature. The cells were analyzed by BD FACSCanto flow cytometer using ModFit LT 3.0 software for cell cycle phases.

Apoptosis assay

Exponentially growing A549 and HeLa cells were cultured at 5×10^5 cells/well in 6-well plates (Greiner, Germany) and incubated for 24 h. The cells were treated with plant extract at final concentrations of 200 µg/mL and 500 µg/mL for 24 h. Annexin V-FITC/PI staining was carried out using the Annexin V-FITC Apoptosis Detection Kit (eBioscience, USA) protocol. Briefly, treated cells were washed with PBS, trypsinized, washed, and resuspended in binding buffer. Then 5 µL of Annexin V-FITC and 10 µL of PI at 20 µg/mL were added to each cell suspension and the cells were incubated for 15 min in the dark. After 500 µL of binding buffer was added, 10,000 cells per group were analyzed by flow cytometry (BD FACSCanto A, BD Biosciences) using BD FACSDiva software v6.13.

Caspase-3 activity assay

Caspase-3 activity of the cell lysates was determined by colorimetric assay kits (Abcam, Cambridge, UK). A549 and HeLa cells were plated at 2×10^6 cells/well in 6-well plates and incubated for 24 h. Then the cells were treated with plant extract at 500 µg/mL for 36 h. After centrifugation, the cells were resuspended in 50 µL of cell lysis buffer and incubated on ice for 10 min. The cell lysates were centrifuged at 10.000 × g for 1 min and the protein concentration of each cell lysate was determined by Bradford assay (1976).[19] Later, 200 µg of protein from each sample was mixed with 50 µL of 2X reaction buffer containing 10 mM DTT and 5 µL of the caspase-3 substrate (4 mM DEVD-*p*-NA), followed by incubation at 37˚C for 2 h. Absorbance of p-NA light emission was read at 405 nm in a microplate reader. Fold increase in caspase-3 activity was determined by comparing the absorbance of p-NA from an apoptotic sample with that of untreated control cells.

Quantitative detection of human VEGF by enzyme-linked immunosorbent assay

To determine the effect of plant extract on VEGF secretion, A549 cells were cultured at a density of 2×10^5 cells/well in a 6-well plate and incubated for 1 h. Then the cells were treated with plant extract at 200 µg/mL and incubated for 6 h. The supernatants were collected after centrifugation and stored at -20˚C until analysis. The untreated cells served as the control. The concentrations of VEGF in the cell culture supernatants were detected by ELISA as described in the manufacturer's procedure (VEGF ELISA kit; Boster Biological Technology, USA). The absorbance of each well was measured using a microplate reader at 450 nm within 30 min. The VEGF concentrations of the cell culture supernatants were interpolated from the standard curve.

Quantitative detection of human interleukin-1α, interleukin-6, and tumor necrosis factor-α by ELISA

In order to examine the effects of plant extract on inflammation, 2×10^5 cells/well of A549 or Daudi cells were plated in triplicate in 6-well plates. The cells were treated with 200 µg/mL *C. solstitialis* extract for 6 h or left untreated to serve as the control. The supernatants were collected and 100 µL of each supernatant was tested for inflammatory cytokine production by ELISA based on the manufacturer's instructions using commercial human ELISA kits for interleukin (IL)-1α, IL-6, and tumor necrosis factor (TNF)-α (Boster Biological Technology, USA). The amount of each cytokine in the supernatants was calculated from the formula of the calibration curve of standard cytokine.

Statistical analysis

The data were analyzed using GraphPad Prism 7.0 (GraphPad Software, Inc., San Diego, CA, USA). Comparisons of treatments among the groups were performed using one-way or two-way ANOVA and post-hoc analysis. Significance was presented as ***($p<0.01$) and ****($p<0.0001$). The data are the mean ± standard deviation of three replicates.

RESULTS

Cytotoxic activity of plant extract on different cancer cell lines

The cytotoxicity of the crude ethanolic extract from the flowering parts of *C. solstitialis* at seven different concentrations was investigated on the A549, Daudi, HeLa, and Beas-2B cell lines to determine the IC_{50} value (µg/mL) that causes 50% cell death. The results demonstrated that the percentage of viable cells changed according to the cell lines used (Figure 1). The viability of all the cancer cells was significantly reduced by the extract in a concentration-dependent manner. However, the extract at concentrations of 15.6 and 31.2 µg/mL did not exert significant cytotoxicity on the normal BEAS-2B cell line, indicating the selectivity of the extract against cancer cells (Figure 1d). The highest cytotoxicity, with an IC_{50} value of 63.18 µg/mL, was observed against HeLa cells (Figure 1c), whereas the IC_{50} values of A549 and Daudi cells were 252.5 µg/mL and 69.27 µg/mL, respectively (Figure 1a and 1b). On the other hand, the extract exhibited a lower cytotoxic effect on normal BEAS-2B cells, with an IC_{50} value of 75.25 µg/mL, when compared with the effects on the HeLa and Daudi cancer cell lines (Figure 1). In other words, in terms of cytotoxicity, HeLa and Daudi cells were the most sensitive cell lines against the extract.

The effect of plant extract on cell cycle distribution

Since the plant extract at 250 µg/mL was cytotoxic against all the cell lines tested, the rest of the analyses for different

parameters were performed with the extract at 200 µg/mL and 500 µg/mL. The changes in cell-cycle progression of the HeLa and A549 cancer cells after treatment with plant extracts at 200 µg/mL and 500 µg/mL for 24 h were analyzed using flow cytometry with PI staining. Plant extract at 200 µg/mL showed virtually no effect in the cell cycle phases of HeLa cells (Figure 2A; a, b, d). At 500 µg/mL, there was a slight increase in the percentage of HeLa cells in the G2 phase and it was accompanied by a decrease in the percentage of cells in the G1 phase from 48.97% to 41.57% (Figure 2A; a, c, d). In addition, treatment of A549 cells with plant extracts at 200 and 500 µg/mL for 24 h resulted in 7.1% and 12.5% increases in cells in the S phase, respectively, and it caused a concomitant decrease in the percentage of cells in the G1 phase (Figure 2B; a-d). Furthermore, the percentage of G2 phase cells increased from 4.8% to 15.6% and 9.6% in A549 cells treated with the extract

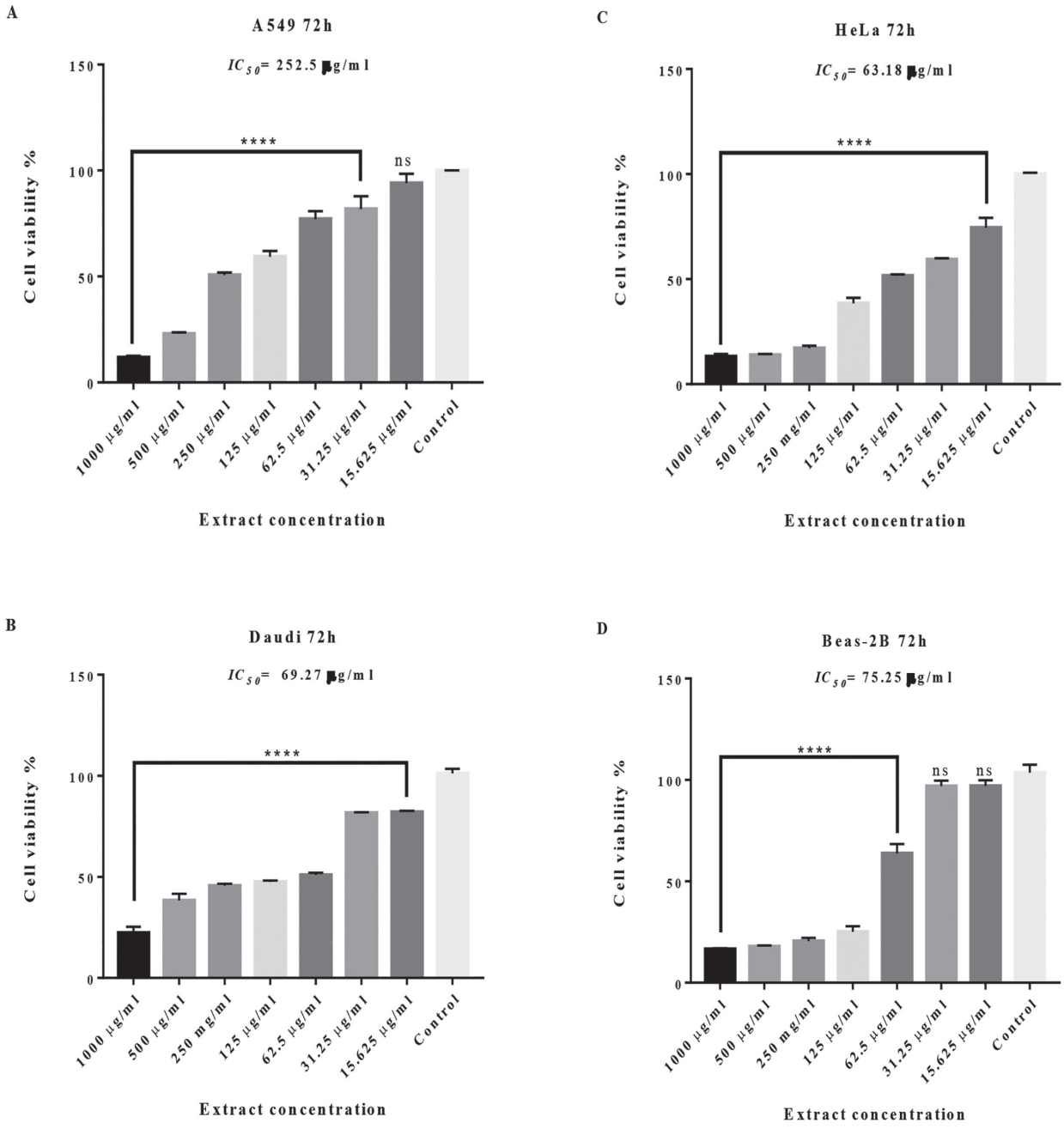

Figure 1. Cytotoxic activity of plant extract against different cancer cell lines. Human cancer cells A549 (A), Daudi (B), HeLa (C), and Beas-2B (D) were treated with ethanolic extract from the flowering parts of *Centaurea solstitialis* for 72 h. Cell viability was determined based on the MTT assay. Data are the means (±standard deviation) of three independent experiments

****: p<0.0001 compared with untreated cells

at 200 and 500 µg/mL, respectively. These results suggest that the plant extract might inhibit cell proliferation by arresting both cells especially in the G2 phase.

Apoptotic effect of plant extract

As cell cycle regulation and apoptosis are closely related, disruption of cell cycle progression may result in apoptotic/necrotic death.[20] Therefore, it was investigated whether or not apoptosis was initiated in cells treated with plant extracts for 24 h. As shown in Figure 3A, the percent of apoptotic HeLa cells (quadrants 2 and 4) increased from 1% to 9.3% and 11.8% after treatment with the extract at 200 and 500 µg/mL, respectively (Figure 3A; a-d). In addition, the percentage of apoptotic A549 cells (quadrants 2 and 4) increased from 3.7% to 4.5% and 31.8% after treatment with 200 and 500 µg/mL extract, respectively (Figure 3B; a-d). These findings demonstrate that the plant extract at 500 µg/mL induces apoptosis in both cell lines, especially in A549. These data were consistent with the results obtained from the cell cycle analysis.

Caspase 3 activation

Caspases play an important role in mediating various apoptotic signaling pathways. In the present study, we analyzed the activity of caspase 3 in A549 and HeLa cells treated with the extract at 500 µg/mL for 36 h. As shown in Figure 4, the extract increased caspase-3 activity about 1.65- and 1.5-fold compared to the control in HeLa and A549 cells, respectively. These results indicate that the plant extract induces apoptosis in both of these cell lines.

VEGF secretion of A549 cells

VEGF is a potent cytokine produced by many cell types including most cancer cells and it has critical roles in physiological and pathological angiogenesis.[21] Because VEGF protein expression was determined in the airway epithelial cancer cell line A549 by Koyama et al.,[22] VEGF secretion of A549 cells was investigated after treatment with the extract at 200 µg/mL by human VEGF ELISA assay. The plant extract caused a 2.5-fold decrease in VEGF secretion of A549 cells compared to untreated control

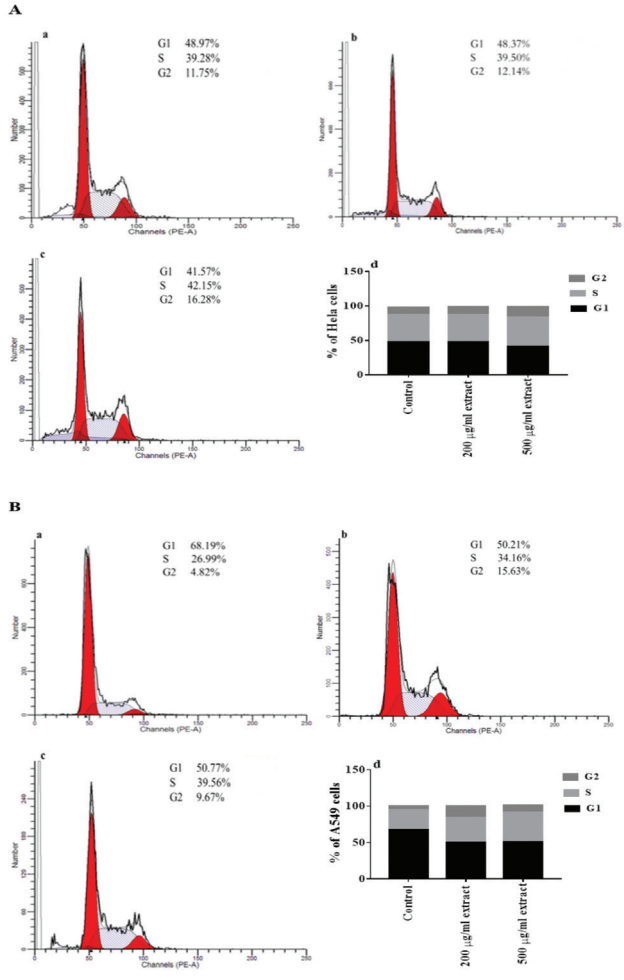

Figure 2. Effect of plant extract on cell cycle distribution of cancer cells. Histograms present a cell cycle distribution of HeLa (A) and A549 (B) cells after treatment with no extract (a), 200 µg/mL (b), and 500 µg/mL (c) extract for 24 h. The percentages of cells at different cell cycle phases are shown (d)

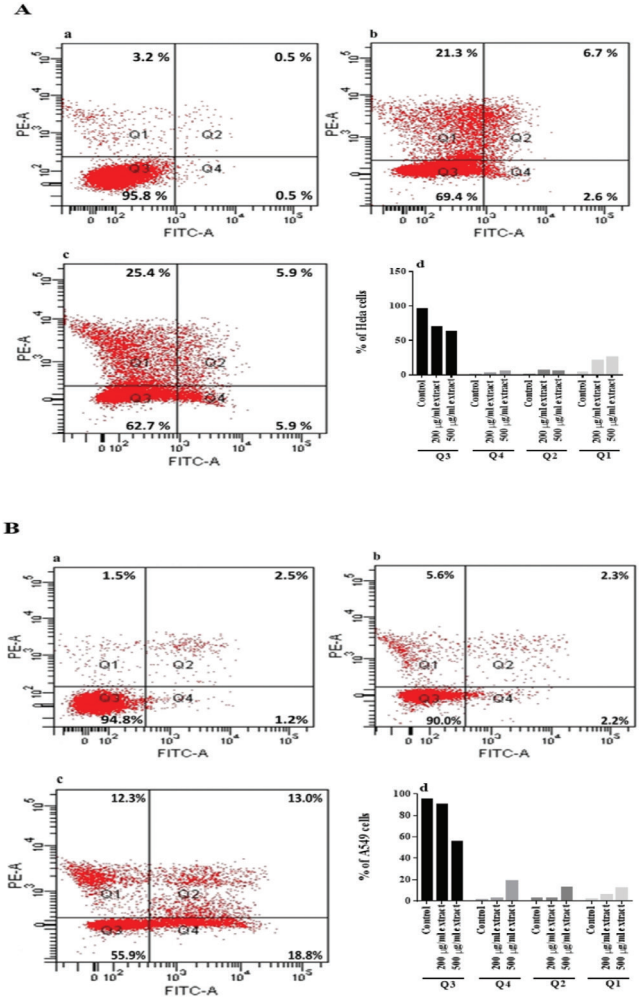

Figure 3. Plant extract induces apoptosis in cancer cells. HeLa (A) and A549 (B) cells were treated with no extract (a), 200 µg/mL (b), and 500 µg/mL extract (c) for 24 h. Cells were distributed into four quadrants: viable cells (Q3), early apoptotic cells (Q4), late apoptotic cells (Q2), and necrotic cells (Q1). The percentage of apoptotic cells (d)

cells (Figure 5), indicating the antiangiogenic function of the extract.

Effect of plant extract on IL-1α, IL-6, and TNF-α secretion

It is known that different cytokines and growth factors may contribute to cancer progression.[23] In the present study, the IL-1α, IL-6, and TNF-α concentrations in A549 and Daudi cell culture supernatants after treatment with plant extract at 200 µg/mL were determined. The effect of plant extract on cytokine secretion varied according to the cell lines used. The highest level of inhibition on the release of cytokines was observed in A549 for IL-6 and Daudi for IL-1α compared to untreated control cells (Figure 6). In contrast, there was a slight increase in the release of IL-1α and TNF-α in A549 cells and IL-6 in Daudi cells.

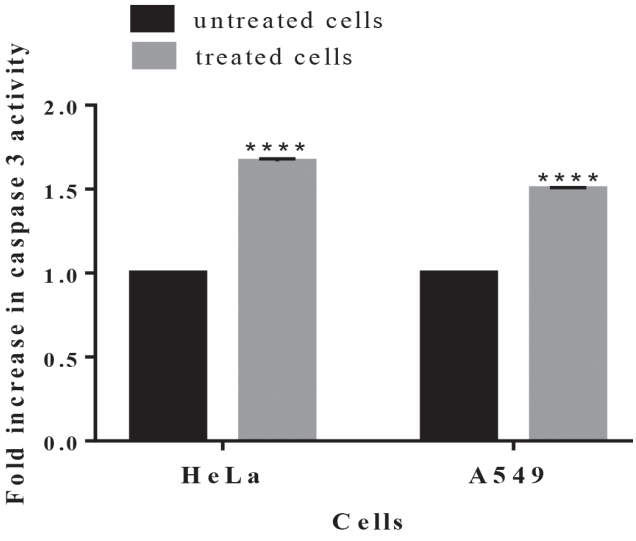

Figure 4. Caspase 3 activity in HeLa and A549 cells after treatment with the plant extract. Cells were treated without or with the extract at 500 µg/mL for 36 h. Caspase 3 activity in untreated cells was taken as 1-fold and the change in the treated cells was expressed by comparing untreated cells. The results are the means (± standard deviation) of three independent experiments

****: p<0.0001

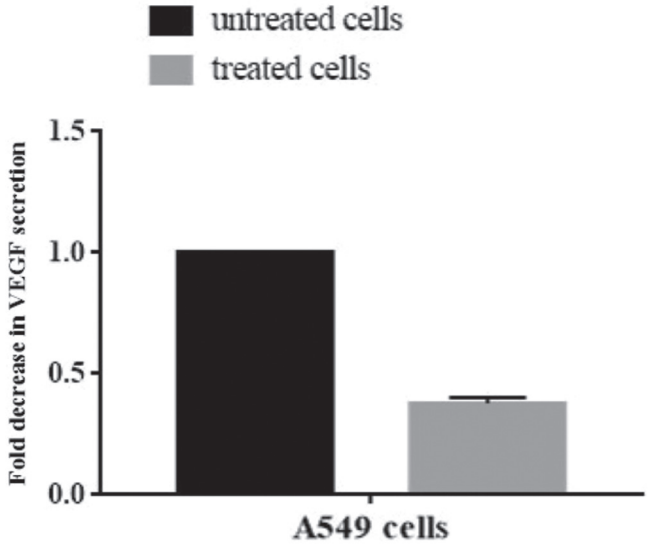

Figure 5. Effects of plant extract on vascular endothelial growth factor secretion of A549 cells. Cells were treated with 200 µg/mL extract for 6 h and vascular endothelial growth factor concentration in supernatants was detected by enzyme-linked immunosorbent assay. Results are presented as fold of change in relation to the control cells. Data are the means (±standard deviation) of three independent experiments

VEGF: Vascular endothelial growth factor

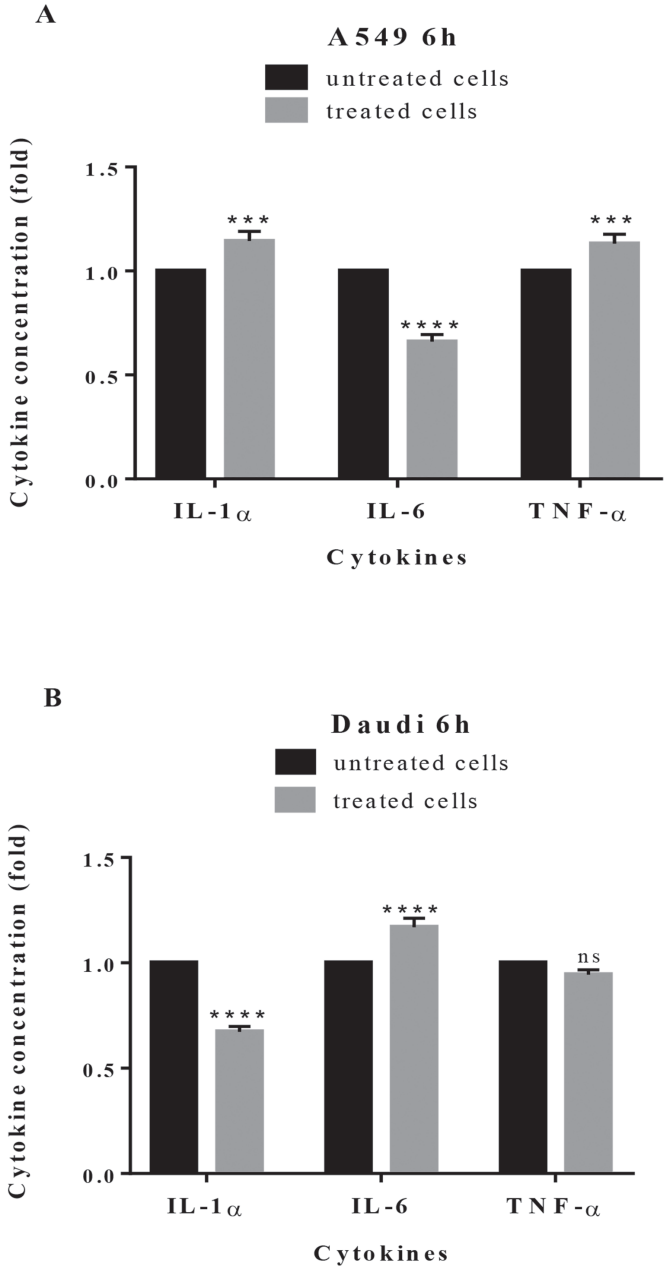

Figure 6. Effects of plant extract on cytokine secretion. A549 cells (A) and Daudi cells (B) were treated with plant extract at 200 µg/mL for 6 h. The concentrations of IL-1α, IL-6, and tumor necrosis factor-α in the supernatants of cancer cells were detected by enzyme-linked immunosorbent assay. Results are presented as fold of change in relation to the control cells. Data are the means (±standard deviation) of three independent experiments

****: p<0.0001, ***: p<0.01, ns: nonsignificant, TNF: tumor necrosis factor, IL: interleukin

In other words, the plant extract caused a significant change in the cytokine levels of cancer cells.

DISCUSSION

Cancer is one of the major causes of death in the world.[24] It has been known for centuries that plants have anticancer properties and they are important resources for new anticancer drugs.[25] The genus *Centaurea* has been the subject of many phytochemical and biological studies because of its widespread application in folk medicine to treat various diseases. Different biological activities such as antioxidant,[26] antimicrobial,[27] antipyretic,[28] and anti-ulcerogenic functions[29] were reported for *C. solstitialis*. However, to the best of our knowledge not much information is available about the anticancer and anti-inflammatory activities of *C. solstitialis* in the literature. Therefore, such biological activities of ethanolic extract from the flowering parts of *C. solstitialis* were examined in the present study.

Investigation of the cytotoxic effect of a plant extract against cancer cells is an important step for the development of plant-based drugs for cancer treatment. Likewise, the cytotoxic effect of ethanolic extract from the flowering parts of *C. solstitialis* on different cancer cell lines was tested. The findings indicated that plant extract showed cytotoxic effects at different levels according to the type of cell lines used. The extract exhibited the highest cytotoxicities in HeLa cells, with an IC_{50} value of 63.18 µg/mL, and Daudi cells, with an IC_{50} value of 69.27 µg/mL, whereas the IC_{50} value in the BEAS-2B normal cell line was 75.25 µg/mL. However, plant extract showed the lowest cytotoxic effect against A549 cells (IC_{50} value of 252.5 µg/mL). Erenler et al.[30] investigated the antiproliferative activities of methanol extract of the root, stem, and flowering parts of *C. solstitialis* L. subsp. *solstitialis* on C6 cells and HeLa cells *in vitro* and found that the methanol extract of the stem exhibited the most antiproliferative activity. In contrast to their study, our previous investigation demonstrated that the flowers were a more effective plant part compared to the stem (unpublished data) and so ethanolic extract only from the flowering parts was used in the present study. The reason for this may have been the type of solvent used for extract preparation. In fact, different solvents result in extraction of chemical compounds at different scales.

Similar to this study, there are publications related to different *Centaurea* species that have cytotoxic effects against the A549 and HeLa cell lines. Tugba Artun et al.[31] reported that among 14 plant extracts the methanol extract of *Centaurea nerimaniae* exhibited the highest cytotoxic effect against the Vero normal cell line and methanolic extract of the endemic *Centaurea antiochia* Boiss. var. *praealta* showed a selective cytotoxic effect against the HeLa cell line, with an IC_{50} value of 427±3.06 µg/mL. In another study, chloroform extracts of *Centaurea cadmea* showed the most inhibitory activities against the HeLa (IC_{50}: 14.24 µg/mL), A549 (IC_{50}: 35.00 µg/mL), and U20S (IC_{50}: 43.10 µg/mL) human cancer cell lines and the 293HEK (IC_{50}: 23.50 µg/mL) noncancer cell line.[32] In addition, Zater et al.[33] stated that chloroformic extract of *C. diluta* Ait. subsp. *algeriensis* exhibited more significant cytotoxic effects on the cancer cells A549, MCF-7, and U373 than the isolated pure compounds. Taken together, these studies indicate that the cytotoxicity level changes depending on the different *Centaurea* species and solvents used for extract preparation and the type of cell lines used for the *in vitro* cytotoxicity test.

Because cell cycle inhibition is a main target in the development and discovery of a drug against cancer, the effect of plant extract on the cell cycle progression of the HeLa and A549 cell lines after 24 h treatment was investigated in the present study. The results indicated that the plant extract blocked cancer cell proliferation by arresting both cell lines especially in the G2 phase of the cell cycle. In contrast to our results, Ghantous et al.[34] reported that inhibition of the cell proliferation of the papilloma and squamous cell carcinoma cell lines by crude extract of *Centaurea ainetensis* and the compound salograviolide A isolated from this plant was due to G0/G1 cell cycle arrest. Other researchers demonstrated that crude extract of *Centaurea ainetensis* induced a progressive increase in the proportion of sub-G1 cells in the HCT-116 cell line.[35]

Apoptosis is an important physiological process that plays a critical role in development and homeostasis in normal tissues; however, the balance between cell division and apoptosis is lost in cancer.[36,37] Therefore, targeting apoptosis in cancer treatment is crucial. In cells undergoing apoptosis, phosphatidylserine (PS) translocates toward the extracellular side of the membrane. Annexin V is a phospholipid-binding protein and so translocation of PS to the outside of the membrane is detected by Annexin V staining and it shows early stage apoptosis.[38] In the literature, only two studies investigated the apoptotic effects of extracts from *Centaurea ainetensis*[34] and *Centaurea fenzlii* Reichardt[39] on different cancer cell lines and they showed the presence of apoptotic cell death. In the present study, Annexin V staining along with flow cytometric analysis was carried out to reveal the mechanism in the cytotoxicity of plant extract on the A549 and HeLa cancer cells. Similar to previous studies, treatment of HeLa and A549 cells with *C. solstitialis* extract induced apoptosis and increased apoptotic cell number in a dose-dependent manner (Figure 3).

Caspases, a family of proteases, play an essential role in the apoptotic pathway and become activated during the early stages of apoptosis.[40] Because elevation in caspase-3 activity is regarded as an apoptotic marker, caspase-3 activity in treated and untreated cancer cell lines was examined. The results indicated that ethanolic extract of the flowering parts of *C. solstitialis* caused an increase in caspase-3 activity in both the HeLa and A549 cell lines (Figure 4). In addition, Yırtıcı et al.[39] reported that dichloromethane extracts-ethyl acetate fractions from *C. fenzlii* Reichardt exhibited an apoptotic effect on MCF-7 cells using flow cytometry and western blot analysis of an apoptosis-related protein, adenosine diphosphate ribose polymerase.

Angiogenesis is defined as the formation of new microvessels from preexisting ones and is required for tumor growth and distribution of tumor cells to distant locations.[41] VEGF is known

to be one of the most potent angiogenic factors. Previous studies indicated that inhibition of VEGF secretion suppresses tumor growth, tumor invasion, and metastasis.[41] A549, an airway epithelial cancer cell line, releases VEGF constitutively.[22] Therefore, the angiogenic potential of the extract on the A549 cell line was investigated by measuring VEGF secretion after 6 h of treatment. A significant inhibition of VEGF secretion in A549 cells implies that the plant extract has potential as an anti-angiogenic agent in cancer therapy.

Inflammatory cytokines play a role in different stages of tumor development and many cytokines such as TNF, IL-1, and IL-6 can be induced by hypoxia, one of the well known properties of cancer cells.[42,43] Here we tested the effect of plant extract on the secretion of IL-1α, IL-6, and TNF-α in A549 and Daudi cells. The plant extract at 200 µg/mL did not decrease TNF-α production in either cell line (Figure 6). The plant extract significantly inhibited the release of IL-6 in A549 and the release of IL-1α in Daudi cells. According to a previous study, production of angiogenic factors such as VEGF could be induced by TNF, IL-1, and IL- 6.[42] A decrease in VEGF production in A549 cells may be associated with decreased IL-6 production in A549 cells in the present study. Similar to our result, Talhouk et al.[44] reported that water extract of *C. ainetensis* inhibited IL-6 production in a dose-dependent manner. In addition, *in vivo* anti-inflammatory effects of some *Centaurea* species were reported as well by Erel et al.[45] and Koca et al.[46] The present study indicates that induction or inhibition of inflammatory cytokines by ethanolic extract of *C. solstitialis* is cell-type dependent.

Study limitations

Crude ethanolic extract from the flowering parts of *C. solstitialis* was investigated for its anticancer and anti-inflammatory potential. Isolation of pure compounds in a future study will show if each constituent alone or in different combinations may exhibit increased anticancer or anti-inflammatory activities.

CONCLUSIONS

Ethanolic extract from the flowering parts of *C. solstitialis* showed significant anticancer and anti-inflammatory potential against different cancer cell lines, indicating that the flowering parts of *C. solstitialis* are a potential source of active compounds for the development of natural drugs against cancer.

ACKNOWLEDGEMENT

This work was supported by grants 15/006 and 15/247 from Scientific Research Projects (BAP) of Muğla Sıtkı Koçman University

Conflict of Interest: No conflict of interest was declared by the authors.

REFERENCES

1. Raskin I, Ribnicky DM, Komarnytsky S, Ilic N, Poulev A, Borisjuk N, Brinker A, Moreno DA, Ripoll C, Yakoby N, O'Neal JM, Cornwell T, Pastor I, Fridlender B. Plants and human health in the twenty-first century. Trends Biotechnol. 2002;20:522-531.
2. Unnati S, Ripal S, Sanjeev A, Niyati A. Novel anticancer agents from plant sources. Chin J Nat Med. 2013;11:16-23.
3. Fan TP, Yeh JC, Leung KW, Yue PY, Wong RN. Angiogenesis: from plants to blood. Trends Pharmacol Sci. 2006;27:297-309.
4. Tahergorabi Z, Khazaei M. A Review on Angiogenesis and Its Assays. Iran J Basic Med Sci. 2012;15:1110-1126.
5. Schottenfeld D, Beebe-Dimmer J. Chronic Inflammation: A Common and Important Factor in the Pathogenesis of Neoplasia. CA Cancer J Clin. 2006;56:69-83.
6. Oppenheim JJ, Murphy WJ, Chertox O, Schirrmacher V, Wang JM. Prospects for Cytokine and Chemokine Biotherapy. Clin Cancer Res.1997;3:2682-2686.
7. Hollman, PC, Katan MB. Dietary Flavonoids: intake, health effects and bioavailability. Food Chem Toxicol.1999;37:937-942.
8. Thun MJ, Henley, SJ, Patrono C. Nonsteroidal Anti-inflammatory Drugs as Anticancer Agents: Mechanistic, Pharmacologic, and Clinical Issues. J Natl Cancer Inst. 2002;94:252-266.
9. Güner A, Özhatay N, Ekim T, Başer K. Flora of Turkey and the East Aegean Islands. Vol 11. Edinburgh: Edinburgh University Press;2000.
10. Altundag E, Ozturk M. Ethnomedicinal studies on the plant resources of east Anatolia. Procedia Soc Behav Sci. 2011;19:756-777.
11. Honda G, Yeşilada E, Tabata M, Sezik E, Fujita T, Takeda Y, Takaishi Y, Tanaka T. Traditional medicine in Turkey VI. Folk medicine in West Anatolia: Afyon, Kütahya, Denizli, Muğla, Aydın provinces. J Ethnopharmacol. 1996;53:75-87.
12. Sezik E, Yeşilada E, Honda G, Takaishi Y, Takeda Y, Tanaka T. Traditional medicine in Turkey X. Folk medicine in Central Anatolia. J Ethnopharmacol. 2001;75:95-115.
13. Bulut G, Tuzlaci E. An ethnobotanical study of medicinal plants in Turgutlu (Manisa-Turkey). J Ethnopharmacol. 2013;149:633-647.
14. Fujita T, Sezik E, Tabata M, Yeşilada E, Honda G, Takeda Y, Tanaka T, Takaishi Y. Traditional Medicine in Turkey VII.Folk Medicine in Middle and West Black Sea Regions. Econ Bot. 1995;49:406-422.
15. Khammar A, Djeddi S. Pharmacological and Biological Properties of some *Centaurea* Species. Eur J Sci Res. 2012;84:398-416.
16. Kaïj-a-Kamb M, Amoros M, Girre L. The chemistry and biological activities of the genus Centaurea. Pharm Acta Helv. 1992;67:178-188.
17. Aktumsek A, Zengin G, Guler GO, Cakmak YS, Duran A. Screening for *in vitro* antioxidant properties and fatty acid profiles of five *Centaurea L.* species from Turkey flora. Food Chem Toxicol. 2011;49:2914-2920.
18. Denizot F, Lang R. Rapid colorimetric assay for cell growth and survival: Modifications to the tetrazolium dye procedure giving improved sensitivity and reliability. J Immunol Methods. 1986;89:271-277.
19. Bradford, MM. A Rapid and Sensitive Method for the Quantitation of Microgram Quantities of Protein Utilizing the Principle of Protein-Dye Binding. Anal Biochem. 1976;72:248-254.
20. Hengartner, MO. The biochemistry of apoptosis. Nature. 2000;407:770-776.
21. Chung AS, Ferrara N. Developmental and Pathological Angiogenesis. Annu Rev Cell Dev Biol. 2011;27:563-584 .
22. Koyama S, Sato E, Tsukadaira A, Haniuda M, Numanami H, Kurai M, Nagai S, Izumi T. Vascular endothelial growth factor mRNA and protein expression in airway epithelial cell lines *in vitro*. Eur Respir J. 2002;20:1449-1456.

23. Dranoff G. Cytokines in cancer pathogenesis and cancer therapy. Nat Rev Cancer. 2004;4:11-22.

24. World Health Organization. World health statistics 2017: monitoring health for the SDGs, Sustainable Development Goals. Geneva: World Health Organization; 2017.

25. Cragg GM, Newman DJ. Natural products: A continuing source of novel drug leads. Biochim Biophys Acta. 2013;1830:3670-3695.

26. Tekeli Y, Sezgin M, Aktümsek A. Antioxidant property of *Centaurea solstitialis* L. from Konya, Turkey. Asian J Chem. 2008;20:4831-4835.

27. Özçelik B, Gürbüz I, Karaoglu T, Yeşilada E. Antiviral and antimicrobial activities of three sesquiterpene lactones from *Centaurea solstitialis* L. ssp. solstitialis. Microbiol Res. 2009;164:545-552.

28. Akkol EK, Arif R, Ergun F, Yesilada E. Sesquiterpene lactones with antinociceptive and antipyretic activity from two *Centaurea* species. J Ethnopharmacol. 2009;122:210-215.

29. Gürbüz İ, Yesilada E. Evaluation of the anti-ulcerogenic effect of sesquiterpene lactones from *Centaurea solstitialis* L. ssp. solstitialis by using various *in vivo* and biochemical techniques. J Ethnopharmacol. 2007;112:284-291.

30. Erenler R, Sen O, Yaglioglu AS, Demirtas I. Bioactivity-Guided Isolation of Antiproliferative Sesquiterpene Lactones from *Centaurea solstitialis* L. ssp. solstitialis. Comb Chem High Throughput Screen. 2016;19:66-72.

31. Tugba Artun F, Karagoz A, Ozcan G, Melikoglu G, Anil S, Kultur S, Sutlupinar N. *In vitro* anticancer and cytotoxic activities of some plant extracts on HeLa and Vero cell lines. J BUON. 2016;21:720-725.

32. Astari KA, Erel ŞB, Köse FA, Köksal Ç, Karaalp C. Cytotoxic and Antibacterial Activities of Centaurea cadmea Boiss. Turk J Pharm Sci. 2014;11:101-106.

33. Zater H, Huet J, Fontaine V, Benayache S, Stévigny C, Duez P, Benayache F. Chemical constituents, cytotoxic, antifungal and antimicrobial properties of *Centaurea diluta* Ait. subsp. algeriensis (Coss. & Dur.) Maire. Asian Pac J Trop Med. 2016;9:554-561.

34. Ghantous A, Tayyoun AA, Lteif GA, Saliba NA, Gali-Muhtasib H, El-Sabban M, Darwiche N. Purified Salograviolide A isolated from Centaurea ainetensis causes growth inhibition and apoptosis in neoplastic epidermal cells. Int J Oncol. 2008;32:841-849.

35. El-Najjar N1, Dakdouki S, Darwiche N, El-Sabban M, Saliba NA, Gali-Muhtasib H. Anti-colon cancer effects of Salograviolide A isolated from *Centaurea ainetensis*. Oncol Rep. 2008;19:897-904.

36. Hanahan D, Weinberg RA. The Hallmarks of Cancer. Cell. 200;100:57-70.

37. Plati J, Bucur O, Khosravi-Far R. Apoptotic cell signaling in cancer progression and therapy. Integr Biol (Camb). 2011;3:279-296.

38. Deepa M, Sureshkumar T, Satheeshkumar PK, Priya S. Purified mulberry leaf lectin (MLL) induces apoptosis and cell cycle arrest in human breast cancer and colon cancer cells. Chem Biol Interact. 2012;200:38-44.

39. Yırtıcı Ü, Göger F, Sarımahmut M, Ergene A. Cytotoxic and apoptotic effects of endemic *Centaurea fenzlii* Reichardt on the MCF-7 breast cancer cell line. Turk J Biol. 2017;41:370-377.

40. Porter AG, Jänicke RU. Emerging roles of caspase-3 in apoptosis. Cell Death Differ. 1999;6:99-104.

41. Masoumi Moghaddam S, Amini A, Morris DL, Pourgholami MH. Significance of vascular endothelial growth factor in growth. Cancer Metastasis Rev. 2012;31:143-162.

42. Balkwill F, Mantovani A. Inflammation and cancer: back to Virchow? Lancet. 2001;357:539-545.

43. Fernandes JV, Cobucci RN, Jatobá CA, Fernandes TA, de Azevedo JW, de Araújo JM. The Role of the Mediators of Inflammation in Cancer Development. Pathol Oncol Res. 2015;21:527-534.

44. Talhouk RS, El-Jouni W, Baalbaki R, Gali-Muhtasib H, Kogan J, Talhouk SN. Anti-inflammatory bio-activities in water extract of *Centaurea ainetensis*. J Med Plant Res. 2008;2:24-33.

45. Erel SB, Demir S, Nalbantsoy A, Ballar P, Khan S, Yavasoglu NU, Karaalp C. Bioactivity screening of five *Centaurea* species and *in vivo* anti-inflammatory activity of C. athoa. Pharm Biol. 2014;52:775-781.

46. Koca U, Süntar IP, Keles H, Yesilada E, Akkol EK. *In vivo* anti-inflammatory and wound healing activities of *Centaurea iberica* Trev.ex Spreng. J Ethnopharmacol. 2009;126:551-556.

Turk J Pharm Sci 2019;16(3):282-291
DOI: 10.4274/tjps.galenos.2018.85619

ORIGINAL ARTICLE

An *In Vitro* Study on the Cytotoxicity and Genotoxicity of Silver Sulfide Quantum Dots Coated with Meso-2,3-dimercaptosuccinic Acid

Mezo-2,3-dimerkaptosüksinik Asitle Kaplanmış Gümüş Sülfit Kuantum Noktalarının Sitotoksisitesi ve Genotoksisitesi Üzerine Bir *In Vitro* Çalışma

Deniz ÖZKAN VARDAR[1], Sevtap AYDIN[2], İbrahim HOCAOĞLU[3], Havva YAĞCI ACAR[4], Nursen BAŞARAN[2]*

[1]Hitit University, Sungurlu Vocational High School, Health Programs, Çorum, Turkey
[2]Hacettepe University, Faculty of Pharmacy, Department of Pharmaceutical Toxicology, Ankara, Turkey
[3]Koç University, Graduate School of Materials Science and Engineering, İstanbul, Turkey
[4]Koç University, College of Sciences, Department of Chemistry, İstanbul, Turkey

ABSTRACT

Objectives: Silver sulfide (Ag_2S) quantum dots (QDs) are highly promising nanomaterials in bioimaging systems due to their high activities for both imaging and drug/gene delivery. There is insufficient research on the toxicity of Ag_2S QDs coated with meso-2,3-dimercaptosuccinic acid (DMSA). In this study, we aimed to determine the cytotoxicity of Ag_2S QDs coated with DMSA in Chinese hamster lung fibroblast (V79) cells over a wide range of concentrations (5-2000 µg/mL).

Materials and Methods: Cell viability was determined by 3-(4,5-dimethylthiazol-2-yl)-2,5-diphenyltetrazolium bromide (MTT) and neutral red uptake (NRU) assays. The genotoxic and apoptotic effects of DMSA/Ag_2S QDs were also assessed by comet assay and real-time polymerase chain reaction technique, respectively.

Results: Cell viability was 54.0±4.8% and 65.7±4.1% at the highest dose (2000 µg/mL) of Ag_2S QDs using the MTT and NRU assays, respectively. Although cell viability decreased above 400 µg/mL (MTT assay) and 800 µg/mL (NRU assay), DNA damage was not induced by DMSA/Ag_2S QDs at the studied concentrations. The mRNA expression levels of *p53, caspase-3, caspase-9, Bax, Bcl-2,* and *survivin* genes were altered in the cells exposed to 500 and 1000 µg/mL DMSA/Ag_2S QDs.

Conclusion: The cytotoxic effects of DMSA/Ag_2S QDs may occur at high doses through the apoptotic pathways. However, DMSA/Ag_2S QDs appear to be biocompatible at low doses, making them well suited for cell labeling applications.

Key words: Meso-2,3-dimercaptosuccinic acid coated silver sulfide quantum dots, genotoxicity, apoptosis

ÖZ

Amaç: Gümüş sülfür (Ag_2S) kuantum noktaları (QD), hem görüntüleme hem de ilaç/gen hedefleme için büyük aktiviteleri nedeniyle biyo-görüntüleme sisteminde oldukça gelecek vaad eden nanomalzemelerdir. Mezo-2,3-dimerkaptosüksinik asit (DMSA) ile kaplanmış Ag_2S QD'lerin toksisitesi hakkında yeterli çalışma yoktur. Bu çalışmada Çin hamster akciğer fibroblast (V79) hücrelerinde DMSA ile kaplanmış Ag_2S QD'lerin geniş bir konsantrasyon aralığında (5-2000 µg/mL) sitotoksisitesini belirlemeyi amaçladık.

Gereç ve Yöntemler: Hücre canlılığı 3-(4,5-dimetiltiyazol-2-il)-2,5-difeniltetrazolium bromid (MTT) ve nötral kırmız alım (NRU) deneyleri ile belirlendi. DMSA/Ag_2S QD'lerin genotoksik ve apoptotik etkileri sırasıyla komet analizi ve gerçek zamanlı polimeraz zincir reaksiyonu tekniği ile değerlendirildi.

Bulgular: Ag_2S QD'lerin en yüksek dozlarında hücre canlılığı MTT ve NRU deneylerinde sırasıyla 54.0±4.8% ve 65.7±4.1% olarak bulundu. Ancak hücre canlılığı 400 µg/mL (MTT deneyi) ve 800 µg/mL (NRU deney) üzerinde azalmıştır. İncelenen konsantrasyonlarda DNA hasarının DMSA/Ag_2S QD'ler tarafından indüklenmediği belirlenmiştir. *P53, kaspaz-3, kaspaz-9, Bax, Bcl-2* ve *survivin* genlerinin mRNA ekspresyon düzeyleri 500 ve 1000 µg/mL DMSA/Ag_2S QD'lere maruz kalan hücrelerde değişmiştir.

Sonuç: DMSA/Ag_2S QD'lerin yüksek dozlarda sitotoksik etkilerinin apoptotik yollarla ortaya çıkabileceği görülmektedir. Bununla birlikte, DMSA/Ag_2S QD'ler, düşük dozlarda biyolojik olarak uyumlu görünmektedir, bu da onları hücre görüntüleme uygulamaları için uygun kılmaktadır.

Anahtar kelimeler: Mezo-2,3-dimerkaptosüksinik asit kaplı gümüş sülfür kuantum noktaları, genotoksisite, apoptoz

*Correspondence: E-mail: nbasaran@hacettepe.edu.tr, Phone: +90 312 305 21 78 ORCID-ID: orcid.org/0000-0001-8581-8933
Received: 06.04.2018, Accepted: 31.05.2018

INTRODUCTION

The number of commercial products containing nanoparticles (NPs) is rapidly increasing and NPs are already widely distributed in air, cosmetics, medicines, and even food. As one of the leading nanomaterials, engineered NPs are currently the focus of considerable research attention due to their various applications such as drug and gene delivery, biosensors, and diagnostic tools. The use of functional nanomaterials in biology and biomedicine has been extensively explored, and it has become one of the fastest moving and most exciting research directions.[1,2]

A key issue in evaluating the utility of these materials is assessing their potential toxicity, which may result from either their inherent chemical composition (e.g., heavy metals) or their nanoscale properties (e.g., inhalation of particulate carbon nanotubes).[1,2] To date, a variety of nanomaterials, such as carbon nanotubes, silicon nanowires, gold/silver NPs, and quantum dots (QDs), have been studied and used in a wide range of biological applications.[3-6] NPs have unique features such as high surface-to-volume ratios, surface curvatures, and surface reactivities. They can also be produced with different sizes, chemical compositions, shapes, and surface charges, which affect their passage across the cell membranes, biodistribution, and toxicity.[7-9] Recently, the use of nanomaterials has also attracted considerable interest in biomedical fields.[10]

QDs are nanometer-scale semiconductor crystals and are defined as particles with physical dimensions smaller than the exciton Bohr radius. QDs, which are composed of group II to VI or III to V elements, are often described as "artificial atoms". They exhibit discrete energy levels, and their band gaps can be precisely modulated by varying their size.[11,12] In 2002, *Applied Spectroscopy* published its first review on QDs, "Quantum Dots: A Primer," by Murphy and Coffer.[13] The applications of luminescent nanocrystals have evolved tremendously over the last decade, particularly in bioimaging and bioanalysis. Since the first demonstration of QDs for biological imaging in 1998,[14,15] thousands of research articles on QDs have been published. Researchers have exploited the brightness, photostability, size-dependent optoelectronic properties, and superior multiplexing capabilities of QDs for a myriad of applications.[16-21] Some of the prominent applications include *in vitro* diagnostics, energy transfer-based sensing, cellular and *in vivo* imaging, and drug delivery and theranostics.[18,22,23] In parallel with these advances in bioimaging and bioanalysis, QDs have also evolved to provide greater flexibility and capability.[24]

QDs are usually synthesized using group II–VI materials, for example, cadmium telluride (CdTe) or cadmium selenide (CdSe).[25,26] Structurally, QDs consist of a metalloid crystalline core and a "cap" or "shell" that shields the core and renders the QD bioavailable. QD cores can be fabricated using different materials with different band gaps for luminescence in the visible or near-infrared region (NIR). Cd or Zn chalcogenides such as CdS, CdSe, CdTe, and ZnS are examples of group II–VI series of QDs[27,28] with luminescence in the visible range; indium phosphate and indium arsenate are examples of group III–V series QDs with emission in the red to NIR.[29,30]

A major limitation with respect to the clinical use of QDs is their potential toxicity due to their chemical composition and nanoscale features.[29] The most popular QDs for biological applications are still based on CdSe core materials, which offer high quality and control over the spectroscopic properties of the nanocrystal. Despite several demonstrations of relatively nontoxic compositions being delivered to cells, concerns remain regarding the cytotoxicity of released cadmium ions and the associated oxidative stress.[31-36]

Within the last decade, tremendous efforts have been devoted to developing Cd-free QDs. Silver sulfide (Ag_2S) QDs emerged recently as new generation QDs satisfying both of these criteria.[37,38] Hocaoglu et al.[38] reported meso-2,3-dimercaptosuccinic acid (DMSA)-coated Ag_2S QDs as one of the most strongly luminescent, anionic, NI-emitting QDs. These particles were significantly internalized by HeLa cells and provided strong intracellular optical signals, suppressing autofluorescence. No reduction in the viability of HeLa cells and only 20% reduction in NIH/3T3 cells at concentrations up to 840 µg/mL were reported, which is quite unusual for a nonpegylated QD. QDs were found quite hemocompatible as well. This composition is of special interest with respect to numerous applications since surface carboxylic acids can be conjugated with target ligands or drugs, producing theranostic NPs.

In the present study, we performed a detailed toxicity analysis to investigate the potential cytotoxicity, genotoxicity, and apoptosis induced by DMSA/Ag_2S QDs in Chinese hamster lung fibroblast (V79) cells. To have a relatively thorough toxicity analysis of DMSA/Ag_2S NIR QDs, the MTT and neutral red uptake (NRU) assays were performed to evaluate the potential cytotoxicity; the comet assay was performed to assess the potential genotoxicity; the real-time polymerase chain reaction (RT-PCR) technique was used to evaluate the regulation of mRNA expression of tumor suppressor gene (*p53*), apoptotic genes (*caspase-3*, *caspase-9*, and *Bax*) and anti-apoptotic genes (*Bcl-2* and *survivin*). The data presented here are the first that give the cytotoxic, genotoxic, and apoptotic effects of DMSA/Ag_2S QDs *in vitro*. Since there is insufficient research on their toxicity, this study provides remarkable information for human health.

MATERIALS AND METHODS

Chemicals

The chemicals were purchased from the following suppliers: hydrogen peroxide (35%) (H_2O_2) from Merck Chemicals (Darmstadt, Germany); 3-(4,5-dimethylthiazol-2-yl)-2,5-diphenyltetrazolium bromide (MTT), acetic acid, dimethyl sulfoxide (DMSO), DMSA, Dulbecco's modified eagle's medium (DMEM), ethanol, ethidium bromide (EtBr), fetal bovine serum (FBS), low melting point agarose, L-glutamin, NR, sodium chloride (NaCl), sodium hydroxide (NaOH), N-lauroyl sarcosinate, normal melting point agarose, silver nitrate

($AgNO_3$), trypsin-EDTA, triton X-100, penicillin/streptomycin, and phosphate buffered saline (PBS) from Sigma-Aldrich Chemicals (St. Louis, MO, USA); and sodium sulfide (Na_2S) from Alfa-Aesar (Thermo Fisher Scientific, Karlsruhe, Germany). Milli-Q water (18.2 MOhm) was used as the reaction medium.

Preparation and characterization of DMSA/Ag_2S NIR QDs

DMSA/Ag_2S NIR QDs were prepared in a one-step reaction. A detailed description and characterization were reported previously by Hocaoglu et al.[38] Briefly, 42.5 mg of $AgNO_3$ (0.25 mmol) was dissolved in 75 mL of deoxygenated deionized water. Then 113.89 mg of DMSA (0.625 mmol) was dissolved and deoxygenated in 25 mL of deionized water at pH 7.5 and added to the reaction mixture. The pH was adjusted to 7.5 using NaOH and CH_3COOH solutions (2 M). The reaction mixture was stirred at 70°C for 4 h. The prepared colloidal DMSA/Ag_2S QDs were washed with deionized water using Amicon-Ultra centrifugal filters (3000 Da cut-off) and stored in the dark at 4°C. In order to calculate the concentration of QDs, a few milliliters of the colloidal solution was dried in a freeze-drier. The concentration of the QD solution was determined as 4.6 mg/mL. The absorbance spectrum of QDs was recorded in a Shimadzu 3101 PC UV-vis-NIR spectrometer in the 300-1000 nm range (Figure 1a). The photoluminescence spectrum was obtained as described in detail previously by Hocaoglu et al.[38] Samples were excited with a DPSS laser operating at 532 nm and emission was recorded by an amplified silicon detector with femtowatt sensitivity in the range of 400-1100 nm with a lock-in amplifier. The QDs have an emission maximum at 790 nm with about 129 nm full-width at half maximum (Figure S1b). A Malvern zetasizer nano ZS was used for the measurement of the hydrodynamic size (2.9 nm) of aqueous QDs and the zeta potential of aqueous QDs (-30 mV). Hydrodynamic size was measured by dynamic light scattering. No agglomeration in the cell culture medium was observed.

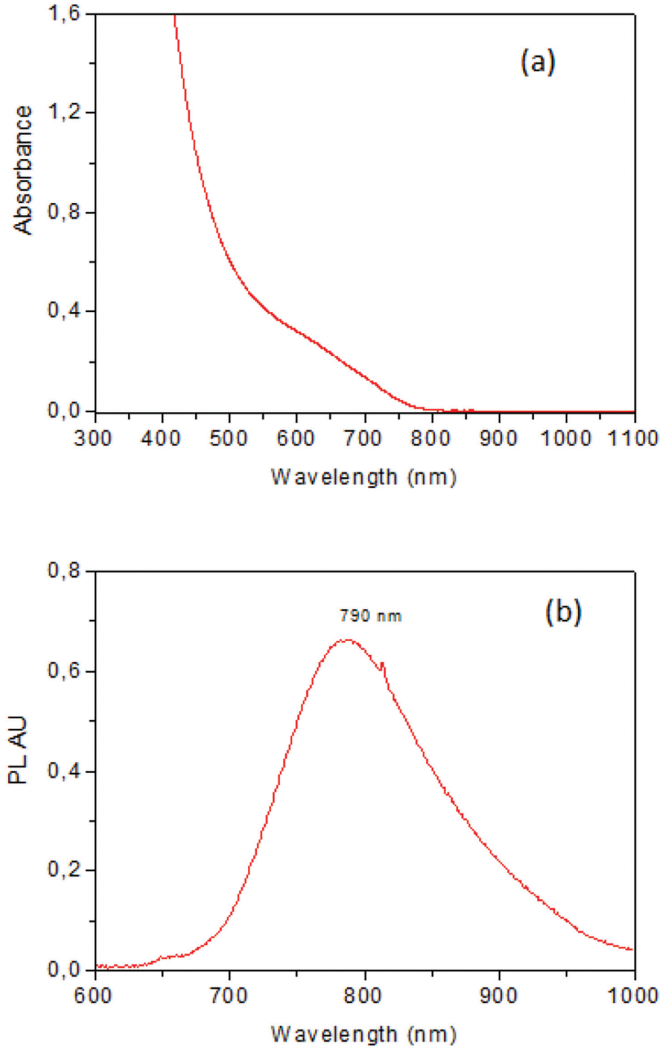

Figure 1. (a) Absorbance spectra, (b) emission spectra of colloidal DMSA/Ag_2S QDs

Ag_2S: Silver sulfide, QDs: quantum dots

Cell culture

V79 cells were obtained from the American Type Culture Collection (ATCC; Rockville, MD, USA). The cells were grown in DMEM supplemented with 10% heat-inactivated FBS, 1% penicillin/streptomycin solution (10.000 units of penicillin and 10 mg of streptomycin in 0.9% NaCl), and 2 mM L-glutamin at 37°C in a humidified atmosphere of 5% CO_2.[39] The culture medium was changed every 3 to 4 days. The passage numbers used in our study were between 6 and 10.

Determination of cytotoxicity by MTT assay

The MTT assay by the method described by Mosmann[40] with the modifications by Hansen et al.[41] and Kuźma et al.[42] was carried out. The cells were disaggregated with trypsin/EDTA and then resuspended in the medium. The suspended cells (a total of 10^5 cells/well) were plated in 96-well tissue-culture plates. The experiment was performed for 12 h, 24 h, and 48 h before and there were no time differences (data not shown). To get a dose range for the further experiments, 24 h incubation was selected. After the incubation for 24 h, the cells were exposed to different concentrations of DMSA/Ag_2S QDs (5, 10, 25, 50, 100, 200, 400, 200, 800, 1000, 2000 µg/mL) in the medium for 24 h. Then the medium was removed and MTT solution (5 mg/mL of stock in PBS) was added (10 µL/well in 100 µL of cell suspension). After the incubation of the cells for an additional 4 h with MTT dye, the dye was carefully taken out and 100 µL of DMSO was added to each well. The absorbance of the plate was measured in a microplate reader at 570 nm. The experiment was repeated three times. The results were expressed as the mean percentage of cell growth. IC_{50} values represent the concentrations that reduced the mean absorbance of 50% of those in the untreated cells.

Determination of cytotoxicity by NRU assay

Determination of the cytotoxicity of DMSA/Ag_2S QDs using NRU assay was performed according to the protocols described by Di Virgilio et al.[43] and Saquib et al.[44] V79 cells were treated with DMSA/Ag_2S QDs as described in the MTT assay. After incubation for 24 h, the medium was aspirated. The cells were washed twice with PBS and incubated for an additional 3 h in

the medium supplemented with NR (50 µg/mL). The absorbance of the solution in each well was measured in a microplate reader at 540 nm and compared with the wells containing untreated cells. The experiment was repeated three times. The results were expressed as the mean percentage of cell growth inhibition. IC_{50} values represent the concentrations that reduced the mean absorbance of 50% of those in the untreated cells.

Determination of genotoxicity by comet assay

V79 cells were treated with DMSA/Ag_2S QDs as described in the MTT assay. Following the disaggregation of the cells with trypsin/EDTA and the resuspension of the cells in the medium, a total of 2×10^5 cells/well were plated in 6-well tissue-culture plates. After 24 h of incubation, the cells were incubated with different concentrations of DMSA/Ag_2S QDs (5-2000 µg/mL) for an additional 24 h at 37˚C. A positive control (50 µM H_2O_2) was also included in the experiments. The cells were embedded in agarose gel and lysed. Fragmented DNA strands were then drawn out by electrophoresis to form a comet. After electrophoresis, the slides were neutralized and then incubated in 50%, 75%, and 98% alcohol for 5 min. The dried microscopic slides were stained with EtBr (20 µg/mL in distilled water, 60 µL/slide) and were examined with a Leica® fluorescence microscope under green light.

The microscope was connected to a charge-coupled device camera and a personal computer-based analysis system (Comet Analysis Software, version 3.0, Kinetic Imaging Ltd, Liverpool, UK) to determine the extent of DNA damage after electrophoretic migration of the DNA fragments in the agarose gel. In order to visualize DNA damage, 100 nuclei per slide were examined at 400× magnification. The results were expressed as the percent of DNA in the tail, "tail intensity". The experiment was performed in duplicate and repeated three times.

Determination of apoptotic genes by RT-PCR

V79 cells were treated with DMSA/Ag_2S QDs at concentrations of 125, 250, 500, and 1000 µg/mL in 6-well plates for 24 h. After the completion of the exposure time, total RNA was extracted with a Qiagen RNeasy Plus Mini Kit (Valencia, CA, USA) according to the manufacturer's protocol. The RNA content was estimated using a Nanodrop 8000 spectrophotometer (Thermo Fisher Scientific, Wilmington, DE, USA), and the integrity of RNA was visualized on 1% agarose gel using a gel documentation system (Thermo Fisher Scientific, Wilmington, DE, USA). First-strand cDNA was synthesized using an RT^2 First Strand Kit (Qiagen, Valencia, CA, USA) according to the manufacturer's instructions. Quantitative RT-PCR was performed by QuantiTect SYBR Green PCR kit (Qiagen) using a Corbett RotorGene Sequence Detection System (Thermo Fisher Scientific, Wilmington, DE, USA). Two microliters of template cDNA was added to the final volume of 20 µL of reaction mixture. The RT-PCR cycle parameters included 10 min at 95˚C followed by 40 cycles involving denaturation at 95˚C for 15 s, annealing at 60˚C for 20 s, and elongation at 72˚C for 20 s. The sequences of the specific sets of primer for *p53*, *caspase-3*, *caspase-9*, *Bax*, *Bcl2,* and *survivin* utilized in the present investigation are given in our previous study.[45] Expressions of selected genes were normalized to the *gapdh* gene and then used as controls. The experiment was performed in duplicate and repeated three times.

Statistical analysis

Statistical analysis was performed with SPSS for Windows 20.0 for the alkaline comet assay. Differences between the means of data were compared by one-way variance analysis and post hoc analysis of group differences by the least significant difference test. The RT-PCR array was analyzed by t-test. Significance in the RT-PCR array was determined based on the fold change from the control ΔΔCt value. The results were expressed as the mean ± standard deviation. A p value of less than 0.05 was considered statistically significant.

RESULTS

Cytotoxicity of DMSA/Ag_2S QDs by MTT assay

The V79 cells were treated with DMSA/Ag_2S QDs and free DMSA to determine the cytotoxicity of the QDs itself and the coating material over a wide range of concentrations between 0 and 2000 µg/mL for 24 h. The cytotoxicity was then evaluated by MTT assay. The data provided in Figure 2a

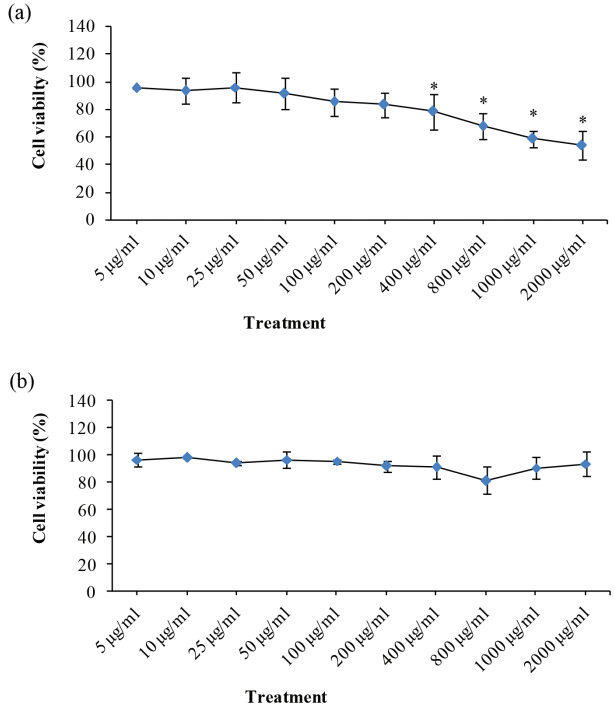

Figure 2. Influence of DMSA/Ag_2S QDs (a) and free DMSA solutions (b) on viability of V79 cells using the MTT assay. Cell viability was plotted as percent of negative control (assuming data obtained from untreated cells as 100%). Results were given as the mean ± standard deviation. Differences between the means of data were compared by one-way analysis of variance and post hoc analysis of group differences by least significant difference test. *Significant difference as compared to the negative control ($p<0.05$). Negative control (1% PBS), positive control (50 µM H_2O_2). The cell viability of the positive control was 48.5%

Ag_2S: Silver sulfide, QDs: Quantum dots, DMSA: Meso-2,3-dimercaptosuccinic acid, MTT: 3-(4,5-dimethylthiazol-2-yl)-2,5-diphenyltetrazolium bromide, PBS: Phosphate buffered saline

exhibited no significant cytotoxicity between 5 and 200 µg/mL and a concentration-dependent decline in the survival of cells exposed to DMSA/Ag_2S QDs at higher concentrations (400-2000 µg/mL) when compared to the untreated control. IC_{50} of DMSA/Ag_2S QDs was not determined at these concentrations. Cell viability was 54.0±4.8% at the highest doses (2000 µg/mL). As shown in Figure 2b, free DMSA did not cause any significant cytotoxicity in V79 cells within the same concentration range.

Cytotoxicity of DMSA/Ag_2S QDs by NRU assay

The results for cytotoxicity as evaluated by NRU cell viability indicated no significant cytotoxicity at concentrations between 5 and 400 µg/mL when compared to the untreated control, but a clear dose-dependent toxicity at higher concentrations (800-2000 µg/mL) was observed (Figure 3a). IC_{50} of DMSA/Ag_2S was not determined. Cell viability was 65.7±4.1% at the highest dose (2000 µg/mL) of Ag_2S QDs. Similar to the results obtained from the MTT assay, DMSA alone did not show cytotoxicity in V79 cells with the same studied doses (Figure 3b).

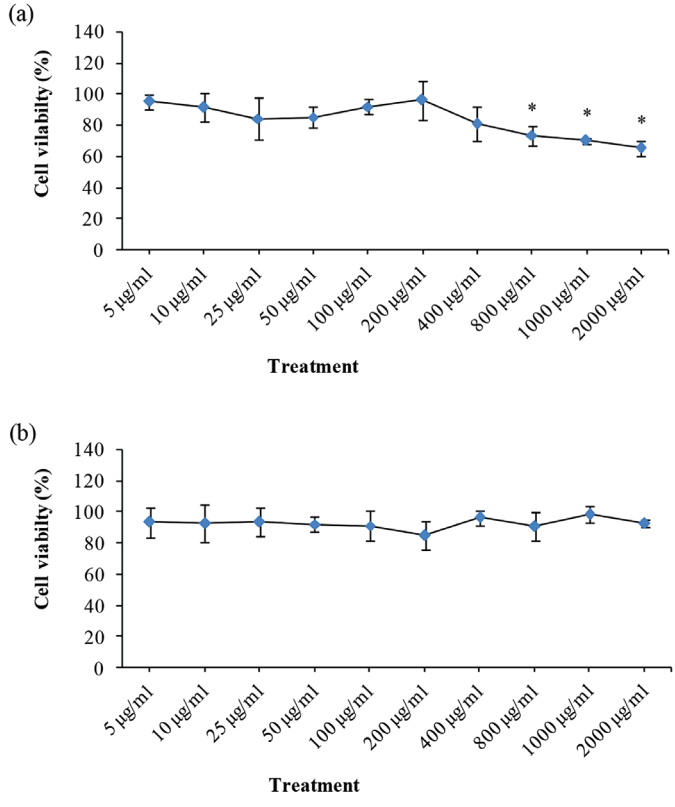

Figure 3. Effects of DMSA/Ag_2S QDs (a) and DMSA solutions (b) on viability of V79 cells using the NRU assay. Cell viability was plotted as percent of negative control (assuming data obtained from untreated cells as 100%). Results were given as the mean ± standard deviation. Differences between the means of data were compared by one-way analysis of variance and post hoc analysis of group differences by least significant difference test *Significant difference as compared to the negative control ($p<0.05$). Negative control (1% PBS), positive control (50 µM H_2O_2). The cell viability of the positive control was 53.6%

Ag_2S: Silver sulfide, QDs: Quantum dots, DMSA: Meso-2,3-dimercaptosuccinic acid, NRU: Neutral red uptake, PBS: Phosphate buffered saline

Genotoxicity of DMSA/Ag_2S QDs

Genotoxicity of these QDs was evaluated by comet assay (Figures 4 and 5). DNA damage, expressed as "DNA tail intensity" in V79 cells, is presented in Figure 4. No significant DNA damage was observed, since DMSA/Ag_2S QDs treatments (5-2000 µg/mL) for 24 h did not change DNA tail intensity in V79 cells (Figure 5).

Effects of DMSA/Ag_2S QDs on the expressions of apoptotic genes

The mRNA expression levels of *p53*, *caspase-3*, *caspase-9*, *Bax*, *Bcl-2*, and *survivin* genes (apoptotic markers) in V79 cells treated with DMSA/Ag_2S QDs at concentrations of 125, 250, 500, and 1000 µg/mL for 24 h was analyzed by RT-PCR assay.

The results demonstrated that the mRNA expression levels of apoptotic genes *p53, caspase-3, caspase-9,* and *Bax* were up-regulated, while the expressions of anti-apoptotic genes *Bcl-2* and *survivin* were down-regulated in V79 cells treated with the highest concentration of DMSA/Ag_2S QDs (1000 µg/mL) ($p<0.05$) (Figure 6). No significant changes were observed in lower concentrations. The ratio of *Bax/Bcl-2* gene expression levels in the cells treated with DMSA/Ag_2S QDs (Figure 7) suggests that these two genes may play a significant role in the pathway of DMSA/Ag_2S QDs via apoptosis.

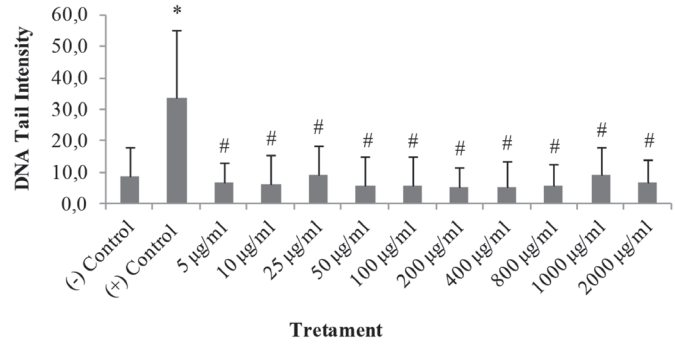

Figure 4. DNA damage expressed as tail intensity in the V79 cells treated with DMSA/Ag_2S QDs. Results were given as the mean ± standard deviation. Differences between the means of data were compared by one-way analysis of variance and post hoc analysis of group differences by least significant difference test. *$p<0.05$, significantly different from the negative control. #$p<0.05$, significantly different from the positive control. Negative control (1% PBS), positive control (50 µM H_2O_2)

Ag_2S: Silver sulfide, QDs: Quantum dots, DMSA: Meso-2,3-dimercaptosuccinic acid, PBS: Phosphate buffered saline

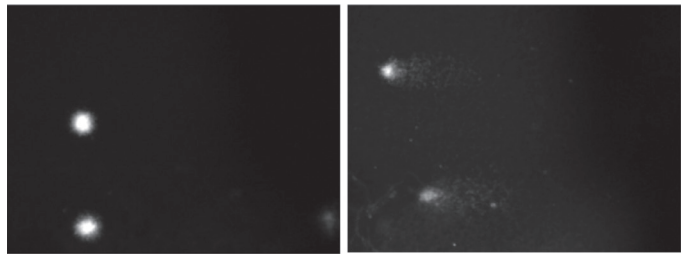

Figure 5. The comet microscopic images of V79 cells. (a) Undamaged cells treated with DMSA/Ag_2S QDs and (b) damaged cells treated with 50 µM H_2O_2 were examined at 400× magnification

Ag_2S: Silver sulfide, QDs: Quantum dots, DMSA: Meso-2,3-dimercaptosuccinic acid

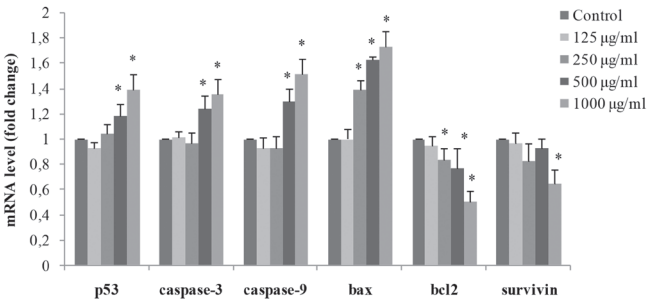

Figure 6. DMSA/Ag_2S QDs-induced apoptosis in V79 cells. Cells were exposed to DMSA/Ag_2S QDs at the dosages of 0, 125, 250, 500, and 1000 µg/mL for 24 h. At the end of exposure, mRNA levels of the *p53, caspase-3, caspase-9, Bax, Bcl2,* and *survivin* genes were measured as described in the Materials and Methods. Results were given as the mean ± standard deviation. The real-time polymerase chain reaction (RT PCR) arrays were analyzed by t-test. Significance in the PCR array was determined based on fold change from the control ΔΔCt value. *Significant difference as compared to the negative control ($p<0.05$). Negative control (1% PBS)

Ag_2S: Silver sulfide, QDs: Quantum dots, DMSA: Meso-2,3-dimercaptosuccinic acid, PCR: Polymerase chain reaction, PBS: Phosphate buffered saline

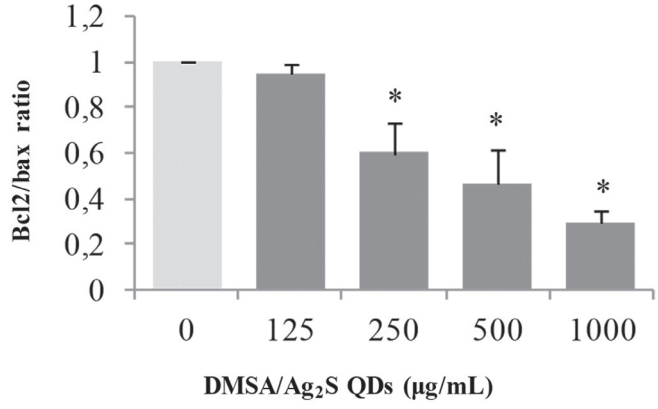

Figure 7. The ratio of *Bcl2/Bax* mRNA in V79 cells. Cells were exposed to DMSA/Ag_2S QDs at the dosages of 0, 125, 250, 500, and 1000 µg/mL for 24 h. *Significant difference as compared to the negative control ($p<0.05$). Negative control (1% PBS)

Ag_2S: Silver sulfide, QDs: Quantum dots, DMSA: Meso-2,3-dimercaptosuccinic acid, PBS: Phosphate buffered saline

DISCUSSION

There has been increasing concern regarding the toxicity of QDs, but further effort is needed to make them safe for biomedical application.[46] The toxic effects of different QDs have already been investigated *in vitro*[34,47-51] as well as *in vivo.*[50,52] QDs are suggested to be cytotoxic and/or to change gene expression[53] and the cores and coatings of QDs may be responsible for their toxicity.[54] Ag_2S QDs were considered to be much less toxic than QDs such as PbSe, PbS, and CdHgTe QDs, because of the lack of toxic metals, such as Pb, Hg, and Cd. Ag_2S QDs are promising fluorescent probes with both bright photoluminescence in the NIR and high biocompatibility, making them highly selective in *in vitro* targeting and imaging of different cell lines.[55] Ag_2S QDs are reported to have no significant effects in altering cell viability, triggering apoptosis or necrosis, forming reactive oxygen species (ROS), or causing DNA damage in *in vitro* toxicity studies.[38,55]

In recent years NP applications towards cell apoptosis have been an increasing focus. Unfortunately, such wide use may pose an unwanted threat to human health and so there is a need for a precise analysis of NP cytotoxicity in living cells. An understanding of the exact role their properties (size, shapes, surface charges, dispersion/agglomeration status) play in the decision about NP safety and suitability is necessary. In addition, some aspects of surface modification may be able to reduce the bioreactivity of NPs, thus alleviating their toxicities in certain circumstances. This may provide a way to design even more effective particles of minimum undesired toxicity.

In the present study, it was aimed to evaluate the cytotoxic, genotoxic, and apoptotic potentials of DMSA/Ag_2S QDs in the V79 cell line. We performed MTT and NRU cytotoxicity assays, since they are generally used tests to determine the cytotoxicity of NPs in different cell lines.[56-59] These assays differ depending on the different mechanisms leading to cell death. Therefore, it is important to check nanotoxicity with different protocols. The NRU assay is a colorimetric assay measuring the uptake of dye by viable cells and its accumulation in functional lysosomes, while the MTT assay is based on the enzymatic conversion of MTT in the mitochondria.[60] The lung fibroblast V79 cell line was used in our experiment. The rationale for choosing this cell line is that it has been widely studied in many nanocytotoxicity and nanogenotoxicity assays, because of its excellent properties in colony formation and also its high sensitivity to many chemicals.[61-65] The question of dose becomes important when comparing studies and when developing predictive models of nanoparticle toxicity. This is very important when comparing *in vitro* and *in vivo* studies, where physicochemical parameters make simple comparisons difficult. Consistent with the previous studies,[61-65] 24 h of exposure was selected to be the optimal time for measurements of the effects of NPs on cell viability. It has been reported that rather high concentrations of NM solutions are used in *in vitro* studies (30 to 400 µg/mL) in the literature.[66] There are no cytotoxicity studies for the doses of DMSA/Ag_2S in V79 cells, and therefore we used wide concentration ranges of DMSA/Ag_2S QDs (0-2000 µg/mL).

In our study, DMSA/Ag_2S QDs reduced cell viability above 400 µg/mL using the MTT assay and above 800 µg/mL using the NRU assay, indicating dose-dependent toxicity in both assays. MTT seems to be more sensitive in detecting changes in viability at low concentrations.[67] In both the MTT and NRU assays, DMSA alone did not significantly induce cell death in the same concentration range between 5 and 2000 µg/mL. It seems that the coating material may prevent cytotoxicity. The biocompatibility of DMSA coupled with the extremely low solubility of Ag_2S core preventing release of high concentration of Ag^+ from the core accounts for the biocompatibility of DMSA/Ag_2S at least in short-term exposure. Munari et al.[54] reported that methyl polyethylene glycol-coated Ag_2S (0.01-50 µg/mL) showed neither genotoxic nor cytotoxic effects.

It is important to use the appropriate method to measure the cytotoxicity of interest without false-negative or -positive misconstruction of the result. The MTT and NRU assays

may sometimes suffer from severe interferences caused by interaction of metallic NPs with assay reagents. Serious consideration is critical to obtain reliable and realistic data.[68] Interference with analytical techniques should be considered in terms of NP intrinsic fluorescence/absorbance and interactions between NPs and assay components. Due to the unique physicochemical properties and increased reactivity of NPs, there is a high potential for these materials to interfere with spectrophotometric and spectrofluorimetric assays. NPs can bind to proteins and dyes and alter their structure and/or function, and it is probable that this process occurs in common toxicity assays. Aluminum NPs showed a strong interaction with the MTT dye, causing significant misreading of the cell viability data.[69,70] Some NPs (iron/graphite magnetic particles, super-paramagnetic magnetite/silica NPs, bare and PEGylated silica NPs, and magnetic composites magnetite/FAU zeolite) in culture medium in the absence of cells have the same wavelength used in MTT assays at 525 nm. This absorbance increases with the NP concentration and can greatly interfere with MTT assay results.[71] However, in our study DMSA/Ag_2S QDs had the emission maximum at 870 nm with broad absorption up to 800 nm. In the MTT and NRU assays the absorbance was 570 nm and 540 nm, respectively. DMSA/Ag_2S QDs appear not to interact with MTT reagent, and therefore there is no absorbance interference.

The comet assay is a sensitive method to detect DNA strand breaks as well as oxidatively damaged DNA at single cell level. The effect of NPs to cause DNA damage is an important issue in mutations and carcinogenesis. Oxidative stress but also other mechanisms may also be involved in the genotoxicity of NPs, including direct NP–DNA interactions and disturbance of the mitotic spindle and its components.[72,73] In our study, DMSA/Ag_2S QD treatments (5-2000 µg/mL) for 24 h did not increase DNA tail intensity in V79 cells, which may indicate no genotoxic effects. The biocompatibility of Ag_2S QDs in the mouse fibroblast L929 cell line, including cell proliferation, cell apoptosis/necrosis, production of ROS, and DNA damage using the comet assay, was investigated by Zhang et al.[55] in a study comparable with ours. They used different Ag_2S QDs with different targeting ligands including dihydrolipoic acid and poly(ethylene glycol) (PEG). The proliferation, ROS production, and DNA damage of L929 cells treated with 6.25, 12.5, 25, 50, and 100 µg/mL Ag_2S QDs for 72 h were not significantly different from those of the negative control. The results presenting negligible toxicity of Ag_2S QDs at concentrations up to 100 µg/mL show that Ag_2S QDs are highly biocompatible in their study. Ag_2S QDs did not interfere with cell proliferation, which makes them suitable for use in the labeling of *in vitro* systems. These observations illustrated the biocompatible nature of Ag_2S without side effects on cell proliferation. Previous studies confirmed that some QDs have high biocompatibilities and low toxicities.[74-76] The coating material may be suggested to reduce cytotoxicity. Consistent with our study, Jebali et al.[77] (2014) reported that free fatty acids-coated Ag NPs had less toxicity, higher uptake, and less ROS generation than unbound Ag NPs. Hocaoglu et al.[78] showed the biocompatibility of 2-mercaptopropionic acid/Ag_2S QDs even at the highest concentration of 600 µg/mL in NIH/3T3 cells after 24 h incubation using the XTT assay. Hocaoglu et al.[38] also showed that DMSA/Ag_2S QDs did not reduce cell viability up to 200 µg/mL in HeLa cells and showed only 20% reduction in cell viability of 3T3 NIH cells over 24 h.

Apoptosis, via extracellular or intracellular signals, triggers the onset of a signaling cascade with characteristic biochemical and cytological signatures with nuclear condensation and DNA fragmentation.[79] Several genes are known to sense DNA damage and apoptosis. In the presence of DNA damage or cellular stress, the p53 protein triggers cell-cycle arrest to provide time for the damage to be repaired or for self-mediated apoptosis.[16] The p53 gene maintains genomic stability via activating cell cycle checkpoints, DNA repair, and apoptosis.[80] Survivin, described as an inhibitor of caspase-9 and a member of the family of inhibitors of apoptotic proteins, functions as a key regulator of mitosis and programmed cell death. Survivin has been reported to play an important role in both cell proliferation and apoptosis.[17] Initially, survivin gene expression is transcriptionally repressed by wild-type p53 and can be deregulated in cancer by several mechanisms, including gene amplification, hypomethylation, increased promoter activity, and loss of p53 function.[81] Downregulation of survivin may cause a cell-cycle defect that leads to apoptosis. The Bax and Bcl-2 proteins regulate apoptotic pathways. The Bcl-2 protein has an antiapoptotic activity, while Bax has a pro-apoptotic effect.[18] The ratio of Bax/Bcl-2 proteins represents a cell death switch, which determines the life or death of cells in response to an apoptotic stimulus; an increased Bax/Bcl-2 ratio decreases the cellular resistance to apoptotic stimuli, leading to apoptosis. It is crucial in mitochondrial outer-membrane permeabilization and the release of cytochrome C in the cytosol.[19,82,83] Moreover, destabilization of mitochondrial integrity by apoptotic stimuli precedes activation of caspases, leading to apoptosis.[84,85] Caspases, essential in cellular DNA damage and apoptosis, are known to play a vital role in both the initiation and execution of apoptosis in many cells.[86]

The transcriptional data on modulation of p53 and Bax/Bcl-2 ratio and release of caspases have strengthened the role of DMSA/Ag_2S QDs in inducing mitochondrial dependent apoptotic pathways. The main intrinsic pathway is characterized by mitochondrial dysfunction, with the release of cytochrome c activation of caspase-9, and subsequently of caspase-3 enzyme.[87,88] Typically, p53 is activated when DNA damage occurs or cells are stressed; p53 is then translocated to the nucleus, where it can induce pro-apoptotic gene expression on the mitochondrial membrane, activate the effector caspases, and accelerate cell death.[88,89] Survivin inhibition induces the activation of caspase-3 and caspase-9 enzymes.[89-91] Taken together, up-regulation of p53 and down-regulation of survivin lead to activation of pro-apoptotic members of the Bcl-2 family. This includes Bax, inducing permeabilization of the outer mitochondrial membrane, which releases soluble proteins from the intermembrane space into the cytosol, where they promote caspase activation.[85,92] The expression of antiapototic protein Bcl-2 was significantly lower, and the expression of pro-apoptotic protein Bax was significantly higher in cells exposed

DMSA/Ag_2S QDs, suggesting that these genes could be excellent molecular biomarkers to assess the apoptotic response of NPs. In our study, no significant changes in mRNA expression levels were observed between 125 and 500 µg/mL, but a clear effect on apoptotic/antiapoptotic gene expression levels was detected at the dose of 1000 µg/mL. The mRNA expression levels of apoptotic genes p53, caspase-3, caspase-9, and Bax were up-regulated, while the expressions of anti-apoptotic genes Bcl-2 and survivin were down-regulated in V79 cells treated with the highest concentration of 1000 µg/mL of DMSA/Ag_2S QDs. The results show that the related gene expression levels may change only at a very high cytotoxic dose, indicating that DMSA/Ag_2S QDs may lead to cell death via apoptotic pathways at very high doses.

CONCLUSIONS

In our study, the potential cytotoxic, genotoxic, and apoptotic effects of DMSA/Ag_2S QDs *in vitro* were evaluated. Ag_2S QDs coated with DMSA had high biocompatibility and low toxicity, since heavy metal-related cytotoxicity was eliminated by using quite a biocompatible and insoluble Ag_2S semiconductor core.

Our data show that DMSA/Ag_2S QDs have neither cytotoxic nor genotoxic effects in V79 cells in medically relevant doses. They may induce apoptosis via p53, survivin, Bax/Bcl-2, and caspase pathways at high dose. The underlying mechanisms of DMSA/Ag_2S QDs should be confirmed by additional experiments in order to prove our results. Further investigation is needed to determine whether *in vivo* exposure consequences may exist for DMSA/Ag_2S QDs application and also to make QDs safe for widespread use.

ACKNOWLEDGEMENTS

This work was supported by TÜBİTAK (Project Number: 114S861).

Conflict of Interest: No conflict of interest was declared by the authors.

REFERENCES

1. Rothenfluh DA, Bermudez H, O'Neil CP, Hubbell JA. Biofunctional polymer nanoparticles for intra-articular targeting and retention in cartilage. Nat Mater. 2008;7:248-254.
2. Kostarelos K, Bianco A, Prato M. Promises, facts and challenges for carbon nanotubes in imaging and therapeutics. Nat Nanotechnol. 2009;4:627-633.
3. Michalet X, Pinaud FF, Bentolila LA, Tsay JM, Doose S, Li JJ, Sundaresan G, Wu AM, Gambhir SS, Weiss S. Quantum dots for live cells, *in vivo* imaging, and diagnostics. Science. 2005;307:538-544.
4. Chen Z, Tabakman SM, Goodwin AP, Kattah MG, Daranciang D, Wang X, Zhang G, Li X, Liu Z, Utz PJ, Jiang K, Fan S, Dai H. Protein microarrays with carbon nanotubes as multicolor Raman labels. Nat Biotechnol. 2008;26:1285-1292.
5. Qian X, Peng XH, Ansari DO, Yin-Goen Q, Chen GZ, Shin DM, Yang L, Young AN, Wang MD, Nie S. *In vivo* tumor targeting and spectroscopic detection with surface-enhanced Raman nanoparticle tags. Nat Biotechnol. 2008;26:83-90.
6. He Y, Fan C, Lee ST. Silicon nanostructures for bioapplications. Nano Today. 2010;5:282-295.
7. McAuliffe ME, Perry MJ. Are nanoparticles potential male reproductive toxicants? A literature review. Nanotoxicology. 2007;1:204-210.
8. Nel A, Xia T, Mädler L, Li N. Toxic potential of materials at the nanolevel. Science. 2006;311:622-627.
9. Oberdörster G, Oberdörster E, Oberdörster J. Nanotoxicology: An emerging discipline evolving from studies of ultrafine particles. Environ Health Perspect. 2005;113:823-839.
10. Singh SK, Kulkarni PP, Dash D. Biomedical Applications of Nanomaterials: An Overview. Bio Nanotechnology: A Revolution in Food. Biomedical and Health Sciences. 2013:1-32.
11. Chan WC, Maxwell DJ, Gao X, Bailey RE, Han M, Nie S. Luminescent quantum dots for multiplexed biological detection and imaging. Curr Opin Biotechnol. 2002;13:40-46.
12. Klimov VI. Spectral and dynamical properties of multiexcitons in semiconductor nanocrystals. Annu Rev Phys Chem. 2007;58:635-673.
13. Murphy CJ, Coffer JL. Quantum dots: A primer. Appl Spectrosc. 2002;56:16-27.
14. Bruchez Jr M, Moronne M, Gin P, Weiss S, Alivisatos AP. Semiconductor nanocrystals as fluorescent biological labels. Science. 1998;281:2013-2016.
15. Chan WCW, Nie S. Quantum dot bioconjugates for ultrasensitive nonisotopic detection. Science. 1998;281:2016-2018.
16. Medintz I. Universal tools for biomolecular attachment to surfaces. Nat Mater. 2006;5:842.
17. Wagner MK, Li F, Li J, Li XF, Le XC. Use of quantum dots in the development of assays for cancer biomarkers. Anal Bioanal Chem. 2010;397:3213-3224.
18. Mattoussi H, Palui G, Na HB. Luminescent quantum dots as platforms for probing *in vitro* and *in vivo* biological processes. Adv Drug Deliv Rev.2012;64:138-166.
19. Frigerio C, Ribeiro DS, Rodrigues SS, Abreu VL, Barbosa JA, Prior JA, Marques KL, Santos JL. Application of quantum dots as analytical tools in automated chemical analysis: A review. Anal Chim Acta. 2012;735:9-22.
20. Frasco MF, Chaniotakis N. Bioconjugated quantum dots as fluorescent probes for bioanalytical applications. Anal Bioanal Chem. 2010;396:229-240.
21. Wu X, Liu H, Liu J, Haley KN, Treadway JA, Larson JP, Ge N, Peale F, Bruchez MP. Immunofluorescent labeling of cancer marker Her2 and other cellular targets with semiconductor quantum dots. Nat Biotechnol. 2003;21:41-46.
22. Algar WR, Prasuhn DE, Stewart MH, Jennings TL, Blanco-Canosa JB, Dawson PE, Medintz IL. The controlled display of biomolecules on nanoparticles: a challenge suited to bioorthogonal chemistry. Bioconjug Chem. 2011;22:825-858.
23. Rosenthal SJ, Chang JC, Kovtun O, McBride JR, Tomlinson ID. Biocompatible quantum dots for biological applications. Chem Biol. 2011;18:10-24.
24. Petryayeva E, Algar WR, Medintz IL. Quantum dots in bioanalysis: A review of applications across various platforms for fluorescence spectroscopy and imaging. Appl Spectrosc. 2013;67:215-252.

25. Alivisatos AP. Semiconductor clusters, nanocrystals, and quantum dots. Science. 1996;271:933-937.
26. Weller H. Quantum size colloids: From size-dependent properties of discrete particles to self-organized superstructures. Curr Opin Colloid Interface Sci. 1998;3:194-199.
27. Dabbousi BO, Rodriguez-Viejo J, Mikulec FV, Heine JR, Mattoussi H, Ober R, Jensen KF, Bawendi MG. (CdSe)ZnS core-shell quantum dots: Synthesis and characterization of a size series of highly luminescent nanocrystallites. J Phys Chem B. 1997;101:9463-9475.
28. Hines MA, Guyot-Sionnest P. Synthesis and characterization of strongly luminescing ZnS-capped CdSe nanocrystals. J Phy Chem. 1996;100:468-471.
29. Hardman R. A toxicologic review of quantum dots: Toxicity depends on physicochemical and environmental factors. Environ Health Perspect. 2006;114:165-172.
30. Kim S, Lim YT, Soltesz EG, De Grand AM, Lee J, Nakayama A, Parker JA, Mihaljevic T, Laurence RG, Dor DM, Cohn LH, Bawendi MG, Frangioni JV. Near-infrared fluorescent type II quantum dots for sentinel lymph node mapping. Nat Biotechnol. 2004;22:93-97.
31. Chan WH, Shiao NH, Lu PZ. CdSe quantum dots induce apoptosis in human neuroblastoma cells via mitochondrial-dependent pathways and inhibition of survival signals. Toxicol Let. 2006;167:191-200.
32. Chen N, He Y, Su Y, Li X, Huang Q, Wang H, Zhang X, Tai R, Fan C. The cytotoxicity of cadmium-based quantum dots. Biomaterials. 2012;33:1238-1244.
33. Cho SJ, Maysinger D, Jain M, Röder B, Hackbarth S, Winnik FM. Long-term exposure to CdTe quantum dots causes functional impairments in live cells. Langmuir. 2007;23:1974-1980.
34. Kirchner C, Liedl T, Kudera S, Pellegrino T, Muñoz Javier A, Gaub HE, Stölzle S, Fertig N, Parak WJ. Cytotoxicity of colloidal CdSe and CdSe/ZnS nanoparticles. Nano Lett. 2005;5:331-338.
35. Li KG, Chen JT, Bai SS, Wen X, Song SY, Yu Q, Li J, Wang YQ. Intracellular oxidative stress and cadmium ions release induce cytotoxicity of unmodified cadmium sulfide quantum dots. Toxicol *In Vitro*. 2009;23:1007-1013.
36. Male KB, Lachance B, Hrapovic S, Sunahara G, Luong JHT. Assessment of cytotoxicity of quantum dots and gold nanoparticles using cell-based impedance spectroscopy. Anal Chem. 2008;80:5487-5493.
37. Gao J, Chen X, Cheng Z. Near-infrared quantum dots as optical probes for tumor imaging. Curr Top Med Chem. 2010;10:1147-1157.
38. Hocaoglu I, Demir F, Birer O, Kiraz A, Sevrin C, Grandfils C, Acar HY. Emission tunable, cyto/hemocompatible, near-IR-emitting Ag2S quantum dots by aqueous decomposition of DMSA. Nanoscale. 2014;6:11921-11931.
39. Rao BS, Shanbhoge R, Rao BN, Adiga SK, Upadhya D, Aithal BK, Kumar MR. Preventive efficacy of hydroalcoholic extract of Cymbopogon citratus against radiation-induced DNA damage on V79 cells and free radical scavenging ability against radicals generated *in vitro*. Hum Exp Toxicol. 2009;28:195-202.
40. Mosmann T. Rapid colorimetric assay for cellular growth and survival: Application to proliferation and cytotoxicity assays. J Immunol Methods. 1983;65:55-63.
41. Hansen MB, Nielsen SE, Berg K. Re-examination and further development of a precise and rapid dye method for measuring cell growth/cell kill. J Immunol Methods. 1989;119:203-210.
42. Kuźma Ł, Wysokińska H, Rózalski M, Krajewska U, Kisiel W. An unusual taxodione derivative from hairy roots of Salvia austriaca. Fitoterapia. 2012;83:770-773.
43. Di Virgilio AL, Iwami K, Wätjen W, Kahl R, Degen GH. Genotoxicity of the isoflavones genistein, daidzein and equol in V79 cells. Toxicol Lett. 2004;151:1511-1562.
44. Saquib Q, Al-Khedhairy AA, Siddiqui MA, Abou-Tarboush FM, Azam A, Musarrat J. Titanium dioxide nanoparticles induced cytotoxicity, oxidative stress and DNA damage in human amnion epithelial (WISH) cells. Toxicol *In Vitro*. 2012;26:351-561.
45. Ahamed M, Akhtar MJ, Siddiqui MA, Ahmad J, Musarrat J, Al-Khedhairy AA, AlSalhi MS, Alrokayan SA. Oxidative stress mediated apoptosis induced by nickel ferrite nanoparticles in cultured A549 cells. Toxicology. 2011;283:101-108.
46. Winnik FM, Maysinger D. Quantum dot cytotoxicity and ways to reduce it. Acc Chem Res. 2013;46:672-680.
47. Manshian BB, Soenen SJ, Brown A, Hondow N, Wills J, Jenkins GJ, Doak SH. Genotoxic capacity of Cd/Se semiconductor quantum dots with differing surface chemistries. Mutagenesis. 2016;31:97-106.
48. Smith WE, Brownell J, White CC, Afsharinejad Z, Tsai J, Hu X, Polyak SJ, Gao X, Kavanagh TJ, Eaton DL. *In vitro* toxicity assessment of amphiphillic polymer-coated CdSe/ZnS quantum dots in two human liver cell models. ACS Nano. 2012;6:9475-9484.
49. Smulders S, Luyts K, Brabants G, Golanski L, Martens J, Vanoirbeek J, Hoet PH. Toxicity of nanoparticles embedded in paints compared to pristine nanoparticles, *in vitro* study. Toxicol Lett. 2015;232:333-339.
50. Smulders S, Luyts K, Brabants G, Landuyt KV, Kirschhock C, Smolders E, Golanski L, Vanoirbeek J, Hoet PH. Toxicity of nanoparticles embedded in paints compared with pristine nanoparticles in mice. Toxicol Sci. 2014;141:132-140.
51. Soenen SJ, Manshian BB, Himmelreich U, Demeester J, Braeckmans K, De Smedt SC. The performance of gradient alloy quantum dots in cell labeling. Biomaterials. 2014;35:7249-7258.
52. Derfus AM, Chan WCW, Bhatia SN. Probing the Cytotoxicity of Semiconductor Quantum Dots. Nano Lett. 2004;4:11-18.
53. Choi O, Clevenger TE, Deng B, Surampalli RY, Ross Jr L, Hu Z. Role of sulfide and ligand strength in controlling nanosilver toxicity. Water Res. 2009;43:1879-1886.
54. Munari M, Sturve J, Frenzilli G, Sanders MB, Brunelli A, Marcomini A, Nigro M, Lyons BP. Genotoxic effects of CdS quantum dots and Ag_2S nanoparticles in fish cell lines (RTG-2). Mutat Res Genet Toxicol Environ Mutagen. 2014;776:89-93.
55. Zhang Y, Hong G, Zhang Y, Chen G, Li F, Dai H, Wang Q. Ag_2S quantum dot: a bright and biocompatible fluorescent nanoprobe in the second near-infrared window. ACS Nano. 2012;6:3695-3702.
56. Akhtar MJ, Kumar S, Murthy RC, Ashquin M, Khan MI, Patil G, Ahmad I. The primary role of iron-mediated lipid peroxidation in the differential cytotoxicity caused by two varieties of talc nanoparticles on A549 cells and lipid peroxidation inhibitory effect exerted by ascorbic acid. Toxicol *In Vitro*. 2010;24:1139-1147.
57. Barillet S, Jugan ML, Laye M, Leconte Y, Herlin-Boime N, Reynaud C, Carrière M. *In vitro* evaluation of SiC nanoparticles impact on A549 pulmonary cells: cyto-, genotoxicity and oxidative stress. Toxicol Lett. 2010;198:324-330.

58. Mahmoudi M, Simchi A, Milani AS, Stroeve P. Cell toxicity of superparamagnetic iron oxide nanoparticles. J Colloid Interface Sci. 2009;336:510-508.

59. Sharma V, Shukla RK, Saxena N, Parmar D, Das M, Dhawan A. DNA damaging potential of zinc oxide nanoparticles in human epidermal cells. Toxicol Lett. 2009;185:211-218.

60. Fotakis G, imbrell JA. *In vitro* cytotoxicity assays: Comparison of LDH, neutral red, MTT and protein assay in hepatoma cell lines following exposure to cadmium chloride. Toxicol Lett. 2006;160:171-177.

61. Chaung W, Mi LJ, Boorstein RJ. The p53 status of Chinese hamster V79 cells frequently used for studies on DNA damage and DNA repair. Nucleic Acids Res. 1997;25:992-994.

62. Chen Z, Wang Y, Ba T, Li Y, Pu J, Chen T, Song Y, Gu Y, Qian Q, Yang J, Jia G. Genotoxic evaluation of titanium dioxide nanoparticles in vivo and *in vitro*. Toxicol Lett. 2014;226:314-319.

63. Darne C, Terzetti F, Coulais C, Fontana C, Binet S, Gaté L, Guichard Y. Cytotoxicity and genotoxicity of panel of single- and multiwalled carbon nanotubes: *in vitro* effects on normal Syrian hamster embryo and immortalized v79 hamster lung cells. J Toxicol. 2014;2014:872195.

64. Guichard Y, Fontana C, Chavinier E, Terzetti F, Gaté L, Binet S, Darne C. Cytotoxic and genotoxic evaluation of different synthetic amorphous silica nanomaterials in the V79 cell line. Toxicol Ind Health. 2016;32:1639-1650.

65. Kang SJ, Kim BM, Lee YJ, Chung HW. Titanium dioxide nanoparticles trigger p53-mediated damage response in peripheral blood lymphocytes. Environ Mol Mutagen. 2008;49:399-405.

66. Gangwal S, Brown JS, Wang A, Houck KA, Dix DJ, Kavlock RJ, Hubal EA. Informing selection of nanomaterial concentrations for ToxCast *in vitro* testing based on occupational exposure potential. Environ Health Perspect. 2011;119:1539-1546.

67. Nogueira DR, Mitjans M, Infante MR, Vinardell MP. Comparative sensitivity of tumor and non-tumor cell lines as a reliable approach for *in vitro* cytotoxicity screening of lysine-based surfactants with potential pharmaceutical applications. Int J Pharm. 2011;420:51-58.

68. Kong B, Seog JH, Graham LM, Lee SB. Experimental considerations on the cytotoxicity of nanoparticles. Nanomedicine (Lond). 2011;6:929-941.

69. Maccormack TJ, Clark RJ, Dang MK, Ma G, Kelly JA, Veinot JG, Goss GG. Inhibition of enzyme activity by nanomaterials: Potential mechanisms and implications for nanotoxicity testing. Nanotoxicology. 2012;6:514-525.

70. Monteiro-Riviere NA, Oldenburg SJ, Inman AO. Interactions of aluminum nanoparticles with human epidermal keratinocytes. J Appl Toxicol. 2010;30:276-285.

71. Díaz B, Sánchez-Espinel C, Arruebo M, Faro J, de Miguel E, Magadán S, Yagüe C, Fernández-Pacheco R, Ibarra MR, Santamaría J, González-Fernández A. Assessing Methods for Blood Cell Cytotoxic Responses to Inorganic Nanoparticles and Nanoparticle Aggregates. Small. 2008;4:2025-2034.

72. Karlsson HL, Di Bucchianico S, Collins AR, Dusinska M. Can the comet assay be used reliably to detect nanoparticle-induced genotoxicity? Environ Mol Mutagen. 2015;56:82-96.

73. Shukla RK, Sharma V, Pandey AK, Singh S, Sultana S, Dhawan A. ROS-mediated genotoxicity induced by titanium dioxide nanoparticles in human epidermal cells. Toxicol *In Vitro*. 2011;25:231-241.

74. Dong B, Li C, Chen G, Chen G, Zhang Y, Zhang Y, Deng M, Wang Q. Facile Synthesis of Highly Photoluminescent Ag_2Se Quantum Dots as a New Fluorescent Probe in the Second Near-Infrared Window for *in vivo* Imaging. Chem Mater. 2013;25:2503-2509.

75. Gu Y-P, Cui R, Zhang Z-L, Xie Z-X, Pang D-W. Ultrasmall Near-Infrared Ag2Se Quantum Dots with Tunable Fluorescence for *in vivo* Imaging. J Am Chem Soc. 2012;134:79-82.

76. Tang H, Yang ST, Yang YF, Ke DM, Liu JH, Chen X, Wang H, Liu Y. Blood Clearance, Distribution, Transformation, Excretion, and Toxicity of Near-Infrared Quantum Dots Ag2Se in Mice. ACS Appl Mater Interfaces. 2016;8:17859-17869.

77. Jebali A, Hekmatimoghaddam S, Kazemi B. The cytotoxicity of silver nanoparticles coated with different free fatty acids on the Balb/c macrophages: an *in vitro* study. Drug Chem Toxicol. 2014;37:433-439.

78. Hocaoglu I, Çizmeciyan MN, Erdem R, Ozen C, Kurt A, Sennaroglu A, Acar HY. Development of highly luminescent and cytocompatible near-IR-emitting aqueous Ag2S quantum dots. J Mater Chem. 2012;22:14674-14681.

79. Gopinath P, Gogoi SK, Sanpui P, Paul A, Chattopadhyay A, Ghosh SS. Signaling gene cascade in silver nanoparticle induced apoptosis. Colloids Surf B Biointerfaces. 2010;77:240-245.

80. Sherr CJ. Principles of Tumor Suppression. Cell. 2004;116:235-46.

81. Ryan BM, O'Donovan N, Duffy MJ. Survivin: A new target for anti-cancer therapy. Cancer Treat Rev. 2009;35:553-562.

82. Chougule M, Patel AR, Sachdeva P, Jackson T, Singh M. Anticancer activity of Noscapine, an opioid alkaloid in combination with Cisplatin in human non-small cell lung cancer. Lung Cancer. 2011;71:271-282.

83. Gao C, Wang AY. Significance of Increased Apoptosis and Bax Expression in Human Small Intestinal Adenocarcinoma. J Histochem Cytochem. 2009;57:1139-1148.

84. Timmer JC and Salvesen GS. Caspase substrates. Cell Death And Differentiation. Cell Death Differ. 2007;14:66-72

85. Youle RJ and Strasser A. The BCL-2 protein family: opposing activities that mediate cell death. Nat Rev Mol Cell Biol. 2008;9:47-59

86. Jänicke RU, Sprengart ML, Wati MR, Porter AG. Caspase-3 is required for DNA fragmentation and morphological changes associated with apoptosis. J Biol Chem. 1998;273:9357-9360.

87. Porter AG, Jänicke RU. Emerging roles of caspase-3 in apoptosis. Cell Death Differ. 1999;6:99-104.

88. Saquib Q, Al-Khedhairy AA, Ahmad J, Siddiqui MA, Dwivedi S, Khan ST, Musarrat. Zinc ferrite nanoparticles activate IL-1b, NFKB1, CCL21 and NOS2 signaling to induce mitochondrial dependent intrinsic apoptotic pathway in WISH cells. Toxicol Appl Pharmacol. 2013;273:289-297.

89. Farnebo M, Bykov VJ, Wiman KG. The p53 tumor suppressor: A master regulator of diverse cellular processes and therapeutic target in cancer. Biochem Biophys Res Commun. 2010;396:85-89.

90. Blanc-Brude OP, Yu J, Simosa H, Conte MS, Sessa WC, Altieri DC. Inhibitor of apoptosis protein survivin regulates vascular injury. Nat Med. 2002;8:987-994

91. Marusawa H, Matsuzawa S, Welsh K, Zou H, Armstrong R, Tamm I, Reed JC. HBXIP functions as a cofactor of survivin in apoptosis suppression. EMBO J. 2003;22:2729-2740.

92. Fuentes-Prior P, Salvesen Guy GS. The protein structures that shape caspase activity, specificity, activation and inhibition. Biochem J. 2004;384:201-232.

Turk J Pharm Sci 2019;16(3):292-302
DOI: 10.4274/tjps.galenos.2018.44265

ORIGINAL ARTICLE

Phytochemical Screening and Metallic Ion Content and Its Impact on the Antipsoriasis Activity of Aqueous Leaf Extracts of *Calendula officinalis* and *Phlebodium decumanum* in an Animal Experiment Model

Calendula officinalis ve P*hlebodium decumanum* Sulu Yaprak Ekstreleri Üzerinde Fitokimyasal Tarama, Metalik İyon İçeriği ve Hayvan Deneyi Modelinde Antipsoriasis Etkisi

Kuntal DAS*, Someswar DEB, Tejaswini KARANTH

Krupanidhi College of Pharmacy, Bangalore, India

ABSTRACT

Objectives: The aim of this study was to evaluate the influence of metal ions present in soil as well as in leaf samples of *Calendula officinalis* and *Phlebodium decumanum* for the treatment of psoriasis.

Materials and Methods: To meet the objective, soil and leaf samples were estimated for metal ions by atomic absorption spectrophotometer to determine the influence in antipsoriatic activity. Thereafter imiquimod-induced dermatitis lesions were created in grouped mice. Two plant extracts (aqueous) separately as well as in combinations and standard Retino-A (0.05%) were used. Psoriasis severity index (PSI) was evaluated according to the phenotypic (redness, erythema, and scales) and histological features (epidermal thickness). Further content of phytochemicals in terms of extract was correlated with the effect of psoriasis activity.

Results: We observed redness, erythema, and scales and the histological features and found a progressive reduction ($P<0.05$) in the severity of psoriatic lesions (redness, erythema, and scales) from days 7 to 21 and decreased epidermal thickness in animals treated with combined extracts at a dose of 200 mg/kg b.w. Furthermore, plant samples procured from the Nandi Hills, Bangalore, showed better uptake of metals with respect to Fe (2.05 mg/kg), Cu (0.78 mg/kg), and Zn (1.12 mg/kg), which showed a positive impact on procurement of maximum amount of extracts that further correlated with the activity, indicating a significant reduction in psoriatic lesions.

Conclusion: The results revealed that the significant dose-dependent antipsoriasis activity of combined aqueous extracts of *C. officinalis* and *P. decumanum* as well as metal ions had an impact on the procurement of extracts and said activity.

Key words: Epidermal thickness, correlation, *Calendula officinalis*, *Phlebodium decumanum*, PSI, psoriasis

ÖZ

Amaç: Bu çalışmanın amacı, *Calendula officinalis* ve *Phlebodium decumanum* yaprak örneklerinde, toprakta da bulunan metal iyonlarının psoriazis tedavisi üzerindeki etkilerini değerlendirmektir.

Gereç ve Yöntemler: Bu amaçla, antipsoriatik etkiyi belirlemek üzere toprak ve yaprak örneklerindeki metal iyonları atomik absorpsiyon spektrofotometresi ile tayin edilmiştir. Daha sonra farelerde, imikimod-nedenli dermatit lezyonları oluşturuldu. İki bitki ekstresi (sulu) ayrı ayrı ve karışım halinde uygulanmış ve standart olarak Retino-A (% 0.05) kullanılmıştır. Psoriasis şiddet indeksi (PSI) fenotipik (kızarıklık, eritem ve pullanma) ve histolojik özelliklere (epidermal kalınlık) göre değerlendirilmiştir. Ekstre içindeki fitokimyasalların, sedef hastalığına karşı etki ile korele olduğu belirlendi.

Bulgular: 200 mg/kg dozda ekstre karışımı uygulanan hayvanlarda kızarıklık, eritem, pullanma ve histolojik özelikler izlenmiş, bunun sonucunda psoriatik lezyonlarda 7. günden 21. güne kadar progresif bir azalma ($p<0.05$) ve epidermal kalınlıkta bir azalma gözlenmiştir. Ayrıca, Nandi Hills, Bangalore'den temin edilen bitki numuneleri üzerindeki çalışmada, bitki numuneleri, Fe (2.05 mg/kg), Cu (0.78 mg/kg) ve Zn (1.12 mg/kg) gibi

*Correspondence: E-mail: drkkdsd@gmail.com, Phone: +919632542846 ORCID-ID: orcid.org/0000-0001-6118-5270
Received: 16.04.2018, Accepted: 31.05.2018

metallerin topraktan daha iyi alımının sağlanması sonucunda ekstrelerin daha yüksek miktarda elde edilmesi ile aktivitede bir korelasyon görülmüş ve psoriatik lezyonların anlamlı derecede azaldığı gözlenmiştir.

Sonuç: Sonuçlar, *C. officinalis* ve *P. decumanum* sulu ekstrelerinin doz bağımlı antipsoriasis aktivitesi üzerinde belirgin bir etkisinin olduğunu ve aynı zamanda metal iyonlarının da hem ekstre miktarının hem de aktivitenin arttırılmasında önemli olduğunu göstermiştir.

Anahtar kelimeler: Epidermal kalınlık, korelasyon, *Calendula officinalis*, *Phlebodium decumanum*, PSI, sedef hastalığı

INTRODUCTION

One of the common immune-based chronic autosomal diseases is psoriasis, which may develop in people of any age. It is also known as a genetically influenced inflammatory disease in skin that is identified as salmon-colored plaques covered by loosely adherent scales that are silver white. This disease spreads to the whole body in a couple of days and causes total body erythema with scaling known as erythroderma. The disease most frequently affects the joints like the skin of the elbow, knees, scalp, lumbosacral areas, intergluteal cleft, and glans penis.[1] People are neglecting this dermatitis but it may sometimes be associated with arthritis, myopathy, enteropathy, spondylitic heart disease, diffuse cutaneous and mucosal pustules, and electrolyte disturbances.[2] Hence, appropriate treatment is required to cure psoriasis at root level. A vast number of allopathic drugs are available for the treatment of psoriasis. Some drugs, i.e. lithium, β-blockers, and chloroquine, are provocative factors[3] and many drugs are associated with various side effects. Therefore, currently the importance of using natural herbs is emphasized for the treatment of skin diseases like psoriasis either in combination or alone in different forms. Whole parts of natural plants such as the root, bark, stem, seed, flowers, or leaves are effective for their versatile therapeutic activities. In the present study *Calendula officinalis* and *Phlebodium decumanum* leaves were selected based on the traditional knowledge. *C. officinalis* (CO) (Family: Asteraceae), commonly known as the pot marigold, is abundantly available throughout India and is cultivated in most soils in a sunny climate. The leaves contain carotenoids such as lutein (80%), zeaxanthin (5%), and beta carotene.[4,5] Apart from that, the leaves also include polyphenols, alkaloids, steroids, tannins, and flavonoids.[6] Many applications are reported with the flowers, whereas traditionally the leaves are used for wound healing and treatment of burns and infections, mainly due to the presence of essential phytoconstituents in the leaves. Scientifically the leaves are also stated to have antimicrobial,[7] hepatoprotective,[8] and wound healing activity.[9] *P. decumanum* (PD) (family Polypodiaceae), commonly known as the ornamental fern, is abundantly available in damp regions in many parts of India.[10] The leaves contains many chemicals, i.e. alkaloids; various fatty acids like oleic acid, linoleic acids, linolenic acids, arachidonic acid, eicosapentaenoic acid, and elaidic acid; arabinopyranosides; ecdysone; ecdysterone; juglanin; kaempferols; and melilotoside.[11] Our literature survey revealed the presence of anti-inflammatory,[12] antioxidant,[13] wound healing, immune system improving,[14] antimicrobial, anthelmintic,[10] etc. activity. The therapeutic activities of plant constituents greatly depend on soil fertility, climatic conditions, and content of metal ions in the accumulated plant parts.[15-19]

Many studies have reported various activities based on the effectiveness of either extracts in combinations or with isolated compounds but there are very few reports on the impact of soil fertility and content of soil metal ions and their uptake by the plant foliage on therapeutic efficacy. No such literature is available on the relation with metal ion content and activity of the plants selected in this investigation. Therefore, in the present study *C. officinalis* and *P. decumanum* leaves were selected from the West Bengal and Karnataka zones of India for establishment of effective treatment as well as the impact of foliage metal ions against psoriasis.

MATERIALS AND METHODS

Selection of experimental zones

In the present investigation, the hilly region of Darjeeling, West Bengal, and the Nandi Hills, Bangalore, Karnataka zones were selected for collection of leaf samples of the said plants because of the soil nature and the natural habitat of the plant species. The hilly region's soil is highly acidic, whereas the soil of the Nandi Hills is slightly basic but both are hill areas (Figure 1). The Terai region lies between latitude 26°30′30″ to 27°8′45″ N 88° and 88°56′15″ E longitude, whereas Bangalore

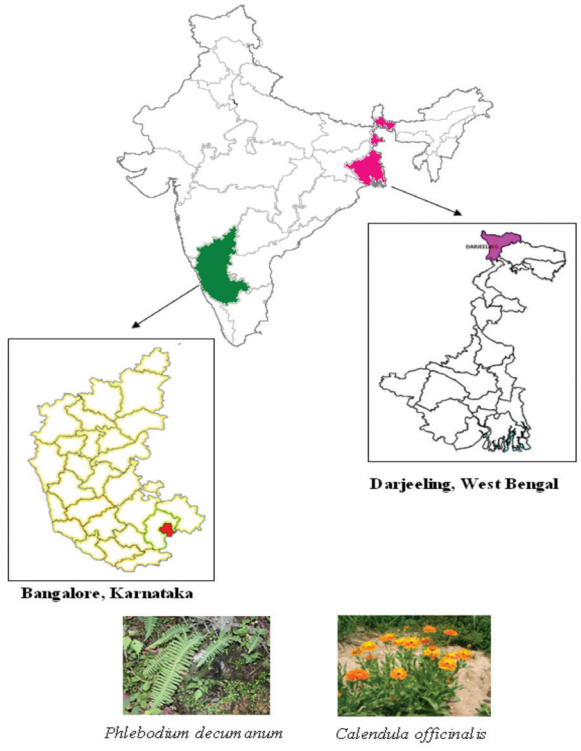

Figure 1. Selection of experimental zones

lies between latitude 12°58′38″ N and longitude 77°35′14″ E in which the Nandi Hills are located at latitude 13.3667° N and longitude 77.6833° E. The average annual rainfall of Darjeeling and Bangalore is about 2547 mm and 870 mm, respectively.

Authentication and preparation of plant samples

The leaves of the said plants were taxonomically identified and authenticated by Dr. Rajasekharan PE, Principal Scientist, Department of Plant Biotechnology, Indian Institute of Horticultural Research, Bangalore. The voucher specimens of both leaves collected from West Bengal and Karnataka (KCP/34/WB-PD/2016-17; KCP/35/WB-CO/2016-17; KCP/36/KAR-PD/2016-17 and KCP/37/KAR-CO/2016-17) have been deposited in the herbarium section of the Pharmacognosy Department of Krupanidhi College of Pharmacy, Bangalore, for future reference.

The leaves were collected in June 2016 from both places and transported in sealed plastic containers to the laboratory for processing. The leaves were cleaned with running tap water and oven dried at 60°C for 2-3 h. Shade drying was not recommended because during the rainy season the moisture content in the environment was high and there was more possibility of microbial growth rather than drying. After oven drying the leaves were blended in a mixer grinder into a coarse powder and separately kept in air tight sealed plastic containers, labeled properly for further investigation.

Analysis of soil samples for metal ion content

Total metals and diethylenetriaminepentaacetic acid (DTPA) extractable metals (iron: Fe; copper: Cu; zinc: Zn; lead: Pb; cadmium: Cd; nickel: Ni; arsenic: As; and chromium: Cr) were determined with the help of an atomic absorption spectrophotometer (AAS, PerkinElmer model: AAnalyst 100; Australia) by acid digestion method. Next 10 g of soil sample was taken in a conical flask and 20 mL of 0.005 M DTPA (0.005 M DTPA; 0.1 M triethanol amine and 0.01 M $CaCl_2$, 2 H_2O) was added to it. Then it was shaken for 2 h on a mechanical shaker and it was filtered with Whatman No. 42 filter paper. Then the filtrate was determined for various metal contents in different soils. Blank samples were also prepared for correction. All the samples were checked by carrying out triplicate analyses for the reproducibility of the method used.

Analysis of leaf samples

Leaf samples were pretreated with concentrated nitric acid in a digestion flask followed by mixing with acid mixtures. Digestion was carried out at 200°C until dense white fumes of H_2SO_4:$HClO_4$ were evolved and finally white residue was obtained. Subsequently the digested samples were diluted with deionized water and the volume made up to 50 mL. Final solutions were analyzed for various heavy metal contents (Cd, Cr, Cu, Fe, Ni, Pb, and Zn) using an AAS (PerkinElmer model: A Analyst 100; Australia). Air acetylene was used as the common oxidant/fuel combination gas in the AAS and the concentration of the above elements was determined using the standard condition. The wavelengths were selected for the analysis based on the concentration ranges of the sample and the linear relation between the absorbance (AU) and concentration of the determined element. Blank samples were also prepared for correction. All the samples were checked by carrying out triplicate analyses for the reproducibility of the method used.

Preparation of plant extracts and their phytochemical screening

Stored coarsely powdered samples (250 g) were used for the preparation of extracts by direct reflux method using distilled water as solvent at 45°C for 8 h. Thereafter extracted liquids were filtered with Whatman No. 1 filter paper and evaporated with a rotary flash evaporator at 45°C and stored in refrigeration condition (at 4°C) in glass bottles for further experimentation. The yield of extracts was calculated and then the presence of various phytochemicals was screened qualitatively by various chemical tests for the detection of constituents like alkaloids, flavonoids, steroids, tannins, glycosides, terpenoids, and others by following standard methods.[20,21]

Selection of animals

Healthy albino mice (50-70 g) obtained from Krupanidhi Pharmacy institutional animal housing facilities were used for the present investigation. The animals were housed in polypropylene cages and were left for 7 days for acclimatization to the animal room and they were kept under controlled conditions (12 h light/dark cycle at 22±2°C) and fed on standard pellet diet and water *ad libitum*. All animals were taken care of ethically as per the guidelines of CPCSEA with approval from the Institutional Animal Ethics Committee (KCP/PCOL/06/2017).

Acute dermal toxicity

Acute dermal toxicity studies were carried out using albino mice in accordance with the Organization for Economic Cooperation and Development guidelines no. 402.[22] The mice (six animals per group) were divided into two groups. The animals' hair was removed from the dorsal portion of the body surface and a dose of 2000 mg/kg body weight for two different extracts was applied. The animals were observed and recorded for changes of redness, erythema, sleep pattern, behavior pattern, and mortality for 14 days. Thereafter a skin irritation test was also carried out with the aqueous extracts over 72 h.

Grouping of animals and experimental method

Based on the toxicity study, the following groupings of animals were carried out (Table 1). Group I is normal (untreated), while group II received standard drug, Retino-A 0.05% (Tretinoin cream U.S.P.) - Janssen-Cilag Pharmaceuticals (Trademark of Johnson & Johnson, USA) in cream form (positive control). The group III to VIII mice were administered a daily topical dose of 62.5 mg of 5% imiquimod cream (IMQ, Aldara; 3M Pharmaceuticals, UK) to a 3 cm×4 cm shaved area on their backs for 7 consecutive days and they were observed for induced psoriasis.

An objective scoring system was applied based on the clinical psoriasis area and severity index.[23] Redness, erythema, and scales were scored independently on a scale from 0 to 4: 0, none; 1, slight; 2, moderate; 3, marked; and 4, very marked. The cumulative score (sum of redness, erythema, and scaling)

served as a measure of the psoriasis severity index (PSI) (scale 0-12).[24] After induced psoriasis from day 8 onwards extract treatment was started once daily, 5 times a week, for 21 days. At the end of the study, the animals were anesthetized using high dose carbon dioxide gas in a closed desiccator. Skin specimens were collected and preserved in glass vials containing 10% formalin solution for histological examination. Longitudinal sections of each mice skin specimen (about 5 mm diameter and 5 µm thickness) were prepared by microtomy and stained with hematoxylin and eosin (H and E) dye for histological examination.

Statistical analysis

The experimental results were represented as mean ± standard deviation and analyzed using one-way analysis of variance by Tukey–Kramer multiple comparisons test. The statistical calculations were performed using GraphPad 5 software (San Diego, CA, USA). $P<0.05$ was considered statistically significant in all the groups. Risk assessment code of metals in the soil was performed following the procedure described by Singh et al.[25] as:

$$\text{RAC (\%)} = \left(\sum_{n=1}^{n=3} F_n \Big/ \sum_{n=1}^{n=6} F_n \right)$$

Here "F_n" is the concentration of metal in the "n^{th}" fraction.

RESULTS

Analysis of soil samples for metal ion content

Soli samples were collected from both geographical locations and analyzed for preliminary soil tests like soil pH, organic carbon, and color of soil. Then total metals and DTPA extractable metals were analyzed by AAS. The results revealed very high acidic soil (pH 4.32) in the Darjeeling region compared to the Nandi Hills soil (pH 5.20). All other results are tabulated in Table 2.

Table 1. Grouping of animals

Groups	Treatments	Number of animals
I	Untreated animals	6
II	The animals received standard drug (Retino-A 0.05%)	6
III	The induced animals treated with 100 mg/kg. b.w. *Phlebodium decumanum*	6
IV	The induced animals treated with 100 mg/kg. b.w. *Calendula officinalis*	6
V	The induced animals treated with 200 mg/kg. b.w. *Phlebodium decumanum*	6
VI	The induced animals treated with 200 mg/kg. b.w. *Calendula officinalis*	6
VII	The induced animals treated with 100 mg/kg. b.w. *Phlebodium decumanum* and *Calendula officinalis* in combination	6
VIII	The induced animals treated with 200 mg/kg. b.w. *Phlebodium decumanum* and *Calendula officinalis* in combination	6

Analysis of leaf samples for metal ion content

Collected leaf samples were also analyzed for uptake of metals separately by AAS and the results revealed that leaf samples collected from the Nandi Hills, Bangalore, contained more metal ion uptake by the leaves. The results are tabulated in Table 3.

Yield of the extracts and phytochemical screening

Yield of the aqueous extracts from both collection areas was calculated and the results are shown in Figure 2. The results revealed that the yield of leaf samples of PD and CO collected from the Bangalore zone was higher than that of samples collected from the Darjeeling, West Bengal zone.

Percentage yield was calculated and it was found that the PD sample was higher (11.48%) than the CO sample (9.68%) collected from the Nandi Hills region and the same trend was followed for samples collected from Darjeeling. The PD sample showed a percentage yield of the leaf sample of 10.52%, whereas for CO extract it was 8.8%.

Table 2. Soil sample analysis from the two different climatic zones

Soil parameters	Darjeeling, West Bengal	Nandi Hills, Bangalore
pH	4.32±0.10[a]	5.18±0.12[b]
Color of soil	Brownish	Grayish brown
Org. carbon (%)	0.64±0.02[a]	0.32±0.11[b]
Total metals (mg/kg)		
Fe	14.21±0.12[a]	22.89±0.10[b]
Zn	5.97±0.01[a]	6.18±0.1[1]b
Cu	1.89±0.14[a]	2.05±0.12[b]
Ni	2.12±0.11[a]	2.62±0.01[a]
Cr	1.06±0.02[a]	1.32±0.11[a]
Cd	0.16±0.11[a]	0.28±0.20[a]
Pb	2.38±0.01[a]	2.52±0.20[a]
DTPA extractable metals (mg/kg)		
Fe	4.88±0.02[a]	5.96±0.02[b]
Zn	0.51±0.02[a]	0.61±0.02[a]
Cu	0.16±0.02[a]	0.24±0.02[a]
Ni	0.45±0.02[a]	0.51±0.02[a]
Cr	0.48±0.02[a]	0.66±0.02[b]
Cd	0.02±0.02[a]	0.04±0.02[a]
Pb	1.12±0.02[a]	1.58±0.02[a]

Values represent mean of three replications ± standard error, same letter(s) in a particular row represent nonsignificant difference between the samples. Detectable limits of Cd, Cr, Cu, Fe, Ni, Pb, and Zn are 0.6 mg/L, 0.3 mg/L, 0.4 mg/L, 0.2 mg/L, 0.1 mg/L, 0.3 mg/L, and 0.3 mg/L, respectively)

Phytochemical screening with respect to chemical tests was carried out and revealed the presence of various group of phytochemicals in all four leaves' aqueous extracts, which is depicted in Table 4.

Acute dermal toxicity

The study revealed the aqueous leaf extract of both CO and PD are nontoxic when tested at maximum dose levels of 2000 mg/kg body weight. Neither mortality nor any sign of toxic reactions was found during the study period. Furthermore, no skin irritation was observed with the applied extracts even after 72 h of study.

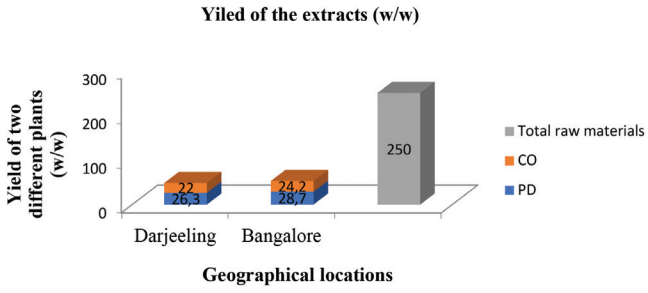

Figure 2. Yield of the extracts from two different climatic zones

CO: *Calendula officinalis*, PD: *Phlebodium decumanum*

A: Untreated animal

B: Induced psoriasis by Imiquimod

Figure 3. Control and induced mice. (a) Untreated animal, (b) Induced psoriasis by Imiquimod

Antipsoriatic activity

Topical application of 62.5 mg of 5% imiquimod was performed for 7 days and resulted in the development of induced psoriasis in each group of mice (groups II-VIII). After 3-4 days, the back skin of the mice started to display signs of erythema, scaling, and thickening (Figure 3).

Various changes such as redness, erythema, and silvery scales on the exposed area were marked visually and found an increase up to day 7 and the cumulative score, PSI, was significantly ($p<0.05$) increased as indicated in Table 5 and Figure 4.

After day 7, from day 8 onwards up to 3 weeks the extracts were applied topically to groups II-VIII. The severity of psoriatic

Table 4. Screening for presence of secondary metabolites through chemical tests

Chemical tests	Darjeeling samples		Nandi Hills samples	
	AEPD	AECO	AEPD	AECO
Protein	++	+	++	--
Carbohydrate	--	+	--	--
Glycoside	--	--	--	--
Alkaloids	++	--	++	--
Saponin	+	++	++	++
Tannins	---	+	--	++
Steroids	++	--	++	--
Terpenoids	++	--	++	--
Flavonoids	+	+	++	++
Polyphenols	--	++	--	++
Resins	--	--	--	--
Fats and oils	++	--	+	--

(++): Active present, (+): Present, (--): Absent

Table 3. Metal content in dried leaves of the two different zones

Metal uptake by leaves	Darjeeling sample		Nandi Hills sample		*RAC/Risk factor	
	Phlebodium decumanum (mg/kg)	*Calendula officinalis* (mg/kg)	*Phlebodium decumanum* (mg/kg)	*Calendula officinalis* (mg/kg)	Darjeeling sample	Nandi Hills sample
Fe	1.89±0.45	1.45±0.22	2.05±0.01	1.88±0.03	N/A	N/A
Zn	0.89±0.15	0.76±0.12	1.12±0.11	0.98±0.22	N/A	N/A
Cu	0.68±0.12	0.54±0.03	0.78±0.01	0.62±0.11	N/A	N/A
Ni	0.20±0.03	0.18±0.04	0.26±0.20	0.22±0.03	1.8±0.18	0.51±0.21
Cr	0.07±0.05	0.08±0.44	0.14±0.11	0.12±0.05	0.05±0.21	1.01±0.10
Cd	0.001±0.11	0.002±0.15	0.002±0.05	0.003±0.11	1.04±0.11	0.9±0.03
Pb	0.27±0.40	0.31±0.11	0.36±0.01	0.37±0.02	0.85±0.23	0.08±0.14

RAC: Risk assessment code, N/A: Not applicable, *RAC: <1 (category 1; no risk), 1-10 (category 2; low risk; >10-30 (category 3, medium risk), >30-50 (category 4, high risk), and >50 (category 5, very high risk)

lesions was evaluated by visual and histological studies. In group II, topical application of Retino-A cream (0.05%) reduced ($p<0.05$) the severity of redness, erythema, and scales from days 7 to 21. Thereafter a drastic reduction ($p<0.01$) in phenotypic changes like redness, erythema, and scales was observed for groups VII and VIII, in which combined extracts were applied and the results showed a dose-dependent manner. Among the responses, the plants procured from the Nandi Hills, Bangalore, Karnataka state, showed more significant results (Tables 6-9) than samples procured from Darjeeling, West Bengal state (Tables 10-13). Combined extracts at 200 mg/kg b.w. resulted in a more significant PSI score ($p<0.01$) on day 14 as well as on day 21 than the later geographical zone. Interestingly the results were better in terms of reduction of redness, erythema, scales, and cumulative score in animals, which showed the therapeutic efficacy of the selected plant samples on induced psoriasis compared to the standard drug applied.

Histopathological study

The histological examination showed an increased epidermal thickness, hyperproliferation of keratinocytes granulocyte infiltration, the presence of microabscesses, and capillary loop dilatation in IMQ-induced mouse skin as compared to normal mouse skin (Figures 5a, 5b). Thereafter the epidermal thickness of extract-treated animals was compared with that of untreated animals, which showed a remarkable decrease in thickness compared to the applied standard (Figure 6).

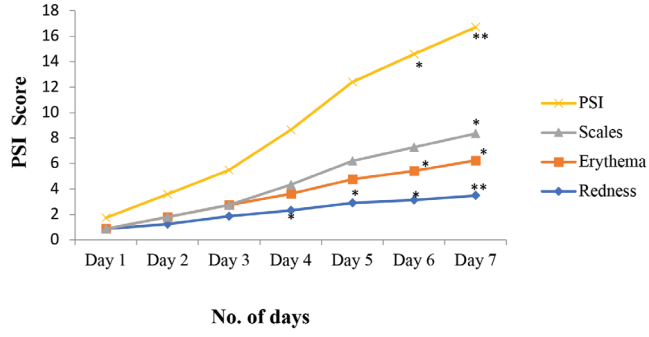

Figure 4. Phenotypic changes during induced psoriasis by imiquimod

PSI: Psoriasis severity index

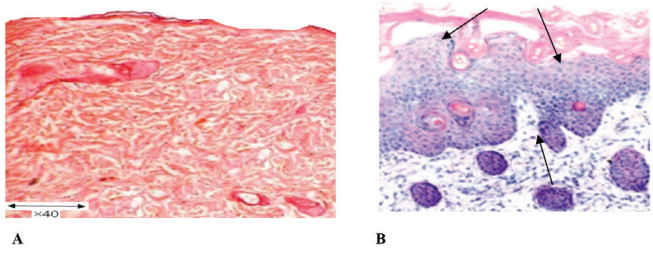

Figure 5. Longitudinal histological sections of mouse skin (H and E, 40×). (a) Section of normal mouse skin and (b) section of IQM-treated mouse skin (The pointed arrows are Munro's microabscess, hyper proliferation of keratinocytes and capillary loop dilatation)

Thickness of the epidermis cell was significantly less (26.18 μM) (**$p<0.01$) when combined PD and CO extracts were applied at 200 mg/kg b.w. compared to the standard (40.14 μM) in terms of reduced epidermal thickness, hyperproliferation, granulocyte infiltration, the presence of microabscesses, and capillary loop dilatation (Figures 7a-c).

Correlation coefficient

The data were analyzed for correlation between uptakes of essential metals in leaves and reduction in epidermal thickness in psoriasis treatment. The results revealed high significance. PD and CO leaf samples procured from the Nandi Hills showed better uptake of Fe (2.05 mg/kg and 1.88 mg/kg, respectively), Cu (0.78 mg/kg and 0.62 mg/kg, respectively), and Zn (1.12 mg/kg and 0.98 mg/kg, respectively) than Darjeeling samples. Extracted plant samples were calculated for percentage of extracts and the results revealed that the Nandi Hills samples gave more extract due to their higher content of metallic ions (Figure 2). These metal contents further correlated with the reduction in epidermal thickness, which showed significant results. The increased content of metals in PD and CO leaf

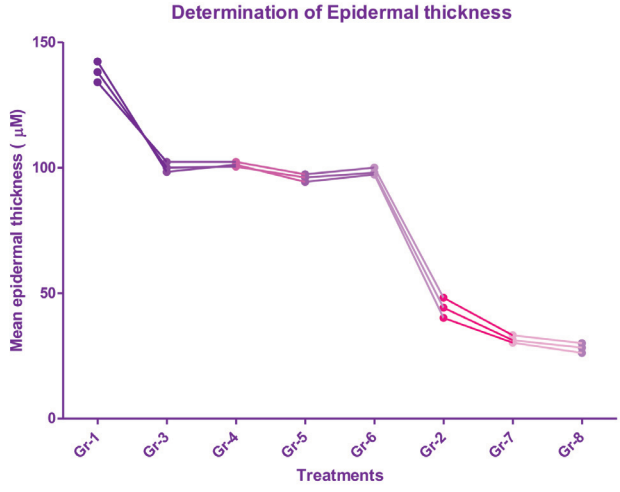

Figure 6. Epidermal thickness determination and comparison with untreated group

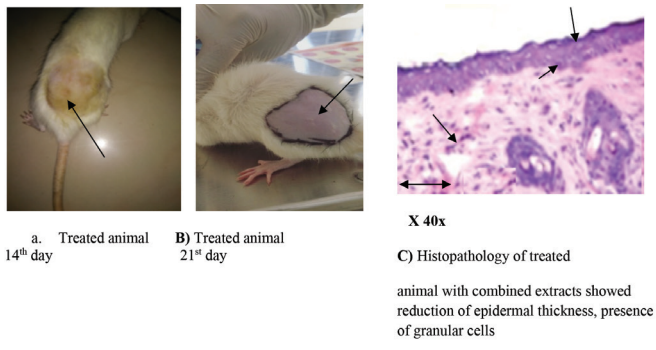

a. Treated animal 14th day

B) Treated animal 21st day

C) Histopathology of treated animal with combined extracts showed reduction of epidermal thickness, presence of granular cells

Figure 7. Histopathology of applied combined *Calendula officinalis* and *Phlebodium decumanum* extracts at 200 mg/kg b.w. (a) Treated animal 14th day, (b) Treated animal 21st day, (c) Histopathology of treated animal with combined extracts showed reduction of epidermal thickness, presence of granular cells 40×

samples decreases the epidermal thickness (94.33 µM and 97.30 µM, respectively, on day 21) (Table 14) more than samples procured from Darjeeling, West Bengal (98.10 µM and 100.20 µM, respectively, on day 21).

DISCUSSION

Metal ion content in soil and leaf sample

The results (Table 2) show that the pH and organic carbon content in the Darjeeling soil were 4.32 and 0.64%, while in the Nandi Hills soil they were 5.18 and 0.32%, suggesting that the soil of Darjeeling was more acidic compared to the Nandi Hills soil. As regards the organic carbon content, it was observed that the amount was much higher (0.64%) in the Darjeeling soil compared to the Nandi Hills soil (0.32%), which might be due to variation in climatic conditions, especially in temperature. The prevailing temperature in the Darjeeling region was much lower compared to the Nandi Hills, which might be explained by the lower loss of organic carbon in the former region resulting from the very little oxidation of organic carbon from the soil compared to that of the latter Nandi Hills soil, causing a greater rate of oxidation of organic carbon.

As regards the total and available heavy metal content in soils, it was found that the amount of both total and available metal concentration was always higher in the Nandi Hills soil compared to the Darjeeling soil, which might be explained by the variation in the initial higher amounts of metals as well as the variation in pedogenic processes of soil formation where the dominant pedogenic process was laterization in the case of the Nandi Hills soil, resulting an accumulation of sesquioxides and loss of silica and the reverse is the case with the Darjeeling soil, where the podzolization process is dominant in which

Table 5. Examination of redness, erythema, and scales in induced mice

Day	Redness	Erythema	Scales	Cumulative score (PSI)
1	0.87±0.02	0	0	0.87±0.02
2	1.23±0.10	0.57±0.12	0	1.8±0.11
3	1.85±0.03	0.89±0.01	0	2.74±0.02
4	2.31±0.02*	1.33±0.22	0.69±0.22	4.33±0.21
5	2.9±0.11*	1.88±0.11	1.42±0.11	6.2±0.11
6	3.12±0.13*	2.3±0.10*	1.87±0.10	7.29±0.11*
7	3.53±0.01**	2.78±0.01*	2.11±0.01*	8.35±0.01**

PSI: Psoriasis severity index, The results represent mean ± standard error of mean (n=6). Data were analyzed by one way ANOVA, followed by Tukey–Kramer multiple comparisons test, values were considered significant at *p<0.05 and **p<0.01

Table 6. Evaluation of redness (score 0-4) after treatment with extracts

Day	Group I	Group II	Group III	Group IV	Group V	Group VI	Group VII	Group VIII
7	3.53±0.01	2.6±0.22	2.78±0.21	2.92±0.03	2.70±0.14	2.84±0.01	2.47±0.14	1.22±0.20
14	3.56±0.11	1.6*±0.20	2.12±0.12	2.78±0.10	2.04±0.23	2.68±0.13	0.68**±0.20	0.59**±0.11
21	3.58±0.21	0.57*±0.03	1.46±0.03	1.74±0.11	1.12±0.13	1.66±0.10	0.48**±0.03	0.30**±0.30
F value			4.182					
R^2 value			0.646					

The results represent mean ± standard error of mean (n=6). Data were analyzed by one way ANOVA, followed by Dunnett comparison test against untreated animals. Values were considered significant at *p<0.05 and **p<0.01

Table 7. Evaluation of erythema (score 0-4) after treatment with extracts

Day	Group I	Group II	Group III	Group IV	Group V	Group VI	Group VII	Group VIII
7	2.78±0.21	1.70±0.10	2.12±0.21	2.32±0.11	1.86±0.21	1.97±0.13	1.54±0.21	1.10±0.02
14	2.82±0.21	0.64*±0.01	1.63±0.23	1.80±0.01	1.46±0.31	1.50±0.21	0.62**±0.11	0.40**±0.20
21	2.84±0.01	0.46*±0.11	0.65±0.32	0.72±0.21	0.57*±0.30	0.62±0.11	0.38**±0.31	0.25**±0.32
F value			3.513					
R^2 value			0.6058					

The results represent mean ± standard error of mean (n=6). Data were analyzed by one way ANOVA, followed by Dunnett comparison test against untreated animals. Values were considered significant at *p<0.05 and **p<0.01

accumulation of silica and loss of sesquioxides occurred.[26] The amount of DTPA extractable Zn content was deficient (0.51 mg/kg) and marginally deficient (0.61 mg/kg) in the Nandi Hills soil based on the critical level of 0.60 mg/kg. However, such decreased availability of Zn and Cu in soils might be explained by their greater fixation and adsorption as well as greater interaction between soil components.[27] The results also reveal that the amounts of DTPA-extractable nonnutrient heavy metals (Cr, Cd, Pb, and Ni) were far below the toxic limit based on the test value.[28] The amounts of DTPA-extractable Ni, Cd, Cr, and Pb contents were recorded at very low values in both the soils of Darjeeling and the Nandi Hills, which might be due to the higher organic carbon content in the former soil and higher pH in the latter soil resulting from the complexation of those heavy metals with organic matter in the Darjeeling soil and the higher adsorption of those metals onto sesquioxides in the Nandi Hills soil. The availability of Ni associated with organic colloids is highly pH dependent, which reduced the rate of dissociation of Ni fulvic acid complexes with increased pH and decreased ionic strength.[28] The availability of nonnutrient heavy metals such as Cr, Cd, Ni, and Pb and also beneficial micronutrients like Fe, Zn, and Cu in soil might be attributed to the individual soil characteristics, particularly soil pH;[29] cation exchange capacity;[30] different oxides of Fe, Al, and Mn;[31] and amount of organic matter content.[32]

The results (Table 3) reveal that the amounts of nonnutrient heavy metals (Cr, Cd, Ni, and Pb) in both PD and CO varied between soil types and kind of medicinal plants, being slightly higher in PD compared to CO in both soils. Such low content of those metals in plants might be due to the very low content of those metals in both soils resulting from the variation in soil reaction as well as amount of organic carbon content in the soils.[28] Karak et al.[33] reported that the concentration of Zn and other nonnutrient heavy metals in soil solution and their availability to crops is controlled by sorption–desorption reactions at the surfaces of soil colloidal materials. The results of the present investigation are similar to those reported by earlier investigators.[34,35]

Table 8. Evaluation of scales (score 0-4) after treatment with extracts

Day	Group I	Group II	Group III	Group IV	Group V	Group VI	Group VII	Group VIII
7	2.11±0.11	1.70±0.13	1.96±0.11	2.02±0.21	1.78±0.10	1.80±0.01	0.98±0.23	0.82±0.01
14	2.46±0.03	0.98±0.03	0.84±0.14	1.42±0.02	0.64*±0.03	0.78±0.12	0.32**±0.13	0.44**±0.01
21	2.58±0.20	0.37±0.02	0.46±0.22	0.87±0.10	0.38*±0.04	0.56±0.12	0.18**±0.01	0.16**±0.02
F value			3.217					
R^2 value			0.5846					

The results represent mean ± standard error of mean (n=6). Data were analyzed by one way ANOVA, followed by Dunnett comparison test against untreated animals. Values were considered significant at *p<0.05 and **p<0.01

Table 9. Evaluation of PSI (score 0-12) after treatment with extracts

Day	Group I	Group II	Group III	Group IV	Group V	Group VI	Group VII	Group VIII
7	8.35±0.10	6.00±0.12	6.86±0.01	7.26±0.10	6.34±0.21	6.61±0.12	4.99±0.03	3.14±0.11
14	8.54±0.13	3.22±0.13	4.59±0.12	6.00±0.10	4.14±0.03	4.96±0.10	1.62**±0.10	1.43**±0.11
21	8.67±0.22	1.40*±0.03	2.57±0.11	3.33±0.02	2.07±0.01	2.84±0.11	1.04**±0.10	0.71**±0.04
F value			3.597					
R^2 value			0.6114					

The results represent mean ± standard error of mean (n=6). Data were analyzed by one way ANOVA, followed by Dunnett comparison test against untreated animals. Values were considered significant at *p<0.05 and **p<0.01, PSI: Proriasis severity index

Table 10. Evaluation of redness (score 0-4) after treatment with extracts

Day	Group I	Group II	Group III	Group IV	Group V	Group VI	Group VII	Group VIII
7	3.53±0.01	2.6±0.22	3.11±0.11	2.98±0.11	2.86±0.13	2.79±0.03	2.64±0.01	2.62±0.13
14	3.56±0.11	1.6±0.20	2.87±0.02	2.76±0.13	2.8±0.20	2.77±0.02	1.64±0.21	1.62±0.21
21	3.58±0.21	0.57**±0.03	2.56±0.20	2.66±0.12	2.5±0.02	2.57±0.13	0.89**±0.11	0.82**±0.11
F value			4.326					
R^2 value			0.654					

The results represent mean ± standard error of mean (n=6). Data were analyzed by one way ANOVA, followed by Dunnett comparison test against untreated animals. Values were considered significant at *p<0.05 and **p<0.01

However, the overall results reveal that the amount of available trace heavy metals including beneficial and nonnutrient metals depends on the nature and properties of soils, pedogenic processes of soil formation, etc. In the case of the Darjeeling soil, exchangeable Al is mainly responsible for the development of soil acidity, while in the Nandi Hills soil, extensive leaching and at the same time accumulation of sesquioxide are responsible for the acidity. Since all those metal concentrations in their available forms in both soils are very low and the absorption in and uptake of those metals by plants are also reportedly low, based on the results of the present investigation, the cultivation of medicinal plants in both soils is suitable without their medicinal value being affected.

Yields of the extracts

Yields of extracts were determined w/w and tabulated. The yield of extract showed a slightly increased amount procured from the Nandi Hills, Bangalore. This may be due to higher accumulation of Fe, Zn, and Cu and lower content of nonessential heavy metals in leaf samples of CO and PD. An earlier report confirmed this result.[19]

Antipsoriasis activity

In recent years many plant extracts in combinations or alone have been applied for psoriasis treatments. However, the main concern is to discover new drugs from plant extracts that are more potent than the extracts against any kind of human health hazards. The main reason behind the selection of the leaves of these two plants was that both the plants enhanced the immunity and act strongly against any infections due to their high antioxidant activities.[10,36] It was revealed that the selected plant extracts showed significant antipsoriasis activity due to the presence of important secondary metabolites (discussed earlier in the Introduction).

It was scientifically proved that prostaglandin E_2 produced by the cyclo-oxygenase pathway results in psoriasis by dilating skin capillaries, which increases leukocyte infiltration and stimulates keratinocyte cell growth.[37] During induction of psoriasis, 5% imiquimod cream was used, which showed redness, erythema, and scales within 7 days in the skin of mice. Histologically, psoriatic skin contains a thickened epidermis with a large number of inflammatory cells and absence of a

Table 11. Evaluation of erythema (score 0-4) after treatment with extracts

Day	Group I	Group II	Group III	Group IV	Group V	Group VI	Group VII	Group VIII
7	2.78±0.21	1.70±0.10	2.71±0.21	2.74±0.11	2.64±0.21	2.68±0.13	1.68±0.21	1.62±0.02
14	2.82±0.21	0.64**±0.01	2.41±0.23	2.57±0.01	2.31±0.31	2.46±0.21	0.60**±0.11	0.50**±0.20
21	2.84±0.01	0.46**±0.11	1.47±0.32	1.89±0.21	1.12± 0.30	1.60±0.11	0.42**±0.31	0.36**±0.32
F value			4.954					
R^2 value			0.6843					

The results represent mean ± standard error of mean (n=6). Data were analyzed by one way ANOVA, followed by Dunnett comparison test against untreated animals. Values were considered significant at *p<0.05 and **p<0.01

Table 12. Evaluation of scales (score 0-4) after treatment with extracts

Day	Group I	Group II	Group III	Group IV	Group V	Group VI	Group VII	Group VIII
7	2.11±0.11	1.70±0.13	2.05±0.01	2.08±0.04	2.00±0.21	2.04±0.02	1.70±0.01	1.65±0.01
14	2.46±0.03	0.98*±0.03	1.46±0.11	1.68±0.21	1.37 ±0.11	1.52±0.03	1.04*±0.11	0.60*±0.11
21	2.58±0.20	0.37*±0.02	1.20±0.21	1.44±0.11	1.10 ±0.11	1.36±0.22	0.34*±0.20	0.27*±0.03
F value			2.818					
R^2 value			0.552					

The results represent mean ± standard error of mean (n=6). Data were analyzed by one way ANOVA, followed by Dunnett comparison test against untreated animals. Values were considered significant at *p<0.05 and **p<0.01,

Table 13. Evaluation of PSI (score 0-12) after treatment with extracts

Day	Group I	Group II	Group III	Group IV	Group V	Group VI	Group VII	Group VIII
7	8.35±0.10	6.00±0.12	7.87±0.04	7.80±0.14	7.50±0.11	7.51±0.02	6.20±0.01	5.89±0.01
14	8.54±0.13	3.22±0.13	6.74±0.10	7.01±0.11	6.48±0.10	6.75±0.13	3.28±0.11	2.72±0.10
21	8.67±0.22	1.40**±0.03	5.23±0.20	5.99±0.12	4.72±0.02	5.53±0.21	1.65*±0.20	1.45**±0.03
F value			4.197					
R^2 value			0.647					

The results represent mean ± standard error of mean (n=6). Data were analyzed by one way ANOVA, followed by Dunnett comparison test against untreated animals. Values were considered significant at *p<0.05 and **p<0.01, PSI: Proriasis severity index

Table 14. Correlation coefficient among essential metal uptake by leaves and decreased epidermal thickness of individual plants

Parameters	Cu content in leaf	Zn content in leaf	Fe content in leaf	Reduction in epidermal thickness
Cu content in leaf	1			
Zn content in leaf	0.882	1		
Fe content in leaf	0.909	0.915	1	
Reduction in epidermal thickness	-0.928***	-0.990***	-0.906***	1

Data were analyzed by one way ANOVA, followed by Tukey's comparative test. Values were considered significant at *p<0.05, **p<0.01, ***p<0.001

granular layer. In the present study fully developed psoriatic lesions were treated with combined herbal aqueous extracts of PD and CO and compared with marketed standard drug along with untreated animals. The results revealed a significant reduction in epidermal thickness after treatment with the aqueous extracts.

Previous studies have established that antioxidants could play an effective role in psoriasis treatment.[38] Plant secondary metabolites such as flavonoids, triterpenoids, and polyphenolic compounds are well known for antioxidant activity and for their anti-inflammatory, antiproliferative, and immunomodulatory activities.[39,40] These characteristics of polyphenolic phytoconstituents are beneficial for the treatment of psoriasis and they are present in huge quantities in PD and CO leaves. Preliminary phytochemical screening through chemical tests revealed the presence of these constituents, which showed antipsoriasis activities.

CONCLUSIONS

The results of this present study demonstrate that the combined extracts of PD and CO provide significant antipsoriasis activity and the effect was dose dependent. The selected plants showed remarkable activity compared to that of the marketed standard drug Retino. Hence, further isolation of newer chemicals and clinical trials are needed for the establishment of effective herbal drug formulations against psoriasis via new drug discovery.

ACKNOWLEDGEMENTS

The authors express their sincere gratitude to The Management, Krupanidhi Group of Institutions for funding the project through Krupanidhi Research Incubator Centre (K-RIC) program under Krupanidhi College of Pharmacy and Dr. S. Parthasarathi, Accendere: CL Educate Ltd.

Conflict of Interest: No conflict of interest was declared by the authors.

REFERENCES

1. Singh S, Prasad R, Tripathi JS, Rai NP. Psoriasis - An Overview. World Journal of Pharmaceutical Sciences. 2015;3:1732-1740.
2. Samuel ML, Donald PM, Hurley JH Jr. Dermatology. WB Philadelphia: Saunders Company; 1986:204.
3. Lo KK, Ho LY. Psoriasis. Handbook of Dermatology and Venereology. 2nd edn. Hong Kong; Social Hygiene Service, Dept of Health; 1997.
4. Tanaka Y, Sasaki N, Ohmiya A. Biosynthesis of plant pigments: anthocyanins, betalains and carotenoids. Plant J. 2008;54:733-749.
5. Zhu C, Bai C, Sanahuja G, Yuan D, Farre G, Naqvi S, Shi L, Capell T, Christou P. The regulation of carotenoids pigmentation in flowers. Arch Biochem Biophy. 2010;504:132-141.
6. Chakraborthy GS. Phytochemical screening of *Calendula officinalis* Linn leaf extract by TLC. IJRAP. 2010;1:131-134.
7. Chakraborthy GS. Antimicrobial activity of the leaf extracts of *Calendula officinalis* (linn). Journal of Herbal Medicine and Toxicology. 2008;2:65-66.
8. Ali J, Khan AH. Preventive and curative effects of *Calendula officinalis* leaves extract on Acetaminophen-induced hepatotoxicity. JPMI. 2006;20:370-373.
9. Sengupta R. Combined wound healing activity of *Calendula officinalis* and Basil leaves. Journal of Pharmacognosy and Phytochemistry. 2017;6:173-176.
10. Das K, Rekha RS, Ibrahim MA, Ahmed SY. Effect of demographic location on *Phlebodium decumanum* (Willd.) J. Sm. for its phytoconstituents and establishment of antioxidant and novel anthelmintic activity of its aqueous and methanolic leaf extracts. Annals of Phytomedicine. 2017;6:101-106.
11. Das K, Einstein JW. Samambaia - The future focus for Indian researchers in the treatment of psoriasis. Thai J Pharm Sci. 2007;31:45-51.
12. Punzon C, Alcaide A, Fresno M. *In vitro* anti-inflammatory activity of Phlebodium decumanum. Modulation of tumor necrosis factor and soluble TNF receptors. Int Immnopharmacol. 2003;3:1293-1299.
13. Díaz-Castro J, Guisado R, Kajarabille N, García C, Guisado IM, De Teresa C, Ochoa JJ. Phlebodium decumanum is a natural supplement that ameliorates the oxidative stress and inflammatory signalling induced by strenuous exercise in adult humans. Eur J Appl Physiol. 2012;112:3119-3128.
14. Gonzalez-Jurado JA, Pradas F, Molina ES, De Teresa C. Effect of *Phlebodium decumanum* on the immune response induced by training in sedentary university students. J Sports Sci Med. 2011;10:315-321.
15. Sekeroglu N, Ozguven M. Effects of different nitrogen doses and plant densities on yield and quality of *Oenothera biennis* L. grown in irrigated lowland and unirrigated dry land conditions. Turk J Agric For. 2006;30:125-135.
16. Orhan IE, Erdem A, Senol FS, Oztürk N, Demirci B, Das K, Sekeroglu N. Comparative studies on Turkish and Indian *Centella asiatica* (L.) Urban (gotu kola) samples for their enzyme inhibitory and antioxidant effects and phytochemical characterization. Industrial Crops and Products. 2013;47:316-322.
17. Özgüven M, Sener B, Orhan I, Sekeroglu N, Kirpik M, Kartal M, Süntar İ, Kaya Z. Effects of varying nitrogen doses on yield, yield components and artemisinin content of *Artemisia annua* L. Industrial Crops and Products. 2008;27:60-64.

18. Das K, Dang R, Shobha Rani HR. Effect of cultural conditions on relative sweetness of Stevia cultivated under acidic soil zone of South India. Int J Agric Environ Food Sci. 2012;2:108-114.

19. Das K, Tribedi S. Effect of Zn, Fe and Cu content on phytochemical investigations and antimicrobial potential of *Alternanthera brasiliana* (L.) O. Kuntze leaf extracts procured from two different States of India. Turk J Pharm Sci. 2015;12:345-356.

20. Harborne JB. Phytochemical Methods: A guide to modern techniques of plant analysis. 3rd ed. Chapman and Hall, London;1998:302.

21. Sazada S, Verma A, Rather AA, Jabeen F, Meghvansi MK. Preliminary phytochemicals analysis of some important medicinal and aromatic plants. Adv Biol Res 2009;3:188-195.

22. Organization Economic for Cooperation and Development (OECD). Guidelines for Testing of Chemicals. Acute Dermal Toxicity, Test No. 402. France: OECD; 2001.

23. Feldman SR, Krueger GG. Psoriasis assessment tools in clinical trials. Ann Rheum Dis 2005;64(Suppl 2):65-68.

24. Srivastava AK, Nagar HK, Chandel HS, Ranawat MS. Antipsoriatic activity of ethanolic extract of *Woodfordia fruticosa* (L.) Kurz flowers in a novel in vivo screening model. Indian J Pharmacol. 2016;48:531-536.

25. Singh KP, Mohan D, Singh VK, Malik A. Studies on distribution and fractionation of heavy metals in Gomti river sediments-a tributary of the Ganges. India J Hydrol. 2005;312:14-27.

26. Das DK. Introductory Sopil Science. 4th ed. Revised and enlarged edn. Kalyani Publishers, New Delhi/ Ludhiana; 2015.

27. Dutta D, Mandal B, Mandal LN. Decrease in availability of zinc and copper in acidic to near neutral soils on submergence. Soil Science. 1989;23:38-46.

28. Das DK. Micronutrients: Their behaviour in soils and plants. 2nd revised edn. Kalyani Publishers, New Delhi/ Ludhiana; 2007.

29. Singh, MV, Abrol IP. Solubility and adsorption of zinc in a sodic soil. Soil Science. 1985;140:406-411.

30. Choudhari JS. Fixation of zinc by arid soil clays. Clay Research. 1984;3:89-92.

31. Harter RD. Micronutrients adsorption-desorption reactions in soils. In: Mortvedt JJ, ed. Micronutrients in Agriculture. 2nd edn . Madison, WI: SSSA. 1991:59-87.

32. Appel C, Ma L. Concentration, pH and surface charge effects on Cd and lead sorption in three tropical soils. J Environ Qual. 2002;31:581-589.

33. Karak T, Singh UK, Das S, Das DK, Kuzykov Y. Comparative efficacy of ZnSO4 and Zn-EDTA application for fertilization of rice (Oryza sativa L). 2005;51:253-264.

34. Das DK, Mandal LN. Effect of puddling and different times of organic matter application before puddling on the availability of iron, manganese, copper and zinc in rice soils. Agrochimica. 1988;32:327-336.

35. Rupa TR, Sukla LM. Adsorption-desorption of zinc and copper in soils of Rayalassema region of Andhra Pradesh. Journal of the Indian Society of Soil Science. 1998;46:207-211.

36. Rigane G, Ben Younes S, Ghazghazi H, Ben Salem R. Investigation into the biological activities and chemical composition of *Calendula officinalis* L. growing in Tunisia. International Food Research Journal. 2013;20:3001-3007.

37. Amigo M, Paya M, De Rosa S, Terencio MC. Antipsoriatic effects of avarol-3'-thiosalicylate are mediated by inhibition of TNF alpha generation and NF-kappa B activation in mouse skin. Br J Pharmacol. 2007;152:353-365.

38. Young CN, Koepke JI, Terlecky LJ, Borkin MS, Boyd Savoy L, Terlecky SR. Reactive oxygen species in tumor necrosis factoralpha-activated primary human keratinocytes: Implications for psoriasis and inflammatory skin disease. J Invest Dermatol. 2008;128:2606-2614.

39. Middleton E Jr, Kandaswami C, Theoharides TC. The effects of plant flavonoids on mammalian cells: Implications forinflammation, heart disease, and cancer. Pharmacol Rev. 2000;52:673-751.

40. González R, Ballester I, López-Posadas R, Suárez MD, Zarzuelo A, Martínez-Augustin O, Sanchez de Medina F. Effects of flavonoids and other polyphenols on inflammation. Crit Rev Food Sci Nutr. 2011;51:331-362.

Turk J Pharm Sci 2019;16(3):303-309
DOI: 10.4274/tjps.galenos.2018.29981

ORIGINAL ARTICLE

Anti-Angiogenic Activity of Flunarizine by *In Ovo*, *In Vitro*, and *In Vivo* Assays

In Ovo, In Vitro ve *In Vivo* Günlüklerinden Flunarizinin Anti-Anjiyojenik Aktivitesi

Chandana KAMILI[1]*, Ravi Shankar KAKARAPARTHY[2], Uma Maheshwararao VATTIKUTI[3]

[1]CMR College of Pharmacy, Hyderabad, Telangana, India
[2]Sri Sai Aditya Institute of Pharmaceutical Sciences and Research, Department of Pharmacology, Surampalem, Andra Pradesh, India
[3]TRR College of Pharmacy, Department of Pharmacognosy, Hyderabad, Telangana, India

ABSTRACT

Objectives: The involvement of T-type calcium channels in cell proliferation and the role of sodium channels in cell migration have been extensively studied in angiogenesis. In the present study, flunarizine, a dual sodium/calcium channel blocker; was selected to evaluate its anti-angiogenic potential. This can be therapeutically beneficial in diseases caused by pathologically excessive angiogenesis.

Materials and Methods: The anti-angiogenic activity of ion channel blocker was screened by chick chorioallantoic membrane assay (*in ovo*), rat aortic ring assay, endothelial cell proliferation assay, transwell migration assay, Matrigel cord-like morphogenesis assay (*in vitro*), and sponge implantation method (*in vivo*). The anti-angiogenic activity of the test drug was compared with the standard anti-angiogenic drug bevacizumab and, in addition, the test responses were compared with the angiogenic factor vascular endothelial growth factor at a maximal concentration of 500 pM.

Results: All the groups were compared with the control group using one-way ANOVA, followed by a post hoc test, Dunnett's test, to compare the mean of all the groups with the control mean. In the chick chorioallantoic membrane assay, the number of branching points and angiogenic score were evaluated and significant results were observed at 10^{-5} M and 10^{-4} M. In the aortic ring assay a reduction in the area of sprouts was observed with 5-10 µM and significant reductions in the weight of sponges, number of blood vessels formed, and hemoglobin content were observed at all three tested concentrations of flunarizine in the sponge implantation method. In the studies on human umbilical vein endothelial cells the test drug (1-100 nM) showed significant inhibition of proliferation and migration and a decrease in the network length of cord-like tubes in a dose-dependent manner.

Conclusion: Flunarizine has significant anti-angiogenic action by inhibiting cell proliferation, migration, and cord-like tube formation, which resulted from blocking of the T-type calcium and sodium channels. Further studies on the structural modifications of flunarizine for repurposing this ion channel modulator will lead to treatment of the diseases due to excessive angiogenesis from the root cause.

Key words: Anti-angiogenesis, chick chorioallantoic membrane assay, rat aortic ring assay, sponge implantation method, human umbilical vein endothelial cells, flunarizine

ÖZ

Amaç: Hücre proliferasyonunda T-tipi kalsiyum kanallarının tutulumu ve hücre göçü içindeki sodyum kanallarının rolü anjiyogenezde kapsamlı olarak incelenmiştir. Bu çalışmada, ikili bir sodyum/kalsiyum kanal blokeri olan flunarizin; anti-anjiyojenik potansiyelini değerlendirmek için seçildi. Bu, patolojik olarak aşırı anjiyogenezin neden olduğu hastalıklarda terapötik olarak yararlı olabilir.

Gereç ve Yöntemler: İyon kanalı blokörünün anti-anjiyojenik aktivitesi, civciv korioallantoik membran deneyi (*in ovo*), sıçan aortik halka deneyi, endotelyal hücre proliferasyon analizi, transwell migrasyon deneyi, Matrigel kord benzeri morfojenez deneyi (*in vitro*) ve sünger implantasyonu ile tarandı. Yöntem (*in vivo*). Test ilacının anti-anjiyogenik aktivitesi standart anti-anjiyojenik ilaç olan bevacizumab ile karşılaştırıldı ve buna ek olarak, test yanıtları, 500 mM'lik bir maksimum konsantrasyonda anjiyojenik faktör vasküler endotel büyüme faktörü ile karşılaştırıldı.

Bulgular: Tüm gruplar kontrol grubu ile tek yönlü ANOVA kullanılarak ve post hoc testi ile karşılaştırıldı, Dunnett testi ile tüm grupların ortalamaları kontrol ortalaması ile karşılaştırıldı. Chick chorioallantoic membran testinde dallanma noktaları ve anjiyojenik skorlar değerlendirildi ve 10^{-5} M ve 10^{-4} M'de anlamlı sonuçlar gözlendi. Aort halkası analizinde, filiz alanında 5-10 µM azalma gözlendi ve sünger implantasyon yönteminde test edilen

*Correspondence: E-mail: chandanakamili@gmail.com, Phone: +9581140044 ORCID-ID: orcid.org/0000-0001-7437-5137
Received: 14.04.2018, Accepted: 31.05.2018

üç flunarizin konsantrasyonunda sünger ağırlığında anlamlı bir azalma, kan damarlarının sayısı ve hemoglobin içeriği gözlendi. İnsan umbilikal ven endotelyal hücreleri üzerindeki çalışmalarda, test ilacı (1-100 nM), proliferasyonun önemli ölçüde engellenmesini, doza ve kordon benzeri tüplerin ağ uzunluğunun doza bağımlı bir şekilde azaldığını gösterdi.

Sonuç: Flunarizin, T-tipi kalsiyum ve sodyum kanallarını bloke ederek hücre proliferasyonu, migrasyon ve kord benzeri tüp oluşumunu inhibe ederek önemli anti-anjiyogenik etkiye sahiptir. Flunarizinin bu iyon kanal modülatörünü yeniden üretmek için yapısal modifikasyonları ile ilgili daha ileri çalışmalar, kök nedeninden aşırı anjiyogenezden kaynaklanan hastalıkları tedavi edebilecektir.

Anahtar kelimeler: Anti-anjiyogenez, civciv korioallantoik membran deneyi, sıçan aortik halka deneyi, sünger implantasyon yöntemi, insan umbilikal ven endotel hücreleri, flunarizin

INTRODUCTION

The term angiogenesis or neovascularization means the formation of new blood vessels from existing vasculature. Blood capillaries supply oxygen: more capillaries can increase tissue oxygen conduction and hence improve energy production; fewer capillaries results in ischemia, hypoxia, and even anoxia in the tissues.[1] Thus, angiogenesis is important for both normal physiology and in pathological conditions.[2-4]

Endothelial cell (EC) structure and functional integrity are important in the maintenance of the vessel wall and circulatory functions, and most of these endothelial functions are regulated by ion channels.[5,6] The role of ion channels in the pathophysiology of diseases has been extensively discussed.[7-9] Despite their prime role in several diseases, there are very few drugs targeting specifically the ion channels as therapeutic inhibitors for the treatment of diseases caused by excessive angiogenesis. Such clinically approved ion channel modulators with well-known safety profiles may be reframed in the treatment of many diseases, saving significant time and money.

In the present study, flunarizine (FLN), a dual Na^+/Ca^{2+} channel blocker, was selected in order to screen its anti-angiogenic potential. FLN, diphenylpiperazine analogue, acts on both Na^+ and Ca^{2+} channels. The test drug is a T-type calcium channel blocker that has been studied as extensively unregulated in most tumor types. The anti-angiogenic potential of the test drug FLN was tested at three different doses in different methods by an *in ovo* method, the chorioallantoic membrane (CAM) assay; an *in vitro* method, the rat aortic ring assay, EC proliferation assay, transwell migration assay, and Matrigel cord-like morphogenesis assay; and an *in vivo* method, the sponge implantation assay.

MATERIALS AND METHODS

Chemicals

FLN, ketamine, xylazine, and tramadol were purchased from N.R. CHEM, India. Matrigel was purchased from Becton Dickinson India Pvt. Ltd, Gurgaon, India. Gel foam and Dulbecco's modified Eagle's medium were supplied by Life Technologies (India) Pvt. Ltd. Well plates were purchased from Hi Media Laboratories Pvt. Ltd, India. Bevacizumab, vascular endothelial growth factor (VEGF), penicillin, streptomycin, amphotericin, gentamycin, heparin, bovine serum albumin, gelatin, and M199 were obtained from Sigma-Aldrich (India). All the chemical and reagents used in the study were of AR grade.

Equipment

All the equipment of CMR College of Pharmacy was used. The BOD incubator, Dona analytical balance, digital pH meter, Evershine 697 homogenizer, laminar airflow unit, and Labomed trinocular microscope were purchased from MH Enterprises, Hyderabad, India.

Experimental animals

Forty-two healthy male Wistar Albino rats weighing 150-200 g were selected for the *in vivo* methods and for the *in vitro* assay. The animals were obtained from Teena Labs Pvt Ltd, Hyderabad, Telangana state, India. Fertilized leghorn chicken eggs were selected for the *in ovo* assay. All the procedures were performed according to the CPCSEA under a protocol approved by the Institutional Animal Ethics Committee (IAEC) (project license numbers CPCSEA/1657/IAEC/CMRCP/PhD-15/42).

Chick CAM assay

This is an *in ovo* angiogenesis assay for identification and quantification of anti-angiogenic agents. Eggs were collected from the hatchery on day 0 and checked for any damage. They were randomly grouped into control, VEGF, bevacizumab, and three test concentrations groups, each containing six eggs. The eggs were disinfected using ethanol and then incubated in constant humidity at a constant temperature of 37°C. On day 3, a hole was drilled at the narrow end and 2-3 mL of albumin was withdrawn using an 18-gauge hypodermic needle. The hole was sealed with sterile tape and the egg returned to incubation. On day 7, a window was opened in the shell and a sterile gel foam or sponge (3 mm×3 mm×1 mm) piece was placed on top of the membrane. The control group was given saline; the test and standard groups were impregnated with their respective doses. The eggs were incubated until day 14. On day 14, CAM tissues directly beneath the sponge were removed from control and treated CAM samples. The tissues were placed in 10% formalin, stained with hematoxylin-eosin, and then examined under a trinocular microscope. The vessel branching points in the square area were counted and analyzed for each treatment group. The resulting angiogenesis index is the mean ± standard error of mean (SEM) of the new branching points in each set of samples. An angiogenesis score of 1-4 was given to each egg based on the number of branching points. If the number of branching points is ≥35, the angiogenesis score is 4. If branches are between 25 and 34, the score is 3 and for 15-24, the score is 2. If the points are <15, the score is 1. The concentrations (10^{-6} M, 10^{-5} M, and 10^{-4} M) were selected based on the results

of previous studies. Previously, the concentration of 10^{-5} M resulted in submaximal efficacy of the drug. The classical molarity formula M=m/V was used to find the required drug amount to provide 10^{-4} M concentration. First the concentration of 10^{-4} M was prepared, and then the other concentrations were prepared from the earlier one by serial dilutions.[10-13]

Rat aortic ring assay

This method is a widely used *in vitro* assay for the evaluation of both angiogenic and anti-angiogenic compounds. One healthy male Wistar albino rat from each group was selected. It was sacrificed by cervical dislocation, the thoracic cavity was cut open, and the visceral organs were separated. The thoracic aorta was identified and isolated by cutting both ends. Immediately it was transferred to cold phosphate buffer solution (PBS) supplied with aeration. The fibro-adipose tissue was isolated, and the proximal and distal 2 mm segments of the aorta were cut away. The aorta was cut into 1 mm ring sections and washed with PBS. These rings were placed in 24-well plates with 150 µL of Matrigel. The rings were overloaded with Matrigel and were left to polymerize for 1-2 h at 37°C. Then they were exposed to hypoxia for 2 h. This hypoxic condition stimulates formation of sprouts. The rings were reoxygenated and then incubated for 7 days. The area of sprouts was quantified by the measurement of length and abundance of microvessel-like extensions from the explants.[14-16]

Sponge implantation method

In the sponge implantation method, the surgical procedure was done by a single investigator to increase the reproducibility of the process. The sponges were implanted subcutaneously (s.c.). All the surgical instruments used in the study were sterilized by autoclaving at 121°C for 25 min. Sponges of 2 cm diameter and 8 mm thickness were prepared and sterilized by soaking in 70% ethanol for 3 h and then boiling at 70°C for 30 min. This *in vivo* method was carried out by anesthetizing the rats using a cocktail of ketamine (80 mg/kg) and xylazine (5 mg/kg). Then the skin was cut open with a surgical blade. A sterile sponge was implanted s.c. by creating an air pocket, which was sutured back by 5/0 silk sutures. Two such sterile sponges were implanted on the mid-dorsal line of the body. When the animals recovered from anesthesia, they were allowed to have normal diet and water. The animals after the surgery were caged individually. Tramadol at a dose of 0.9 mg/kg was injected intramuscularly (i.m.) twice a day in the morning and evening; gentamycin at a dose of 2 mg/kg was injected i.m. in the morning. The analgesic and antibiotic drugs were given for the 3 days postoperatively. Standard and test drugs were applied to the sponges of their respective groups for 13 days after the implantation. On day 14 the animals were sacrificed and the sponges were dissected out. The sponges were weighed and the amount of hemoglobin and the number of vessels per sponge were quantified. The drug concentrations were expressed as mg/kg. The therapeutic

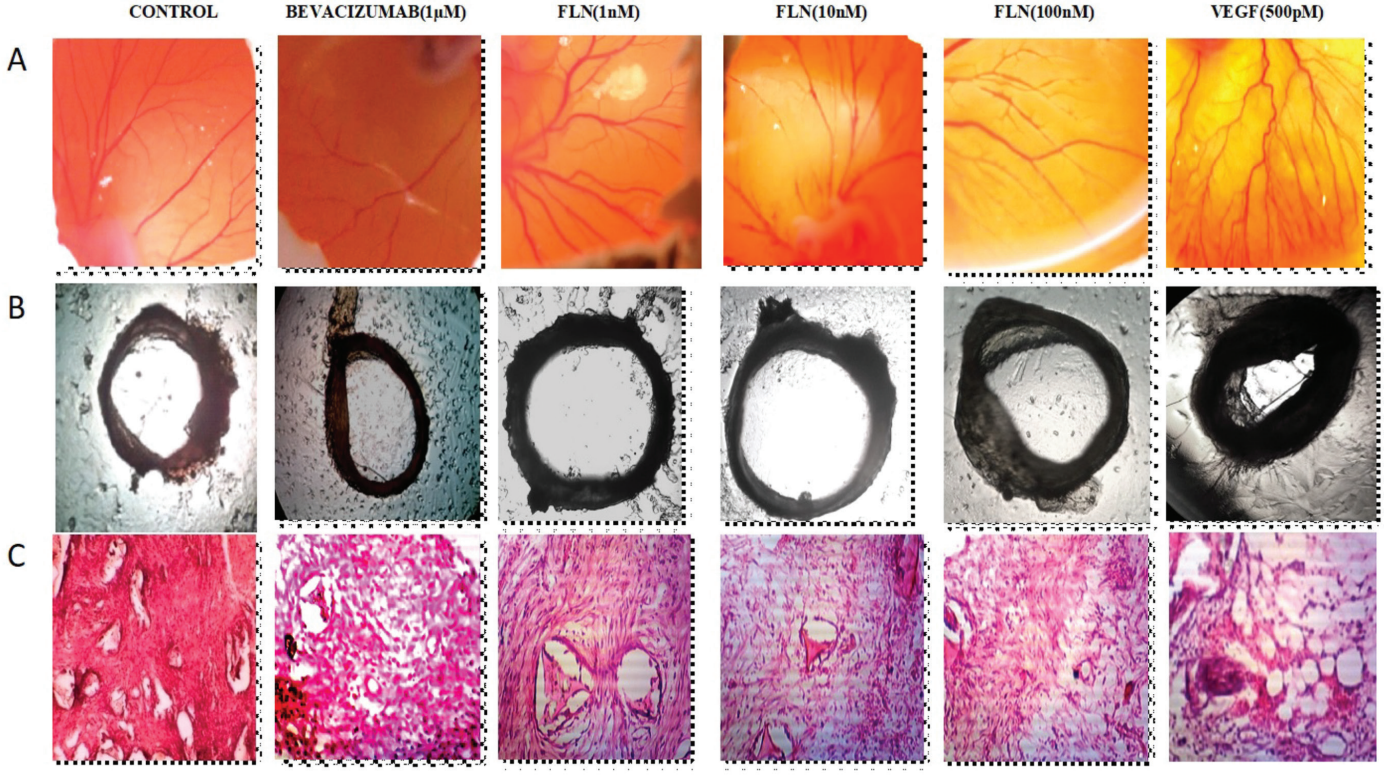

Figure 1. FLN intibited angiogenesis *in ovo*, *in vitro* and *in vivo*. (a) In the CAM assay numbers of branching points from each major vessel were counted. (b) Photographs of explants in the aortic ring assay show the micro vessel like extensions. (c) The histological sections of the sponges show circular spaces amidst the fibroblast region representing the newly formed blood vessels

FLN: Flunarizine, CAM: Chorioallantoic membrane, VEGF: Vascular endothelial growth factor

human range of each drug in the subcutaneous route was obtained from the literature and three animal doses were calculated by the formula;

$$\text{Dose of the animal} = \frac{\text{Surface area of animal}}{\text{Surface area of human}} \times \text{Human dose}$$

Here,

Rat surface area=0.025 m^2

Human surface area=1.6 m^2

First the highest concentration of each drug was prepared and then the other concentrations were prepared from the earlier one by serial dilutions.[17-19]

Procedure for determining hemoglobin content: The sponges after removal from the rats were soaked in double distilled water and homogenized completely over an ice platform for 5 min. The homogenate was centrifuged at 10,000 rpm in a cooling centrifuge for 5 min and the supernatant liquid obtained was used to estimate hemoglobin content (g/dL).

Procedure for determining number of blood vessels formed per sponge: The sponges were bisected and fixed in saline at 4°C for 1 h. The sponges were immersed in 75% ethanol for 30 min and finally kept in 10% formalin. Then paraffin sections (10 pm) were prepared and stained with hematoxylin-eosin. The prepared slides were then observed under a trinocular microscope. The circular spaces amidst the fibroblast regions present were counted as they represent vessels formed in the sponges.

Endothelial cell culture

Human umbilical vein EC (HUVECs) were grown on gelatinized dishes in M199 supplemented with 15% fetal calf serum, 50 U/mL penicillin, 50 mg/mL streptomycin, 50 mg/mL gentamycin, 2.5 mg/mL amphotericin B, 5 U/mL heparin, and 150-200 mg/mL EC growth supplement. Cells were used between passages 1 and 3. Each experiment shown is derived from three independent repeats, each time using different pools (isolates) and/or passages of cells.[20]

Endothelial cell proliferation assay

The HUVECs were seeded in 24-well plates at a density of 6000 cells/cm^2 and incubated overnight in Dulbecco's modified Eagle's medium. The cells were exposed to different concentrations of FLN, bevacizumab, VEGF, or vehicle and allowed to proliferate for 48 h. At the end of this incubation time, the cells were trypsinized, and their number was determined using a Neubauer hemocytometer.[21]

Transwell migration assay

The capacity of EC to migrate through a pore-bearing membrane was assessed using 6.5-mm diameter transwell chambers with polycarbonate membrane inserts (8 mm pore size). Control or ECs were serum starved overnight. The cells were trypsinized and 1×10^5 cells were added to each transwell in 100 mL of serum-free medium containing 0.2% bovine serum albumin in the control and in the presence of different concentrations of FLN (1 nM, 10 nM, and 100 nM), bevacizumab, and VEGF. The cells were allowed to migrate for 4 h, after which the nonmigrated cells at the top of the transwell filter were removed with a cotton swab. The migrated cells on the bottom side of the filter were fixed in Carson's solution for 30 min at room temperature and then were stained with toluidine blue. The migrated cells were scored and averaged from eight random fields per transwell as previously described elsewhere.[22]

Matrigel cord-like morphogenesis assay

The formation of cord-like structures by ECs (HUVECs) was assessed in growth factor-reduced Matrigel. The cell groups were plated in 96-well plates precoated with 45 mL of Matrigel per well. After 8 h of incubation, cord-like structure formation was quantified. One image per well was analyzed and used for the statistical analysis.[21,23]

Statistical analysis

The statistical analysis was carried out using GraphPad Prism 5. The results were presented as mean ± SEM. The differences between the groups were compared by one-way ANOVA followed by post hoc Dunnett's test. In the statistical analysis all the groups were compared with the control group. The results were considered statistically significant at p values <0.05. In all the groups of the CAM assay, rat aortic ring assay, and sponge implantation method, n=6 (Figures 2, 3).

RESULTS

In the chick CAM assay (*in ovo*), the dual ion channel blocker exhibited marked anti-angiogenic activity at all the tested concentrations. In the rat aortic ring assay (*in vitro*), a reduction in the area of sprouts was observed. A noticeable reduction in the weight of sponges and inhibition in the growth of new blood vessels, and a very sharp reduction in hemoglobin content were observed, which was better than the standard drug response (*in vivo*).

Results of the chick CAM assay

In the assay, on day 14 the CAM tissues directly beneath the sponge were removed from control and treated CAM samples. The vessel branching points in the square area equal to the region of each sponge were counted (Figure 1). An angiogenesis score of 1-4 was given to each egg based on the number of branching points. Effects of the drug treatment on the two evaluation parameters, that is the number of branching points and angiogenic score, are presented in Figures 2a and 2b. The results of three doses of FLN, the standard anti-angiogenic drug bevacizumab, and VEGF were statistically compared with the control results. Significant results were observed with all three test doses selected: 10^{-6} M, 10^{-5} M, and 10^{-4} M.

Results of the rat aortic ring assay

Photographs showing the abundance of microvessel-like extensions from the explants are given in Figure 1. A significant reduction in the area of sprouts was observed with 5 µM and 10 µM of the drug (Figure 2c).

Results of the sponge implantation method

In the sponge implantation method, the evaluation parameters are weight of the sponge, number of vessels per sponge, hemoglobin content, and the histopathology of the sponge. A moderate reduction in weight of sponges and a prompt inhibition in the growth of new blood vessels and hemoglobin content were observed at 1.0 mg/kg and 10 mg/kg of the drug (Figures 2d-2f). Sections of the sponges were observed under a trinocular microscope. The circular spaces amidst the fibroblast regions were counted as they represent new vessels formed in the sponges. In the VEGF group large numbers of vessels were identified, in the standard very few microvessels were formed due to the strong anti-angiogenic action, and the test drug caused a dose-dependent decrease in the number of blood vessels per sponge (Figure 1).

Results of the endothelial cell proliferation assay and transwell Matrigel and cord-like morphogenesis assay

Na^+ and Ca^{2+} channels are important for cell proliferation, migration, and cord-like network formation. To further test the link between channel inhibition and anti-angiogenesis, EC-based assays triggering proliferation and mobilization were performed. In the cell proliferation assay VEGF resulted in elevated proliferation (increase of 49%), whereas bevacizumab and the three doses of FLN showed significant inhibition of proliferation (inhibition by 50%, 79.3%, 69.7%, and 58.3%, respectively). In addition, test doses of FLN inhibited cell motility through transwell compartments comparable to the vehicle control, respectively. To further assess the anti-angiogenic property of the test drug, a cord-like tube formation assay was performed. Significant inhibition was observed with the test doses (69.3%, 59.7%, and 48.3%, respectively) (Figures 3 and 4).

DISCUSSION

FLN is a dual sodium/calcium blocker.[24] It acts on sodium and Ca^{2+} channels, blocking influx of Ca^{2+} ions. Ca^{2+} ions have long been known to be secondary messengers in various cellular signaling resulting in angiogenesis. The fact that deprivation of extracellular Ca^{2+} leads to cell growth arrest in G1/S indicates that Ca^{2+} is required for cell cycle progression.[25-27]

One of the Ca^{2+} regulation mechanisms is binding of calcium to calmodulin protein. Intracellular Ca^{2+} binds with calmodulin II, in turn activates calcium–calmodulin-dependent protein kinases, and regulates pro-survival transcriptional proteins.

In the chick CAM assay, the ion channel blocker exhibited potent anti-angiogenic activity at all three test concentrations of 10^{-6} M, 10^{-5} M, and 10^{-4} M. A reduction in the area of sprouts in the

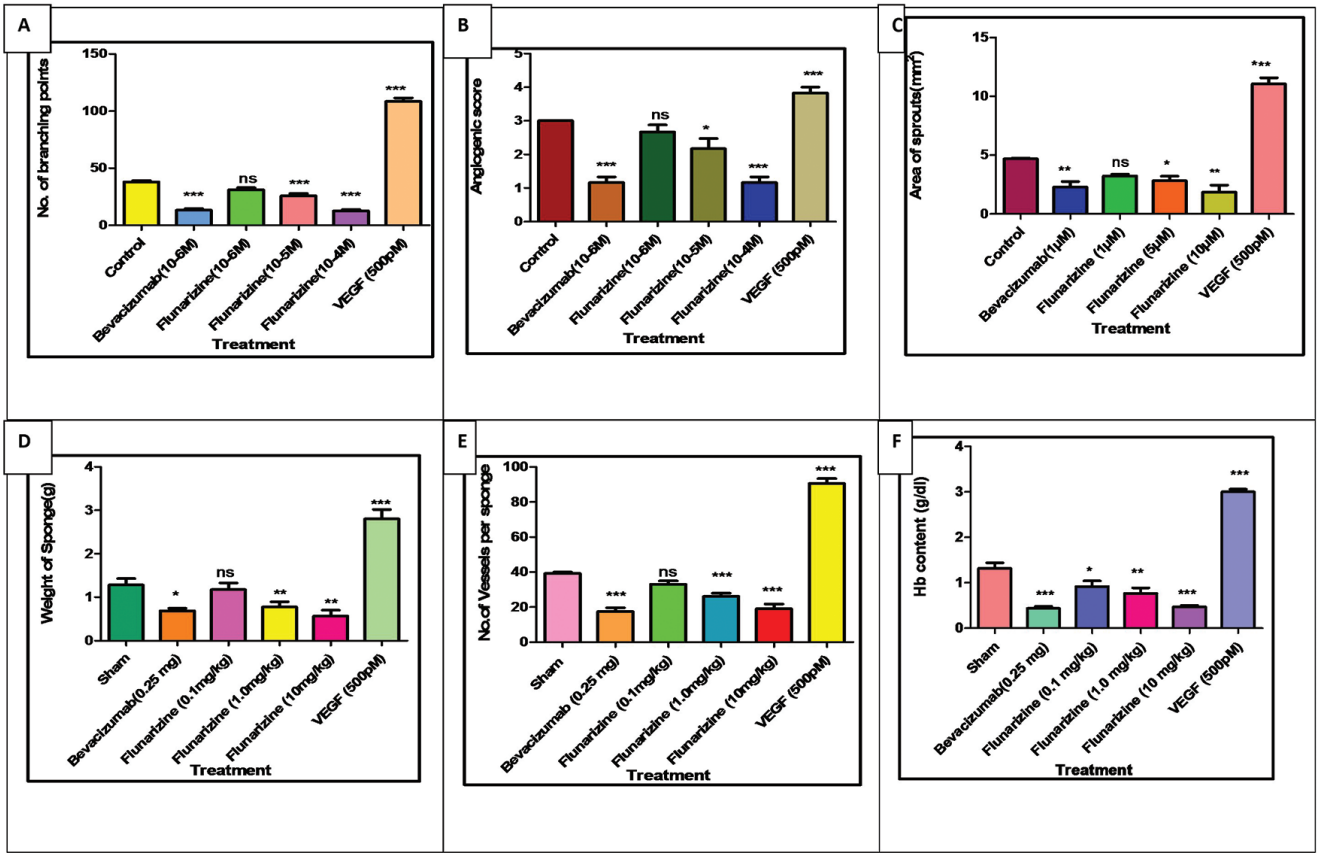

Figure 2. Graphs showing the effect of FLN on (A) number of branching points in CAM assay (B) angiogenic score in CAM assay (C) area of sprouts in aortic ring assay (D) weight of sponge in sponge implantation method (E) number of vessels per sponge (F) Hemoglobin content per sponge in sponge implantation method. All the results were expressed as mean ± standard error of mean; n=6. ***p<0.001, **p<0.01, *p<0.05 vs control

ns: Non-significance, FLN: Flunarizine, CAM: Chorioallantoic membrane, VEGF: Vascular endothelial growth factor

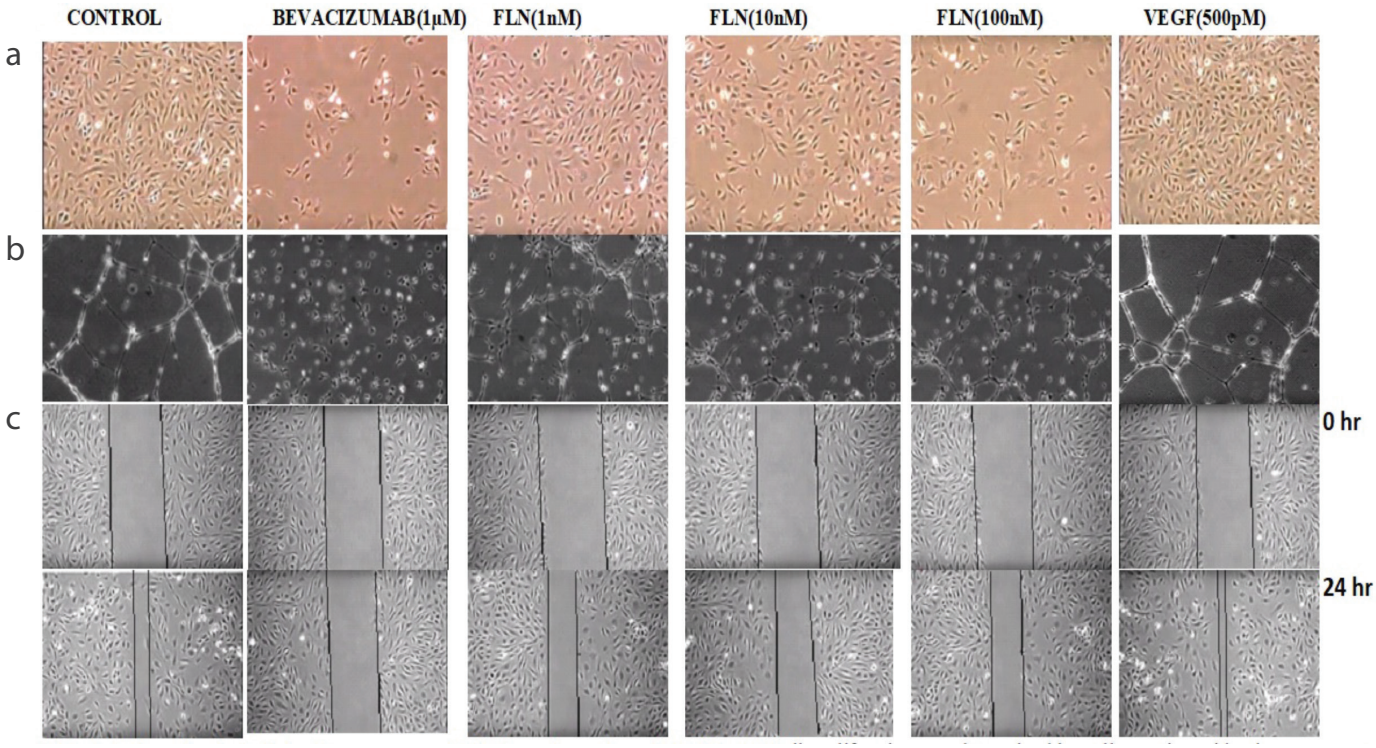

Figure 3. Modulation of endothelial cell responses to FLN, Bevacizumab and VEGF. (a) Cell proliferation was determined by cell counting with a hemocytometer. (b) Representative images of tube formation after being treated with FLN for 2 h following VEGF stimulation. (c) Quantitative data of scratch wound-healing inhibition in HUVECs treated with FLN for 24 h under VEGF stimulation. Cord-like network morphogenesis in vitro is affected by K_{ATP} modulation

FLN: Flunarizine, VEGF: Vascular endothelial growth factor, HUVECs: Human umbilical vein endothelial cells

rat aortic ring assay was observed with 5 µM and 10 µM of FLN. A significant reduction in the weight of sponges, number of blood vessels formed, and hemoglobin content were observed at 1 mg/kg and 10 mg/kg. The results revealed that FLN has significant inhibition of sprout formation and branching in a dose-dependent manner. Modulation of EC response to FLN was significant at all the test doses of 1 nM, 10 nM, and 100 nM on the EC proliferation, migration, and tube formation assays. FLN, being a strong blocker of Ca^{2+} ion influx, gave significant anti-angiogenic results. This drug serves as good chemical template that can be structurally modified for more site-specific actions for anti-angiogenic therapy.

CONCLUSIONS

The anti-angiogenic property of an ion channel modulator, FLN, was thoroughly evaluated by *in ovo*, *in vitro*, and *in vivo* studies. The test drug showed very potent anti-angiogenic activity, even better than that of the standard drug bevacizumab at a concentration range of 5-10 µM. The very strong anti-angiogenic potential is due to effective blockage of Ca^{2+} influx. Na^{+}/Ca^{2+} dual blocker inhibits the Ca^{2+} influx with double the strength. Calcium dynamics play a crucial role in the critical steps of angiogenesis like cell migration, proliferation, and even cell death. Molecular modifications of the ion channel modulator used in the present study will evolve EC targeted chemical moieties. Furthermore, such endothelial targeted chemical moieties can be formulated suitably to achieve a site specific action that minimizes side effects.

ACKNOWLEDGEMENT

We thank the management of CMR College of Pharmacy for their support to us to perform the research in the institution. The research was partially supported by University grants commission, minor research project grant (proposal number: 3228; ROMRP-SERO-PHAR-2015-16-68663).

Conflict of Interest: No conflict of interest was declared by the authors.

REFERENCES

1. Adair TH, Montani JP. Angiogenesis. Colloquium series on integrated systems physiology: From molecule to function. Morgan & Claypool Life Sciences. 2010
2. Tahergorabi Z, Khazaei M. A review on angiogenesis and its assays. Iran J Basic Med Sci. 2012;15:1110-1126.
3. Folkman J. Angiogenesis in psoriasis: therapeutic implications. J Invest Dermatol. 1972;59:40-43.
4. Khurana R, Simons M, Martin JF, Zachary IC. Role of angiogenesis in cardiovascular disease. Circulation. 2005;112:1813-1824.
5. Galley HF, Webster NR. Physiology of the endothelium. Br J Anaesth. 2004;93:105-113.
6. Karamysheva AF. Mechanisms of Angiogenesis. Biochemistry (Moscow). 2008;73:751-762.
7. Munaron L. Systems biology of ion channels and transporters in tumor angiogenesis: An omics view. Biochim Biophys Acta. 2015;1848:2647-2656.

8. Nilius B, Droogmans G. Ion channels and their functional role in vascular endothelium. Physiol Rev. 2001;81:1415-1459.

9. Arcangeli A, Becchetti A. New trends in cancer therapy: targeting ion channels and transporters. Pharmaceuticals (Basel). 2010;3:1202-1224.

10. Lokman NA, Elder AS, Ricciardelli C, Oehler MK. Chick chorioallantoic membrane (CAM) assay as an *in vivo* model to study the effect of newly identified molecules on ovarian cancer invasion and metastasis. Int J Mol Sci. 2012;13:9959-9970.

11. Peifer C, Dannhardt G. A novel quantitative chick embryo assay as an angiogenesis model using digital image analysis. Anticancer Res. 2004;24:1545-1551.

12. Cruz A, Parnot C, Ribatti D, Corvol P, Gasc JM. Endothelin-1, a regulator of angiogenesis in the chick chorioallantoic membrane. J Vasc Res. 2001;38:536-545.

13. Yıldız Ç, Cetin A, Demirci F, Polat ZA, Kiyan T, Altun A, Cetin M, Yildiz ÖK, Goze İ. Anti-Angiogenic Effects of Diltiazem, Imatinib, and Bevacizumab in the CAM Assay. International Journal of Scientific and Research Publications. 2013;3:1-8.

14. AlMalki WH, Shahid I, Mehdi AY, Hafeez MH. Assessment methods for angiogenesis and current approaches for its quantification. Indian J Pharmacol. 2014;46:251-256.

15. Goodwin AM. *In vitro* assays of angiogenesis for assessment of angiogenic and anti-angiogenic agents. Microvasc Res. 2007;74:172-183.

16. Khoo CP, Micklem K, Watt SM. A Comparision of Methods for Quantifying Angiogenesis in the Matrigel Assay *in vitro*. J Tissue Eng Part C Methods. 2011;17:895-906.

17. Veeramani VP, Veni G. An essential review on current techniques used in angiogenesis assays. International Journal of PharmTech Research. 2010;2:2379-2387.

18. Lokman NA, Elder AS, Ricciardelli C, Oehler MK. Chick chorioallantoic membrane (CAM) assay as an *in vivo* model to study the effect of newly identified molecules on ovarian cancer invasion and metastasis. Int J Mol Sci. 2012;13:9959-9970.

19. Lee MS, Moon EJ, Lee SW, Kim MS, Kim KW, Kim YJ. Angiogenic activity of pyruvic acid in *in vivo* and *in vitro* angiogenesis models. Cancer Res. 2001;61:3290-3293.

20. Geer JJ, Dooley DJ, Adams ME. K(+)-stimulated 45Ca^{2+} flux into rat neocortical mini-slices is blocked by omega-Aga-IVA and the dual Na^{+}/Ca^{2+} channel blockers lidoflazine and flunarizine. Neurosci Lett. 1993;158:97-100.

21. Le Guennec JY, Ouadid-Ahidouch H, Soriani O, Besson P, Ahidouch A, Vandier C. Voltage-gated ion channels, new targets in anti-cancer research. Recent Pat Anticancer Drug Discov. 2007;2:189-202.

22. El-Kenawi AE, El-Remessy AB. Angiogenesis inhibitors in cancer therapy: mechanistic perspective on classification and treatment rationales. Br J Pharmacol. 2013;170:712-729.

23. Urrego D, Tomczak AP, Zahed F, Stühmer W, Pardo LA. Potassium channels in cell cycle and cell proliferation. Philos Trans R Soc B Sci. 2014;369:20130094.

24. Su M, Huang J, Liu S, Xiao Y, Qin X, Liu J, Pi C, Luo T, Li J, Chen X, Luo Z. The anti-angiogenic effect and novel mechanisms of action of Combretastatin A-4. Sci Rep. 2016;6:28139.

25. Pyriochou A, Tsigkos S, Vassilakopoulos T, Cottin T, Zhou Z, Gourzoulidou E, Roussos C, Waldmann H, Giannis A, Papapetropoulos A. Anti-angiogenic properties of a sulindac analogue. Br J Pharmacol. 2007;152:1207-1214.

26. Umaru B, Pyriochou A, Kotsikoris V, Papapetropoulos A, Topouzis S. ATP-sensitive potassium channel activation induces angiogenesis *in vitro* and *in vivo*. J Pharmacol Exp Ther 2015;354:79-87.

27. Papapetropoulos A, Pyriochou A, Altaany Z, Yang G, Marazioti A, Zhou Z, Jeschke MG, Branski LK, Herndon DN, Wang R, Szabó C. Hydrogen sulfide is an endogenous stimulator of angiogenesis. Proc Natl Acad Sci U S A. 2009;106:21972-21977.

Turk J Pharm Sci 2019;16(3):310-316
DOI: 10.4274/tjps.galenos.2018.15013

ORIGINAL ARTICLE

Superior Solubility and Dissolution of Zaltoprofen via Pharmaceutical Cocrystals

Farmasötik Cocrystal ile Zaltoprofen'in Üstün Çözünürlük ve Çözünmesi

Prabhakar PANZADE*, Giridhar SHENDARKAR

Center for Research in Pharmaceutical Sciences, Nanded Pharmacy College, Opp. Kasturba Matruseva Kendra, Sham Nagar, Nanded, India

ABSTRACT

Objectives: Pharmaceutical cocrystals are a promising tool to enhance the solubility and dissolution of poorly soluble drugs. Zaltoprofen (ZFN) is nonsteroidal anti-inflammatory drug with a prevalent solubility problem. The present study was undertaken to enhance the solubility and dissolution of ZFN through pharmaceutical cocrystals by screening various coformers.

Materials and Methods: Cocrystals of ZFN were prepared in 1:1 and 1:2 ratio of drug:coformer by the dry grinding method. The melting point and solubility of the crystalline phase were determined. The potential cocrystals were characterized by differential scanning calorimetry (DSC), infrared spectroscopy, and powder X-ray diffraction (PXRD). Cocrystals were subjected to dissolution rate and stability study.

Results: ZFN-nicotinamide (NIC) cocrystals demonstrated deviation in melting point and solubility. The cocrystals were obtained in both 1:1 and 1:2 ratios with NIC. The infrared analysis noticeably indicated the shifting of characteristic bands of ZFN. The crystallinity of the cocrystals was evident from the XRPD pattern and notable difference in the 2θ values of intense peaks. The DSC spectra of the cocrystals exhibited altered endotherms analogous to melting point. The cocrystals showed a faster dissolution rate and a 55% increase in the extent of dissolution compared to pure drug. The cocrystals were stable at room temperature and accelerated conditions.

Conclusion: The prepared cocrystals exhibited greater solubility and dissolution compared to the pure drug and were stable at room temperature and accelerated conditions.

Key words: Pharmaceutical cocrystal, zaltoprofen, solubility, dissolution

ÖZ

Amaç: Farmasötik kokristal, zayıf çözünür ilaçların çözünürlüğünü ve çözünmesini arttırmak için umut veren bir araçtır. Zaltoprofen (ZFN) yaygın çözünürlüğe sahip nonsteroid antiinflamatuvar ilaçtır. Bu çalışma, çeşitli koformerlerin taranması yoluyla farmasötik kokteyli aracılığıyla ZFN'nin çözünürlüğünü ve çözünmesini arttırmak için üstlenilmiştir.

Gereç ve Yöntemler: Kuru öğütme yöntemi ile 1:1 ve 1:2 oranında ilaç:koformer oranında ZFN kristalleri hazırlanmıştır. Erime noktası ve kristalin fazın çözünürlüğü belirlenmiştir. Potansiyel kristaller differansiyel tarama kalorimetrisi (DSC), kızılötesi spektroskopi ve toz X ışını kırınımı (PXRD) ile karakterize edilmiştir. Kokristaller çözünme hızına ve stabilite çalışmasına tabi tutulmuştur.

Bulgular: ZFN-nikotinamid (NIC) kokristal erime noktasında ve çözünürlükte sapma göstermiştir. Kristaller, NIC ile hem 1:1 hem de 1:2 oranında elde edilmiştir. Kızılötesi analizi, ZFN karakteristik bantlarının kaymasını belirgin bir şekilde göstermiştir. Kristallerin kristallenmesi XRPD paterninden belirgin olarak görülmüştür ve 2θ değerindeki yoğun zirvelerdeki kayda değer farklılıklar gözlenmiştir. Kristallerin DSC spektrumları, erime noktasına benzer değiştirilmiş endotermler sergilemiştir. Kristaller, daha hızlı çözünme oranı ve saf ilaçla karşılaştırıldığında çözünme derecesinde % 55 artış göstermiştir. Kristaller, oda sıcaklığında ve hızlandırılmış koşullarda kararlı bulunmuştur.

Sonuç: Hazırlanan kristaller, saf ilaca kıyasla daha fazla çözünürlük ve çözünme sergilemiş ve oda sıcaklığında ve hızlandırılmış koşullarda sabit bulunmuştur.

Anahtar kelimeler: Farmasötik kokristal, zaltoprofen, çözünürlük, çözünme

***Correspondence: E-mail:** prabhakarpanzade@gmail.com, **Phone:** +91-9921830320 **ORCID-ID:** orcid.org/0000-0003-1247-9197
Received: 24.03.2018, **Accepted:** 07.06.2018

INTRODUCTION

After oral administration the solubility and dissolution rate of a drug are crucial factors for its sufficient bioavailability. These factors are the main challenge to the formulation scientist for the development and formulation of effective drugs. More than 40% of drugs in development suffer from bioavailability problems owing to poor solubility. Alternative strategies have been introduced to enhance solubility, the dissolution rate, and bioavailability. These involve salt formation, solid dispersion, cyclodextrin complexation, microemulsification, solubilization, micronization, etc.[1-4]

Recently pharmaceutical cocrystals have attracted considerable attention from formulation experts busy in formulation development. Due to the inherent thermodynamic stability of crystalline active pharmaceutical ingredients (APIs), these are preferred in the pharmaceutical industry. Pharmaceutical cocrystals have emerged as an effective tool to tailor the physical properties of APIs like solubility and dissolution along with stability. The principal advantage of this technique is that the pharmacological effect of the drug remains unchanged.[5-7] Cocrystals are defined as stoichiometric multicomponent systems united by noncovalent interactions in which two diverse components are solid under ambient conditions. The documented advantages of cocrystals are improved stability against humidity, chemical stability, improved dissolution and bioavailability, and tabletability. Various methods were studied to enhance solubility like hydrotropy and solid dispersion. To the best of our knowledge, pharmaceutical cocrystals of zaltoprofen (ZFN) have not been reported to date.[8-14]

ZFN is a nonsteroidal anti-inflammatory propionic acid class drug. It is used in the treatment of acute and chronic inflammation and rheumatoid arthritis. It is practically insoluble in water and associated with side effects like ulcerogenicity, bellyache, and indigestion. Moreover, ZFN is weakly ionizable and so salt formation cannot enhance the solubility of the drug. Rapid onset and improved bioavailability are desired for analgesics. Hence there is a strong scientific and clinical need to prepare novel forms of ZFN possessing modified solubility and dissolution rates that can be formulated for oral administration. Accordingly, the aim of the present study was to prepare novel pharmaceutical cocrystals of ZFN with improved solubility and dissolution.[15,16]

MATERIALS AND METHODS

Materials

ZFN was received as a gift sample from ICPA Laboratory Ltd. (Mumbai, India). All other chemicals were purchased from the SD Fine Chemicals (Mumbai, India). Double distilled water was used throughout the research.

Preparation of cocrystals

The dry grinding method was adopted for the preparation of ZFN cocrystals. The drug and coformers were mixed in different molar ratios (1:1 and 1:2) in a mortar and pestle for 45 min to form cocrystals. They were dried overnight at ambient temperature and stored in tight containers.[17] Twenty-five coformers were screened for the preparation of cocrystals, i.e. salicylic acid, nicotinamide (NIC), glutaric acid, malonic acid, benzoic acid, tartaric acid, oxalic acid, citric acid, urea, succinic acid, saccharine sodium, Pluronic 68 AR, magnesium stearate, crotonic acid, P-hydroxy benzoic acid, caffeine, 3,5 dihydroxy benzoic acid, piperazine citrate, cinnamic acid, adipic acid, hydroquinone, isonicotinic acid, acetamide, maleic acid, and ascorbic acid.

Evaluation of cocrystals

Drug content

Cocrystal powder equivalent to 10 mg of drug was accurately weighed and dissolved in a 10 mL volumetric flask and the volume was adjusted with phosphate buffer pH 6.8. The resulting solution was filtered, suitably diluted, and the absorbance of the solution was measured at 243 nm (Shimadzu UV 1800).[18]

Determination of melting points

Melting points of the compounds were determined using a digital melting point apparatus (Labtronics Ltd).

Saturation solubility

An excess amount of pure drug and cocrystals were dissolved in 10 mL vials containing the drug to estimate solubility. The vials were agitated on rotary shaker and allowed to stand for equilibration for 24 h. The samples were filtered after 24 h, suitably diluted with distilled water, and analyzed by UV spectrophotometer at 243 nm.

Infrared spectroscopy

Infrared (IR) spectroscopy was employed to determine the possible interaction between the drug and coformers. Samples were mixed with potassium bromide and compressed into discs before scanning between 4000 and 400 cm^{-1} with resolution of 4 cm^{-1} by Shimadzu IR spectrophotometer.

Differential scanning calorimetry

The thermal behavior of the drug alone and cocrystals was determined on a Mettler Toledo DSC 822e Module. Weighed samples were loaded into an aluminum pan before crimping and heated at a rate of 5°C/min, covering the 0 to 300°C temperature range, under a nitrogen stream. The instrument was calibrated using indium and an empty aluminum pan was used as a reference.

Powder X-ray diffraction

Silicon sample holders were utilized to get diffraction patterns for pure ZFN and cocrystals (Bruker D8 Advance diffractometer). The instrument was equipped with a fine focus X-ray tube and each sample was placed onto a goniometer head that was motorized to permit spinning of the sample during data acquisition.

In vitro dissolution study

Pure ZFN and its cocrystals were subjected to dissolution study by USP type II apparatus (Electrolab, Mumbai, India). The dissolution study was performed in 900 mL of pH 6.8

phosphate buffer at 37±0.5°C and 50 rpm for 60 min. The pure drug and cocrystals equivalent to 80 mg of drug were used for the study. Then 5 mL samples were withdrawn after specified time intervals and analyzed by UV spectrophotometer at 243 nm.[19]

Stability study

The selected cocrystals were subjected to a stability study at room temperature and 40±2°C with 75±5% RH for 3 months. A sample of 1 g was placed in an eppendorf tube in a stability chamber throughout the stability duration and analyzed after 30 days, 60 days, and 90 days. Different attributes were studied to assess the stability, i.e. drug content, melting point, solubility, *in vitro* drug release, etc.

RESULTS AND DISCUSSION

The 25 coformers were screened to prepare cocrystals with ZFN by the dry grinding method. The coformers were selected based on a literature survey and to increase the chances of formation of new cocrystals. Among the various coformers studied, NIC successfully interacted with ZFN, giving novel cocrystal forms. The obtained ZFN cocrystals were subjected to evaluation and stability studies.

Drug content

The drug content of ZFN-NIC 1:1 and 1:2 cocrystals was determined in phosphate buffer pH 6.8 as 95.87±0.98% and 95.88±1.10%, respectively.

Melting points and saturation solubility

The melting points of pure drug, coformers, and cocrystals were estimated and are reported in Table 1. In addition, the saturation solubility of pure drug and cocrystals was also determined and is reported in Table 1. These parameters were used for preliminary screening of the cocrystals. The melting points of the ZFN-NIC cocrystals were lower than that of the pure drug. This may be attributed to the multicomponent system and the probable formation of cocrystals. The altered melting points might be due to an interaction between ZFN and NIC, modified crystallinity of molecules, or distinct packing arrangement. This interaction results in an altered molecular arrangement, which leads to novel crystal forms with distinct physical properties.[20,21]

The solubility of a few cocrystals was improved but ZFN-NIC cocrystals exhibited a remarkable increase in solubility, indicating successful interaction of drug and coformer. However, greater solubility was obtained with ZFN-NIC 1:2 cocrystals (1.516±0.467 mg/mL) than with 1:1 (0.926±0.134 mg/mL). The ZFN-NIC 1:1 and 1:2 cocrystals showed 42-fold and 66-fold increases in solubility in comparison to the pure drug. The results were compared using Dunnet's test and statistically significant differences were found in solubility ($p<0.05$) between the pure drug and cocrystals. This indicates an interaction between ZFN and NIC leading to cocrystal formation. The interaction between the oxygen atom of the drug and the primary amide hydrogen of the NIC might have formed the cocrystal. Similar studies were reported on cocrystals of meloxicam, lornoxicam, aceclofenac, etc.[22,23]

On the basis of the results, ZFN-NIC 1:1 and 1:2 cocrystals were further characterized and confirmed.

IR spectroscopy

The IR spectra for the pure drug, coformer, and ZFN cocrystals were recorded and are shown in Figures 1 and 2. The principle bands were identified and related changes were recorded. The IR spectrum of pure ZFN shows the presence of the characteristic peaks, which were recorded at 1699 cm^{-1} and 1668 cm^{-1} for stretching of the carboxylic group, -C-S-C- aromatic stretching peaks observed at 939.39 cm^{-1}, OH stretching in the carboxylic group at 2950 cm^{-1}, and CH_3 stretching at 1330 cm^{-1}. The IR spectrum of NIC revealed an absorption band at 3145 cm^{-1} for NH_2 stretching of primary amide and 3342 cm^{-1} for the pyridine ring region, NH bending is observed at 1593 cm^{-1}, and aromatic C=C peaks are observed at 1614 cm^{-1}. These spectra are in good agreement with the published data. The IR bands were significantly changed in the cocrystals in comparison to the pure drug and coformer, indicating an interaction between drug and coformer.[24]

In the case of the 1:1 cocrystal changes were observed in the peaks corresponding to carboxylic group stretching, which was observed at 1634 cm^{-1}, OH stretching at 3000 cm^{-1} in comparison to the drug, and NH_2 stretching and NH bending at 3450 and 1583 cm^{-1} as compared to NIC and 1654 cm^{-1}, 3000 cm^{-1}, 3300 cm^{-1}, and 1583 cm^{-1} for the 1:2 cocrystal, respectively.

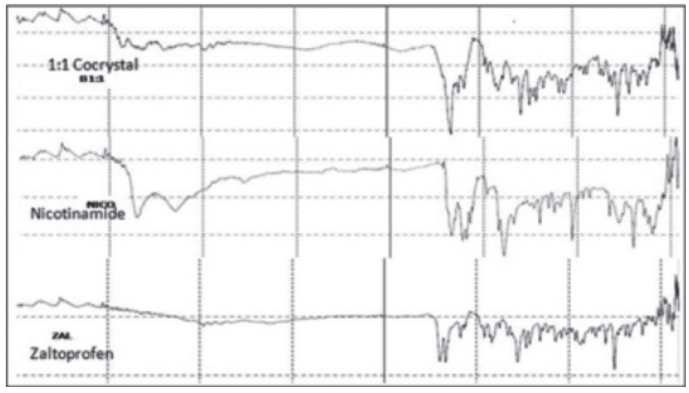

Figure 1. Overlay IR spectra of 1:1 cocrystal

IR: Infrared spectroscopy

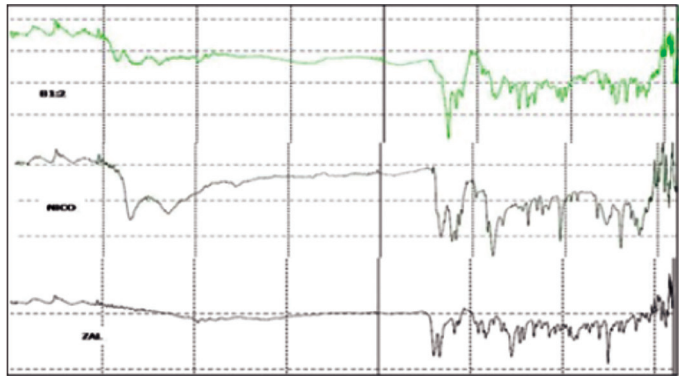

Figure 2. Overlay IR spectra of 1:2 cocrystal

IR: Infrared spectroscopy

A new peak at 3450 cm^{-1} and one at 3400 cm^{-1} were observed, indicating the formation of a hydrogen bond between the drug and coformer in the ZFN-NIC 1:1 and 1:2 cocrystals, respectively, prepared by the neat grinding method.[25]

Similar changes in the IR spectra of other drugs like piroxicam and hydrochlorothiazide were reported and considered as a sign of cocrystal formation.[26,27] Hence the changes recorded in the present study can be regarded as a indicator of cocrystal formation between the drug and coformer.

Differential scanning calorimetry

ZFN, NIC, and ZFN-NIC cocrystals were characterized by DSC. The pure drug and NIC showed characteristic endothermic peaks at 137.69°C and 129.67°C, respectively, corresponding to their melting points. Similar thermal behavior was reported for the drug and coformer.[28]

ZFN-NIC (1:1 and 1:2) cocrystals exhibited melting points at 109.20°C and 123.50°C, respectively, which are significantly different from that of the pure drug. Moreover, the peak onset for the pure drug was obtained at 131.52°C and at 102.40°C and 120.02°C for 1:1 and 1:2 cocrystals, respectively.

The changes in the thermal properties were reported as evidence for the formation of cocrystals.[29] Hence the present investigation indicates the formation of cocrystals (Figure 3).

Powder X-ray diffraction

The powder X-ray diffraction (PXRD) patterns for ZFN, NIC, and ZFN-NIC cocrystals are shown in Figures 4 and 5. The materials in the powder state give different peaks of varying intensities at certain positions. The diffractogram of the ZFN showed characteristic numerous sharp, intense diffraction peaks at

Table 1. Melting point and solubility of cocrystals

Drug/potential cocrystal	Melting point of coformer (°C)	Cocrystal melting point (1:1) (°C)	*Cocrystal solubility (mg/mL) (1:1)	Cocrystal melting point (1:2) (°C)	*Cocrystal solubility (mg/mL) (1:2)
ZFN	133-135		0.022±0.005		
ZFN-Salicylic acid	158-159	133.5	0.452±0.078	135	0.445±0.095
ZFN-Nicotinamide	122-124	128	0.926±0.134	121	1.516±0.467
ZFN-Glutaric acid	96	119.5	0.0136±0.0089	120.5	0.0819±0.023
ZFN-Malonic acid	130	113.5	0.0083±0.093	116.5	0.0077±0.001
ZFN-Benzoic acid	122	103	0.416±0.098	100	0.721±0.278
ZFN-Tartaric acid	164-167	146.5	0.0218±0.013	146.5	0.0103±0.008
ZFN-Oxalic acid	99	117	0.0147±0.017	115.5	0.0261±0.009
ZFN-Citric acid	148-150	135.5	0.0098±0.00097	134.5	0.0080±0.002
ZFN-Urea	131	129.5	0.367±0.067	128.5	0.228±0.090
ZFN-Succinic acid	184	152	0.0287±0.008	153	0.0210±0.007
ZFN-Sodium saccharine	226-230	126.5	0.154±0.069	181	0.207±0.067
ZFN-Pluronic 68 AR	53-54	65.5	0.152±0.089	62.5	0.139±0.083
ZFN-Magnesium stearate	88.5	91.5	0.761±0.284	126.5	0.536±0.132
ZFN-Crotonic acid	74-75	124	0.064±0.016	95	0.0714±0.021
ZFN-Phydroxy benzoic acid	208	160	0.820±0.349	164.5	0.980±0.230
ZFN-Caffeine	238	175.5	0.354±0.078	152	0.435±0.098
ZFN-3,5 dihydroxy benzoic acid	236-238	184.5	0.256±0.086	187.5	0.372±0.068
ZFN-Piperazine citrate	183-187	197	0.160±0.067	199.5	0.179±0.043
ZFN-Cinnamic acid	132-134	113	0.339±0.129	117.5	0.440±0.065
ZFN-Adipic acid	151-154	141	0.0282±0.009	143	0.0202±0.009
ZFN- Hydroquinone	172.3	123.5	0.109±0.008	124.5	0.0597±0.006
ZFN-Isonicotinic acid	310	284	0.0950±0.021	292	0.103±0.089
ZFN-Acetamide	79-81	98.5	0.0246±0.026	92	0.0232±0.007
ZFN- Maleic acid	135	124.5	0.0700±0.039	130.5	0.0785±0.013
ZFN-Ascorbic acid	190	158	0.0593±0.009	160	0.0525±0.013

ZFN: Zaltoprofen, *Average of three determinations mean ± standard deviation

different 2θ values (15, 17.5, 19, 31, 32.5, and 42), indicating a crystalline nature. In addition, the diffraction peaks obtained for NIC were 25, 30, 34.5, 37, 47.5, and 50.5 2θ values. Similar diffraction patterns were reported in previous investigations. The PXRD pattern of the cocrystal was distinguishable from that of its components and some additional diffraction peaks appeared that did not exist in the pure drug or coformer. The additional diffraction peaks for 1:1 and 1:2 cocrystals were obtained at 2θ values of 16, 17, 18, 19, 20, 30.5, and 37.5 and 17.5, 18.5, 26.5, 34.5, 37.5, 40.5, and 50.5, respectively. The appearance of new diffraction peaks in the diffractogram of cocrystals shows the formation of a new crystalline phase

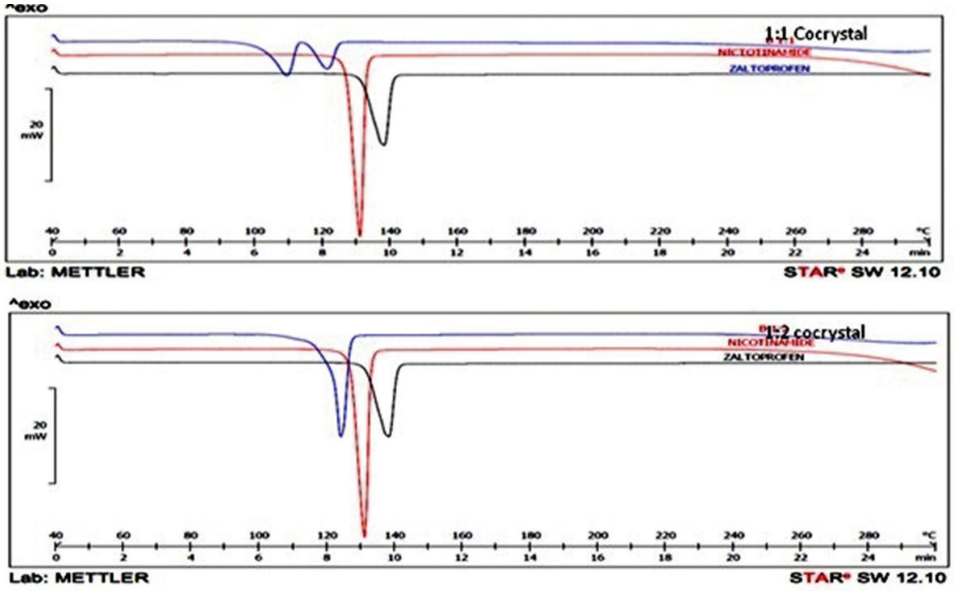

Figure 3. Overlay DSC thermogram of 1:1 and 1:2 cocrystals

DSC: Differential scanning calorimetry

Table 2. Stability study of cocrystals

Parameters	Sampling	Zaltoprofen (accelerated)	Zaltoprofen (room temperature)	Cocrystal neat grinding (accelerated)		Cocrystal neat grinding (room temperature)	
				1:1	1:2	1:1	1:2
Melting point (°C)	Initial	133-134	133-134	111-114	120-121	111-114	120-121
	1 month	133-134	133-135	114-115	115-117	116-117	124-126
	2 month	132-133	131-133	115-118	117	116-118	115-117
	3 month	132-134	131-134	114-116	116	115-116	116-118
Solubility (mg/mL)	Initial	0.01513	0.0151	0.926	1.516	0.9261	1.516
	1 month	0.01518	0.0131	1.016	1.202	1.077	1.159
	2 month	0.01464	0.0136	1.126	1.268	1.126	1.308
	3 month	0.01445	0.0131	0.913	1.070	1.020	1.149
In vitro dissolution (%)	Initial	52.01	52.01	98.32	98.89	98.32	98.89
	1 month	64.76	65.49	98.78	94.51	99.26	99.45
	2 month	64.81	64.81	98.74	98.39	98.74	98.39
	3 month	64.06	63.63	99.53	99.74	98.69	98.81
Drug content	Initial	-	-	95.87	95.88	95.87	95.88
	1 month	-	-	95.70	95.3	95.74	95.57
	2 month	-	-	95.2	94.96	95.47	95.90
	3 month	-	-	95.00	95.05	95.08	95.59

(cocrystals). The formation of cocrystals based on the PXRD pattern was reported and showed new peaks that differ from the peaks corresponding to its input components.[30,31]

In vitro dissolution study

The dissolution rate plays a crucial role in the bioavailability of drugs with poor solubility. The dissolution experiment was conducted on the pure drug and cocrystals. The dissolution profile of the pure drug and the prepared cocrystals is shown in Figure 6. The dissolution profile of the pure drug indicates a slow dissolution rate with only 27.17±0.89% of the drug being dissolved in the first 10 min. The total amount of drug dissolved in 60 min was 43.82±1.06% and the calculated dissolution efficiency was only 27.4%. However, cocrystals of the ZFN resulted in a substantial increase in the dissolution rate. The amount of drug dissolved in first 10 min was 50.66±0.32% and 46.67±0.65% for the 1:1 and 1:2 cocrystals, respectively. The maximum amount of drug dissolved was 98.89±0.48% for the 1:2 cocrystal with dissolution efficiency of 86.71%, whereas it was 94.14±0.91% for the 1:1 cocrystal, having a dissolution efficiency of 81.78%. This can indicate a weaker crystalline structure of the formed cocrystal as evident from the higher dissolution rate. Moreover, greater dissolution of ZFN from the cocrystal can be attributed to enhanced solubility of the cocrystal in the dissolution media. Cocrystallization had been well documented as a suitable technique for dissolution enhancement.[32] The similarity factor test denoting the dissolution of pure drug showed dissimilarity to the prepared cocrystals (F2 value 20% and 22% for 1:1 and 1:2 cocrystals).

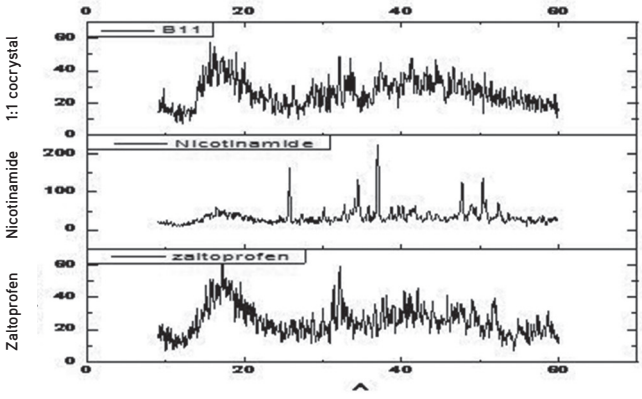

Figure 4. Overlay PXRD pattern for 1:1 cocrystal (1:1 cocrystal)

PXRD: Powder X-ray diffraction

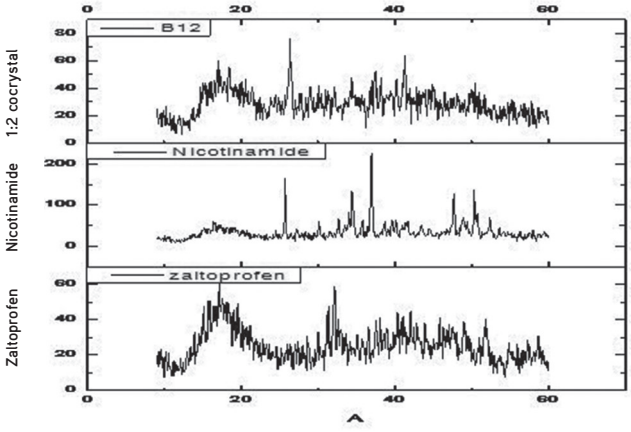

Figure 5. Overlay PXRD pattern for 1:2 cocrystal (1:2 cocrystal)

PXRD: Powder X-ray diffraction

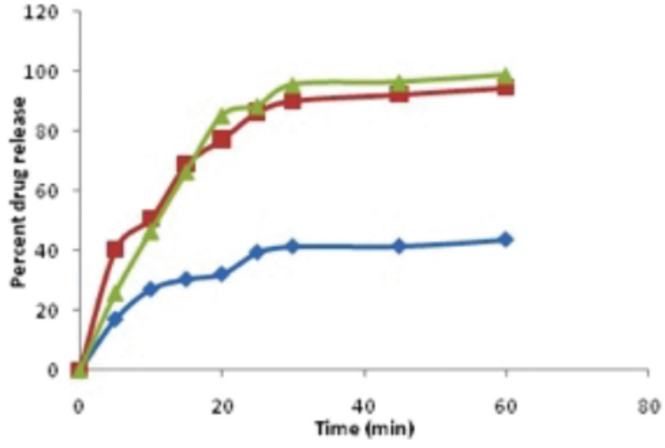

Figure 6. *In vitro* drug release

Stability study

The drug and cocrystals were subjected to a stability study at room temperature and accelerated conditions for 3 months to assess the stability of cocrystals. All the cocrystals were stable at both storage conditions and no substantial change in the estimated parameters like melting point, solubility, *in vitro* drug release, and drug content was obtained except ZFN:NIC 1:2 cocrystal solubility at accelerated conditions. However, the pure drug exhibited changes in solubility and percent dissolution during the stability period, indicating instability. Hence cocrystal stability was enhanced in comparison to the pure drug. This demonstrates the potential of cocrystals to improve drug stability. Similar results have been reported for theophylline.[33] The results are given in Table 2.

CONCLUSIONS

Dry grinding of ZFN with NIC resulted in cocrystal formation. This was ascertained by melting point transformations, DSC changes, shifts in infrared bands, and changes in 2θ values in XRPD that mutually supported each other. The newly prepared cocrystals exhibited greater solubility and dissolution as compared to the pure drug and were stable at room temperature and accelerated conditions. The study endorsed the high potential of the technique for future applications with other drugs.

Conflict of interest: No conflict of interest declared by authors.

REFERENCES

1. Schultheiss N, Newman A. Pharmaceutical cocrystals and their physicochemical properties. Cryst Growth Des. 2009;9:2950-2967.
2. Miroshnyk I, Mirza S, Sandler N. Pharmaceutical co-crystals–an opportunity for drug product enhancement. Expert Opin Drug Deliv. 2009;6:333-341.

3. Blagden N, De Matas M, Gavan PT, York P. Crystal engineering of active pharmaceutical ingredients to improve solubility and dissolution rates. Adv Drug Deliv Rev. 2007;59:617-630.

4. Qiao N, Li M, Schlindwein W, Malek N, Davies A, Trappitt G. Pharmaceutical cocrystals: an overview. Int J Pharm. 2011;419:1-11.

5. Bolla G, Nangia A. Pharmaceutical cocrystals: walking the talk. Chem Commun. 2016;52:8342-8360.

6. Steed JW. The role of co-crystals in pharmaceutical design. Trends Pharmacol Sci. 2013;34:185-193.

7. Krishnamohan Sharma CV. Crystal Engineering-Where Do We Go from Here? Cryst Growt Des. 2002;2:7-10.

8. Rodríguez-Hornedo N. Cocrystals: Molecular design of pharmaceutical materials. Mol Pharm. 2007;4:299-300.

9. Box KJ, Comer J, Taylor R, Karki S, Ruiz R, Price R, Fotaki N. Small-Scale Assays for Studying Dissolution of Pharmaceutical Cocrystals for Oral Administration. AAPS Pharm Sci Tech. 2016;17:245-251.

10. Rahman Z, Agarabi C, Zidan AS, Khan SR, Khan MA. Physico-mechanical and stability evaluation of carbamazepine cocrystal with nicotinamide. AAPS Pharm Sci Tech. 2011;12:693-704.

11. Rodriguez-Aller M, Guillarme D, Veuthey JL, Gurny R. Strategies for formulating and delivering poorly water-soluble drugs. J Drug Deliv Sci Technol. 2015;30:342-351.

12. Kale DP, Zode SS, Bansal AK. Challenges in Translational Development of Pharmaceutical Cocrystals. J Pharm Sci. 2017;106:457-470.

13. Perlovich GL, Manin AN. Design of pharmaceutical cocrystals for drug solubility improvement. Russ J Gen Chem. 2014;84:407-414.

14. Gadade DD, Pekamwar SS. Pharmaceutical Cocrystals: Regulatory and Strategic Aspects, Design and Development. Adv Pharm Bull. 2016;6:479-494.

15. Baek J, Lim J, Kang J, Shin S, Jung S, Cho C. Enhanced transdermal drug delivery of ZFN using a novel formulation. Int J Pharm. 2013;453:358-362.

16. Ratnesh M, Kedar S P, Lokesh Kumar B. Preparation, optimization, and evaluation of Zaltoprofen-loaded microemulsion and microemulsion-based gel for transdermal delivery. J Liposome Res. 2016;26:297-306.

17. Shiraki K, Takata N, Takano R, Hayashi Y, Terada. K. Dissolution improvement and the mechanism of the improvement from cocrystallization of poorly water-soluble compounds. Pharm Res. 2008;25:2581-2592.

18. Goud NR, Gangavaram S, Suresh K, Pal S, Manjunatha SG, Nambiar S, Nangia A. Novel furosemide cocrystals and selection of high solubility drug forms. J Pharm Sci. 2012;101:664-680.

19. Rodriguez-Aller M, Guillarme D, Veuthey JL, Gurny R. Strategies for formulating and delivering poorly water-soluble drugs. J Drug Deliv Sci Technol. 2015;30:342-351.

20. Shan N, Perry ML, Weyna DR, Zaworotko MJ. Impact of pharmaceutical cocrystals: the effects on drug pharmacokinetics. Expert Opin Drug Metab Toxicol. 2014;10:1255-1271.

21. Maddileti D, Jayabun SK, Nangia A. Soluble cocrystals of the xanthine oxidase inhibitor febuxostat. Cryst Growth Des. 2013;13:3188-3196.

22. Nijhawan M, Santhosh A, Babu PR, Subrahmanyam CV. Solid state manipulation of lornoxicam for cocrystals--physicochemical characterization. Drug Dev Ind Pharm. 2014;40:1163-1172.

23. Yamamoto K, Tsutsumi S, Ikeda Y. Establishment of cocrystal cocktail grinding method for rational screening of pharmaceutical cocrystals. Int J Pharm. 2012;437:162-171.

24. Ganesh M, Jeon UJ, Ubaidulla U, Hemalatha P, Saravanakumar A, Peng MM, Jang HT. Chitosan cocrystals embedded alginate beads for enhancing the solubility and bioavailability of aceclofenac. Int J Biol Macromol. 2015;74:310-317.

25. El-Gizawy SA, Osman MA, Arafa MF, El Maghraby GM. Aerosil as a novel co-crystal co-former for improving the dissolution rate of hydrochlorothiazide. Int J Pharm. 2015;478:773-778.

27. Shayanfar A, Jouyban A. Physicochemical characterization of a new cocrystal of ketoconazole. Powder Technol. 2014;262:242-248.

28. Panzade P, Shendarkar G, Shaikh S, Rathi P. Pharmaceutical Cocrystal of Piroxicam: Design, formulation and evaluation. Adv Pharm Bull. 2017;7399-408.

29. Yadav AV, Dabke AP, Shete AS. Crystal engineering to improve physicochemical properties of mefloquine hydrochloride. Drug Dev Ind Pharm. 2010;36:1036-1045.

30. Sarkar A, Rohani S. Molecular salts and co-crystals of mirtazapine with promising physicochemical properties. J Pharm Biomed Anal. 2015;110:93-109.

31. Sanphui P, Kumar SS, Nangia A. Pharmaceutical cocrystals of niclosamide. Cryst Growth Des. 2012;12:4588-4599.

32. Mulye SP, Jamadar SA, Karekar PS, Pore YV, Dhawale SC. Improvement in physicochemical properties of ezetimibe using a crystal engineering technique. Powder Technol. 2012;222:131-138.

33. Trask AV, Motherwell WS, Jones W. Physical stability enhancement of theophylline via cocrystallization. Int J Pharm. 2006;320:114-123.

Turk J Pharm Sci 2019;16(3):317-325
DOI: 10.4274/tjps.galenos.2018.26879

ORIGINAL ARTICLE

Effect of Extracts of the Aerial Parts and Roots from Four *Ferulago* Species on Erectile Dysfunction in Rats with Streptozotocin-Induced Diabetes

Streptozotosin ile Oluşturulan Diyabetik Sıçanlarda Dört *Ferulago* Türünün Toprak Üstü ve Kök Ekstrelerinin Erektil Disfonksiyon Üzerine Etkisi

Songül KARAKAYA[1]*, Didem YILMAZ ORAL[2], Serap GÜR[2], Hayri DUMAN[3], Ceyda Sibel KILIÇ[4]

[1]Atatürk University, Faculty of Pharmacy, Department of Pharmacognosy, Erzurum, Turkey
[2]Ankara University, Faculty of Pharmacy, Department of Pharmacology, Ankara, Turkey
[3]Gazi University, Faculty of Science, Department of Biology, Ankara, Turkey
[4]Ankara University, Faculty of Pharmacy, Department of Pharmaceutical Botany, Ankara, Turkey

ABSTRACT

Objectives: The extracts of *Ferulago* species are used as aphrodisiacs in Turkey and so we aimed to demonstrate *in vivo* and *in vitro* the relaxant effect of four *Ferulago* species' extracts on the corpus cavernosum (CC).

Materials and Methods: A total of 30 adult male Sprague Dawley rats were divided into control and diabetic groups. Diabetes was induced by a single intraperitoneal injection of 40 mg/kg streptozotocin. *In vivo* erectile responses were obtained by stimulation of the cavernosal nerves and repeated after intracavernosal injection of extracts in rats, and the data were expressed as intracavernosal pressure (ICP)/mean arterial pressure and total ICP. The relaxant and contractile responses of CC strips were analyzed in the presence or absence of extracts.

Results: The extracts were active in both control and diabetic rats. The extract-induced maximum relaxation responses (especially of methanol extract of the root of *Ferulago bracteata*) (98.30±2.6%) were decreased after incubation with L-NAME (44.8±1.8). ODQ, a soluble guanylate cyclase inhibitor, inhibited 77% of extract-induced maximum relaxation in the CC from the control rats.

Conclusion: These species can be utilized in erectile dysfunction and may be an herbal alternative to synthetic drugs.

Key words: Aphrodisiacs, Apiaceae, *Ferulago*, erectile function

ÖZ

Amaç: *Ferulago* türlerine ait ekstreler Türkiye'de afrodizyak olarak kullanılmaktadır, bu nedenle *in vivo* ve *in vitro* olarak dört *Ferulago* türüne ait ekstrelerin korpus kavernosum (CC) üzerindeki gevşetici etkisini göstermeyi amaçladık.

Gereç ve Yöntemler: Kontrol ve diyabetik gruba ayrılan toplam 30 yetişkin erkek Sprague Dawley sıçanı, 40 mg/kg Streptozotocin ile intraperitonal olarak tek seferlik enjeksiyon ile indüklenmiştir. Kavernosal sinirlerin uyarılmasıyla *in vivo* erektil yanıtlar elde edildi ve sıçanlarda intrakavernozal ekstraktların enjeksiyonu sonrasında tekrarlandı ve veriler intrakavernozal basınç (ICP)/ortalama arteriyel basınç ve toplam ICP olarak ifade edildi. CC striplerin gevşetici ve kasılma yanıtları, ekstraktların varlığında veya yokluğunda analiz edildi.

Bulgular: Ekstraktların hem kontrol hem de diyabetik sıçanlar üzerinde aktif olduğu bulundu. Ekstraktlar (özellikle *Ferulago bracteata* kök metanol ekstresi) ile maksimum gevşeme yanıtları (%98.30±2.6) L-NAME (44.8±1.8) ile inkübasyondan sonra azalmıştır. ODQ, çözünebilir guanilat siklaz inhibitörü, kontrol sıçanlarından CC'de ekstraktların indüklediği maksimum gevşemenin %77'sini inhibe ettiği görülmüştür.

Sonuç: Sonuç olarak bu türler erektil disfonksiyonda kullanılabilir ve sentetik ilaçlara karşı bitkisel alternatif oluşturabilir.

Anahtar kelimeler: Afrodizyak, Apiaceae, *Ferulago*, erektil disfonksiyon

*Correspondence: **E-mail:** ecz-songul@hotmail.com, **Phone:** +90 442 231 52 50 **ORCID-ID:** orcid.org/0000-0002-3268-721X
Received: 14.03.2018, **Accepted:** 07.06.2018

INTRODUCTION

Diabetes is one of the most prevalent causes of erectile dysfunction (ED), which eminently influences the quality of life, and the risk of developing ED in diabetic men is threefold higher than that in healthy men.[1,2] As compared with the other complications of diabetes, the development of ED begins at an earlier age. Moreover, the incidence and severity of ED increase with the duration of diabetes[3] and multifactorial mechanisms including neurogenic and vasculogenic factors are involved in diabetic ED. The efficacy of some ED treatments is limited for diabetes-associated ED. For example, men with diabetes frequently show a poor response to first-line oral phosphodiesterase type 5 (PDE-5) inhibitors.[4] An alternative therapy choice may be phytotherapy for diabetic ED.

In the present study, we examined the effect of lyophilized aqueous and methanol extracts of *Ferulago* species growing naturally in Turkey on erectile tissue. In Turkey these species are known as "çağşır" or "çakşır" and are utilized conventionally as an aphrodisiac in South and Southeast Anatolia. Actually, many species that belong to the genera *Ferulago*, *Prangos*, and *Ferula* have been utilized for this aim. These species are utilized in rutting of goats and sheep, and water decoctions of the roots and aerial parts are administered orally as aphrodisiacs.[5] In Turkey *Ferulago* species are usually well known for their aphrodisiac activities like various plants in other countries.[6] Apart from their medicinal usage, they have been consumed in salads or as spices due to their special odor, and used as food for goats and deer.[7]

Ferulago W. Koch. (Apiaceae) is represented by 34 taxa in Turkey, 19 of which are endemic. For this reason Anatolia is considered to be the gene center of this genus.[8] *Ferulago blancheana* Post ex Boiss., *Ferulago pachyloba* (Fenzl) Boiss., and *Ferulago bracteata* Boiss. & Hausskn. are endemic perennial species growing only in Kayseri, Central Anatolia; Niğde, Central Anatolia; and Gaziantep, Southeastern Anatolia, Turkey, respectively, but *Ferulago trachycarpa* Boiss. is not an endemic species, growing in Antalya.[9] During our studies, we found that aqueous and methanol extracts of the roots and aerial parts from *Ferulago* species produced relaxation in precontracted rat corpus cavernosum (CC). Therefore, we planned to investigate the pharmacological profile of their relaxant effect by using isolated CC tissue *in vivo* and *in vitro*. This study aims to give the first report to evaluate the effect of extracts from *F. blancheana*, *F. pachyloba*, *F. trachycarpa*, and *F. bracteata* on ED in rats with streptozotocin (STZ)-induced diabetes.

MATERIALS AND METHODS

Plant material

Flowering plants of *F. blancheana*, *F. pachyloba*, *F. trachycarpa*, and *F. bracteata* were collected in 2014 from Kayseri, Niğde, Antalya, and Gaziantep (Turkey), respectively, and identified by Prof. Dr. Hayri Duman, a plant taxonomist at the Department of Biology, Faculty of Science, Gazi University. The voucher specimens are kept in the Herbarium of Ankara University, Faculty of Pharmacy (herbarium numbers AEF 26673, AEF 26674, AEF 26677, and AEF 26676, respectively).

Extraction

The air-dried roots and aerial parts of these species were powdered and macerated three times with methanol for 8 h in a water bath not exceeding 45°C (3×200 mL) using a mechanical mixer at 300 rpm, separately. The extracts were filtered and concentrated until dryness by rotary evaporator (Heidolph VV2000, Germany). Moreover, 50 g of roots and aerial parts from these plants were ground and macerated with 200 mL of distilled water for 8 h/3 days at 30 to 35°C, separately. The aqueous extract was filtered, frozen (Sanyo Medical Freezer, Germany), and lyophilized (Christ® Gamma 2-16 LSC, Germany) to give aqueous extracts from the roots and aerial parts. The amounts of the powdered plants and extracts obtained are given in Table 1.

Animals

Adult male Sprague Dawley rats (350-400 g) received a dose of streptozotocin (STZ, 40 mg/kg, i.p.) within a citrate buffer (pH 5.5) on the day of use.[10] Measurement of blood glucose levels was carried out using an Accu-Chek glucometer (Roche Diagnostics, Indianapolis, IN, USA) after the induction of diabetes. The animals were housed in separate cages on a 12-h light–dark cycle and were fed standard water and chow ad libitum. This study was approved by the Institutional Animal Care and Use Committee of Ankara University (2014-15-86).

In vivo assessment of erectile function

To assess erectile function *in vivo*, intracavernosal pressure (ICP) (ICP, mmHg) was monitored in the rats. The rats were anesthetized with ketamine (50 mg/kg, i.p.) and the trachea was cannulated [polyethylene, (PE)-240 tubing] to keep the airway open, and the carotid artery was cannulated (PE-50 tubing) to measure the main arterial pressure (MAP, mmHg), by a transducer (Statham, Oxnard, CA, USA) attached to a data acquisition system (Biopac MP 100 System, Santa Barbara, CA, USA). A 25-gauge needle filled with 250 U/mL heparin and connected to polyethylene-50 tubing was placed in the right crus of the penis connected to a pressure transducer to measure ICP indissolubly. The right major pelvic ganglion and cavernosal nerve (CN) were represented. A stainless-steel bipolar hook electrode for stimulation was installed around the CN postero-lateral to the prostate on one side, and the MAP

Table 1. Amounts of the powdered plants and obtained extracts

Species	Used parts	Powdered (g)	MeOH (g)	Lyophilized aqueous (g)
F. blancheana	Root	50	6.62	5.78
	Aerial part	50	3.22	4.78
F. pachyloba	Root	50	7.25	6.98
	Aerial part	50	3.32	4.01
F. trachycarpa	Root	50	6.77	7.76
	Aerial part	50	3.41	3.67
F. bracteata	Root	50	7.94	5.99
	Aerial part	50	3.65	4.88

(mmHg) and ICP (mmHg) were indissolubly measured with pressure transducers. The CN was stimulated (2.5, 5, and 7.5 V, 15 Hz, 30 s train duration) with a square pulse stimulator (Grass Instruments, Quincy, MA, USA) and electrical stimulation was inducted distally to the ligature. The measurements were repeated after intracavernosal administration of extracts (1 µM) in groups.[10]

Isometric tension measurements

Cavernosal tissue (CC) strips were placed in organ bath chambers and maintained in Krebs-bicarbonate solution (containing, mM: KCl 4.7, NaCl 118.1, $MgSO_4$ 1.0, KH_2PO_4 1.0, $NaHCO_3$;25.0, glucose 11.1, and CaCl 22.5, pH 7.4). The strips (1×1×9 mm^3) were dissected and combined under 1 g of resting tension in a 20 mL organ bath. The organ chamber temperature was kept at 37°C by a circulating water bath and continuous bubbling with a mixture of 95% O_2 and 5% CO_2. The tissues were permitted to equilibrate for a minimum of 60 min, and the bath solution was changed every 15 min. Electrical field stimulation (EFS) of the autonomic nerves (duration: 15 s; amplitude: 50-90 V; frequency: pulse width: 5 ms) was achieved by the use of platinum electrodes, placed on either side of the tissue strip (Grass Instruments, Quincy, MA, USA).

In the first series of trials, CC strips were precontracted with phenylephrine (Phe, 10^{-5} M) and allowed to relax after administration of the extracts. The relaxation response curves to the extracts were also acquired in the presence of the nonspecific nitric oxide (NO) synthase inhibitor L-NAME (L-N(G)-nitroarginine methyl ester, 100 µM) and soluble guanylate cyclase inhibitor ODQ (1H-[1,2,4]-oxadiazolo[4,3-a] quinoxaline-1-one, 30 µM).

In the second series of trials, acetylcholine (ACh)-, EFS-, sildenafil-, and sodium nitroprusside (SNP)-induced relaxation responses were stimulated after precontraction of CC strips with Phe (10^{-5} M) in the presence or absence of the extracts (100 µM).

Statistical analysis

All results are expressed as mean ± standard error and differences between means were statistically analyzed using one-way ANOVA followed by Bonferroni's complementary analysis, with $p<0.05$ considered to indicate statistical significance. At the end of the experiment, each CC strip was weighed. All contractile responses were expressed as mg of tension developed per mg of corporal tissue and relaxant responses were calculated as a percentage of Phe-contraction.

Drugs

All drugs were purchased from Sigma Chemical Co. (St. Louis, MO, USA).

RESULTS

Extraction

Methanol and lyophilized aqueous extracts of the roots and aerial parts from *Ferulago* species were evaluated for their effect on ED.

Characteristics of animals

Body weight of the diabetic rats was considerably lower than that of the control rats (Figure 1a, $p<0.001$). Blood glucose levels in the diabetic group were considerably higher than those in the control group (Figure 1b, $p<0.001$).

In vivo erectile responses in both groups

ICP/MAP values in the control rats were higher than in the diabetic rats ($p<0.001$; Figure 2), which was reversed by intracavernosal administration of the extracts (1 µM). Moreover, total ICP values were decreased in the diabetic group compared with the control group ($p<0.001$; Figure 2). After the intracavernosal administration of the extracts (1 µM) total ICP values were restored in the diabetic group at all voltage levels, except for the 7.5 voltage level (Figure 2).

In vitro responses of CC strips

The extract-induced maximum relaxation responses (especially methanol extract of the roots from *F. bracteata*) (98.30±2.6%) were decreased after incubation with L-NAME (44.8±1.8, Figure 3a). ODQ, a soluble guanylate cyclase inhibitor, inhibited 77% of extract-induced maximum relaxation in the CC from the control rats (Figure 3).

The endothelial-dependent relaxation response to ACh (1 mM) in the control rats was higher than in the diabetic rats, which was increased after the incubation of the extracts (100 µM) in the control and diabetic groups (Figure 4).

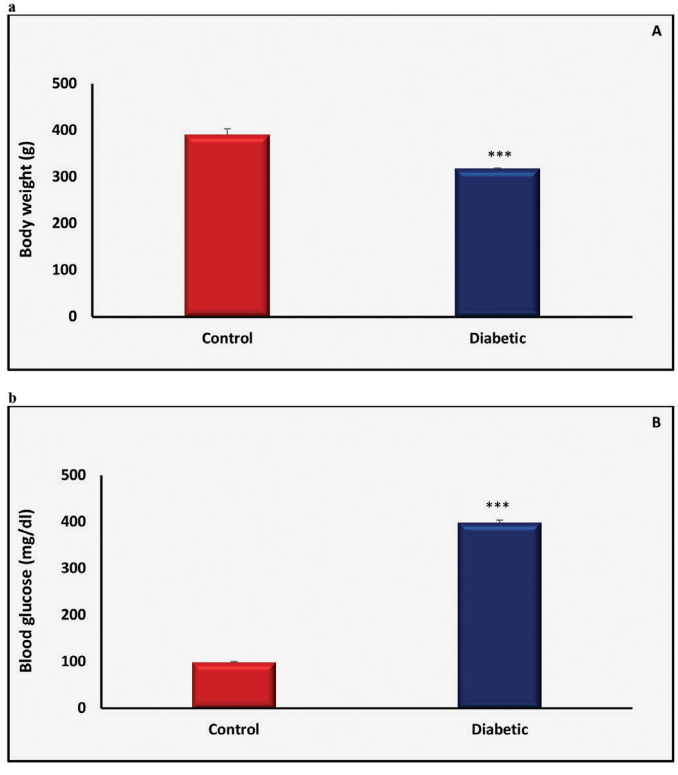

Figure 1. Bar graph showing body weight of the control and diabetic groups (a) and glucose levels (b) in the control and diabetic groups. Data are mean ± standard error of mean (n=6) and ***$p<0.001$ vs control

EFS-induced relaxation response at 20 Hz was decreased in the diabetic group compared with the control group, which was restored by the incubation with the extracts (100 µM). There was no difference in EFS-induced relaxation response in the control rats between the presence and absence of the extracts (Figure 5).

SNP-induced endothelial-independent relaxation response at 0.1 µM dose relaxation was not different in the control rats when compared with the diabetic rats (Figure 6). However, relaxation responses to SNP were enhanced in the presence of the extracts (100 µM) in the diabetic and control rats.

The relaxation response induced by the PDE-5 inhibitor sildenafil at 1 µM dose was considerably reduced in the diabetic rats when compared with the control rats (Figure 4d). After incubation of the extracts (100 µM), relaxation responses to sildenafil were higher in the diabetic and control rats (Figure 7).

DISCUSSION

In the present study, we aimed to examine the relaxant effect of methanol and lyophilized aqueous extracts of the roots and aerial parts of *F. blancheana*, *F. pachyloba*, *F. trachycarpa*, and *F. trachycarpa* in the CC with *in vivo* and *in vitro* studies. Corporal smooth muscle relaxation plays a significant role in erection. Smooth muscle relaxation, which is interceded by NO throughout sexual stimulation, is synthesized in the nerve terminals of parasympathetic noncholinergic and non-adrenergic nerves in the penis as well as by the endothelial cells lining the blood vessels and lacunar spaces of the CC.[11]

The first data provide basic mechanistic information concerning the extract-induced dose-dependent relaxation in rat CC. The major findings of the study show that (i) the extracts relax rat CC in a concentration-dependent manner; (ii) the NO-cGMP pathway plays an important role in mediating extract-induced relaxation; and (iii) they partially restore *in vivo* erectile function in diabetic rats.

Penile erection in response to CN stimulation was confirmed *in vivo* in a diabetic animal model. Our data showed that diabetes reduced the *in vivo* erectile response and the *in vitro* relaxant response of the CC to EFS. Amazingly, erectile responses (ICP/MAP and total ICP) gained after cavernous nerve stimulation except 7.5 V were augmented in the extract-injected diabetic group, as compared with the vehicle-injected diabetic group. In *in vitro* studies, the nitrergic relaxation response to EFS in the diabetic rats was increased by the incubation of extracts. There were no previous data to evaluate the effect of these species on erectile function. However, the extract treatment reduced the diabetes-induced renal damage related to the diabetic nephropathy.[12] Moreover, the treatment improved the activities of enzymatic and nonenzymatic antioxidants,[13] and also *in vitro* increased the glycolytic activities.[14] These results indicate a rationale for more studies using combinations of extracts and phosphodiesterase-5 inhibitors in diabetes-induced ED.

The present study showed that extract-induced relaxation in the CC from the diabetic group was not changed compared with that from the control group. The data support the intracavernosal administration of extracts to augment erectile responses. It seems that the extract responses serve as the normal activity *in*

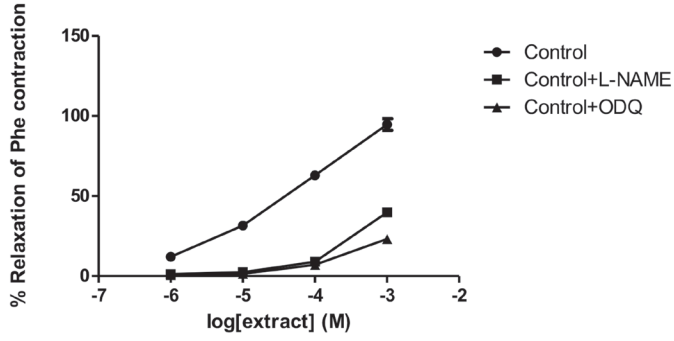

Figure 3. Concentration–response curves to extract (10^{-6}-10^{-3} M) in the corpus cavernosum after precontraction with phenylephrine (Phe, 10 µM) in the presence of L-NAME (100 µM, A) and ODQ (30 µM, B). Data represent mean ± standard error of mean of 6-8 observations. ***p<0.001 vs control value

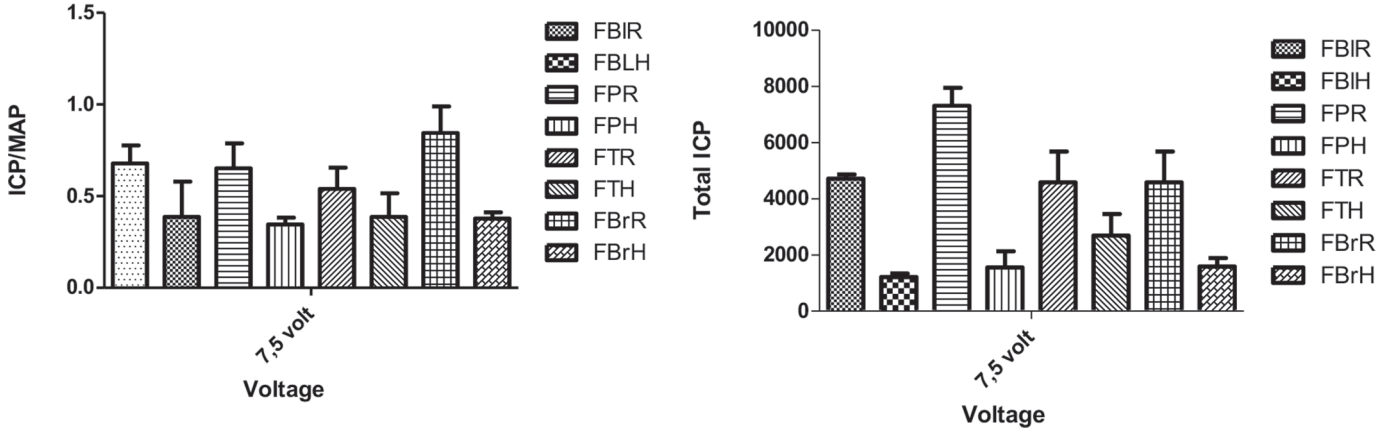

Figure 2. *In vivo* intracavernosal effect of extracts from roots on control and diabetic rat penile erection. Bar graphs showing ICP/MAP total ICP. Data represent mean ± standard error of mean of 6-8 observations (p=0.1413)

FBlR: Root of *F. blancheana*, FBlH: Aerial part of *F. blanchean*, FPR: Root of *F. pachyloba*, FPH: Aerial part of *F. pachyloba*, FTR: Root of *F. trachycarpa*, FTH: Aerial part of *F. trachycarpa*, FBrR: Root of *F. bracteata*, FBrH: Aerial part of *F. bracteate*, ICP: Intracavernosal pressure, MAP: Mean arterial pressure

vivo and *in vitro* in diabetes. Moreover, relaxation to the extracts was calmly inhibited after precontraction with KCl. Potential sensitive calcium channels are forced by depolarization of the plasma membrane when the extracellular K^{+1} concentration is augmented. Potential sensitive calcium channels were activated by depolarization of the plasma membrane when the extracellular K+ concentration was enhanced.

In the current study, we researched the underlying mechanism of the extracts' effects on erectile responses that can be mediated by the NO/cGMP-dependent pathway, which is damaged in diabetes. No earlier study appears to have been done on the mechanism of the extracts in penile tissue. The extracts are most likely to have a role in the NO-cGMP signaling pathway, mediating CC relaxation responses.

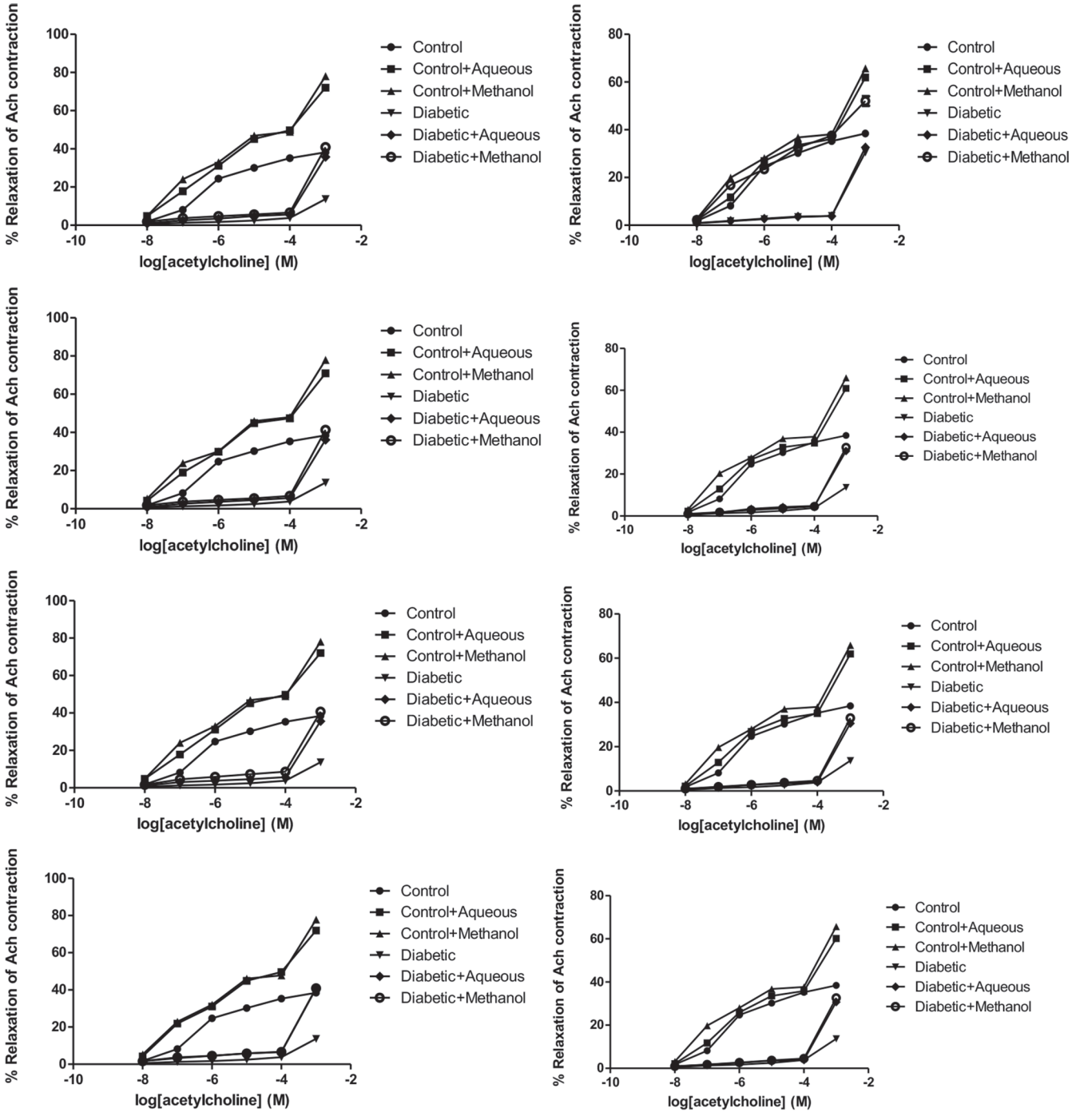

Figure 4. Relaxation responses to single doses of ACh in the presence of extract of FBlR, FBlH, FPR, FPH, FTR, FTH, FBrR, and FBrh, respectively. Data represent mean ± standard error of mean of 6-8 observations. *p<0.05, ***p<0.001 vs. control value. §p<0.05, §§p<0.01 vs diabetic value

ACh: Acetylcholine, FBlR: Root of *F. blancheana*, FBlH: Aerial part of *F. blanchean*, FPR: Root of *F. pachyloba*, FPH: Aerial part of *F. pachyloba*, FTR: Root of *F. trachycarpa*, FTH: Aerial part of *F. trachycarpa*, FBrR: Root of *F. bracteata*, FBrH: Aerial part of *F. bracteate*

In the isolated CC from the diabetic group, the endothelium-dependent relaxation response to ACh was considerably reduced, which was potentialized in the presence of the extracts. There were no previous supporting data similar to these findings.

There was no difference in the endothelial-independent relaxation response to SNP between the control and diabetic rats, which was enhanced in the groups after incubation of the extracts. In previous studies, SNP-induced relaxant responses did not change in diabetic rats when compared with the controls.[15,16]

In the present study, relaxation responses to the PDE-5 inhibitor sildenafil in CC strips were lower in the diabetic rats than in the control rats. There was no difference in relaxant response to sildenafil between the control and diabetic rats' CC after incubation of the extracts. This finding indicates that these species have a potential effect on penile function by means of various pathways to contribute to erectile function in diabetic rats.

As shown in Figure 1, among the extracts, the methanol extracts of roots (especially roots of *F. bracteata*) showed the best activity. On the other hand, lyophilized aqueous extracts

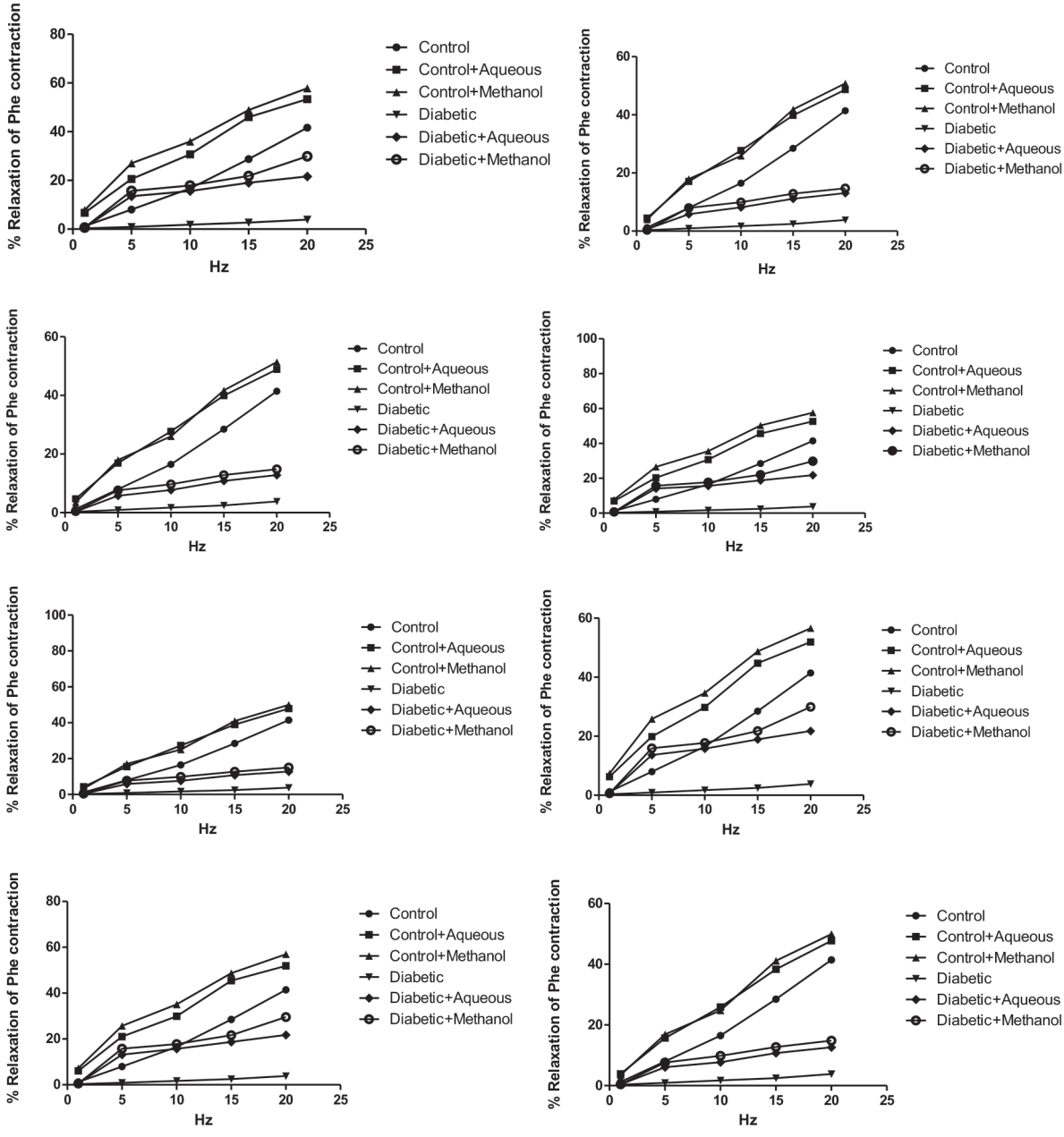

Figure 5. Relaxation responses to single doses of EFS in the presence of extract of FBlR, FBlH, FPR, FPH, FTR, FTH, FBrR, and FBrh, respectively. Data represent mean ± standard error of mean of 6-8 observations. *p<0.05, ***p<0.001 vs control value. §p<0.05, §§p<0.01 vs diabetic value

EFS: Electrical field stimulation, FBlR: Root of *F. blancheana*, FBlH: Aerial part of *F. blanchean*, FPR: Root of *F. pachyloba*, FPH: Aerial part of *F. pachyloba*, FTR: Root of *F. trachycarpa*, FTH: Aerial part of *F. trachycarpa*, FBrR: Root of *F. bracteata*, FBrH: Aerial part of *F. bracteate*

of the aerial parts (especially *F. blancheana*) showed the worst activity. EFS relaxation responses decreased from 40% in the controls rats to 3% in the diabetes rats. However, as a result of 15-min incubation of the extracts, the EFS relaxation responses increased to 21%. Similarly, acetylcholine relaxation responses decreased from 38% in the controls to 13% in the diabetic rats. However, as a result of 15-min incubation of the extracts, acetylcholine relaxation responses were increased by 40% and were higher than those in the controls. Sildenafil relaxation responses were 92% in the controls and 74% in the diabetic rats, but, as a result of 15-min incubation of the extracts, acetylcholine relaxation responses were increased by

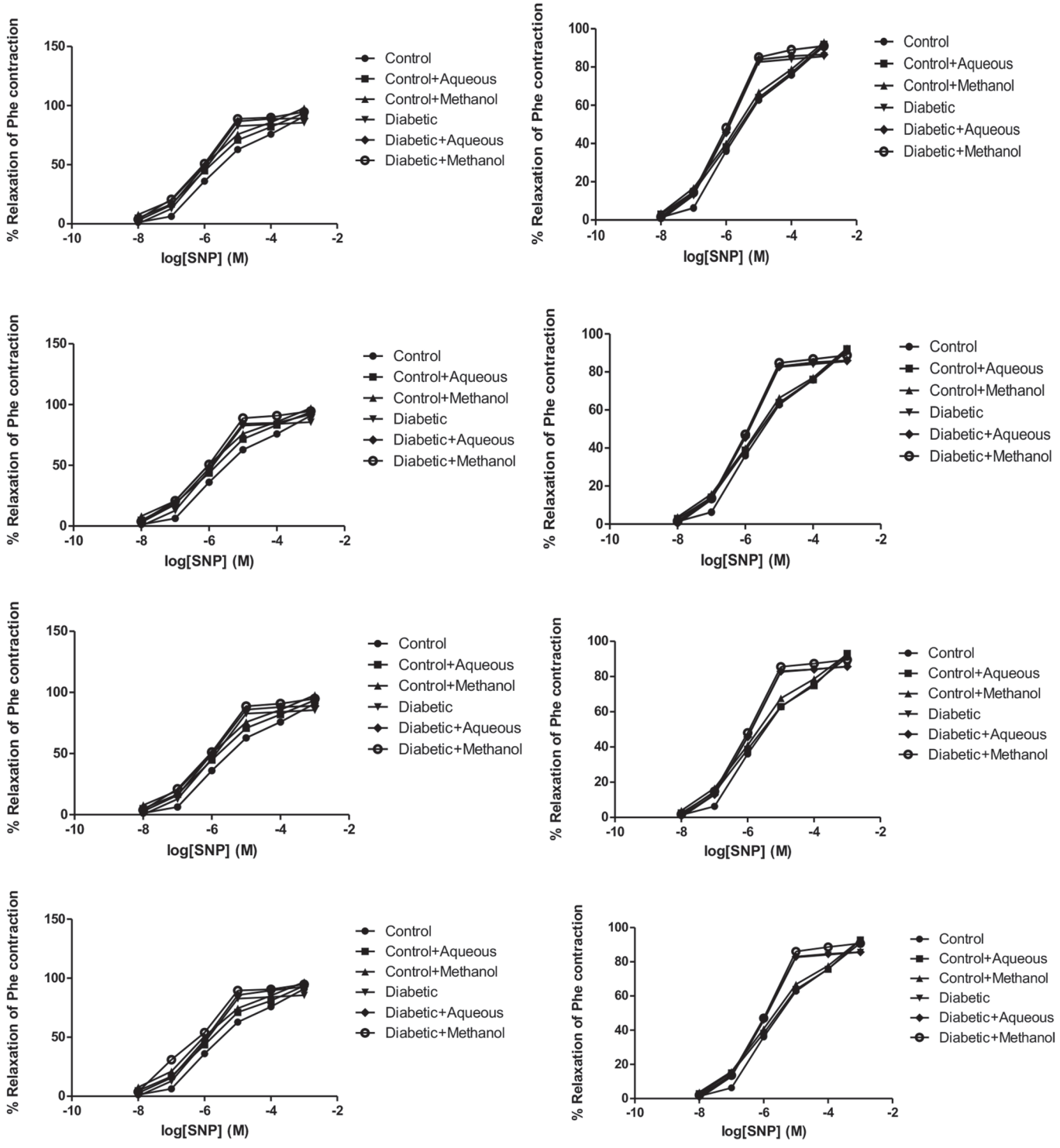

Figure 6. Relaxation responses to single doses of SNP in the presence of extract of FBlR, FBlH, FPR, FPH, FTR, FTH, FBrR, and FBrh, respectively. Data represent mean ± standard error of mean of 6-8 observations. *p<0.05, ***p<0.001 vs control value. §p<0.05, §§p<0.01 vs diabetic value

SNP: Sodium nitroprusside, FBlR: Root of *F. blancheana*, FBlH: Aerial part of *F. blanchean*, FPR: Root of *F. pachyloba*, FPH: Aerial part of *F. pachyloba*, FTR: Root of *F. trachycarpa*, FTH: Aerial part of *F. trachycarpa*, FBrR: Root of *F. bracteata*, FBrH: Aerial part of *F. bracteate*

95% and were higher than those in the controls. SNP relaxation responses were 90% in the controls and 85% in the diabetic rats. However, as a result of 15-min incubation of the extracts, acetylcholine relaxation responses were increased by up to 94% and were higher than those in the controls. The results are shown in Figures 1-7.

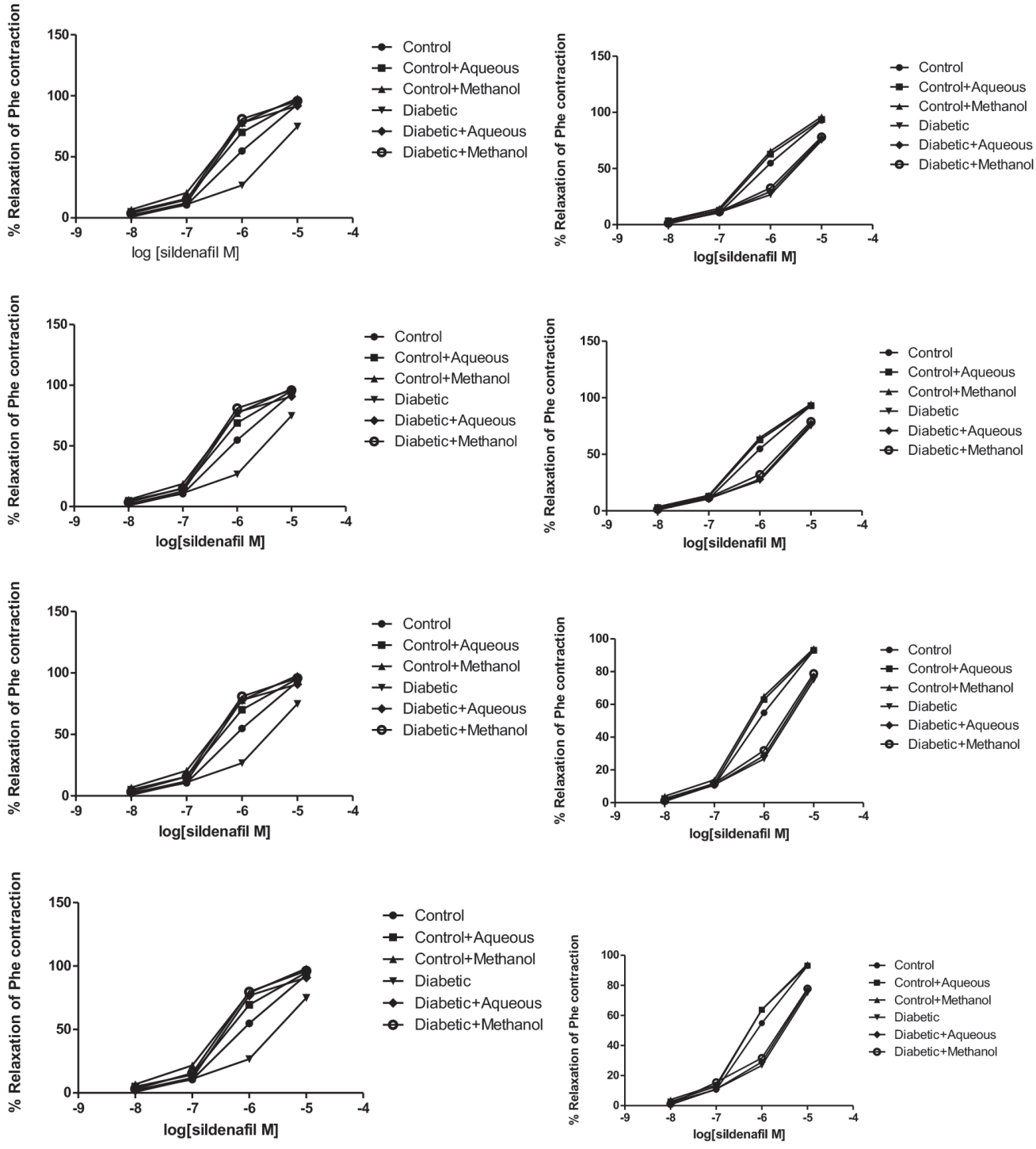

Figure 7. Relaxation responses to single doses of sildenafil in the presence of extract of FBlR, FBlH, FPR, FPH, FTR, FTH, FBrR and FBrh, respectively. Data represent mean ± standard error of mean of 6-8 observations. *p<0.05, ***p<0.001 vs control value. §p<0.05, §§p<0.01 vs diabetic value

FBlR: Root of *F. blancheana*, FBlH: Aerial part of *F. blanchean*, FPR: Root of *F. pachyloba*, FPH: Aerial part of *F. pachyloba*, FTR: Root of *F. trachycarpa*, FTH: Aerial part of *F. trachycarpa*, FBrR: Root of *F. bracteata*, FBrH: Aerial part of *F. bracteate*

CONCLUSIONS

The present study primarily revealed the useful effect of intracavernosal administration of extracts in improving erectile function in diabetic rats, which is dependent on the NO/cGMP pathway. The preclinical findings should extend our information of the beneficial effects of the extracts on penile function to develop preventive or therapeutic agents and combinations of them, and phosphodiesterase-5 inhibitors may be a beneficial option for diabetes-induced ED.

ACKNOWLEDGEMENTS

This study was supported by the Scientific and Technological Research Council of Turkey (TUBITAK 115S009).

Conflict of Interest: No conflict of interest was declared by the authors.

REFERENCES

1. Mazzilli R, Elia J, Delfino M, Benedetti F, Scordovillo G, Mazzilli F. Prevalence of Diabetes Mellitus (DM) in a population of men affected by Erectile Dysfunction (ED). Clin Ter. 2015;166:317-320.
2. Rastrelli G, Corona G, Mannucci E, Maggi M. Vascular and Chronological Age in Subjects with Erectile Dysfunction: A Cross-Sectional Study. J Sex Med. 2015;12:2303-2312.
3. Johannes CB, Araujo AB, Feldman HA, Derby CA, Kleinman KP, Mckınlay JB. Incidence of erectile dysfunction in men 40 to 69 years old: longitudinal results from the Massachusetts male aging study. J Urol. 2000;163:460-463.
4. Ruan Y, Li M, Wang T, Yang J, Rao K, Wang S, Yang W, Liu J, Ye Z. Taurine Supplementation Improves Erectile Function in Rats with Streptozotocin-induced Type 1 Diabetes via Amelioration of Penile Fibrosis and Endothelial Dysfunction. J Sex Med. 2016;13:778-785.
5. Baytop T. Therapy with Medicinal Plants in Turkey-Past and Present (2nd ed). Istanbul; Nobel Medical Publ; 1999.
6. Ibrahim JA, Muazzam I, Jegede IA, Kunle OF. Medicinal plants and animals sold by the "Yan-Shimfidas" of Sabo Wuse in Niger State, Nigeria. Afr J Pharm Pharmacol. 2010;4:386-394.
7. Erdurak CS. Investigations on *Ferulago isaurica* Peşmen and *F. syriaca* Boiss. (Umbelliferae) species. Ankara; Ankara University, PhD thesis; 2003.
8. Güner A. Türkiye Bitkileri Listesi (Damarlı Bitkiler), Flora Dizisi .1 (1st ed). İstanbul; Nezahat Gökyiğit Botanik Bahçesi Publ; 2012:62-64.
9. Davis PH. Flora of Turkey and the East Aegean Islands (4th ed). Edinburgh; University Press; 1972:4;462-464.
10. Yilmaz Oral D, Bayatli N, Gur S. The Beneficial Effect of Fesoterodine, a Competitive Muscarinic Receptor Antagonist on Erectile Dysfunction in Streptozotocin-induced Diabetic Rats. Urology. 2017;107:271.
11. Ozturk B, Gur S, Coskun M, Kosan M, Erdurak CS, Hafez G, Gonulalan U, Cetinkaya M. A new relaxant on human corpus cavernosum: *Ferulago syriaca* root extract. Afr J Pharm Pharmacol. 2012;6:2652-2656.
12. Garud MS, Kulkarni YA. Attenuation of renal damage in type I diabetic rats by umbelliferone - a coumarin derivative. Pharmacol Rep. 2017;69:1263-1269.
13. Ramu R, S Shirahatti P, S NS, Zameer F, Lakkappa Dhananjaya B, M N NP. Assessment of *In Vivo* Antidiabetic Properties of Umbelliferone and Lupeol Constituents of Banana (*Musa* sp. var. Nanjangud Rasa Bale) Flower in Hyperglycaemic Rodent Model. PLoS One. 2016;11:e0151135.
14. Gao D, Zhang YL, Xu P, Lin YX, Yang FQ, Liu JH, Zhu HW, Xia ZN. *In vitro* evaluation of dual agonists for PPARγ/β from the flower of *Edgeworthia gardneri* (wall.) Meisn. J Ethnopharmacol. 2015;162:14-19.
15. Cengiz T, Kaya E, Oral DY, Ozakca I, Bayatli N, Karabay AZ, Ensari TA, Karahan T, Yilmaz E, Gur S. Intracavernous Injection of Human Umbilical Cord Blood Mononuclear Cells Improves Erectile Dysfunction in Streptozotocin-Induced Diabetic Rats. J Sex Med. 2017;14:50-58.
16. Yilmaz D, Bayatli N, Un O, Kadowitz PJ, Sikka SC, Gur S. The effect of intracavernosal avanafil, a newer phosphodiesterase-5 inhibitor, on neonatal type 2 diabetic rats with erectile dysfunction. Urology. 2014;83:508.

Turk J Pharm Sci 2019;16(3):326-334
DOI: 10.4274/tjps.galenos.2018.99266

ORIGINAL ARTICLE

Development and Optimization of a Floating Multiparticulate Drug Delivery System for Norfloxacin

Norfloksasin için Yüzen Çok Partiküllü Bir İlaç Salım Sisteminin Geliştirilmesi ve Optimizasyonu

Vaibhav SALVE, Rakesh MISHRA*, Tanaji NANDGUDE

Dr. D.Y. Patil Institute of Pharmaceutical Science and Research, Department of Pharmaceutics, Maharashtra, India

ABSTRACT

Objectives: Norfloxacin is a synthetic broad-spectrum antibacterial drug having poor bioavailability and pH-dependent solubility. The purpose of the present study was to develop a gastroretentive floating multiparticulate drug delivery system for norfloxacin.

Materials and Methods: Norfloxacin core pellets were prepared using microcrystalline cellulose (MCC) and polyvinylpyrrolidone K30 (PVP K30) by extrusion and spheronization. A 3-level, 3-factor, 17-run experimental Box–Behnken design was adopted to optimize levels of variables in the pellets' formulations. The selected independent variables were amounts of MCC and PVP K30 and spheronizing speed and the dependent variables were aspect ratio and hardness of pellets. Sodium bicarbonate and hydroxypropyl methylcellulose K15M in the ratios of 1:1, 1:2, and 2:1 (w/w) on a dry solid basis were incorporated into the norfloxacin pellets and they were further coated with Eudragit RL 100 using a fluidized bed processor to obtain weight gain of 5%, 10%, and 15% w/w. The fourier transform infrared spectrum, scanning electron microscopy, physical characterization, particle size distribution analysis, floating studies, and *in vitro* drug release studies of the pellets were evaluated.

Results: Among the floating multiparticulate pellets batches, batch B-22 was found to be optimized based on the criteria of attaining the minimum floating lag time (<10 min) and the maximum value of drug released 82.11% in 8 h. The percentage drug release for batches B-21 and B-23 was 91.12% in 5 h and 60.67% in 8 h, respectively. The drug release studies indicated that as the Eudragit RL 100 polymer coat increases the drug release decreases, producing sustained release of norfloxacin. The floating studies revealed that 70%-90% of pellets remained floating for up to 8 h. All the batches have excellent flow properties with angle of repose in the range of 25.5±0.49° to 28.02±0.30°, and Carr's index and Hausner's ratio in the range of 5% to 15% and 1.05±0.3 to 1.14±0.3, respectively.

Conclusion: The significant outcome obtained in the study is that such an approach can be effectively employed for improvement of the bioavailability of drugs having poor absorption in the lower part of the gastrointestinal tract with enhanced therapeutic efficacy.

Key words: Gastroretentive, floating multiparticulate, norfloxacin, spheronization, Box–Behnken design

ÖZ

Amaç: Norfloksasin zayıf biyoyararlanımı olan ve pH'a bağlı çözünürlüğe sahip sentetik geniş spektrumlu bir antibakteriyel ilaçtır. Bu çalışmanın amacı, norfloksasin için gastroretentif bir yüzen çok partiküllü ilaç salım sistemi geliştirmektir.

Gereç ve Yöntemler: Norfloksasin çekirdek pelletleri, ekstrüzyon ve sferonizasyonla mikrokristalli selüloz (MCC) ve polivinilpirolidon K30 (PVP K30) kullanılarak hazırlanmıştır. Pelletlerin formülasyonlarındaki değişken seviyelerini optimize etmek için 3 seviyeli, 3 faktörlü, 17 çalışma deneysel bir Boxn Behnken tasarımı benimsenmiştir. Seçilen bağımsız değişkenler, MCC ve PVP K30 miktarları ve sferonizasyon hızı ve bağımlı değişkenler, boyut oranı ve pelletlerin sertliği idi. Kuru katı bazda 1:1, 1:2 ve 2:1 (a/a) oranlarında sodyum bikarbonat ve hidroksipropil metilselüloz K15M norfloksasin peletlerine katılmış ve %5, %10 ve %15 a/a ağırlık artışı elde etmek için akışkanlaştırılmış yatak kullanılarak Eudragit RL 100 ile kaplanmıştır. Fourier transform infrared spektrumu, taramalı elektron mikroskobu, fiziksel karakterizasyon, partikül büyüklüğü dağılım analizi, yüzme çalışmaları ve pelletlerin *in vitro* etken madde salım çalışmaları değerlendirilmiştir.

Bulgular: Yüzen çok partiküllü pelet partileri arasında, B-22 partisi minimum yüzme gecikme süresine (<10 dakika) ve 8 saat içinde maksimum etken madde salım değeri %82.11'e ulaşma kriterlerine dayanarak optimize edilmiştir. B-21 ve B-23 partileri için etken madde salım yüzdesi, sırasıyla 5

*Correspondence: E-mail: mishrarakesh287@gmail.com, Phone: +9579790159 ORCID-ID: orcid.org/0000-0002-8520-1412
Received: 27.04.2018, Accepted: 11.06.2018

saatte %91.12 ve 8 saatte %60.67 idi. Etken madde salım çalışmaları, Eudragit RL 100 polimer kaplaması arttıkça, etken madde salınımının azaldığını ve sürekli olarak norfloksasin salımı sağladığını göstermiştir. Yüzme çalışmaları, pelletlerin %70-90'ının 8 saate kadar yüzer şekilde kaldığını ortaya koymuştur. Tüm partiler, 25.5±0.49°-28.02±0.30° aralığında yığın açısı ve sırasıyla %5 ila %15 ve 1.05±0.3 ila 1.14±0.3 aralığında Carr indeksi ve Hausner oranı ile mükemmel akış özelliklerine sahiptir.

Sonuç: Çalışmada elde edilen önemli sonuç, bu tür bir yaklaşımın, gastrointestinal sistemin alt kısmında zayıf bir şekilde absorpsiyonu olan ilaçların biyoyararlanımının arttırılması ve terapötik etkinliklerinin iyileştirilmesinde etkili bir şekilde kullanılabileceğidir.

Anahtar kelimeler: Gastroretentif, yüzen çok partiküllü ilaç salım sistemi, norfloksasin, sferonizasyon, Box–Behnken tasarımı

INTRODUCTION

The oral route plays an important role in therapy as it is the most preferred and convenient route for drug delivery systems.[1] Gastroretentive drug delivery systems (GRDDSs) are an advanced approach for the novel drug-delivery systems in which the drug is retained in the stomach for a prolonged period.[2,3] GRDDSs are particularly suitable for drugs having a narrow absorption window, drugs that act locally in a part of the gastrointestinal tract, drugs that are unstable in intestinal fluids, and drugs that exhibit poor solubility in the intestinal tract.[4]

Floating drug delivery systems (FDDSs) are one of the most prominent approaches of GRDDs, characterized by the capacity of the formulation to float in and over the gastric contents. FDDSs are low density systems, which allows them to remain buoyant in the stomach for a prolonged period. In the development of FDDSs based on the mechanism of buoyancy the widely employed technology is effervescent systems. In effervescent systems, carbon dioxide gas production occurs due to the reaction of carbonates and bicarbonates present in the formulation with gastric fluid. The gas that forms is entrapped in the polymers, which allows the system to remain buoyant. The FDDSs are effectively used to design sustained drug delivery systems and improve the overall oral bioavailability of drugs.[5-7]

Norfloxacin is fluoroquinolone anti-infective antibacterial drug firstly used in the treatment of urinary tract infections, prostatitis, gonorrhea, and genital tract infections.[8] It has 30%-40% bioavailability with a plasma half-life of 3 to 4 h, thus requiring multiple dosing to maintain adequate plasma concentration during treatment.[9] Norfloxacin is also poorly absorbed from the lower part of the gastrointestinal tract and it is well absorbed from the stomach. The solubility of norfloxacin in water is pH-dependent, increasing sharply with decreasing pH below 5.[10,11]

The therapeutic dose of norfloxacin is very high (400 mg orally twice daily) in the treatment of urinary tract infections.[12] Many novel approaches have been reported that are used for bioavailability enhancement of norfloxacin, either directed towards the development of a single unit system or unable to produce a significant effect on improvement of bioavailability. Thus it was decided to develop a floating multiparticulate drug delivery system for norfloxacin that could produce sustained release so as to maintain drug plasma levels for improving bioavailability and therapeutic effects.

A floating multiparticulate system was developed in which norfloxacin pellets containing different ratios of sodium bicarbonate ($NaHCO_3$):hydroxypropyl methylcellulose (HPMC) K15M were prepared by extrusion spheronization. The pellets were coated with Eudragit RL 100 on a fluidized bed processor by the bottom spray technique. The amount of the effervescent agent and coating level of Eudragit RL 100 polymeric membrane were evaluated and optimized in terms of floating ability and drug release properties.

MATERIALS AND METHODS

Materials

Norfloxacin was a kind gift provided by Aarti Drugs Ltd, Mumbai, India. Eudragit RL 100 was provided by Evonik, Mumbai, India. All the other chemicals were used as received and were of analytical reagent grade.

Preparation method for norfloxacin pellets

Extrusion and spheronization

The norfloxacin core pellets were prepared using wet granulation by extrusion and spheronization. A powder mixture of norfloxacin and microcrystalline cellulose was mixed in a mortar for 20 min. This was followed by addition of binding liquid consisting of 3% polyvinylpyrrolidone K30 in water. The obtained wet mass was passed through BSS sieve no. 16 to get the extrudates. The prepared extrudates were then transferred to a spheronizer (Shakti Pharmatech, Ahmedabad, India) and spheronized at different spheronizing speeds to get pellets. The prepared core pellets were oven dried overnight at 60°C.

Experimental design

A 3-level, 3-factor, 17-run experimental Box–Behnken design was adopted to optimize levels of variables in the pellet formulations. The selected independent variables were amount of MCC, i.e. microcrystalline cellulose (X1), PVP (K30), i.e. polyvinylpyrollidone (X2), and spheronizing speed (X3) as shown in Table 1. The dependent variables were aspect ratio (Y1) so as to predict the sphericity and hardness (Y2).The generation of experimental runs, ANOVA study and optimization were carried out by Design-expert® software 10. The formulation batches prepared are indicated in (Table 2a).

The optimized norfloxacin pellet batch in terms of sphericity and hardness was selected followed by incorporation of $NaHCO_3$ and HPMC K15M in the ratios of 1:1, 1:2, and 2:1 (w/w) on a dry solid basis as indicated in Table 2b.

Coating of norfloxacin pellets containing $NaHCO_3$:HPMC K15M

The norfloxacin pellets containing $NaHCO_3$:HPMC K15M in the ratio of 1:1 were further coated with Eudragit RL 100 using a

fluidized bed processor (ACG, Miniquest-F, Mumbai, India) to obtain weight gain of 5%, 10%, and 15% w/w as shown in Table 2b. The coating solution was prepared by dissolving the desired amount of Eudragit RL 100 in isopropyl alcohol and stirring to obtain a clear solution.

The layering conditions were as follows: batch size, 7.5 g; inlet temperature, 40˚C; product temperature, 35˚C; air flow, 0.8-1.0 bar; spray pressure, 0.5-0.9 bar; spray rate, 0.130 g/min; and final drying at 40˚C for 15 min.

Evaluation of floating norfloxacin pellets

Spectroscopic studies

Calibration curve of norfloxacin in 0.1 N HCl

First 10 mg of norfloxacin was accurately weighed and dissolved in 100 mL of 0.1 N HCl in a volumetric flask to get 100 µg/mL stock solution. This solution was further diluted with 0.1 N HCl to get solutions in the concentration range of 1 to 10 µg/mL. Absorbance of these solutions was determined spectrophotometrically (Shimadzu 1700, Japan) at 273 nm.[13,14]

Table 1. Experimental design parameters

Factors	Levels used (coded value)			Actual value (%)		
	Low	Medium	High	Low	Medium	High
Microcrystalline cellulose	-1	0	+1	25	30	35
Polyvinylpyrrolidone K30	-1	0	+1	4	6	8
Spheronizing speed (rpm)	-1	0	+1	750	850	950

Table 2a. Composition of experimental formulations

Batch number	Microcrystalline cellulose (%)	Polyvinylpyrrolidone K30 (%)	Spheronizing speed (rpm)
B-1	25	4	850
B-2	35	6	750
B-3	30	6	850
B-4	35	6	950
B-5	30	6	850
B-6	35	8	850
B-7	25	8	850
B-8	30	4	950
B-9	35	4	850
B-10	30	6	850
B-11	30	6	850
B-12	30	6	850
B-13	30	8	750
B-14	25	6	750
B-15	25	6	950
B-16	30	4	750
B-17	30	8	950

Fourier transform infrared spectrum

The powder sample of norfloxacin, Eudragit RL 100, and physical mixture of norfloxacin and polymer (Eudragit RL 100) was kept in a dryer to make it moisture-free. The dry sample of powders was separately mixed and triturated with dry potassium bromide. This mixture was placed in a DRS assembly sample holder. The infrared spectrum was recorded and the spectral analysis was done (Shimadzu, 8400S, Japan).[15]

Drug content

Norfloxacin pellets equivalent to 400 mg were ground using a mortar and pestle and transferred into a 50 mL volumetric flask containing 0.1 N HCl and the volume was made up to 50 mL. The mixture was sonicated for 10 min to ensure complete extraction of the drug. The solution was filtered through Whatman filter paper and assayed spectrophotometrically (Shimadzu 1700, Japan) at 273 nm to determine the percent drug content.[16,17]

In vitro drug release studies

Drug release studies of the norfloxacin pellets were performed by USP Dissolution Apparatus-I (Veego DA-8D, India). The dissolution studies were carried out with 900 mL of 0.1 N HCl as dissolution medium at 37±0.5˚C and at 50 rpm. Pellets equivalent to 400 mg of norfloxacin were weighed and transferred to the dissolution apparatus. A 10 mL aliquot was withdrawn and immediately replaced by the same volume of fresh medium to maintain sink condition. The aliquot was filtered through Whatman filter paper and absorbance was measured at 273 nm using a UV spectrophotometer (Shimadzu 1700, Japan) to determine the drug release.[16-18]

In vitro buoyancy studies[19-21]

The time required for the pellets to rise to the surface and float as floating lag time and total duration of time for which pellets remain buoyant, i.e. total floating time, were determined. The

Table 2b. Composition of experimental formulations containing different ratios of $NaHCO_3$:HPMC K15M and Eudragit RL 100 coating

Ingredients (g)	Batch number					
	B-18	B-19	B-20	B-21	B-22	B-23
Norfloxacin	3.33	3.33	3.33	3.33	3.33	3.33
Microcrystalline cellulose	1.27	1.27	1.27	1.27	1.27	1.27
Polyvinylpyrrolidone K30	0.3	0.3	0.3	0.3	0.3	0.3
Sodium bicarbonate	1.25	0.83	1.66	1.25	1.25	1.25
Hydroxypropyl methylcellulose K15	1.25	1.66	0.83	1.25	1.25	1.25
Eudragit RL 100 (% weight gain)	-	-	-	5	10	15

floating pellets (100) was kept in a USP Type-I dissolution apparatus, the dissolution medium used was 0.1 N HCl, and the conditions were 37±5°C at 50 rpm. The percentage of floating pellets was determined by the following equation:

$$\text{Floating pellets (\%)} = \frac{\text{number of floating pellets at measuring time}}{\text{initial number of pellets}} \times 100$$

Scanning electron microscopy

The surface morphology of the optimized coated pellets was examined using a scanning electron microscope. Scanning electron microscopy (SEM) analysis was performed using a Carl Zeiss Supra 5 scanning electron microscope (Germany). The pellet samples were mounted directly onto aluminum stubs and were sputter coated with a gold/palladium mixture for 1 min under an argon atmosphere. The coated pellets were mounted onto the stubs using double-sided adhesive tape.[22]

Particle size distribution analysis

The size distribution of the gastroretentive pellets was determined using a mechanical sieve shaker (Make-Kumar). A series of BSS standard stainless steel sieves of no. 8, 10, 22, 36, 44, 60, and 100 were arranged in order of decreasing aperture size. An accurately weighed amount of drug-loaded gastroretentive pellets from each batch was placed on the uppermost sieve. The sieves were shaken for 10 min and the material retained on each sieve was weighed separately. A graph of mean size vs % weight retained was plotted to analyze pellet size distribution.[23,24]

Physical characterization

The micromeritic properties (bulk density, tapped density, Carr's index, Hausner's ratio, and angle of repose) of the floating pellets were determined. Friability of the pellets was determined using a USP friability test apparatus. Friability of the pellet formulations was determined as the percentage of weight loss after 200 revolutions of 6.5 g of the core pellets in a friabilator (Roche Friability Tester, India). The hardness of the pellets was determined using a digital hardness tester (Veego, India).[25-27]

Pellet sphericity

Pellet sphericity was determined by measuring the Feret diameter and perpendicular diameter of pellets by vernier caliper. From that aspect ratio was calculated (i.e. ratio of longest Feret diameter and its longest perpendicular diameter).[28]

RESULTS AND DISCUSSION

UV spectrum of norfloxacin in 0.1 N HCl

The λ max of norfloxacin in 0.1 N HCl was 273 nm. The calibration curve of norfloxacin was obtained in 0.1 N HCl at the respective λ max value as indicated in Figure 1.

Fourier transform infrared spectrum

The IR spectrum of norfloxacin, Eudragit RL 100, and a physical mixture of norfloxacin and polymer (Eudragit RL 100) was obtained by fourier transform infrared (FTIR) (Figure 2). The interpretations of the IR frequencies were done and the absorption bands were consistent with the structure of norfloxacin and Eudragit RL 100. The FTIR spectra of the physical mixture indicated compatibility of norfloxacin and Eudragit RL 100. The FTIR spectra of pure drug showed functional peaks at 3600 to 3250, 1492.95, 2524.46, 1267.27, and 1614.47 cm^{-1}. Eudragit RL 100 IR spectra showed peaks at 2920.32, 1720.56, and 1072.46, while the physical mixture showed peaks at 3491.27, 3365.90, 3012.91, 2850.8, 1745.64, 1610.61, 1456.30, and 1269.20 cm^{-1} with negligible shift in wave number.

Drug content

The drug content in all pellet formulations was determined by UV spectroscopy and was found to be between 96.75±0.8% and 98.78±0.45%, which indicated that the coating on the pellets also gives good reproducibility of drug content.

Optimization of norfloxacin pellets

To optimize the pelletization process MCC, PVP K30, and spheronizing speed were varied at different levels. Seventeen batches were prepared using a Box–Behnken design, and the aspect ratio and hardness of pellets were determined as response as indicated in Table 3.

The sphericity and hardness of pellets are essential properties to obtain effective coating. Spherical pellets provide a uniform surface, whereas sufficiently hardened pellets can withstand the mechanical stress during the subsequent coating process. The sphericity of pellets was determined in terms of aspect ratio. An aspect ratio value equal to unity indicates spherical

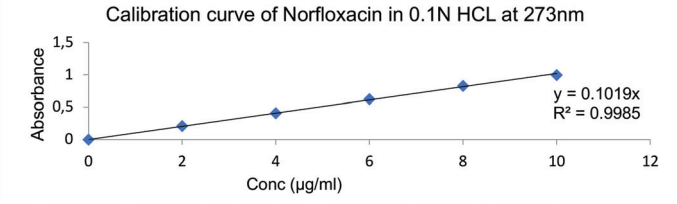

Figure 1. Calibration curve of norfloxacin in 0.1 N HCl at 273 nm

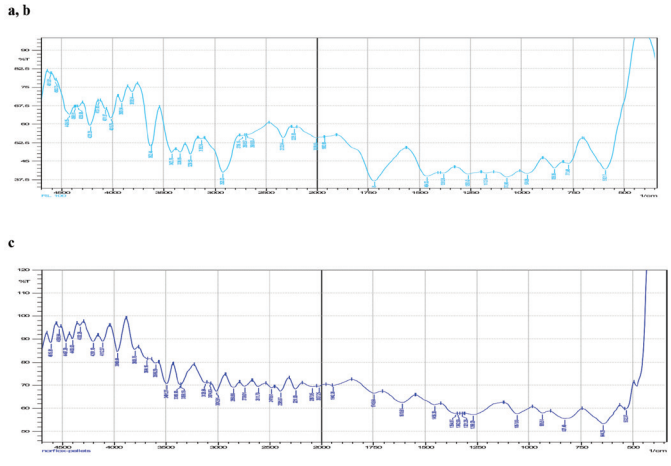

Figure 2. IR spectrum of (a) norfloxacin (b) Eudragit RL 100, and (c) physical mixture of norfloxacin and polymer (Eudragit RL 100)

IR: Infrared

pellets. The response surface plots of aspect ratios obtained indicate that increasing the MCC amount and spheronizing speed yields pellets having an aspect ratio near to 1, which is desirable, whereas increasing the amount of PVP K30 yields pellets having an aspect ratio greater than 1. The response surface plots of hardness obtained indicate that with increasing amount of PVP K30 the hardness of pellets also increases, as indicated in Figure 3. From the results of the experimental design batch number B-4 was selected, having aspect ratio 1.1 and hardness 0.59, for incorporation of $NaHCO_3$:HPMC K15M in different ratios and the subsequent coating process.

Regression equations of the fitted quadratic model:

Aspect ratio (Y1) = +1.41+0.036 * A-0.16 * B-0.013 * C-0.16 * A^2-0.030 * B^2+0.018 * C^2-0.030 * A * B-0.038 * A * C+0.13 * B * C.

Hardness (Y2) = +0.48-0.028 * A-0.055 * B+5.000E-003 * C+0.068 * A^2+0.16 * B^2-0.081 * C^2-0.10 * A * B-0.050 * A * C+0.023 * B * C.

Here A, B, and C are spheronizing speed, MCC, and PVP K 30, respectively.

It was observed from the regression equation that the independent variable MCC has a negative effect on the aspect ratio (Y1). This proves that an increasing amount of MCC leads to a decrease in the aspect ratio, i.e. near to unity, which is desirable. On hardness (Y2) a positive effect of PVP K30 was observed. As the concentration of PVP K30 increases the hardness of pellets also increases.

Table 3. Aspect ratio and hardness of experimental formulations

Batch number	Spheronizing speed (rpm)	Microcrystalline cellulose (%)	Polyvinyl pyrrolidone K30 (%)	Aspect ratio (mm)	Hardness (kg/cm^2)
B-1	850	25	4	1.90	0.72
B-2	750	35	6	1.16	0.77
B-3	850	30	6	1.41	0.47
B-4	950	35	6	1.15	0.59
B-5	850	30	6	1.41	0.47
B-6	850	35	8	1.16	0.42
B-7	850	25	8	1.39	0.56
B-8	950	30	4	1.26	0.37
B-9	850	35	4	1.14	0.50
B-10	850	30	6	1.41	0.47
B-11	850	30	6	1.41	0.47
B-12	850	30	6	1.41	0.47
B-13	750	30	8	1.36	0.65
B-14	750	25	6	1.24	0.60
B-15	950	25	6	1.35	0.83
B-16	750	30	4	1.09	0.41
B-17	950	30	8	1.38	0.41

Subsequently, $NaHCO_3$:HPMC K15M was incorporated in the selected batch (B-4) in different ratios, i.e. 1:1, 1:2, and 2:1, to prepare three additional batches (B-18, B-19, and B-20). Drug release and floating studies were conducted on the prepared batches. The batch (B-19) containing $NaHCO_3$ and HPMC K15M in the ratio of 1:2 yielded irregular shape and size pellets due to the higher amount of HPMC K15M, which was difficult to pass through the sieve, and the affecting spheronization process was not studied for drug release and floating behavior.

The plain norfloxacin pellet batch (B-4) showed 87.43% drug release within 1 h. The norfloxacin pellet batch containing $NaHCO_3$ and HPMC K15M in the ratios of 1:1 and 2:1 exhibited 84.19% in 4 h (B-18) and 92.42% in less than 2 h (B-20), respectively, as shown in Figure 4. The drug release in batch B-18 was sustained for 4 h but batch B-20 exhibited higher release in less than 2 h, as it contained more sodium bicarbonate and the generated CO_2 gas did not get entrapped in the polymer. The floating lag time for batches B-18 and B-20 was 8 s and 3 s, respectively, in 0.1 N HCl. As the amount of sodium bicarbonate increases the floating lag time decreases. The total floating time of batches B-18 and B-20 was quite short, i.e. 4 h and 2 h, respectively, as shown in Table 4. In batch B-18 the time required to release above 80% of drug and total floating time were 4 h. This type of behavior could be attributed to fact that once the HPMC was dissolved there was no polymeric membrane that could entrap the generated CO_2 gas. Hence, batch B-18 containing $NaHCO_3$ and HPMC K15M in the ratio of 1:1 was further selected for coating with Eudragit RL 100 to design complete floating drug delivery system pellets. A Eudragit RL 100 coating was given in order to increase the total floating time and to sustain the release of norfloxacin. Three batches (B-21, B-22, and B-23) were prepared with Eudragit RL 100 coating with weight gain of 5%, 10%, and 15% and evaluated for drug release and floating behavior.

The percentage drug release for batches B-21, B-22, and B-23 was 91.12% in 5 h, and 82.11% and 60.67% in 8 h, respectively, as shown in Figure 5. The drug release studies indicated that as the Eudragit RL 100 polymer coat increases the drug release decreases. The higher coat led to a thicker membrane over pellets, which retarded dissolution medium penetration and hence sustained drug release was obtained. The floating lag time for batches B-21, B-22, and B-23 was 290 s, 440 s, and 795 s, respectively, in 0.1 N HCl. The total floating time of batches B-21, B-22, and B-23 was 5 h, 8 h, and 8 h, respectively,

Table 4. Floating studies of batches (B-18, B-20, B-21, B-22, and B-23)

Batch number	Floating lag time (s)	Total floating time (h)
B-18	9±1	4.07±0.75
B-20	4±1	1.89±0.105
B-21	300±10	4.99±0.1
B-22	430±10	8±0.05
B-23	805±10	7.85±0.15

Mean ± standard deviation; n=3

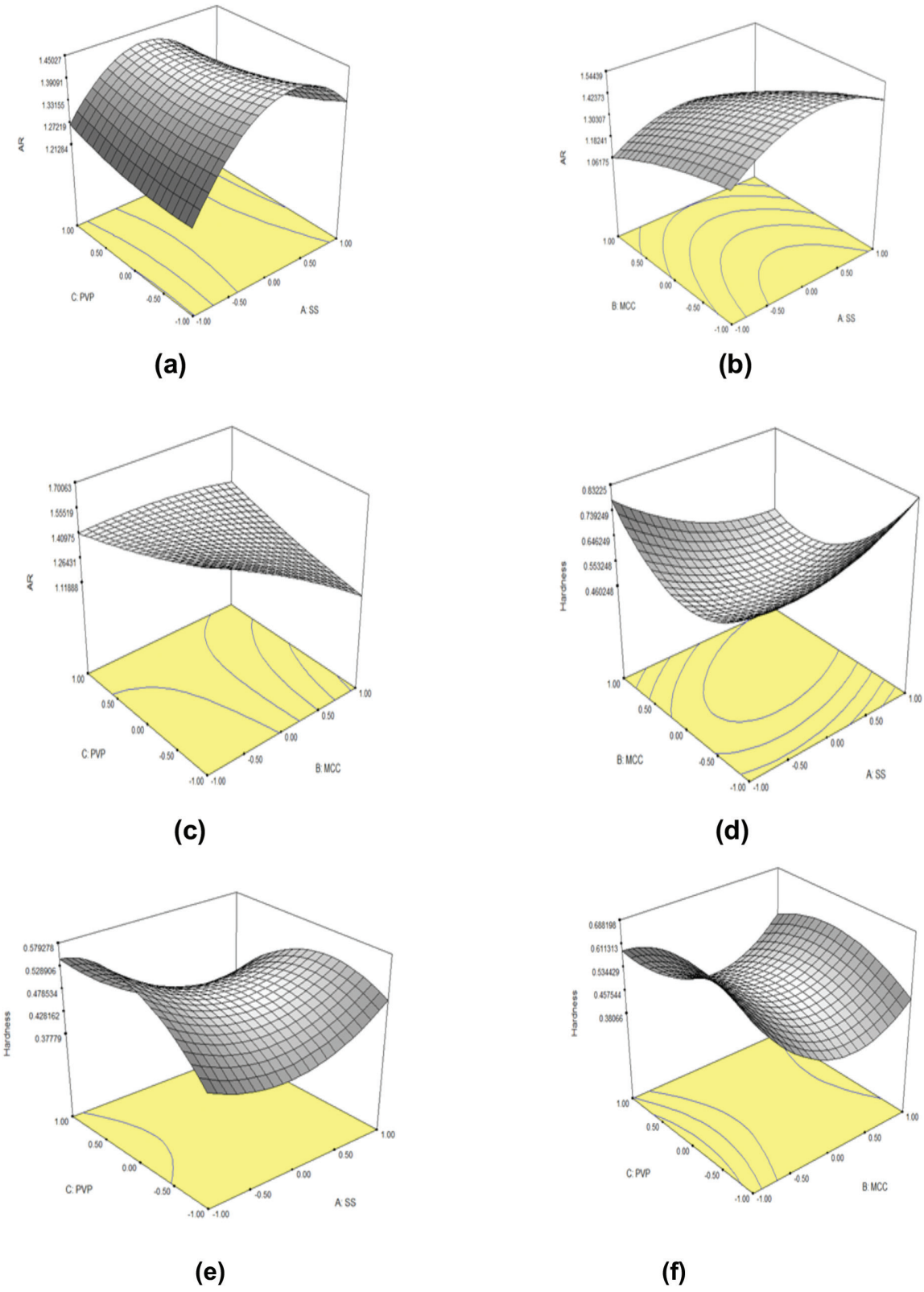

Figure 3. Response surface plot. (a, b, c) Aspect ratio (PVP vs SS, MCC vs SS, PVP vs MCC) respectively. (d, e, f) Hardness (MCC vs SS, PVP vs SS, PVP vs MCC) respectively

PVP: Polyvinylpyrrolidone, MCC: Microcrystalline cellulose

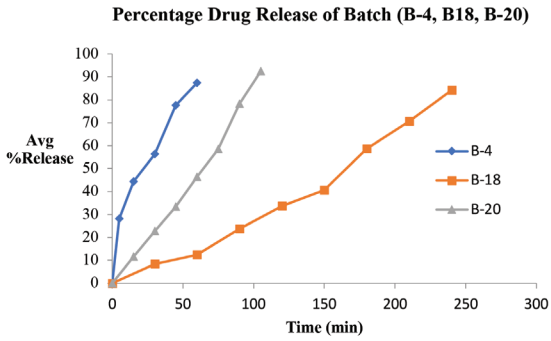

Figure 4. Percentage drug release of batch (B-4, B18, B-20) in 0.1 N HCl. Mean ± standard deviation; n=3

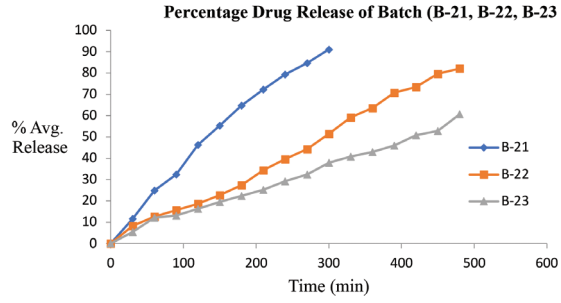

Figure 5. Percentage drug release of batch (B-21, B22, B-23) in 0.1 N HCl. Mean ± standard deviation; n=3

as shown in Table 4. Batches B-22 and B-23 had satisfactory floating ability, with 70%-90% of pellets remaining floating for up to 8 h. The floating studies reveal that an increasing level of polymeric membrane coating increases floating lag time as well as total floating time. Due to the thicker polymer coat water penetration is retarded, which in turn delays CO_2 gas generation, leading to increased floating lag time. However, once the CO_2 gas is generated the increasing amount of polymer coat inhibits the permeation of gas out of the floating pellets system and maintains the buoyancy for a longer period.

Among the three complete floating drug delivery system pellet batches B-21, B-22, and B-23, batch B-22 was found to be optimized based on the criteria of attaining minimum floating lag time (less than 10 min), maximum total floating time, and maximum value of drug released in 8 h.

Scanning electron microscopy

The surface morphology of the norfloxacin uncoated pellet batch (B-4) and coated pellet batch (B-22) was studied through SEM. The uncoated norfloxacin pellets' surface was wrinkled and rough, whereas the polymer-coated pellets showed smoother surfaces as indicated in Figures 6a and 6b.

Particle size distribution analysis of pellets

The particle size distribution analysis of pellets indicates a narrow size distribution in which most of the pellets are in the size range of 1000 µm to 1200 µm, as shown in Figure 7.

Physical characterization of pellets

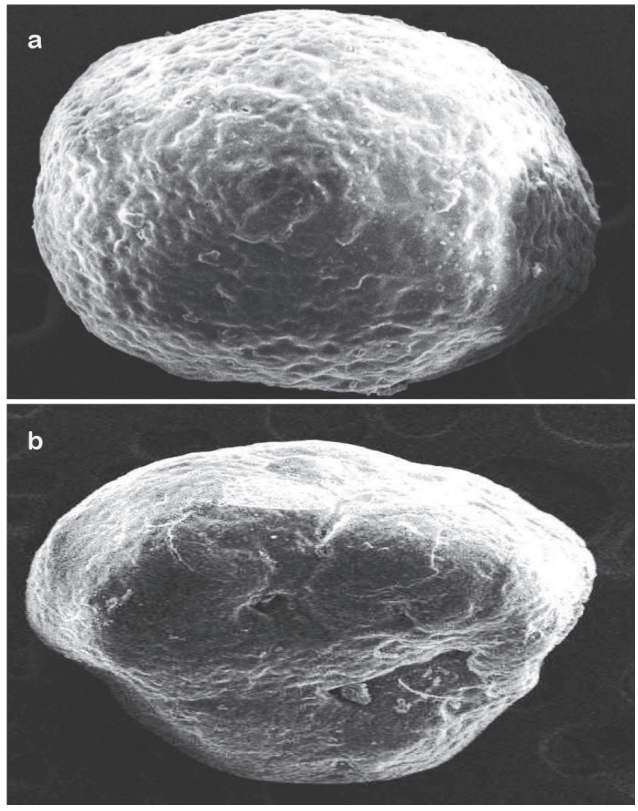

Figure 6. Scanning electron microphotographs of (a) uncoated norfloxacin pellets and (b) norfloxacin pellets coated with polymer at 100× magnification

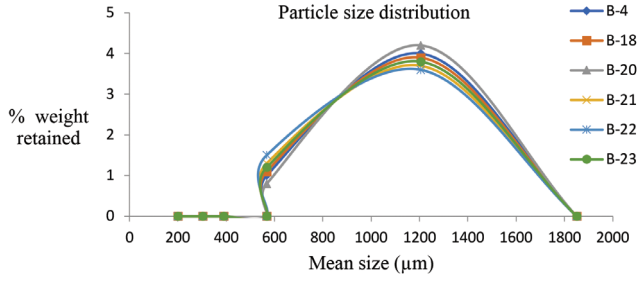

Figure 7. Particle size distribution curve

From the physical characterization of pellets, it was clearly observed that all the batches have excellent flow properties, with an angle of repose in the range 25.5±0.49° to 28.02±0.30° **and** Carr's index and Hausner's ratio in the range of 5% to 15% and 1.05±0.3 to 1.14±0.3, respectively (Table 5). The aspect ratio of pellets obtained was near to unity. Hardness and friability were in the range of 0.49±0.01 to 0.61±0.01 kg/cm^2 and 0.17±0.52%, respectively.

CONCLUSIONS

A gastroretentive multiparticulate drug delivery system for norfloxacin based on the gas generation technique was successfully designed and developed. The identification and purity of drug were affirmed by conducting infrared and UV spectroscopy studies. A 3-level, 3-factor, 17-run experimental Box–Behnken design was employed to optimize the norfloxacin

Table 5. Physical characterization of pellet batches (B-4, B18, B-20, B-21, B-22, and B-23)

Batch number	Angle of repose (°)	Carr's index (%)	Hausner's ratio	Aspect ratio (mm)	Hardness (kg/cm²)	Friability (%)
B-04	27.07±0.6	14.85±0.65	1.12±0.02	1.17±0.02	0.59±0.005	0.30±0.1
B-18	27.85±0.3	9.23±0.66	1.05±0.3	1.14± 0.02	0.49±0.01	0.48±0.2
B-20	26.19±0.5	12.13±0.63	1.08±0.07	1.13±0.01	0.57±0.02	0.52±0.09
B-21	23.16±0.3	7.51±0.37	10.6±0.01	1.14±0.03	0.61±0.01	0.35±0.02
B-22	25.5±0.49	5.62±0.42	1.03±0.01	1.18±0.005	0.54±0.025	0.16±0.01
B-23	28.02±0.3	11.62±0.36	1.01±0.005	1.09±0.06	0.56±0.015	0.21±0.1

Mean ± standard deviation; n=3

pellets in terms of sphericity and hardness required to attain effective coating subsequently. The pellet batch obtained at spheronizing speed 950 rpm containing 35% MCC with 6% PVP K 30 produced pellets with the desired sphericity and hardness. $NaHCO_3$ and HPMC K15M in the ratios of 1:1, 1:2, and 2:1 (w/w) on a dry solid basis were incorporated into the norfloxacin pellets and they were further coated with Eudragit RL 100 using a fluidized bed processor to obtain weight gain of 5%, 10%, and 15% w/w. The floating ability and *in vitro* drug release of the system were dependent on the ratio of $NaHCO_3$ to HPMC K15M and the percentage of Eudragit RL 100 polymer coat. As the amount of sodium bicarbonate increases floating lag time decreases. The drug release studies indicated that as the Eudragit RL 100 polymer coat increases the drug release decreases, producing sustained release of norfloxacin. The floating multiparticulate pellet batch containing $NaHCO_3$ and HPMC K15M in the ratio of 1:1 with 10% Eudragit RL 100 coating showed the minimum floating lag time (<10 min) and 82.11% average drug release in 8 h. The floating study reveals that 70%-90% of pellets remained floating for up to 8 h. The significant result obtained with the study was that a floating multiparticulate drug delivery system based on the effervescent mechanism can be effectively employed for improvement of the bioavailability and therapeutic effect of drugs having poor absorption in the lower part of the gastrointestinal tract.

ACKNOWLEDGEMENTS

The author acknowledges Aarti Drugs Ltd, Mumbai, India for providing the gift sample of norfloxacin. The author is also thankful to Savitribai Phule Pune University for conducting the scanning electron microscopic studies.

Conflict of Interest: No conflict of interest was declared by the authors.

REFERENCES

1. Vo AQ, Feng X, Morott JT, Pimparade MB, Tiwari RV, Zhang F, Repka MA. A novel floating controlled release drug delivery system prepared by hot-melt extrusion. Eur J Pharm Biopharm. 2016;98:108-121.
2. Singh BN, Kim KH. Floating drug delivery systems: an approach to oral controlled drug delivery via gastric retention. J Control Release. 2000;63:235-259.
3. Lopes CM, Bettencourt C, Rossi A, Buttini F, Barata P. Overview on gastroretentive drug delivery systems for improving drug bioavailability. Int J Pharma. 2016;510:144-158.
4. Mandal UK, Chatterjee B, Senjoti FG. Gastro-retentive drug delivery systems and their *in vivo* success: A recent update. Asian J Pharma Sci. 2016;11:575-584.
5. Sharma AR, Khan A. Gastroretentive drug delivery system: an approach to enhance gastric retention for prolonged drug release. Int J Pharma Sci Res. 2014;5:1095-1106.
6. Narang N. An updated review on: floating drug delivery system (FDDS). Int J Applied Pharma. 2011; 3:1-7.
7. Thahera PD, Latha K, Shailaja T, Nyamathulla S, Uhumwangho MU. Formulation and evaluation of Norfloxacin gastro retentive drug delivery systems using natural polymers. Int Current Pharma J 2012;1:155-164.
8. Srivastava R, Chaturvedi D. Formulation, Characterization and Evaluation of Gastro-Retentive Floating Tablets of Norfloxacin hydrochloride. J. Pharmacy and Pharma Sci.2015:33-38
9. Guguloth M, Bomma R, Veerabrahma K. Development of Sustained Release Floating Drug Delivery. PDA J. Pharm Sci Technol. 2011;65:198-206
10. Oliveira PR, Bernardi LS, Strusi OL, Mercuri S, Segatto Silva MA, Colombo P, Sonvico F. Assembled modules technology for site-specific prolonged delivery of norfloxacin. Int J Pharm. 2011;405;90-96.
11. Bomma R, Naidu RS, Yamsani M, Veerabrahma K. Development and evaluation of gastroretentivenorfloxacin floating tablets. Actapharma. 2009;59:211-221.
12. Bhattacharya SA, Prajapati BG. Formulation, design and development of ciprofloxacin hydrochloride floating bioadhesive tablet. e-J Sci Tech. 2017;12;40-70.
13. Rajaiya P, Mishra R, Nandgude T, Poddar S. Solubility and dissolution enhancement of albendazole by spherical crystallization. Asian J Biomedical Pharma Sci. 2016;6:9-14.
14. Nandgude T, Bhise K. Characterization of Drug and Polymers for Development of Colon Specific Drug Delivery System. Asian J Biomedical Pharma Sci. 2011;1:17-21.
15. Parmar S, Mishra R, Shirolkar S. Spherical agglomeration for Solubility and Dissolution Enhancement of Simvastatin, Asian J Pharm Clinical Res. 2016;9:65-72.
16. Nandgude T, Saifee M, Bhise K. Formulation and evaluation of fastdisintegrating tablet of Diphenhydramine Tannate. Asian J Pharma. 2006;1:41-45.

17. Amrutkar PP, Chaudhari PD. Design and *in vitro* evaluation of multiparticulate floating drug delivery system of zolpidem tartarate. Colloids Surf B Biointerfaces. 2012;89:182-187.

18. Katakam VK, Reddy S, Somagoni JM, Panakanti PK, Yamsani MR. Design and Evaluation of a Novel Gas Formation-Based Multiple-Units as a Biphasic Gastro-Retentive Floating Drug Delivery System for Alfuzosin Hydrochloride. Research and Reviews. J Pharmacy Pharma Sci. 2013;2:33-46.

19. Zhang C, Xu M, Tao X, Tang J, Liu Z, Zhang Y, Lin X, He H, Tang X. A floating multiparticulate system for ofloxacin based on a multilayer structure: *In vitro* and *in vivo* evaluation. Int J Pharm. 2012;430:141-150.

20. Pagariya TP, Patil SB. Development and optimization of multiparticulate drug delivery system of alfuzosin hydrochloride. Colloids Surf B Biointerfaces. 2013;102:171-177.

21. Kendre PN, Chaudhari PD. Effect of polyvinyl caprolactam–polyvinyl acetate–polyethylene glycol graft copolymer on bioadhesion and release rate property of eplerenone pellets. Drug Dev Ind Pharm. 2017;43:751-761.

22. Chakravarthy KK, Younus M, Shaik S, Pisipati SV. Formulation and Evaluation of Enteric Coated Pellets of Omeprazole. Int J Drug Dev Res. 2012;4;257-264.

23. Tubati VP. Murthy GK, Rao SS. Formulation Development and Statistical Optimization of Ivabradine Hydrochloride Floating Pulsatile Microspheres Using Response Surface Methodology. Asian J Pharm. 2016;10:1-11

24. Patil SM, Mishra RV, Shirolkar SV. Development and Evaluation of Sustain Release Simvastatin Pellets. Res J Pharm Techn. 2017;10:2467-2473.

25. Diggikar SS, Nandgude TD, Poddar SS. Formulation of Modified Release Pellets of Montelukast Sodium. Res J Pharm Techn. 2018;11:31-37.

26. Muley s, Nandgude T, Poddar S. Extrusion-spheronization a promising pelletization technique: In-depth review. Asian J Pharma Sci. 2016;11:684-699.

27. Muley SS, Nandgude T, Poddar S. Formulation and Optimization of Lansoprazole Pellets Using Factorial Design Prepared by Extrusion-Spheronization Technique Using Carboxymethyl Tamarind Kernel Powder. Recent Pat Drug Deliv Formul. 2017;11:54-66.

28. Raval MK, Ramani RV, Sheth NR. Formulation and evaluation of sustained release enteric-coated pellets of budesonide for intestinal delivery. Int J Pharm Investig. 2013;3:203-211.

Turk J Pharm Sci 2019;16(3):335-339
DOI: 10.4274/tjps.galenos.2018.02419

ORIGINAL ARTICLE

Impact of Particle-Size Reduction on the Solubility and Antidiabetic Activity of Extracts of Leaves of *Vinca rosea*

Partikül Büyüklüğünün Azaltılmasının *Vinca rosea* Yaprak Ekstresinin Çözünürlüğü ve Antidiyabetik Aktivitesi Üzerine Etkisi

Khalid HUSSAIN*, Abida QAMAR, Nadeem Irfan BUKHARI, Amjad HUSSAIN, Naureen SHEHZADI, Shaista QAMAR, Sajida PARVEEN

University of the Punjab, Punjab University College of Pharmacy, Lahore, Pakistan

ABSTRACT

Objectives: The present study aimed to enhance the aqueous solubility of methanol extract of leaves of *Vinca rosea* (family: *Apocynaceae*) by particle-size reduction using milling and to evaluate its antidiabetic activity.

Materials and Methods: The methanol extract (ME) was micronized using a vibratory ball mill, operated at a vibratory speed of 15 Hz for 60 min at room temperature, and the resulting extract micronized ME (MME) was investigated to determine particle size, solubility, UV/visible profile, and i*n vitro* antidiabetic activity.

Results: The average particle size of MME was 0.753±0.227 µm, which was less than half of that of the ME (2.007±0.965 µm). The solubility of MME was greater than that of the ME. MME exhibited 65.63%, 18.0%, and 96.87% higher antidiabetic activity in the glucose uptake by the yeast cells method, hemoglobin glycosylation assay, and the alpha amylase inhibition assay, respectively ($p<0.05$).

Conclusion: The results of the present study indicate that micronization effectively enhanced the aqueous solubility and antidiabetic activity of methanol extract of leaves of *Vinca rosea*.

Key words: *Vinca rosea*, methanol extract, micronization, solubility, antidiabetic activity

ÖZ

Amaç: Bu çalışmada *Vinca rosea* (familya: *Apocynaceae*) yapraklarının metanol ekstresinin öğütme işlemi kullanılarak partikül büyüklüğünün azaltılması ile sudaki çözünürlüğünün artırılması ve antidiyabetik aktivitesinin değerlendirilmesi amaçlanmıştır.

Gereç ve Yöntemler: Metanol ekstresi (ME) titreşimli bir bilyalı değirmen kullanılarak oda sıcaklığında 60 dakika boyunca 15 Hz'lik bir titreşim hızında mikronize ME (MME) edilmiş ve elde edilen ekstrenin partikül büyüklüğü, çözünürlüğü, UV/görünür bölge profili ve *in vitro* antidiyabetik aktivitesi araştırılmıştır.

Bulgular: MME'nin ortalama partikül büyüklüğünün 0.753±0.227 µm olduğu ve bu değerin ME'nin partikül büyüklüğünün (2.007±0.965 µm) yarısından az olduğu belirlenmiştir. MME'nin çözünürlüğünün, ME'ninkinden daha fazla olduğu saptanmıştır. MME, glukoz alımında, maya hücreleri yöntemi, hemoglobin glikozilasyon ve alfa amilaz inhibisyon deneylerinde, sırasıyla %65.63, %18.0 ve %96.87 daha yüksek antidiyabetik aktivite sergilemiştir ($p<0.05$).

Sonuç: Bu çalışmanın sonuçları, mikronizasyonun, *Vinca rosea* yapraklarının metanol ekstresinin suda çözünürlüğünü ve antidiyabetik aktivitesini etkili bir şekilde artırdığını göstermektedir.

Anahtar kelimeler: *Vinca rosea*, metanol ekstresi, mikronizasyon, çözünürlük, antidiyabetik aktivite

***Correspondence: E-mail:** hussain_761@yahoo.com, **Phone:** +92 332 424 93 23 **ORCID:** orcid.org/0000-0001-9627-8346
Received: 01.04.2018, **Accepted:** 03.07.2018

INTRODUCTION

The surge in interest among the public towards plant-based drugs is increasing day by day. However, mostly such products show poor aqueous solubility and oral bioavailability, leading to challenges in formulation development and efficacy. As a result, active constituents cannot reach the target site at a rate and extent needed to elicit therapeutic response. Several techniques may be used to improve aqueous solubility and oral bioavailability. Among such techniques, particle-size reduction (micronization) is one of the oldest approaches to improving solubility.[1] Micronization, a conventional technique for size reduction, is commonly used for enhancing solubility. This technique reduces particle size up to 2-5 µm usually, but sometimes below 1 µm.[2] For such purpose, jet milling, ball milling, and high-pressure homogenization machines are used frequently.[1] In the present study, a ball mill was used to reduce the particle size of extract of leaves of a traditional medicinal plant, *Vinca rosea.*

The plant is well known due to its alkaloids such as vincristine and vinblastine for treating cancer.[3] As a folkloric medicine, fresh leaves of the plant are chewed to manage diabetes. The scientific evidence for this use was reported due to isolation of alkaloids such as vindoline, vindolidine, vindolicine, and vindolinine, which had antidiabetic activity.[4] The three alkaloids exhibited quite high median inhibitory concentration for cell viability and hence are considered safe to consume. Moreover, such alkaloids are poorly soluble in aqueous medium and suspected to have a low systemic level so that they exhibit cytotoxicity. The extracts of the plant contain flavonoids and polyphenols that have antidiabetic activity as well.[5] The activity of extract of the plant may be enhanced by increasing aqueous solubility by micronization. Therefore, the present study aimed to reduce the particle size of methanol extract (ME) of leaves of *V. rosea* and evaluate the antidiabetic activity of micronized ME (MME). The results of the present study may enhance the utilization of this plant for managing diabetes.

MATERIALS AND METHODS

Collection and extraction

The plant was acquired from the National Agricultural Research Centre, Islamabad, Pakistan. The leaves were separated, washed, dried under shade, and pulverized. Powdered material (75 g) was macerated with 200 mL of methanol for 5 days. The solvent was removed and the extraction was repeated three times using the same volume of methanol. The extract was filtered and dried *in vacuo* at 40°C, and termed ME.

Micronization of extract

A vibratory ball mill (locally manufactured, Lahore, Pakistan) was used in this study. It was fitted with two stainless steel cylinders (10 cm in length, 32 mm in internal diameter) each containing one stainless steel ball (25 mm in diameter). A total of 3 g of ME was added to each of the cylinders, fitted in the mill, and micronized by operating the machine at a vibratory speed of 15 Hz for 60 min at room temperature. The resulting extract was termed MME.

Chemicals

Metronidazole (Siza International, Lahore, Pakistan), alpha amylase and hemoglobin (China), acarbose (Bayer, Pakistan), methanol (RCI Labscan, Thailand), glucose, starch, gallic acid, and enthrone reagent (Sigma Aldrich) were procured from the local market.

Characterization of ME and MME

ME and MME were subjected to scanning electron microscopy (SEM) to determine the particle morphology in the magnification range from lower to higher (1.00 kx and 25.0 kx). The various sized particles were observed in the magnification range of 10.0 kx and average particle size was determined by ImageJ (software). Both the extracts were dissolved in methanol to obtain solutions having a final concentration of 1.0 mg/mL. These solutions were scanned in the UV/visible range (800-200 nm) and the spectra were compared with each other. The aqueous solubility of ME and MME was assessed by taking 10 mg of extract in separate test tubes containing 10 mL of water. The samples were allowed to dissolve by shaking by hand and if not soluble were subjected to sonication for 1 min. The formation of a clear homogeneous solution indicated solubility.

Antidiabetic activity

Glucose uptake by yeast cells

The method described by Kumar et al.[6] was used to study glucose uptake by yeast cells. Briefly, the yeast cells were rinsed with distilled water by centrifugation at 2500 rpm for 5 min and the procedure was repeated until the supernatant became clear. Then a yeast cell pellet was suspended in water to prepare 10% suspension (v/v). One milliliter of 10 mM glucose solution and 1 mL of each extract/standard (metronidazole) were mixed and incubated at 37°C for 10 min. Then 100 µL of yeast suspension was added and mixed and incubation was continued for 1 h at 37°C. Afterwards, the mixture was centrifuged at 2500 rpm for 5 min and the supernatant was used to determine the glucose concentration. The percentage glucose uptake was computed using the following formula:

$$\text{Percentage uptake} = \frac{[\text{Absorbance of control-Absorbance of sample}]}{\text{Absorbance of control}}$$

Hemoglobin glycosylation inhibition activity

The activity was determined using the procedure described by Parker et al.[7] Briefly, 1 mL of hemoglobin (0.06%, w/v), gentamycin (0.02%, w/v), sample/standard (gallic acid) solution, and glucose (2%, w/v) were mixed and incubated in the dark at room temperature for 72 h. Then the absorbance was measured at 440 nm and the percentage inhibition of hemoglobin glycosylation was determined using the formula given as follows:

$$\text{Percentage activity} = \frac{[\text{Absorbance of control-Absorbance of sample}]}{\text{Absorbance of control}}$$

Alpha amylase inhibition activity

The activity was determined using the method developed by Ramakrishna et al.[8] Briefly, 1 mL of enzyme solution (0.5 mg/mL, in 20 mM phosphate buffer of pH 6.9) and 1 mL of extract/standard (acarbose) solution were mixed and incubated at 37°C for 10 min. Then 1 mL of 1% starch solution was added and the reaction mixture was again incubated at 37°C for 10 min. Finally, the reaction was stopped by adding 2 mL of dinitrosalicylic acid and the mixture was further heated in a boiling water bath for 8 min. The contents were cooled and the absorbance was measured at 540 nm. The % inhibition of the enzyme activity was calculated by the formula given as follows:

$$\text{Percentage activity} = \frac{[\text{Absorbance of control-Absorbance of sample}]}{\text{Absorbance of control}}$$

Statistical analysis

The data were analyzed by one-way ANOVA with Bonferroni post hoc multiple comparison. A p value <0.05 was considered significantly different.

RESULTS AND DISCUSSION

Micronization and characterization of extracts

The MME and ME of leaves of *V. rosea* were compared with each other in terms of morphology, size distribution, solubility, UV/visible absorbance behavior, and antidiabetic activity. The morphology of ME and MME, determined by SEM at lower and higher magnification (1.0 kx and 25.0 kx), is shown in Figures 1 and 2, respectively. The particle-size distribution, determined in the magnification range of 10.0 kx, of ME and MME is given in Figure 3. The particles of ME appeared angular with low sphericity, whereas the particles of MME appeared rounded with medium sphericity. The spherical smaller particles showed agglomeration due to the micronization process. These results show that micronization enhanced flowability, packing, and interaction with fluids and the covering power of pigments, which are much needed properties of a pharmaceutical material.

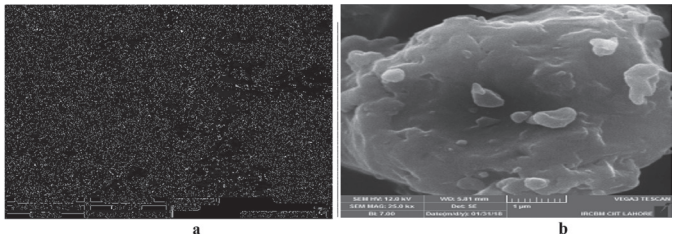

Figure 1. Scanning electron microscopy images of methanol extract of leaves of *Vinca rosea* at lower (a) and higher magnification (b)

SEM: Scanning electron microscopy

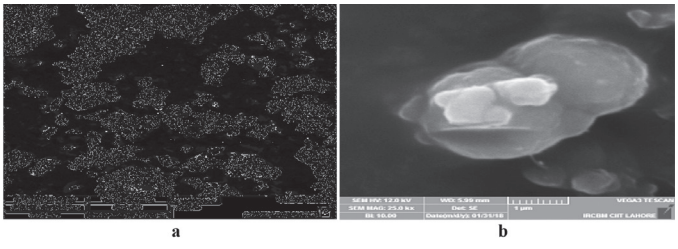

Figure 2. Scanning electron microscopy images of micronized methanol extract of leaves of *Vinca rosea* at lower (a) and higher magnification (b)

The average particle size of ME prior to micronization, determined from SEM data by applying ImageJ, was 2.007±0.0965 µm, whereas the average particle size of MME was 0.753±0.227 µm (62.48% reduction in size). Hence, the milling had increased the surface area of the particles.

The impact of micronization on the aqueous solubility of the extract was positive. The solubility of ME in distilled water was 2 mg/mL with sonication, whereas MME was soluble in water in the same proportion without sonication. This ease of solubility was due to smaller particle size as described by the Noyes–Whitney equation, which indicated that when particles became smaller the surface area to volume ratio was increased. The larger surface area allowed greater interaction with the solvent molecules, which resulted in increased solubility. The reduction in the particle size increases the rate of solution because of the large surface area.[9]

The overlays of the UV/visible spectra of ME and MME of leaves of *V. rosea* are shown in Figure 4. The spectra of both the extracts were superimposable, indicating chemical similarity of the extracts. These results clearly indicated that milling had not affected the chemical nature of the constituents of the extract. Thus, the solubility was increased due to milling but without any chemical change.

The improvement in the solubility of MME of leaves of *V. rosea* is of great importance. The plant is reported to contain antidiabetic alkaloids and polyphenols/flavonoids that are either insoluble or poorly soluble in water. In the present study, plant material was defatted with petroleum ether and then its alkaloidal contents were further reduced by extracting the residue with chloroform, in which alkaloids were soluble. The residue was extracted with methanol so that the extract contained polar compounds such as polyphenols and flavonoids in higher proportions. This extract was subjected to milling to enhance the aqueous solubility of MME and its chemical constituents, leading to higher efficacy. To confirm this fact, both types of extracts were investigated for antidiabetic activity, the traditional use of the plant, using different *in vitro* models.

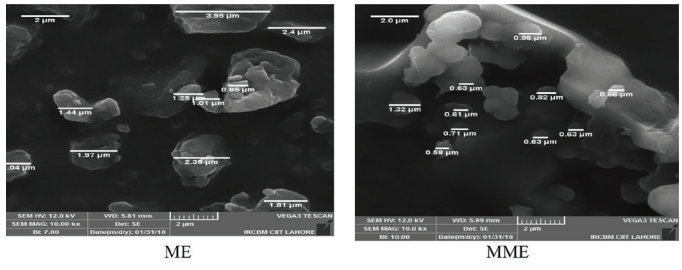

Figure 3. Scanning electron microscopy images of methanol and micronized methanol extracts showing particles of various sizes in the magnification range of 10.0 kx

ME: Methanol extract, MME: Micronized methanol extract

Antidiabetic activity

The effect of micronization on the antidiabetic activity of ME and MME of leaves of the plant using three *in vitro* models is shown in Figure 5. In all three models, MME showed higher activity as compared to ME and standard drug ($p<0.05$). The activity of MME was 63% higher in glucose uptake by the yeast cell assay, 18.0% higher in inhibition in the hemoglobin-glycosylation inhibition assay, and 96.87% higher in the alpha amylase inhibition assay than that of ME. These results explicitly indicate the positive effect of physical modification of particle size on hypoglycemic activity.

In the present study, MME showed higher uptake of glucose in yeast cells as compared to ME. This increase in activity is due to the reduction in particle size and higher aqueous solubility. Owing to such behavior the constituents of the extract can enter yeast cells at a higher rate and extent, thereby facilitating glucose utilization within the cell. This creates a concentration gradient

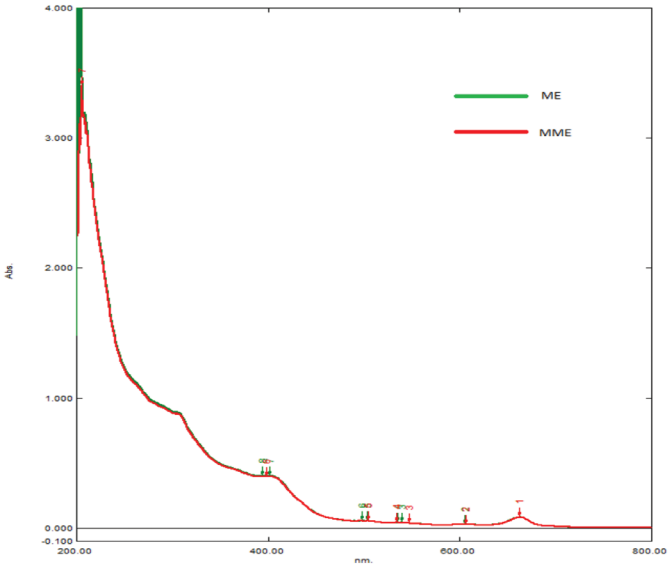

Figure 4. Overlays of UV/visible profiles of methanol extract and micronized methanol extract of leaves of *Vinca rosea*

UV: Ultraviolet

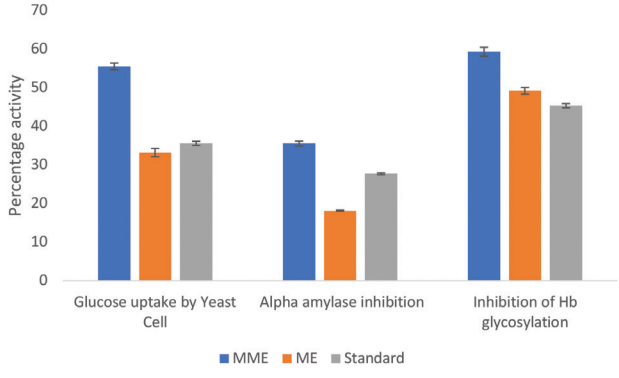

Figure 5. Antidiabetic activity of MME, ME, and standard using glucose uptake by yeast cells, hemoglobin glycosylation, and alpha amylase inhibition assay

across the membrane and facilitates the movement of glucose from the solution to the cell. It is reported that glucose uptake in yeast cells takes place through facilitated diffusion catalyzed by glucose transporter and hence the compounds enhancing the activity of the transporter can increase glucose uptake.[10] As the glucose enters the yeast cell, phosphorylation takes place, which prevents the glucose molecules from diffusing back and creating a concentration gradient.[10] Therefore, MME entered the cells much faster than ME and enhanced the transport of glucose from the solution to the cells due to facilitated diffusion and phosphorylation.

Likewise, the inhibition of Hb glycosylation with MME is higher as compared to ME. The glycosylation can be inhibited in two ways: blocking the glucose so that it cannot interact with the amino group of the beta chain of hemoglobin, and blocking the amino group of the hemoglobin. The activity of the extract may be multifaceted because it contains alkaloids, soluble proteins, polyphenols, and flavonoids. The nitrogen groups of the alkaloids and soluble proteins may block the aldehyde group of glucose, thus reducing its availability to react with hemoglobin. The polyphenols and flavonoids can act as proton donors to reduce the aldehyde group of the glucose. The same is reported about the glycosylation inhibition activity of polyphenols and flavonoids.[11,12] The extract might have shown all such effects in glycosylation inhibition.

Hb glycosylation has attained much importance in the modern world due to its use as a scale in the long-term control of diabetes. Glycosylation is a nonenzymatic process of attaching glucose molecules with the amino group of Hb, leading to the formation of advanced glycated end products. Antioxidants prevent this oxidation process and so in a way inhibit Hb glycosylation.[12]

The inhibitory response of MME against alpha amylase, an important therapeutic target of diabetic control, was also superior to that of ME. This enzyme hydrolyzes the alpha glycosidic bond and converts starch into glucose. The phenolic compounds of the extract can show alpha amylase inhibition action as reported earlier.[13] The inhibitory potential of these metabolites is related to the presence of a hydroxyl group that forms hydrogen bonding between the hydroxyl group and catalytic residue of the binding site of enzyme.[13] The difference in activity between ME and MME was due to the micronization process. The extracts due to differential solubility interacted with the enzyme differently. The micronization process converted the extract into amorphous particles, which resulted in improved solubility. The amorphous form is more readily soluble because of higher Gibbs free energy.[14] The above-mentioned results indicated that smaller particles with larger surface area might have an improved antidiabetic effect.

Traditional micronization has some limitations such as morphology and particle properties that are uncontrolled as compared to novel size reduction techniques. Heterogeneous particle shape and agglomeration are observed in the ball milling method, which can be prevented by particle engineering techniques. Micronization using other methods such as jet

milling and high pressure homogenization can be used to observe the difference between the results.

Study limitations

Traditional micronization has some limitations such as morphology and particles properties that are uncontrolled as compared to novel size reduction techniques. Heterogeneous particle shape and agglomeration are observed in the ball milling method, which can be prevented by particle engineering techniques. Most of the new chemical entities in drug research are poorly water soluble. Therefore, attempts should be made to enhance water solubility by micronization, which would in turn increase the pharmacological activity.

CONCLUSIONS

The results of the present study show that micronization increases the solubility and antidiabetic activity of methanol extract of leaves of *V. rosea* without causing any chemical change.

ACKNOWLEDGEMENTS

We are grateful to COMSATS, Lahore Campus, Pakistan, for the SEM studies.

Conflict of Interest: No conflict of interest was declared by the authors.

REFERENCES

1. Khadka P, Ro J, Kim H, Kim I, Kim JT, Kim H, Cho JM, Yun G, Lee J. Pharmaceutical particle technologies: An approach to improve drug solubility, dissolution and bioavailability. Asian J Pharm Sci. 2014;9:304-316.
2. Rawat N, Kumar MS, Mahadevan N. Solubility: Particle size reduction is a promising approach to improve the bioavailability of lipophillic drugs. Int J Adv Pharm Res. 2012;1:8-18.
3. Farnsworth NR, Bingel AS. Problems and prospects of discovery new drugs from higher plants by pharmacological screening. Springer Verlag, Berlin. 1977;1-22.
4. Tiong SH, Looi CY, Hazni H, Arya A, Paydar HJ, Wong WF, Cheah SC, Mustafa MR, Awang K. Antidiabetic and antioxidant properties of alkaloids from *Catharanthus roseus* (L.) G. Don. Molecules. 2013;18:9770-9784.
5. Umeno A, Horie M, Murotomi K, Nakajima Y, Yoshida Y. Antioxidative and antidiabetic effects of natural polyphenols and isoflavones. Molecules. 2016;21:708.
6. Kumar B, Dinesh A, Mitra M. *In vitro* and *in vivo* studies of antidiabetic Indian medicinal plants. A review. J Herb Med Tox. 2009;3:9-14.
7. Parker KL, England JD, Da Costa J, Hess RL, Goldstein DE. Improved colorimetric essay for glycosylated haemoglobin. Clin Chem. 1981;25:669-672.
8. Ramakrishna SV, Suseela T, Ghilyan NP, Jalil A, Prema P, Lonsane BK, Ahmed SY. Recovery of amyloglucosidase from moulay bran. Indian J Technol. 1982;20:476-480.
9. Chaudhary A, Nagaich U, Gulati N, Sharma VK, Khosa RL. Enhancement of solubilization and bioavailability of poorly soluble drugs by physical and chemical modifications: A recent review. J Adv Pharm Edu Res. 2012;2:32-67.
10. Weusthuis RA, Pronk JT, Broek PJA, Dijken JPV. Chemostat cultivation as a tool for studies on sugar transport in yeasts. Microbiol Rev. 1994;616-630.
11. Yeh WJ, Hsia SM, Lee WH, Wu CH. Polyphenols with antiglycation activity and mechanisms of action: a review of recent findings. J Food Drug. 2017;25:84-92.
12. Sadowska BI, Galiniak SBG. Kinetics of glycoxidation of bovine serum albumin by glucose, fructose and ribose and its prevention by food components. Molecules. 2014;19:18828-18849.
13. Sales PMD, Souza PMD, Simeoni LA, Magalhaes PDO, Silveira D. α-amylase inhibitors. A review of raw material and isolated compounds from plant source. J Pharm Pharmaceut Sci. 2012;15:141-183.
14. Graeser KA, Patterson JE, Zeitler JA. The role of configurational entropy in amorphous systems. Pharmaceutics. 2010;2:224-244.

Turk J Pharm Sci 2019;16(3):340-347
DOI: 10.4274/tjps.galenos.2018.24861

ORIGINAL ARTICLE

Design and *In Vitro* Evaluation of Eudragit-Based Extended Release Diltiazem Microspheres for Once- and Twice-Daily Administration: The Effect of Coating on Drug Release Behavior

Günde Bir ve İki Kez Uygulama için Eudragit Esaslı Uzatılmış Salımlı Diltiazem Mikrokürelerin Tasarımı ve *İn Vitro* Değerlendirilmesi: Kaplamanın Etken Madde Salım Şekline Etkisi

Noushin BOLOURCHIAN*, Maryam BAHJAT

Department of Pharmaceutics and Pharmaceutical Nanotechnology, School of Pharmacy, Shahid Beheshti University of Medical Sciences, Tehran, Iran

ABSTRACT

Objectives: The aim of this investigation was to develop an extended release formulation of diltiazem hydrochloride (DL) for once- and twice-daily administration, based on Eudragit (Eud) RL and RS microspheres using emulsion solvent evaporation.

Materials and Methods: Formulations with different drug–polymer concentrations were produced and characterized in terms of yield, encapsulation efficiency (EE), particle size, and surface morphology. The drug release and thermal behavior of the microspheres were also investigated. Selected microspheres were then coated with Eud RS by continuous solvent evaporation, in order to modify the microspheres' properties and burst release.

Results: According to the results, the EE was in the range of 56%-93% for uncoated microspheres. The mean particle size of microspheres was different from 470 to above 1000 µm, based on various formulation variables. No difference was observed between the mean size of particles prepared with Eud RL and Eud RS. Microspheres showed sustained release behavior, which was affected by the drug:polymer ratio as well as particle size. Coating the microspheres not only improved the EE values (82%-92%) but also reduced the mean dissolution rate as well as the burst release.

Conclusion: Microspheres prepared with DL:Eud RL ratios of 1:3 and 1:4 showed release profiles in accordance with the USP criteria for a DL extended release product for dosing every 12 and 24 h, respectively.

Key words: Coating, diltiazem hydrochloride, Eudragit RL and RS, extended release, microspheres

ÖZ

Amaç: Bu araştırmanın amacı, emülsiyon çözücü buharlaştırma kullanarak hazırlanan Eudragit (Eud) RL ve RS mikro küreleri ile günde bir ve iki kez uygulama için diltiazem hidroklorürün (DL) uzatılmış salım formülasyonunu geliştirmektir.

Gereç ve Yöntemler: Farklı etken madde-polimer konsantrasyonlarına sahip formülasyonlar üretilmiş ve verim, enkapsülasyon etkinliği (EE), partikül büyüklüğü ve yüzey morfolojisi açısından karakterize edilmiştir. Mikrokürelerin etken madde salınımı ve termal davranışı da incelenmiştir. Seçilen mikro küreler daha sonra mikro kürelerin özelliklerini modifiye ve hızlı ilk salınımını değiştirmek için sürekli çözücü buharlaştırma yoluyla Eud RS ile kaplanmıştır.

Bulgular: Sonuçlara göre, kaplanmamış mikroküreler için EE %56 -%93 aralığındadır. Mikrokürelerin ortalama partikül büyüklüğü, çeşitli formülasyon değişkenlerine bağlı olarak 470 ila 1000 um'nin üzerinde olmuştur. Eud RL ve Eud RS ile hazırlanan partiküllerin ortalama ortalama partikül büyüklüğü arasında bir fark gözlenmemiştir. Mikroküreler, etken madde: polimer oranının yanı sıra partikül boyutundan etkilenen sürekli salım davranışı göstermiştir. Mikrokürelerin kaplanması sadece EE değerlerini iyileştirmemiş (%82 -%92), aynı zamanda hızlı ilk çıkış yanı sıra ortalama çözünme oranınıda (MDR) azaltmıştır.

*Correspondence: E-mail: bolourchian@sbmu.ac.ir, Phone: +982188200072 ORCID-ID: orcid.org/0000-0002-8178-1624
Received: 22.04.2018, Accepted: 20.06.2018

Sonuç: 1:3 ve 1:4 oranlarında DL:Eud RL mikroküreler, sırasıyla her 12 ve 24 saatte bir dozlama için DL uzatılmış salım ürünü için USP kriterlerine uygun salım profilleri göstermiştir.

Anahtar kelimeler: Kaplama, diltiazem hidroklorür, Eudragit RL ve RS, uzatılmış salınım, mikroküreler

INTRODUCTION

Diltiazem hydrochloride (DL) is a highly soluble calcium channel blocker drug that is used in the treatment of high blood pressure and angina pectoris.[1] Due to its short elimination half-life of 2-5 h, the conventional oral dosage forms are administered 3-4 times a day, to maintain an effective plasma concentration, which results in low and variable bioavailability.[2] Using a sustained release form of this medication is vital for its efficacy by achieving relative constant blood concentrations and improving the clinical efficacy of the drug, as well as patient compliance.

However, along with the benefits of using extended release single-unit tablets, there are some limitations for these systems, such as the dose adjustment problem and the effect of food on drug release. Moreover, breaking the tablets before taking them could cause different release behavior and serious side effects.[3] The above-mentioned problems could be overcome using microspheres as multiple-unit dosage forms. Microspheres are uniformly distributed in the gastrointestinal tract and result in more uniform drug absorption, limited fluctuation within a therapeutic range, decreased dose frequency, and reduced patient-to-patient variability.[4]

The physical properties and release behavior of microspheres are dependent on different factors such as drug and polymer nature as well as the method of manufacturing. According to the literature, the existence of drug particles on the surface and particles embedded in the surface layers as well as high porosity of microspheres are considered the main reasons for initial burst release. Coating of microspheres is one of the approaches to reduce the burst release and modify the drug release behavior.[5] Preparation and separation of initial microspheres and then using them in a separate coating process would be time and cost consuming. Therefore, application of a continuous preparation and coating process for microspheres seems to be preferable.

To date, modified-release microspheres of DL using different polymers and methods were developed in order to extend its clinical effects.[2,6-11] Only a few studies were performed on the preparation of Eudragit (Eud) RS-based DL microspheres by solvent evaporation.[12-14]

The objective of the present research was to design and evaluate DL-loaded Eud RL and RS matrix-type microspheres as extended release systems for both once- and twice-daily administration, in order to reduce its dosing frequency. With the aim of achieving both systems, different drug–polymer concentrations were applied and examined. In addition, the effect of coating of microspheres by Eud RS on drug release behavior and the burst effect was also evaluated. Emulsion solvent evaporation was used for microsphere preparation as well as continuous coating. This is a simple method that has been used to prepare microspheres of different soluble and insoluble compounds.[15-17]

MATERIALS AND METHODS

Materials

DL powder (Zambon Group SPA, Italy), Eud RL and RS 100 (Röhm Pharma GmbH, Germany), span 60 (Sigma-Aldrich, St. Louis, MO, USA), n-hexane (Carlo Erba, France), and liquid paraffin (Merck, Germany) were used in this study. The materials and excipients used in preparing the microspheres were of pharmacopoeial grade.

Microsphere preparation

DL-loaded Eud RL and RS microspheres were produced by emulsion solvent evaporation.[18] Different amounts of drug and polymer were dissolved in 3 mL of ethanol (dispersed phase), which was then slowly (at the rate of 1 mL/min) added to a beaker containing a mixture of 50 mL of liquid paraffin and 0.1% w/v span 60 (continuous phase) with stirring at 500 rpm using a mechanical stirrer (IKA, Germany). The mixture was stirred until the organic solvent evaporated completely. The prepared microspheres were collected by filtration and washed three times with n-hexane until all the paraffin was removed. Finally, the microspheres were dried at room temperature for 24 h and kept in air-tight containers for further studies.

Coating of microspheres

A one-step continuous solvent evaporation technique was used for the coating process. Primary microspheres were prepared by the above-mentioned method, but before completing the process and collecting the microspheres a 3.3% w/v Eud RS ethanolic solution was added dropwise to the continuous phase and stirred until complete solvent evaporation.[9] The other steps were similar to the previous method.

Characterization of microspheres

The prepared microspheres were characterized in terms of yield value, encapsulation efficiency (EE), morphology, drug release, particle size, and thermal analysis. The yield value of each formulation was calculated by the following equation:[19]

Yield value(%) = (weight of dried microspheres/total solid material amount in the dispersed phase) × 100

Drug content

Ten milligrams of dried microspheres was accurately weighed and transferred to a beaker containing 10 mL of methanol and stirred for 15 min to dissolve the microspheres completely. The solution was analyzed for DL content by a UV spectrophotometer (Shimadzu UV1201, Japan) at 240 nm after dilution. The drug loading and EE were calculated using the following equations:[20]

Drug loading (%) = (weight of drug in microspheres/weight of microspheres) × 100

Drug EE (%) = (actual drug loading/theoretical drug loading) × 100

In vitro drug release

Drug release of all microspheres was carried out using a USP type II dissolution test apparatus (Erweka DT6R, Germany) in 900 mL of phosphate buffer solution (pH 7.2) at 37±0.5°C at 50 rpm (in accordance with the USP test number 5 for DL extended release form dosing every 12 h). Then 3 mL of the medium was withdrawn at predetermined time intervals and replaced with the same amount of fresh dissolution medium after each sampling. The sample solutions were analyzed for drug content at 240 nm by a UV spectrophotometer.

The dissolution test was also performed on selected microspheres in compliance with the USP test number 2 for DL extended release form dosing every 24 h, using an apparatus II at 100 rpm and 900 mL of dissolution medium (distilled water) for 15 h. All experiments were performed in triplicate for each formulation.

All formulations were compared using different dissolution parameters.[21] Mean dissolution time (MDT), which was applied to analyze dissolution profiles, was calculated arithmetically by the following equation:

$$MDT = \frac{\sum_{i=1}^{n} ti\ \Delta Mi}{\sum_{i=1}^{n} \Delta Mi}$$

where ΔM_i is the fraction of drug released in time t_i (calculated by $(t_i+t_{i-1})/2$) and i is the sample number.

In addition, the area under the dissolution curve [dissolution efficiency (DE)] was calculated by the formula below:

$$DE = \frac{\int_o^t y.dt}{y100.t} \times 100$$

where y is the percentage of drug dissolved at time t. Mean dissolution rate (MDR) was also calculated based on the following equation:

$$MDR = \frac{\sum_{i=1}^{n} \Delta Mi/\Delta t}{n}$$

where Δt is the time at the midpoint between t and t_{-1} and n is the number of dissolution sample times.

Particle size

The mean particle size of the DL microspheres was determined by optical microscopy. At least 200 microspheres were analyzed for each preparation and the mean diameter was calculated.

Surface morphology

The appearance and surface morphology of microspheres were evaluated by scanning electron microscopy [scanning electron microscopy (SEM), Philips XL30, the Netherlands]. The microspheres were attached to a specimen holder with double-sided adhesive tape and coated under vacuum by gold sputter coater (Bal-Tec SCD 005, Switzerland) prior to observation.

Differential scanning calorimetry

Differential scanning calorimetry (DSC) analysis of the drug, polymer, selected DL-loaded microspheres, and related physical mixture was conducted. After calibrating the apparatus (Shimadzu DSC-60, Japan) by indium standard, accurately weighed samples (5 mg) were placed in sealed aluminum pans. The containers were placed in the DSC apparatus and heated at a constant rate of 10/min over a temperature range of 25 to 300°C. An empty standard aluminum pan was used as reference.

Statistical analysis

Statistical analysis of the different variables was carried out using ANOVA followed by Tukey's *post hoc* test. Significance was tested at the 0.05 level of probability.

RESULTS AND DISCUSSION

DL microspheres were successfully prepared by emulsion solvent evaporation using ethanol as the drug–polymer solvent (dispersed phase) and a liquid paraffin–span 60 mixture as the continuous phase. The yield value was in the range of 62.8%-92.4% for the initial microspheres and 81.3%-97.6% for the Eud RS-coated microparticles.

Characterization of microspheres

Encapsulation efficiency and particle size

Table 1 shows the composition and properties of the Eud RL- and RS-based microspheres prepared with different drug:polymer ratios. Increasing the amount of Eud RL from 300 to 800 mg led to a 25% enhancement in the EE values. In fact, the size of emulsion droplets was increased due to the higher viscosity of the polymeric solution, which in turn decreased the surface area and also drug molecule transport from dispersed to continuous phases.[22] The particle size of those microspheres was also increased significantly ($p<0.001$), which was expected. Similar results were obtained for the microspheres prepared with higher DL concentrations. Based on the results (Table 1), there is a significant difference between the EE values of M8L and M4L ($p<0.05$). In addition, using higher drug:polymer ratios resulted in significantly ($p<0.001$) increased particle size. Although the effect of polymer concentration on particle size seemed to be more than that of the drug, the results revealed that in certain drug concentrations its effect on particle size cannot be neglected.

The application of various drug:polymer concentrations with the same ratio (M1L, M2L, and M7L) resulted in microspheres with different EEs and mean particle sizes. An increase of 20% was found for the EE value of M7L (higher DL-Eud RL concentration) compared to M1L and M2L. In other words, an appropriate simultaneous increase in drug and polymer concentrations led to more drug entrapment in the microspheres. The same trend was also observed for microparticles size, which could be attributed to the higher viscosity and emulsion droplet size of this formulation. However, the difference observed between M2L and M1L was far smaller.

By changing the polymer type from Eud RL to Eud RS (Table 1), no difference was observed in EE % for lower drug:polymer concentrations (M1L and M1S). However, the opposite was found for the formulations prepared with higher drug:polymer concentrations, in which M2S showed an improved EE value compared to M2L, which is in accordance with some reports in the literature.[23,24] Eud RL is more permeable and the diffusion of drug molecules from the droplets to the surrounding medium during the preparation process is more probable than with Eud RS. In addition, the repulsion between the quaternary ammonium groups of Eud RL and the cationic drug could facilitate DL removal to the external phase and reduce the EE.

According to the results, coating of microspheres improved the EE % significantly ($p<0.001$) compared to the uncoated microspheres (Table 2). It is probable that application of the Eud RS coating on the surface of the initial microspheres prevents the drug molecules' transport to the emulsion external phase during the preparation process. Meanwhile, no difference was observed in the EE values of the coated microspheres with different inner polymers. As was expected, the mean particle size of the microparticles was increased following the coating process. The higher mean particle size of M2LS and M2SS compared to M1LS and M1SS was related to the higher inner polymer concentration used to prepare the initial microspheres.

SEM

The SEM micrographs (Figure 1) show that the microspheres prepared in the presence of a lower polymer concentration (M2L) were more spherical with wrinkled surfaces compared to M5L (higher polymer amount). Using a higher DL concentration in the formulations, did not affect the microspheres' shape, but increased their roughness mainly due to the existence of drug crystals on the surface layers of the microspheres. No difference was observed between the microspheres prepared with Eud RL and RS (M1L and M1S) in terms of shape or surface properties, which was in accordance with previous research.[24]

Based on the results, following the coating of microspheres, they were still spherical with more uniform surfaces compared to the initial uncoated microparticles. The study of the surface morphology of M1LS and M1SS (Figure 1) confirmed the absence of drug crystals on the surface of the microparticles and suitable coverage of the initial microspheres during the continuous coating process.

Drug release studies

The release profiles of DL from microspheres prepared with different formulations are presented in Figure 2. Based on the results, the drug release rate decreased apparently with increasing polymer concentration (Figure 2a). The DL released after 3 h of the experiment for M2L and M5L was 73.28% and 26.09%, respectively. This trend was also observed in MDR and DE values (Table 1). Furthermore, decreasing the drug release rate led to an increase in MDT values. In fact, a higher polymer concentration resulted in larger particle size with less surface

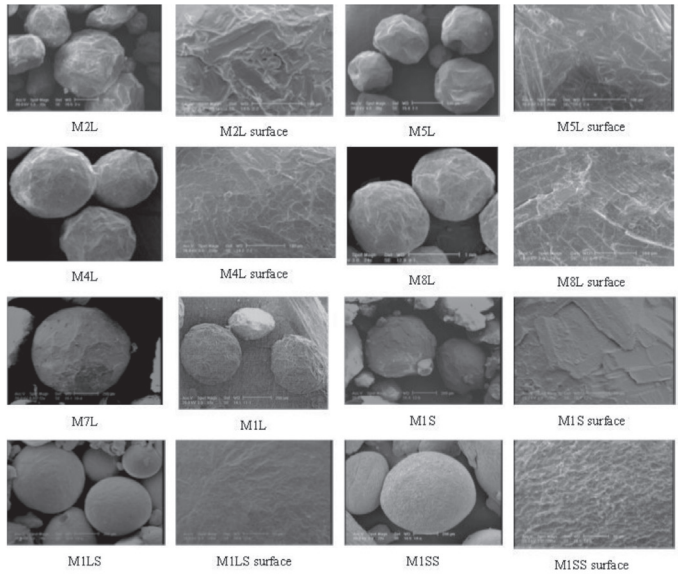

Figure 1. Scanning electron microscopy micrographs of different microspheres and their surfaces

Table 1. Composition and physicochemical properties of diltiazem hydrochloride microspheres (mean ± standard deviation, n=3)

Formulation	Drug (mg)	Polymer (mg)	EE[c] (%)	Mean particle size (μm)	MDT[d] (min)	DE[e] (%)	MDR[f] (%min^{-1})
M1L[a]	100	150	61.43±1.33	452.9±7.29	82.45±4.17	83.78±0.98	0.331±0.005
M2L	200	300	62.15±1.09	513.8±10.09	94.38±4.05	75.29±0.58	0.210±0.004
M3L	200	500	56.62±3.75	620.0±5.82	150.70±6.77	74.96±0.54	0.174±0.007
M4L	200	600	81.46±2.60	665.7±6.71	197.11±5.62	61.43±1.11	0.086±0.004
M5L	200	800	87.70±3.57	720.1±12.58	210.27±2.34	54.00±1.19	0.068±0.006
M6L	300	600	82.18±0.84	745.9±5.58	235.95±7.86	58.29±1.09	0.064±0.002
M7L	400	600	84.97±3.53	813.2±2.33	201.50±4.26	66.98±0.43	0.147±0.005
M8L	500	600	92.86±3.90	1027.3±6.50	114.94±6.45	80.78±1.91	0.246±0.007
M1S[b]	100	150	59.53±1.19	463.5±4.05	116.74±5.05	65.00±1.93	0.211±0.005
M2S	200	300	77.09±1.05	528.6±3.35	122.57±1.71	63.95±0.36	0.224±0.011

[a]L: Eudragit RL, [b]S: Eudragit RS, [c]EE: Encapsulation efficiency, [d]MDT: Mean dissolution time, [e]DE: Dissolution efficiency, [f]MDR: Mean dissolution rate

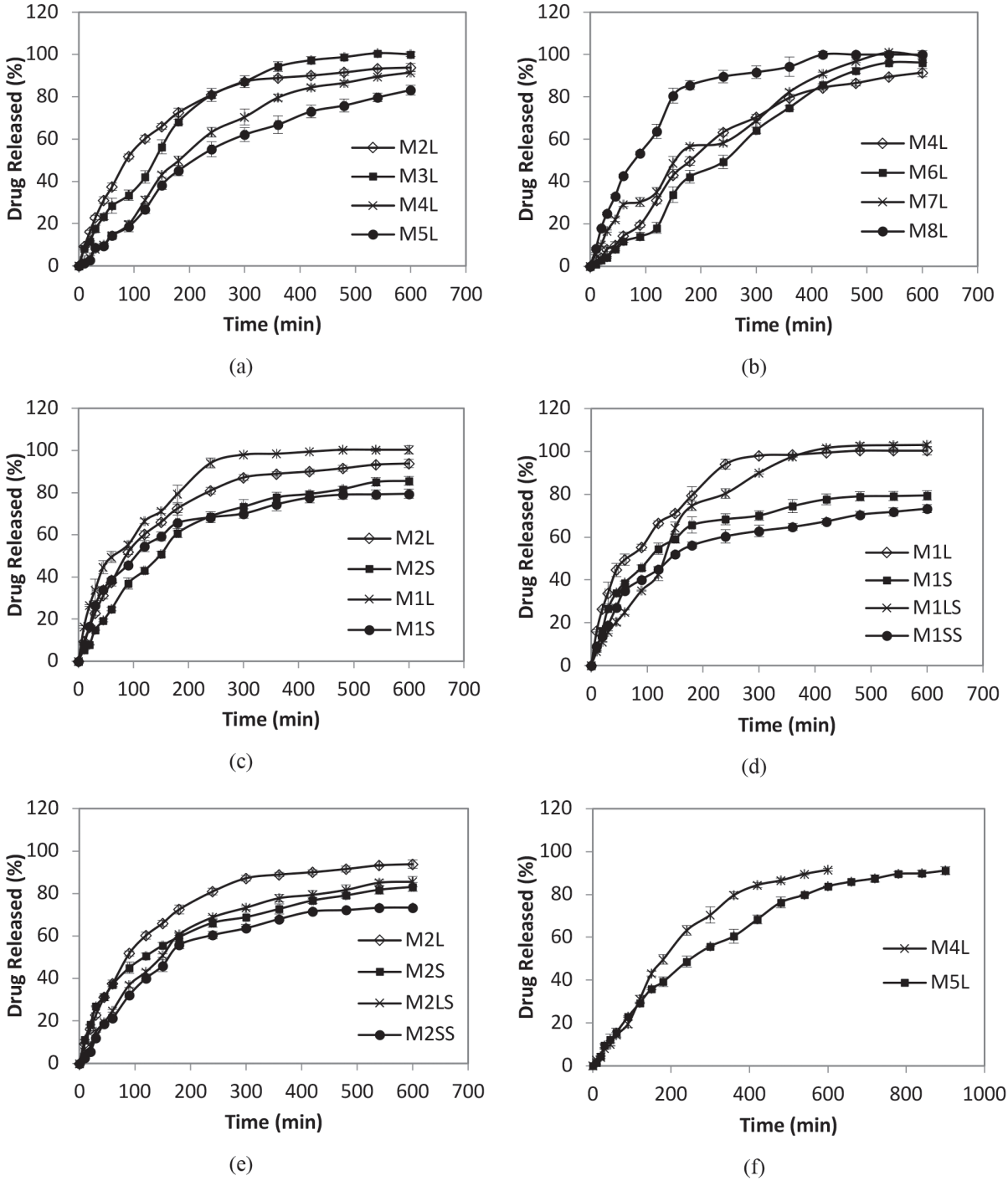

Figure 2. Release profiles of DL from (a-c) microspheres with different formulation variables in phosphate buffer (pH 7.2), (d, e) coated versus uncoated microspheres, (f) M4L in phosphate buffer (pH 7.2) and M5L in water (n=3)

area and therefore a lower release rate. A burst release of about 37% was observed for M2L during the first hour of the study, which could be attributed to the lower polymer content and particle size, as well as more drug particles on the surface layers of the microspheres.

Using higher drug concentrations with a fixed amount of polymer enhanced the drug release apparently (Figure 2b) and about 90% of DL was dissolved over 5 h from M8L (DE=80.78±1.91%). Table 1 shows that MDR was significantly increased in the formulations prepared with higher drug concentrations ($p<0.0001$). In addition, the burst release of these microspheres was in the range of 11.88%-42.70%. It seems that the presence of more drug particles on the surface layers of the microspheres prepared with higher drug levels enhanced the drug release rate in spite of the larger particle size.[15] In fact, reduction of the drug diffusion pathway is possible in microspheres with higher drug loading.[25] Moreover, removal

of drug particles from microspheres leads to the formation of a more porous structure, which plays an important role in accelerating drug release.[26]

Using various drug:polymer concentrations with the same ratio also led to microspheres with different release behavior. Based on Table 1, M7L prepared with a higher drug:polymer concentration extended the drug release more than M2L and M1L ($p<0.001$), mainly due to its larger particle size. The significant decrease in the MDR value for M7L ($p<0.001$) corresponds to an increase of more than 110 min in MDT of this formulation in comparison to M1L. All those three microspheres showed a burst release in the range of 30%-50%.

Figure 2c shows the release profiles of DL from microspheres prepared with Eud RL and RS. It is obvious that the drug release from the Eud RS-based microspheres was slower than that of the particles made with Eud RL. The difference observed between M1L and M1S was more evident. Based on Table 1, a reduction of more than 18% in DE and about 1.5-fold in MDR was observed for M1S compared to M1L. The MDT values for M1S and M2S were also significantly greater than for M1L and M2L ($p<0.001$). Since the mean particle size was not affected very much by the polymer type, the results obtained could be attributed to the lower permeability of Eud RS.

The effect of coating microspheres on the DL release profile is illustrated in Figures 2d and 2e. The drug release from all coated particles decreased clearly compared to the uncoated microspheres. Based on Table 2, a significant reduction in MDR and DE values was observed for coated particles. The lowest MDR was for the formulation M2SS, which was about half that of M2S. The lowest DE % was also obtained for M2SS. A decreasing release rate was observed with increasing MDTs. A significant difference was observed between the MDTs of M1L and M1LS and also M2L and M2LS ($p<0.01$). Following the coating process, MDT of the microspheres with Eud RL as inner polymer was enhanced more than that of Eud RS. Furthermore, although the burst release declined for all coated microspheres, this was more noticeable for the microspheres with Eud RL as core polymer.

The results revealed that although coating of microspheres was helpful in decreasing the drug release rate, it was not as effective as using an appropriate drug:polymer concentration in the preparation process, without any coating. Formulations M5L and M6L showed the lowest MDRs and the highest MDT values among all coated and uncoated microspheres. It seems that the drug particles in the mass of microspheres were much more than the particles in the surface layers and controlling their diffusion was more important in achieving the desirable extended release behavior. However, application of a higher polymer concentration in the coating process could cause different effects.

DL microspheres for once- and twice-daily administrations

Figure 2f shows the release profiles of two selected formulations (M4L and M5L) in phosphate buffer solution (pH 7.2) (USP test number 5) and water (USP test number 2), respectively. The results indicated that the microspheres prepared with DL: Eud RL ratios of 1:3 (M4L) and 1:4 (M5L) were in accordance with the USP test for DL extended release form dosing every 12 and 24 h, respectively, without any further treatment.

The release kinetics of these formulations was investigated using three different models, i.e. zero order, first order, and the Higuchi equation. Based on the squared correlation coefficient (R^2), the release profile of M4L was best fitted with zero order (R^2=0.989) compared with first order and the Higuchi model (R^2=0.973 and 0.944, respectively). Although the R^2 values calculated for M5L based on first order (0.991) and the Higuchi equation (0.994) were higher than that of zero order (0.954), there is no evidence to specify the dominant kinetics model for this formulation.

DSC

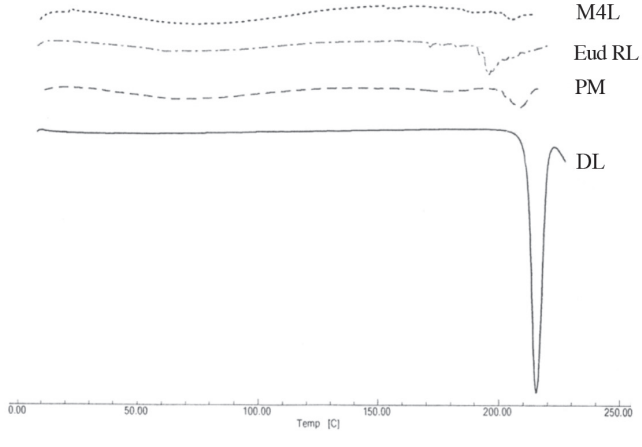

Figure 3. Differential scanning calorimetry thermograms of DL, Eudragit RL, M4L, and related physical mixture

PM: Physical mixture

Table 2. Composition and physicochemical properties of diltiazem hydrochloride microspheres coated with Eud RS (mean ± standard deviation, n=3)

Formulation	Core drug (mg)	Core polymer (mg)	Type of core polymer	EE[a] (%)	Mean particle size (μm)	MDT[b] (min)	DE[c] (%)	MDR[d] (%min^{-1})
M1LS	100	150	Eudragit RL	91.99±0.82	510.4±5.85	118.04±3.27	77.42±0.69	0.195±0.004
M1SS	100	150	Eudragit RS	88.32±1.31	500.2±3.05	131.16±5.71	57.25±1.48	0.184±0.007
M2LS	200	300	Eudragit RL	82.08±2.05	641.1±7.81	125.18±5.32	63.92±1.53	0.146±0.004
M2SS	200	300	Eudragit RS	83.84±1.92	610.5±3.52	138.87±2.30	56.33±0.20	0.106±0.002

[a]EE: Encapsulation efficiency, [b]MDT: Mean dissolution time, [c]DE: Dissolution efficiency, [d]MDR: Mean dissolution rate

The DSC thermograms of DL, Eud RL, selected microsphere (M4L), and related physical mixture (PM) are depicted in Figure 3. A characteristic endotherm appeared for the drug at the onset temperature of 210.08°C, which could be attributed to the melting of DL.[27] A broad peak in the range of 50-60°C was observed in the thermogram of Eud RL, which is related to its glass transition temperature.[28] The DSC curve obtained for the microspheres presented the same thermal profile as that of the physical mixture, both containing a drug melting peak with a slight shift toward lower temperatures. These minor changes in the drug endotherm could be attributed to the presence of polymer, which lowers the drug purity.[29] This result suggests no interaction between the drug and the polymer during the preparation process.

CONCLUSIONS

DL:Eud RL extended release microspheres for once- and twice-daily administration for the treatment of hypertension and angina pectoris were successfully produced in this study by a simple method of solvent evaporation using suitable formulation variables. The results confirmed that a one-step continuous emulsion solvent evaporation process was a practical technique to prepare coated microspheres with improved physical properties (especially EE %) and reduced burst release. Using suitable drug:polymer ratios and external coating polymer concentration could modify the particle size, surface morphology, porosity, and the amount of drug particles on the surface layers, which are essential to obtain desirable results.

Conflict of Interest: No conflict of interest was declared by the authors.

REFERENCES

1. Frishman WH, Charlap S, Kimmel B, Goldberger J, Phillippides G, Klein N. Calcium-channel blockers for combined angina pectoris and systemic hypertension. Am J Cardiol. 1986;57:22-29.
2. Sultana Y, Mall S, Maurya D, Kumar D, Das M. Preparation and *in vitro* characterization of diltiazem hydrochloride loaded alginate microspheres. Pharm Dev Technol. 2009;14:321-331.
3. Sun C, Liu H, Zhao X, He H, Pan W. In vitro and *in vivo* evaluation of a novel diltiazem hydrochloride polydispersity sustained-release system. Drug Dev Ind Pharm. 2013;39:62-66.
4. Mundargi RC, Shelke NB, Rokhade AP, Patil SA, Aminabhavi TM. Formulation and in-vitro evaluation of novel starch-based tableted microspheres for controlled release of ampicillin. Carbohydrate Polymers. 2008;71:42-53.
5. Yeo Y, Park K. Control of encapsulation efficiency and initial burst in polymeric microparticle systems. Arch Pharm Res. 2004;27:1-12.
6. Das MK, Maurya DP. Evaluation of diltiazem hydrochloride-loaded mucoadhesive microspheres prepared by emulsification-internal gelation technique. Acta Pol Pharm. 2008;65:249-259.
7. Morkhade DM. Evaluation of gum mastic (*Pistacia lentiscus*) as a microencapsulating and matrix forming material for sustained drug release. Asian Journal of Pharmaceutical Sciences. 2017;12:424-432.
8. Kristmundsdottir T, Gudmundsson OS, Ingvarsdottir K. Release of diltiazem from Eudragit microparticles prepared by spray-drying. Int J Pharm. 1996;137:159-165.
9. Das SK, Das NG. Preparation and *in vitro* dissolution profile of dual polymer (Eudragit® RS100 and RL100) microparticles of diltiazem hydrochloride. J Microencapsul. 1998;15:445-452.
10. Sengel CT, Hascicek C, Gönül N. Development and *in-vitro* evaluation of modified release tablets including ethylcellulose microspheres loaded with diltiazem hydrochloride. J Microencapsul. 2006;23:135-152.
11. Shailesh T, Vipul P, Girishbhai J, Manish C. Preparation and *in vitro* evaluation of ethylcellulose coated egg albumin microspheres of diltiazem hydrochloride. J Young Pharm. 2010;2:27-34.
12. Nappinnai M, Kishore V. Formulation and evaluation of microspheres of diltiazem hydrochloride. Indian Journal of Pharmaceutical Sciences. 2007;69:511-514.
13. Sengel-Türk CT, Hascicek C, Gönül N. Microsphere-based once-daily modified release matrix tablets for oral administration in angina pectoris. J Microencapsul. 2008;25:257-266.
14. Cetin EO, Gundogdu E, Kirilmaz L. Novel microparticle drug delivery systems based on chitosan and Eudragit® RSPM to enhance diltiazem hydrochloride release property. Pharm Dev Technol. 2012;17:741-746.
15. Bolourtchian N, Karimi K, Aboofazeli R. Preparation and characterization of ibuprofen microspheres. J Microencapsul. 2005;22:529-538.
16. Lee JH, Park TG, Choi H. Effect of formulation and processing variables on the characteristics of microspheres for water-soluble drugs prepared by w/o/o double emulsion solvent diffusion method. Int Pharm. 2000;196:75-83.
17. Masaeli R, Kashi TSJ, Dinarvand R, Tahriri M, Rakhshan V, Esfandyari-Manesh M. Preparation, characterization and evaluation of drug release properties of simvastatin-loaded PLGA microspheres. Iran J Pharm Res 2016;15:205-211.
18. Singh V, Chaudhary AK. Preparation of Eudragit E100 microspheres by modified solvent evaporation method. Acta Pol Pharm. 2011;68:975-980.
19. Kılıçarslan M, Baykara T. The effect of the drug/polymer ratio on the properties of the verapamil HCl loaded microspheres. Int J Pharm. 2003;252:99-109.
20. Farhangi M, Dadashzadeh S, Bolourchian N. Biodegradable Gelatin Microspheres as Controlled Release Intraarticular Delivery System: The Effect of Formulation Variables. Indi J Pharm Scie. 2017;79:105-112.
21. Asare-Addo K, Šupuk E, Al-Hamidi H, Owusu-Ware S, Nokhodchi A, Conway BR. Triboelectrification and dissolution property enhancements of solid dispersions. Int J Pharm. 2015;485:306-316.
22. Yang C-Y, Tsay S-Y, Tsiang R-C. Encapsulating aspirin into a surfactant-free ethyl cellulose microsphere using non-toxic solvents by emulsion solvent-evaporation technique. J Microencapsul. 2001;18:223-236.
23. Kiliçarslan M, Baykara T. Effects of the permeability characteristics of different polymethacrylates on the pharmaceutical characteristics of verapamil hyhdrochloride-loaded microspheres. J Microencapsul. 2004;21:175-189.
24. Kim BK, Hwang SJ, Park JB, Park HJ. Preparation and characterization of drug-loaded polymethacrylate microspheres by an emulsion solvent evaporation method. J Microencapsul. 2002;19:811-822.
25. Chiao C, Price J. Formulation, preparation and dissolution characteristics of propranolol hydrochloride microspheres. J Microencapsul. 1994;11:153-159.

26. Cirpanli Y, Ünlü N, Çalış S, Atilla Hincal A. Formulation and *in-vitro* characterization of retinoic acid loaded poly (lactic-co-glycolic acid) microspheres. J microencapsul. 2005;22:877-889.

27. Al-Zoubi N, Al-obaidi G, Tashtoush B, Malamataris S. Sustained release of diltiazem HCl tableted after co-spray drying and physical mixing with PVAc and PVP. Drug Dev Ind Pharm. 2016;42:270-279.

28. Soltani S, Zakeri-Milani P, Barzegar-Jalali M, Jelvehgari M. Design of eudragit RL nanoparticles by nanoemulsion method as carriers for ophthalmic drug delivery of ketotifen fumarate. Iran J Basic Med Sci. 2016;19:550-560.

29. Moyano M, Broussalis A, Segall A. Thermal analysis of lipoic acid and evaluation of the compatibility with excipientes. Journal of Thermal Analysis and Calorimetry. 2009;99:631-637.

Turk J Pharm Sci 2019;16(3):348-355
DOI: 10.4274/tjps.galenos.2018.75046

ORIGINAL ARTICLE

Formulation Design of Hydrocortisone Films for the Treatment of Aphthous Ulcers

Aftöz Ülser Tedavisi için Hidrokortizon Filmlerin Formülasyon Tasarımı

Mohammed Gulzar AHMED*, Sanjana ADINARAYANA

Yenepoya Pharmacy College and Research Centre, Department of Pharmaceutics, Mangalore, India

ABSTRACT

Objectives: Research and development in oral drug delivery has evolved to the changeover of solid dosage forms from tablets to oral films. These films offer an elegant route for systemic drug delivery, with an advantage for patients who are suffering from difficulty in swallowing larger oral dosage forms. Aphthous ulcers are the most common oral lesions and are round or oval, with a grayish yellow, crateriform base. For the treatment of aphthous ulcers various marketed product are available, such as vitamin B12 tablets, benzydamine hydrochloride mouthwash or spray, steroid lozenges, and local anesthetics. Hence hydrocortisone is selected as the drug of choice for the treatment of aphthous ulcers, exhibiting anti-inflammatory and immunosuppressant properties that inhibit the clinical manifestations. The main aim of the present study was to develop a hydrocortisone film in order to improve the therapeutic efficacy and bioavailability of hydrocortisone for the treatment of aphthous ulcers.

Materials and Methods: The hydrocortisone film was developed containing various concentrations of methylcellulose and propylene glycol (1.0-2.0% w/v) by solvent casting. The prepared films were evaluated for various characterization studies like film forming capacity, visual appearance, thickness, weight variation, folding endurance, surface pH, drug content, disintegration time, tensile strength, *in vitro* release study, *ex vivo* study, and stability studies.

Results: A total of five formulations were developed, out of which formulation F2 (1.25% w/v) is considered the optimized formulation as it showed the best results with respect to all characterization studies. A disintegration time of 44 s and maximum *in vitro* drug release, i.e. 97.55%, were observed. Further, no significant changes were observed during stability studies for the optimized formulation.

Conclusion: Hydrocortisone oral films can be formulated as a potentially useful tool for effective treatment of aphthous ulcers with improved bioavailability, rapid onset of action, and increased patient compliance.

Key words: Aphthous ulcers, hydrocortisone, oral films, solvent casting method, tensile strength, *ex vivo* study

ÖZ

Amaç: Oral ilaç salımında araştırma ve geliştirme, katı dozaj formlarının tabletlerden oral filmlere geçişine doğru gelişmiştir. Bu filmler, daha büyük oral dozaj formlarını yutmakta zorluk çeken hastalar için sistemik ilaç salımında avantaj sağlayan, çok iyi bir yol sunar. Aftöz ülserleri en sık görülen yuvarlak veya oval, krater formunda bir tabanı olan grimsi sarı oral lezyonlardır. Aftöz ülserlerin tedavisi için B12 vitamini tabletleri, benzidamin hidroklorür gargarası veya spreyi, steroid pastiller ve lokal anestezikler gibi çeşitli ticari ürünler mevcuttur. Bu nedenle hidrokortizon, klinik belirtileri engelleyen anti-enflamatuvar ve immünsüpresif özellikler sergileyen aftöz ülserlerin tedavisi için tercih edilen etken madde olarak seçilmiştir. Bu çalışmanın temel amacı, aftöz ülserlerin tedavisinde hidrokortizonun terapötik etkinliğini ve biyoyararlanımını artırmak için hidrokortizon filmi geliştirmektir.

Gereç ve Yöntemler: Çözücü dökümüyle çeşitli konsantrasyonlarda metilselüloz ve propilen glikol (1.0-2.0% w/v) içeren hidrokortizon filmi geliştirilmiştir. Hazırlanan filmler, film oluşturma kapasitesi, görsel görünüm, kalınlık, ağırlık değişimi, katlanma dayanıklılığı, yüzey pH'ı, etken madde içeriği, dağılma süresi, gerilme direnci, *in vitro* salım çalışması, *ex vivo* çalışma ve stabilite çalışmaları gibi çeşitli karakterizasyon çalışmaları için değerlendirilmiştir.

Sonuçlar: Toplam beş formülasyon geliştirilmiştir; bunlardan F2 formülasyonu (%1.25 a/h), tüm karakterizasyon çalışmalarına göre en iyi sonuçları gösterdiği için optimize edilmiş formülasyon olarak kabul edilmiştir. 44 s'lik bir dağılma süresi ve maksimum *in vitro* etken madde salımı, yani %97.55, gözlenmiştir. Ayrıca, optimize edilmiş formülasyon için stabilite çalışmaları sırasında önemli bir değişiklik gözlenmemiştir.

Bulgular: Hidrokortizon oral filmler, gelişmiş biyoyararlanım, hızlı etki başlangıcı ve artan hasta uyumu ile aftöz ülserlerin etkili tedavisi için potansiyel olarak faydalı bir araç olarak formüle edilebilmiştir

Anahtar kelimeler: Aftöz ülserler, hidrokortizon, oral filmler, çözücü döküm yöntemi, çekme dayanımı, *ex vivo* çalışma

*Correspondence: **E-mail:** mohammedgulzar1@gmail.com, **Phone:** +09448401238 **ORCID-ID:** orcid.org/0000-0002-9226-9984
Received: 08.03.2018, **Accepted:** 21.06.2018

INTRODUCTION

Over the past few decades there has been a tremendous change in the design of various drug delivery systems to achieve rapid onset of action. Travelling through the various milestones from discovering a conventional tablet, capsules, and modified release tablets and capsules, oral disintegrating tablets/wafers to achieve oral drug administration were quite popular. Now another potential milestone in the novel era of formulating films,[1] mouth dissolving films are novel dosage forms that disintegrate or dissolve in the oral cavity. These are ultrathin postage stamp size formulations with an active agent or pharmaceutical excipients. These dosage forms are placed on the tongue or any mucosal tissue. When wet with saliva, the films rapidly hydrate and adhere to the site of application. They rapidly dissolve or disintegrate to release the drug for mucosal absorption or with modification allow for oral gastrointestinal tract absorption with quick dissolving properties. An important benefit of these dosage forms is accurate dosing as compared to liquid dosage form.[2] Films are the most advanced form of oral solid dosage forms since they improve the efficacy of APIs by dissolving within a minute in the oral cavity after contact with less saliva as compared to fast dissolving tablets, without chewing and with no need for water for administration.[1] They give quick absorption and instant bioavailability of drugs due to high blood flow and permeability of the oral mucosa, which is 4-1000 times greater than that of the skin.[3]

Aphthous ulcers belong to the group of chronic inflammatory diseases of the oral mucosa. The most characteristic symptom of the disease is the recurrent onset of single or multiple painful erosions and ulcers that appear mainly on unattached oral mucosa of the lips, cheeks, and tongue. Occasionally the lesions may also be observed on strongly keratinized palatal and gingival mucosa. The eruptions are surrounded by a characteristic erythematous halo and covered with a fibrous coating.

Aphthous ulcers are classified as minor, major, and herpetiform. Minor aphthous ulcers involve the presence of one to five ulcers at a time, with each ulcer less than 1 cm in diameter. In major aphthous ulcers there are 1-10 ulcers at a time, the ulcers exceed 1 cm in diameter, and they persist for up to 6 weeks. In herpetiform recurrent aphthous ulcers there are 10-100 ulcers at a time, their size is usually 1-3 cm, and they form clusters that coalesce into widespread areas of ulceration lasting 7-10 days. These ulcers are only herpes-like in appearance.[4]

Corticosteroids are a class of drugs that includes steroid hormones. Topical corticosteroid when used for aphthous ulcers is intended to limit the inflammatory process associated with the formation of aphthae. Corticosteroids may act directly on T lymphocytes or alter the response of effector cells to precipitants of immunopathogenesis. Hydrocortisone is a corticosteroid with both glucocorticoid and to a lesser extent mineralocorticoid activity. It exhibits anti-inflammatory and immunosuppressant properties inhibiting the clinical manifestations.[5] It is chemically designated as pregn-4-ene-3,20-dione,21 (acetyloxy)-11,17-dihydroxy-, (11β)-. It is a white to partially white, odorless, crystalline powder that is well absorbed after oral administration, achieving peak blood concentrations after 1 h. Plasma protein binding is greater than 90%, primarily bound to plasma globulin as globulins have a high affinity for hydrocortisone but low binding capacity. These pharmacokinetic parameters make hydrocortisone a suitable candidate for film formulation.[6]

Thus, the main objective of the present investigation was to formulate oral films containing hydrocortisone by solvent casting, which is simple and cost effective to minimize the first pass effect, increase the oral bioavailability, and provide rapid onset of action, thereby increasing patient compliance.

Although the research concerning local drug delivery for the treatment of aphthous ulcer has attracted much attention, there is greater potential in the treatment offered by local drug delivery, and research has proved this to be an alternative method of current conventional treatment.

MATERIALS AND METHODS

Materials

Hydrocortisone was procured from Yarrow Chem. Products, Mumbai. Methyl cellulose and sodium citrate were procured from SD Fine Chemicals, Mumbai. All other ingredients used were of analytical grade.

Formulation method of mouth dissolving films

Different composition formulas were optimized as a primary film former for the formulation (Table 1). Aqueous solution of methylcellulose was prepared by dissolving it in 50 mL of hot water with continuous stirring to form a homogeneous solution and then the solution was kept for swelling of the polymer. Propylene glycol and sodium citrate were dissolved in 10 mL of distilled water and the drug was also separately dissolved

Table 1. Formulation design of oral film

Formulation code	Hydrocortisone (%w/v)	Methylcellulose (%w/v)	Sodium citrate (%w/v)	Propylene glycol	Distilled water
F1	1	1.00	0.25	1.00	Q.S
F2	1	1.25	0.25	1.25	Q.S
F3	1	1.50	0.25	1.50	Q.S
F4	1	1.75	0.25	1.75	Q.S
F5	1	2.00	0.25	2.00	Q.S

in distilled water to form a solution. Both of these solutions were mixed in a polymer solution with continuous stirring and kept for 2 h for removal of the air bubbles. Then the prepared solutions were cast onto moulds and kept in air for drying and then in a hot air oven for 24 h at 40°C. Finally, the films were removed from the mould and cut to 0.5 cm×0.5 cm size.[7]

Evaluation parameters for films

Fourier transform infrared studies

The compatibility of the drug in the formulation was confirmed by IR spectra of pure drug alone and the formulations were determined using a Shimadzu fourier transform infrared (FTIR)-8400S spectrophotometer by the KBr disc method.[7]

Scanning electron microscopy

The morphology and surface topography of the film were examined by scanning electron microscopy (SEM). The samples to be examined were mounted on a SEM sample stub using double-sided adhesive tape. The samples mounted were coated with gold (200 Å) under reduced pressure (0.001 torr) for 5 min to improve the conductivity using an ion sputtering device.[8]

Differential scanning calorimetry

Thermal properties of the pure drug and the formulation were evaluated by differential scanning calorimetry (DSC). It is used to determine drug excipient compatibility studies and also used to observe more phase changes, such as glass transitions, crystallization, and amorphous forms of drugs and polymers. The analysis was performed at 5 to 200°C under nitrogen flow.[8]

Thickness

Film thickness was evaluated using a screw gauge with a range of 0-10 mm and revolution 0.001 mm. The anvil of the thickness gauge was turned and the film was inserted after making sure that the pointer was set to zero. The film was held on the anvil and the reading on the dial was noted down. The estimations were carried out in triplicate.[9]

Variation in mass

The mass of 0.5 cm^2 film from different batches of the formulations was noted on an electronic balance. The estimations were carried out in triplicate.[9]

Folding endurance

Folding endurance was determined by repeated folding of the film at the same place until the film broke. This gives an indication of the brittleness of the film. The number of times the film was folded without breaking was computed as the folding endurance value. The estimations were carried out in triplicate.[8]

Surface pH

The surface pH of the film is determined in order to investigate the possibility of any irritation *in vivo*. As an acidic or alkaline pH may cause irritation to the oral mucosa, it is necessary to keep the surface pH as close to neutral as possible. A combined pH electrode was used for this purpose. The film was slightly wet with the help of water and the pH was measured by bringing the electrode in contact with the surface of the oral film. This study was performed in triplicate and mean ± standard deviation calculated.[10]

Drug content

Film of 0.5 cm^2 size was put in a 10 mL volumetric flask and dissolved in 5 mL of methanol and then the final volume was made up with methanol. Samples were suitably diluted with artificial saliva and the absorbance was measured at 242 nm. The estimations were carried out in triplicate.[10]

In vitro disintegration studies

Disintegration time gives an indication about the disintegration characteristics and dissolution characteristics of the film. In the case of films the disintegration and dissolution procedures are hardly distinguishable. If the film disintegrates it concurrently dissolves in a small amount of saliva, which makes it difficult to mimic these natural conditions and measures with an adequate method. However, in the present investigation two methods of disintegration were adopted.[8]

Drop method: In the first method one drop of distilled water was dropped by a pipette onto the oral films. The films were placed on a glass slide and then the glass slide was placed planar on a petri dish. The time until the film dissolved and caused a hole in the film was measured. The estimations were carried out in triplicate.

Petri dish method: In this method 2 mL of distilled water was placed in a petri dish and one film was added to the surface of the water and the time required until the oral film dissolved completely was measured. Drug-loaded films were investigated under both methods. The estimations were carried out in triplicate.

Tensile strength

Tensile strength is the maximum stress applied to a point at which the film specimen breaks. It is calculated by the load at rupture divided by the cross-sectional area of the film as given below:

$$\text{Tensile strength} = \frac{\text{Force at break (N)}}{\text{Initial cross-sectional area of the sample } (mm^2)}$$

It was measured using a Shimadzu AG-100kNG (Winsoft tensile and compression testing). Film of size 5×5 cm^2 and free of physical imperfections was placed between two clamps held 10 mm apart. The film was pulled by a clamp at a rate of 5 mm/min. The whole experiment was carried out in triplicate.[9]

In vitro dissolution studies

The *in vitro* dissolution studies were conducted using 500 mL of artificial saliva as dissolution medium with a modified type I dissolution apparatus. A temperature of 37°C and speed of 50 rpm were used. Each film with dimensions of appropriate size equivalent to 5 mg of hydrocortisone was placed on a watch glass covered with nylon wire mesh. The watch glass was then dropped into a dissolution flask (Figure 1). Then 5-mL samples were withdrawn after 1, 2, 3, 4, 5, 6, 7, and 8 h and every time replaced with 5 mL of fresh dissolution medium. The samples were analyzed by measuring absorbance at 242 nm. The dissolution experiments were conducted in triplicate.[7]

Ex vivo diffusion studies

An *ex vivo* release study was conducted using fresh chicken skin. The skin was soaked in sodium bromide solution for 5-6 h and washed with water to remove the adhering fat tissue. Then the skin was mounted in a diffusion cell containing phosphate buffer of pH 6.8. The temperature of the medium was thermostatically controlled at 37±1.0°C and 5 mL of the sample was withdrawn at predetermined intervals and spectrophotometrically estimated at 242 nm against the respective blank formulation.[10]

Drug release kinetics

Investigation of the drug release from the films was done by studying the release data with zero order and first order kinetics and the Higuchi equation. The release mechanism was understood by fitting the data to the Korsmeyer–Peppas model.[9]

Stability study

The stability study for the oral films was carried out for all the batches for a short-term period of 3 months. After predetermined time intervals, the films were evaluated for drug content, pH, thickness, disintegration study, and physical appearance.[10]

RESULTS AND DISCUSSION

FTIR studies

The infrared spectra of the pure drug hydrocortisone and combinations of the drug with polymers (methylcellulose) were obtained and are shown in figures. All the characteristic peaks of hydrocortisone were present in the spectrum of the drug and polymer mixture, indicating compatibility between drug and polymer. The spectrum confirmed that there is no significant change in the chemical integrity of the drug and the formulation and it is shown in Figure 2.

SEM analysis

Macroscopically the prepared hydrocortisone films were clear. The scanning electron photomicrographs of the selected films at 400× magnification are shown in Figure 3. The SEM photographs of the films showed smooth surfaces without any scratches or transverse striations, indicating that hydrocortisone is uniformly distributed and no crystals of hydrocortisone were observed in the films.

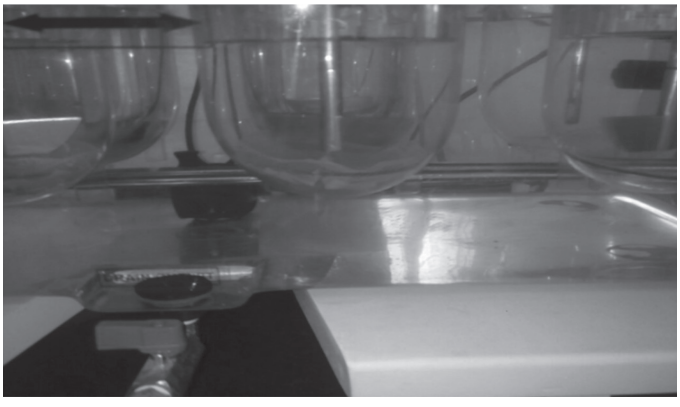

Figure 1. Drug release profile of the formulations

DSC study

The DSC study of the pure drug showed a sharp endothermic peak at 220.26°C. Similar endothermic peaks were obtained in the formulations at 202.62°C, clearly indicating that there was no drug–polymer interaction. The results of the DSC thermogram are shown in Figure 4.

Thickness of the films

Thickness was measured with a screw gauge at different places of the film in order to evaluate the reproducibility of the preparation method. The thickness was in the range of 470±0.09 to 490±0.03 µm. Around 90% of wet film thickness was lost during drying. The results are given in Table 2. For the prepared film a good uniformity of thickness was observed.

Weight variation of the films

Films of 0.5 cm^2 were cut from different batches and weighed. The weights of different formulations were in the range of 0.0098 to 0.0100 g and the results are given in Table 2. The same mass of film was obtained with three batches of films, indicating reproducibility of the preparation method and formulation.

Folding endurance

All the prepared films have an acceptable folding endurance. The folding endurance test was in the range of 122 to 146 folds and no films developed any visible cracks or breaks, thus showing good folding endurance. Among the five different formulations, F5 has the highest folding endurance due to the presence of a higher concentration of methylcellulose (2.00% w/v) when compared with the other films. The results are shown in Table 2.

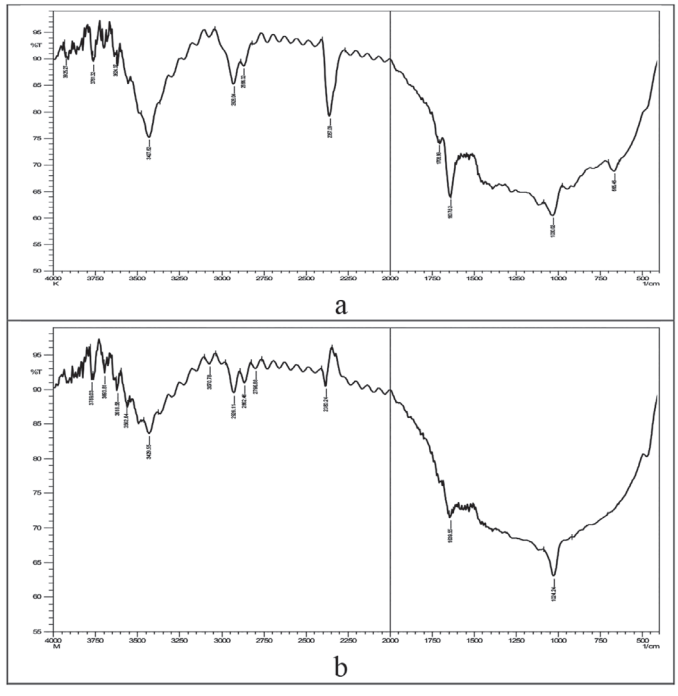

Figure 2. (a) FTIR of pure drug, (b) FTIR of drug with polymer

FTIR: Fourier transform infrared

Surface pH of the films

The surface pH of all films was in the range of 6.37±0.08 to 6.79±0.01. This assured that there will not be any kind of irritation to the mucosal lining of the oral cavity and the results are tabulated in Table 2.

Disintegration time

The disintegration time was in the range of 40 to 55 s in the drop method, whereas in the petri dish method it was e in the range of 43 to 56 s as shown in Table 2. These results indicated that the formulation F1 disintegrated faster than the other formulations in the drop method. With the petri dish method F1, F2, and F3 disintegrated/dissolved faster than the other formulations.

Drug content

Films of 0.5 cm^2 were cut from different places of the whole films for the estimation of drug content. The results were in the range of 95.6% to 98.4% as given in Table 3. These results

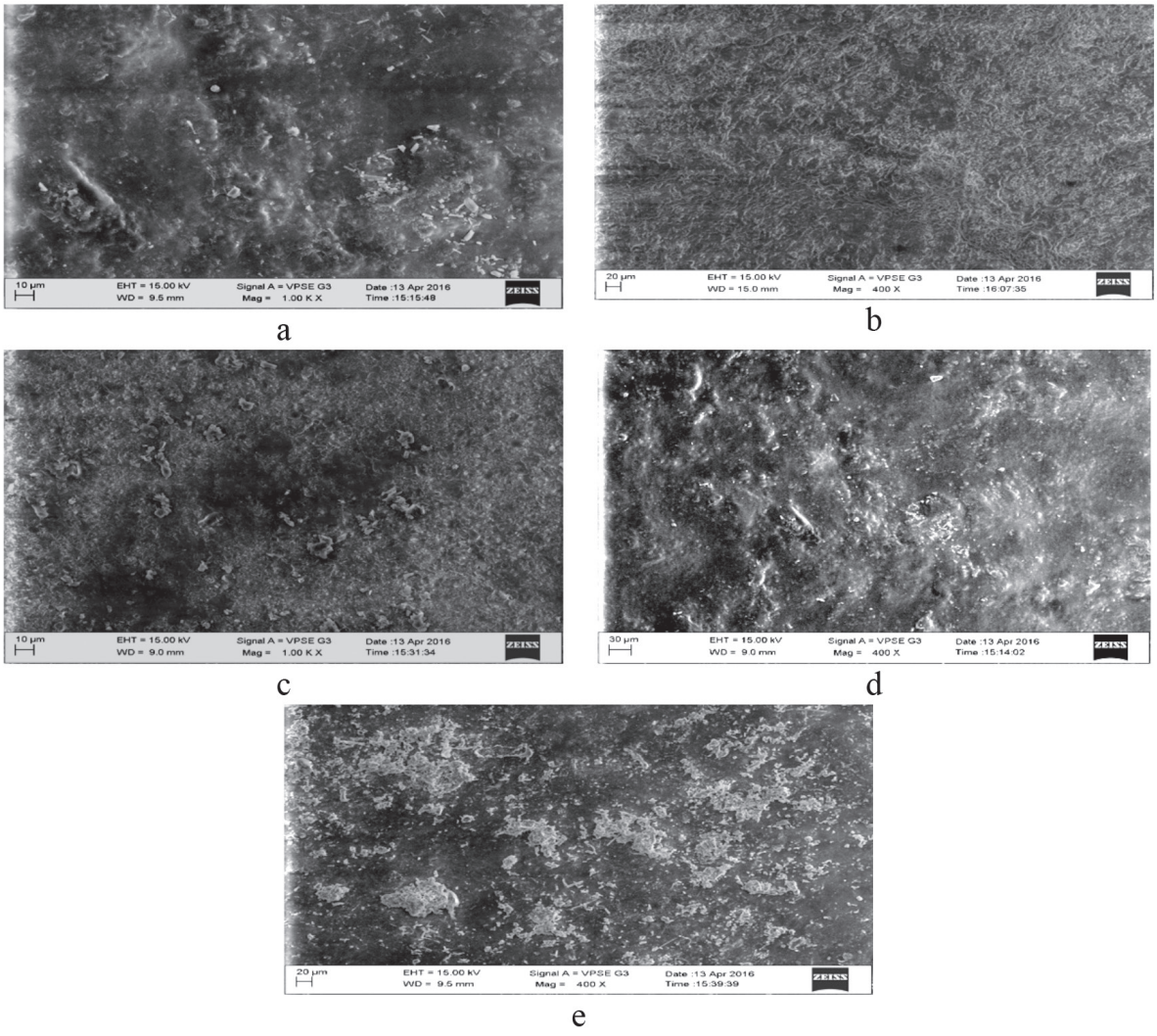

Figure 3. a. SEM of formulation (F1), b. SEM of formulation, (F2) c. SEM of formulation, (F3) d. SEM of formulation, (F4) E. SEM of formulation (F5)

SEM: Scanning electron microscopy

Table 2. Characterization studies

Formulation code	Variation in mass (g)	Thickness (µm)	Surface pH	Disintegration time (s)		Folding endurance
				Drop method	Petri dish method	
F1	0.0098±0.0004	470±0.09	6.52±0.016	40±0.045	430±1.57	122
F2	0.0100±0.0007	490±0.03	6.79±0.024	44±1.27	480±2.56	130
F3	0.0094±0.0006	475±0.07	6.55±0.022	47±0.55	520±1.32	134
F4	0.0100±0.0003	476±1.66	6.62±0.015	50±0.58	550±1.70	140
F5	0.0097±0.0005	480±2.04	6.49±0.019	55±1.32	568±2.54	146

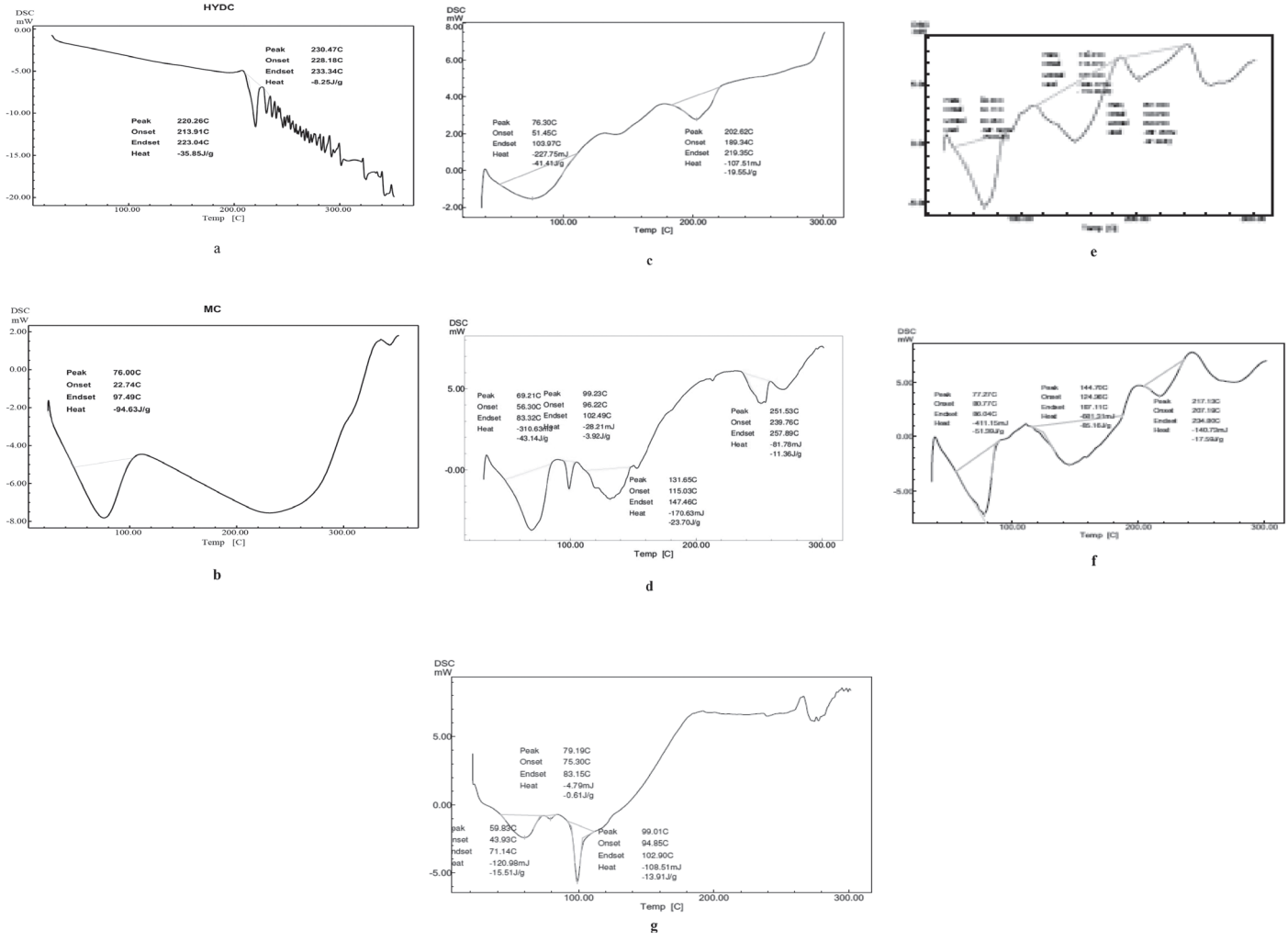

Figure 4. (a) DSC of pure drug, (b) DSC of polymer, (c) DSC of formulation (F1), (d) DSC of formulation (F2), (e) DSC of formulation (F3), (f) DSC of formulation (F4), (g) DSC of formulation (F5)

DSC: Differential scanning calorimetry

indicated a good uniformity of hydrocortisone within the films, and overall good solubilization of hydrocortisone in the formulations was observed.

Tensile strength

Films should possess moderate tensile strength, high % elongation (E), and high percentage of drug release. The results revealed that all the films showed moderate tensile strength values ranging from 0.614 to 0.872 (kg/mm^2). Among all the formulations, F2 showed the highest % E and tensile strength. The nature and concentration of the polymer affect the tensile strength and % elongation. F2, having the optimum concentration of methylcellulose (1.25%), showed the highest % of tensile strength and % elongation. The results are given in Table 3.

In vitro dissolution studies

The hydrocortisone films were prepared using methylcellulose as film-forming polymer with sodium citrate. The *in vitro* dissolution profiles of the hydrocortisone films were performed for all the different formulations and are shown in Figure 5. The cumulative percent of released hydrocortisone increased to the end of 8 h. The release rate from different films shows that the release of drug increased with an increase in the concentration of the release retardant polymer at a certain level, i.e. 1.25%, and a further increase in the concentration of the polymer decreased the release behavior of the formulation significantly.

Table 3. Tensile strength and elongation strength

Batch code	Tensile strength (kg/ mm^2)	Elongation (%)	Drug content (%)
F1	0.614±0.034	6.67±0.071	95.6
F2	0.872±0.044	7.67±0.005	98.4
F3	0.72±0.072	6.1±0.008	96.0
F4	0.863±0.008	6.01±0.072	97.6
F5	0.75±0.023	5.52±0.003	96.8

Table 4. Release exponent values and rate constant values for different formulations

Formulation code	Kinetic models				
	Zero order	First order	Higuchi	Korsmeyer–Peppas	
	R^2	R^2	R^2	R^2	n
F1	0.976	0.323	0.933	0.333	1.564
F2	0.977	0.596	0.818	0.713	1.835
F3	0.984	0.334	0.878	0.511	1.688
F4	0.998	0.317	0.904	0.440	1.613
F5	0.979	0.319	0.856	0.459	1.662

Table 5. Stability study

Formulation (F2)	Surface pH	Disintegration time (s)		Drug content (%)
		Drop method	Petri dish method	
Before	6.79±0.024	44±1.27	480±2.56	98.4
After	6.74±0.015	46±1.03	460±1.22	95.6

Release kinetics

In order to determine the release kinetics, the data of the release profile were subjected to various kinetics models. The release exponent 'n' values of the Korsmeyer–Peppas model were from 1.564 to 1.853, indicating the drug release pattern was a super case II mechanism. The data of the kinetics studies are shown in Table 4.

Ex vivo studies

Among the five different formulations the best formulation was subjected to an *ex vivo* release study through chicken skin using a diffusion cell. *Ex vivo* release would give a better estimate of drug permeation characteristics through animal skin. The amount of drug that permeated through the skin after 8 h from the formulation is shown in Figure 6.

Stability study

The selected optimized formulation F2 was subjected to short-term accelerated stability studies for 3 months at 25°/60% and 40°/75% RH. The samples were evaluated for any physical changes, disintegration rate, pH, and drug content. No discernible change in the physical appearance was seen in the samples and the disintegration rate, pH, and drug content values were found to be the same. The film was white, smooth, nonsticky, and flexible after the stability studies (Table 5).

CONCLUSIONS

The main objective of the study was to formulate and evaluate an oral film containing hydrocortisone. The films can be easily formulated by solvent casting using polymers such as methylcellulose in different ratios with a suitable plasticizer like propylene glycol. The compatibility of hydrocortisone with polymers was confirmed by FTIR, SEM, and DSC studies. It was observed that the physicochemical characteristics such as uniformity of weight, thickness, folding endurance, surface pH, and uniformity of drug content of all the film samples

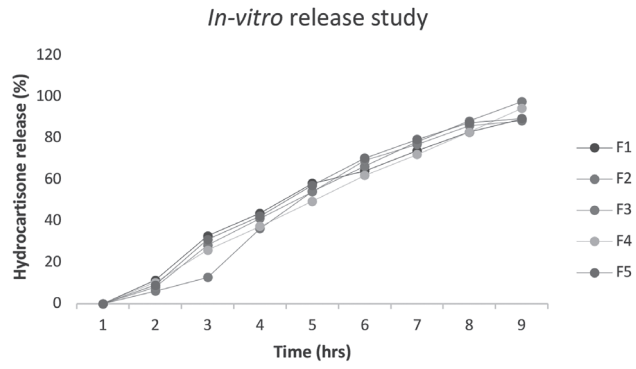

Figure 5. Comparative drug release profile of the formulations

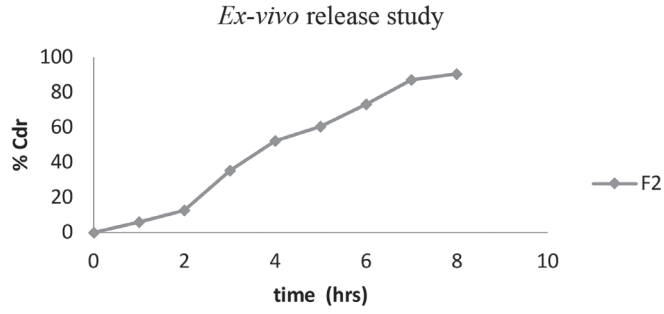

Figure 6. *Ex vivo* release studies

showed satisfactory results with respect to variation in these parameters between films of the same formulation. Tensile strength and percentage elongation of the films increased with an increase in the concentration of methylcellulose polymer. Disintegration time of the films was 40 to 55 s. Based on the physicochemical parameters and *in vitro* drug release studies, formulations F2 and F4 were considered the best formulations, exhibiting drug release of 97.54% and 94.29%, respectively, at the end of 8 h. *Ex vivo* drug release studies through chicken skin also showed similar results. The present study reveals that all five formulated films showed satisfactory film parameters. Out of these five formulations, F2 (1.25% w/v) showed better results when compared to the other formulations. From the present investigation it can be concluded that film formulation can be a potential novel drug dosage form for pediatric and geriatric populations and also for the general population.

ACKNOWLEDGEMENT

The authors are sincerely thankful to the principal of Sri Adichunchanagiri College of Pharmacy, B.G. Nagara, for providing us with the infrastructure facilities and moral support to carry out this research work.

Conflict of Interest: No conflict of interest was declared by the authors.

REFERENCES

1. Kumar RK, Sulochana MM. Formulation and evaluation of Fast dissolving films of Lercandipine Hydrochloride. IJIDD. 2014;4:46-53.

2. Ketul P, Patel KR, Patel MR, Patel NM. Fast dissolving films: A Novel approach to oral drug dilivery. AJPST. 2013;3:25-31.
3. Vucicevic Boras V, Savage NW. Recurrent aphthous ulcerative disease: Presentation and management. Aust Dent J. 2007;52:10-15.
4. Barrons RW. Treatment strategies for recurrent oral aphthous ulcers. Am J Health Syst Pharm. 2001;58:41-50.
5. Grover NK, Babu R, Bedi SPS. Steroid therapy- current indications in practice. Ind J Anesth. 2007;51:389-393.
6. Gupta P, Bhatia V. Corticosteroid physiology and principal of therapy. Ind J Pediat. 2008:1039-1044.
7. Maheshwari KM, Devineni PK, Deekonda S. Development and evaluation of mouth dissolving films of Amlodipine besylate for enhanced therapeutic efficacy. Hindawi J Pharm. 2014:1-10.
8. Patidar MK, Karjikar FA, Patel FA, Rathi SS, Thokal SB, Bhingare CL. Formulation and evaluation of mouth dissolving films of zolpidem tartrate by exploration on polymers combination. Int J Pharm. 2013;3:716-721.
9. Aviral K, Prajapati SK. Formulation and evaluation of dental film for periodontaitis. IRJP. 2012;3:143-148.
10. Rani JL. Formulation and *in vitro* and *in vivo* evaluation of oral dispersable films of loronoxicam. Int J Sci Tec. 2014;24:1649-1655.

Turk J Pharm Sci 2019;16(3):356-361
DOI: 10.4274/tjps.galenos.2018.69783

ORIGINAL ARTICLE

Investigation of Gelatinase Gene Expression and Growth of *Enterococcus faecalis* Clinical Isolates in Biofilm Models

Enterococcus faecalis Klinik İzolatlarının Üreme ve Gelatinaz Gene Ekspresyonlarının Biyofilm Modellerinde Araştırılması

Didem KART[1]*, Ayşe Semra KUŞTİMUR[2]

[1]Hacettepe University, Faculty of Pharmacy, Department of Pharmaceutical Microbiology, Ankara, Turkey
[2]Gazi University, Faculty of Medicine, Department of Medical Microbiology, Ankara, Turkey

ABSTRACT

Objectives: *Enterococcus faecalis* is the major reason for biofilm-related infections and it also interacts with *Staphylococcus aureus* in biofilms. Gelatinase (gelE) enzyme is an important virulence factor of *E. faecalis* for biofilm formation. This study aimed to compare the biofilm producing *E. faecalis* isolates from urine and urinary catheters. The influence of *S. aureus* on the growth of *E. faecalis* biofilm cells was also investigated in a dual biofilm model *in vitro*. Another aim was to evaluate *E. faecalis* gelE gene expression during biofilm formation.

Materials and Methods: Firstly, crystal violet staining was used to measure the total biofilm biomass of the isolates. Secondly, plate counting was performed to determine the biofilm formation ability of *E. faecalis* isolates and the effect of *S. aureus* on *E. faecalis* biofilm formation. Finally, the gelE expression profile of the isolates was assessed by quantitative real time-polymerase chain reaction.

Results: According to crystal violet staining and plate counting, all *E. faecalis* isolates were biofilm producers and the number of *E. faecalis* sessile cells increased in the presence of *S. aureus*. Among the 21 *E. faecalis* isolates, ten expressed high levels of the gelE gene, while eight of them had low expression profiles ($p<0.05$).

Conclusion: When they grow together, *S. aureus* may give some advantages to *E. faecalis* such as increasing sessile cell growth. The expression of the gelE gene was not affected by *E. faecalis* biofilm formation of the isolates collected from the patients with urinary tract infections.

Key words: Dual biofilm, *E. faecalis*, *S. aureus*, gelatinase, quantitative reverse transcription polymerase chain reaction

ÖZ

Amaç: *Enterococcus faecalis* biyofilm ilişkili enfeksiyonların ana sebebidir ve biyofilmlerde *Staphylococcus aureus* ile de etkileşimde bulunurlar. Jelatinaz (gelE) enzimi biyofilm oluşumunda *E. faecalis* için önemli bir virulans faktörüdür. Bu çalışma idrar ve üriner kateterlerden izole edilmiş biyofilm oluşturan *E. faecalis* izolatlarını karşılaştırmayı amaçlamaktadır. Aynı zamanda *S. aureus*'un *E. faecalis* biyofilm hücrelerinin üremesi üzerindeki etkisi de *in vitro* iki türlü biyofilm modelinde incelenmiştir. Bir diğer amacımız biyofilm oluşumu sırasında *E. faecalis* gelE gen ekspresyonunu değerlendirmektir.

Gereç ve Yöntemler: İzolatların total biyofilm biyokütlesinin ölçümünde ilk olarak kristal viyole boyama yöntemi kullanılmıştır. İkinci olarak, *E. faecalis* izolatlarının biyofilm oluşturma kapasitesini ve *S. aureus*'un *E. faecalis* biyofilmleri üzerinde etkisini değerlendirmek için plak sayım yöntemi uygulanmıştır. Son olarak, izolatların gelE ekspresyon profilleri kantitatif gerçek zamanlı-polimeraz zincir reaksiyonu ile belirlenmiştir.

Bulgular: Kristal viyole ve plak sayım yöntemine göre, tüm *E. faecalis* izolatlarının biyofilm oluşturdukları ve *E. faecalis* sesil hücre sayılarının *S. aureus* varlığında arttığı belirlenmiştir. Yirmi bir *E. faecalis* izolatı arasında, 10'u gelE gen ekspresyonunu yüksek oranda arttırmış, ancak 8'i azaltmıştır ($p<0.05$).

Sonuç: Birlikte üredikleri zaman; *S. aureus*, *E. faecalis*'e sesil hücre üremesini arttırmak gibi bazı avantajlar sağlayabilmektedir. GelE gen ekspresyonu idrar yolu enfeksiyonlu hastalardan izole edilmiş *E. faecalis* izolatlarının biyofilm oluşumundan etkilenmemiştir.

Anahtar kelimeler: İkili biyofilm, *E. faecalis*, *S. aureus*, jelatinaz, kantitatif gerçek zamanlı-polimeraz zincir reaksiyonu

*Correspondence: **E-mail:** dturk@hacettepe.edu.tr, **Phone:** +90 312 305 14 99 **ORCID-ID:** orcid.org/0000-0001-7119-5763
Received: 13.05.2018, **Accepted:** 21.06.2018

INTRODUCTION

Biofilms are defined as biotic or abiotic surface-attached microbial consortia and have multiple stages such as initial reversible attachment; production of an extracellular polymeric matrix (EPM) including proteins, polysaccharides, and nucleic acids; irreversible attachment; etc.[1,2] Biofilm formation is an important problem causing failure in antimicrobial treatment because sessile cells in the biofilm are highly resistant to antimicrobial agents. It has been highlighted that 65%-80% of all infections are biofilm-related. Biofilm cells are phenotypically, physiologically, and genotypically different from nonattached (planktonic) cells. Moreover, high concentrations of antimicrobial agents are necessary to kill sessile cells in a mature biofilm vs planktonic cells.[3]

It has been recently shown that most diseases are caused by polymicrobial communities.[4-8] Although some infections are considered predominantly monomicrobial, they may be influenced by other microorganismal associations during active infection.[4] The physiology of microbial cells in the biofilm has been frequently changed by these interactions and leads to various advantages being obtained, such as resistance to antimicrobials or the human immune system, metabolic cooperation, quorum sensing systems, and more productive gene sharing.[9-12]

Enterococcus species have been recognized as opportunistic pathogens for many nosocomial infections and are natural inhabitants of the human intestinal and oral flora. *Enterococcus faecalis* is the most common species leading to many infections among the other enterococcus species.[13,14] They can readily form biofilms and keep growing on various medical devices' surfaces such as urinary catheters despite a serious inflammatory response.[15] *Staphylococcus aureus* has become an important cause of hospital-acquired infection associated with indwelling medical devices and surgical wounds. It may cause chronic infections that cannot be treated with antibiotics because of the ineffective host immune response. Moreover, staphylococci have nonspecific resistance mechanisms such as biofilm formation.[16-18]

Changing expression levels of virulence factors of *E. faecalis* have been shown whether they formed a biofilm or not. Among the virulence factors, the gelatinase (gelE) enzyme is an important factor that hydrolyzes gelatin, casein, and collagen.[19] Although there have been many studies on biofilm formation and gelE expression by *E. faecalis*, it is still not clear how gelE expression levels change in mono- or polymicrobial biofilms.[20-22]

In the present study, we evaluated the biofilm ability of *E. faecalis* isolates by quantification assays and then we set up an *in vitro* dual biofilm model in a repeatable style and determined the influence of the presence of *S. aureus* on the growth of *E. faecalis* by plating assay. Finally, the *gelE* gene expression levels of *E. faecalis* were measured by quantitative real time-polymerase chain reactions (qRT-PCRs).

MATERIALS AND METHODS

Strains used in the study

A total of 20 *E. faecalis* clinical isolates and a strain as a positive control (*E. faecalis* ATCC 29212) were used in this study. These isolates were taken from urinary catheter (n=10) and urine samples (n=10) from hospitalized intensive care unit patients admitted to a University Hospital from 2000 to 2011.

For dual biofilm formation, all the *E. faecalis* isolates and *E. faecalis* ATCC 29212 were cultured with *S. aureus* ATCC 29213.

Mono and dual biofilm formation in microtiter plates

Final inoculum suspensions of all clinical *E. faecalis* strains were adjusted to approximately 10^6 colony-forming units (CFU) mL^{-1}. Each experiment included the biofilm-forming *E. faecalis* ATCC 29212 strain as a positive control. For dual species biofilms, *E. faecalis* isolates were co-cultured with a laboratory strain of *S. aureus* (10^6 CFU/mL) and incubated at 37°C without shaking. Sterile tryptic soy broth (TSB) (Becton Dickinson GmbH, Heidelberg, Germany) with 0.25% glucose was used as a blank. For each test condition, 12 wells of a flat-bottomed polystyrene 96-well microtiter plate were inoculated with 100 µL of the final inoculum suspension. After 4 h of incubation at 37°C without shaking, nonadhered cells were removed and rinsed with 100 µL of 0.9% physiological saline (PS), then 100 µL of fresh TSB with 0.25% glucose was added, and the plates were incubated for an additional 20 h for biofilm maturation. After 24 h, the supernatants were removed and each well was rinsed with PS before the sessile cells were quantified.

Quantification of the biofilms

Crystal violet staining

The biomass quantification of *E. faecalis* biofilms was performed according to an optimized assay.[19] After washing with sterile PBS, the wells were stained with 100 µL of a solution of 0.2% crystal violet for 15 min. The stained biofilms were rinsed again three times with PBS to remove excess dye and dried for 15 min at room temperature. The bound dye was solubilized in 150 µL of acetone/ethanol solution. The optical densities (ODs) of the stained adherent cells were read at 570 nm using a micro-ELISA plate reader. We defined the cut-off OD (0.282) as three standard deviations above mean OD of the negative control. Each isolate was tested in 12 wells in each assay and each assay was carried out in duplicate (n=24).

Plate counting

Quantification of the number of cells in mature biofilms was done via plate counting using tryptic soy agar (TSA) medium.

Table 1. The primers for quantifying the genes of *E. faecalis* by RT-qPCR

Gene	Forward primer (5'-3')	Reverse primer (5'-3')
16sRNA	CCGAGTGCTTGCACTCAATTGG	CTCTTATGCCATGCGGCATAAAC
gelE	TGGATTAGATGCACCCGAAAT	CGGAACATACTGCCGGTTTAGA

Biofilms were detached by vortexing (5 min) followed by sonication (5 min). The sonicated fluids were serially diluted and plated on TSA to determine the number of CFU per mL of the isolates. Bile esculin azide agar was used for plating of *E. faecalis* isolates in mature dual biofilms that were formed by *E. faecalis* and *S. aureus*.

Expression of the gelE gene in planktonic and biofilm cells of E. faecalis

Total RNA was extracted from the mono- and dual-species biofilm cells with the RNeasy® Mini Kit according to the manufacturer's recommendations (Qiagen GmbH, Germany). All RNA extracts were prepared as 100 ng μL^{-1} per sample and transcribed into cDNA using a Transcriptor High Fidelity cDNA Synthesis Kit according to the manufacturer's instructions (Roche Diagnostics GmbH, Germany). RT-PCR (Roche Light Cycler 2.0) was performed with LightCycler Faststart DNA Master SYBR Green1 (Roche Diagnostics GmbH) in a total volume of 20 µL. Primer sequences for the housekeeping gene 16sRNA and gelE were obtained from the literature and are listed in Table 1.[17] The 16sRNA gene was used to normalize the expression level of gelE. Melt curve analysis was carried out to assess the specificity of each primer pair. The comparative C_T method for relative quantification ($^{\Delta\Delta}C_T$ method) was performed to analyze the data.[23]

Statistical analysis

The independent samples t-test was used to compare biofilm cell CFU counts between the two groups (with/without *S. aureus* biofilms). One-way ANOVA was used to evaluate CFU differences within a group. The CFU counts were log-transformed before the statistical tests. A p value <0.05 was considered significant. For gene expression, the results were analyzed by t-tests and only differences of more than twofold up- or down- regulation and with a p-value <0.05 were considered significant.

RESULTS

Detection of biofilm production by E. faecalis isolates

In total 20 *E. faecalis* isolates were analyzed to determine the ability of biofilm formation. All of the isolates were found to be biofilm-positive by plate counting and crystal violet staining (Figures 1 and 2). In terms of biofilm-forming ability no statistically significant difference was determined between the isolates from catheters and not from catheters (Figure 2).

In the co-culture of *E. faecalis* with *S. aureus*, the cell counts of *E. faecalis* were significantly higher than those in their mono-species biofilm (Figure 2). Our results showed that *S. aureus* contributed to the growth of *E. faecalis* biofilm cells by an unknown mechanism.

GelE gene expression in planktonic and biofilm cells of E. faecalis clinical isolates

We used qRT-PCR to compare the expression levels of gelE in planktonic and biofilm cells of 21 *E. faecalis* isolates (including a positive control) from urine and urinary catheter samples from hospitalized patients and *E. faecalis* ATCC 29212. According to the results obtained from the mRNA levels of gelE in planktonic and biofilm cells of *E. faecalis*, 12 of the 21 *E. faecalis* strains (including the positive control) exhibited increased gelE gene

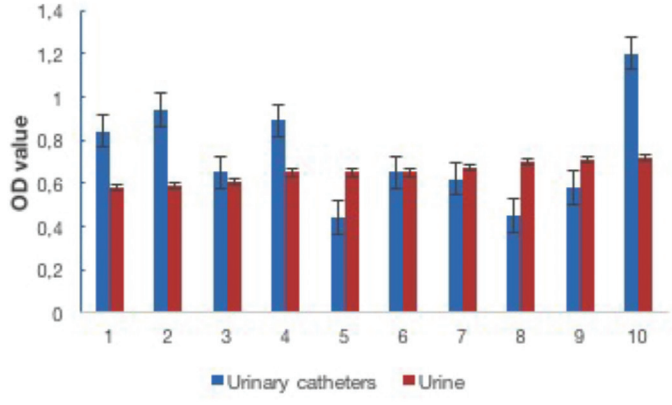

Figure 1. Biofilm forming ability of the *Enterococcus faecalis* isolates from the urine and urinary catheter samples of hospitalized patients by crystal violet staining assay

[a]Biofilm formation degrees of the isolates were determined by crystal violet staining assay. Results are means of at least three different experiments, OD: Optical density

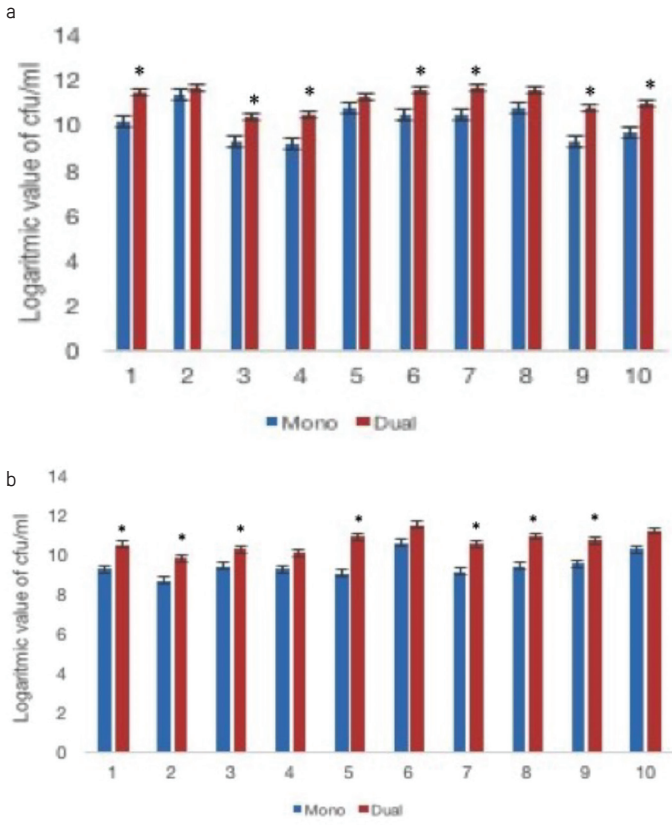

Figure 2. Biofilm forming ability of the *Enterococcus faecalis* isolates in mono and dual biofilms. Numbers of the sessile cells of the *E. faecalis* isolates in mono and dual species biofilms were determined by plate counting assay. (a) The results of isolates from the urinary catheter samples, (b) The results of isolates from the urine samples. Results are means of at least three different experiments. Mono: only *E. faecalis* biofilms, Dual: *E. faecalis* and *S. aureus* biofilms, CFU: Colony forming unit,

*: Statistically significant

expression; however, only ten of them (including the positive control) were statistically significant ($p<0.05$). Eight isolates showed significantly decreased expression levels ($p<0.05$) (Figure 3).

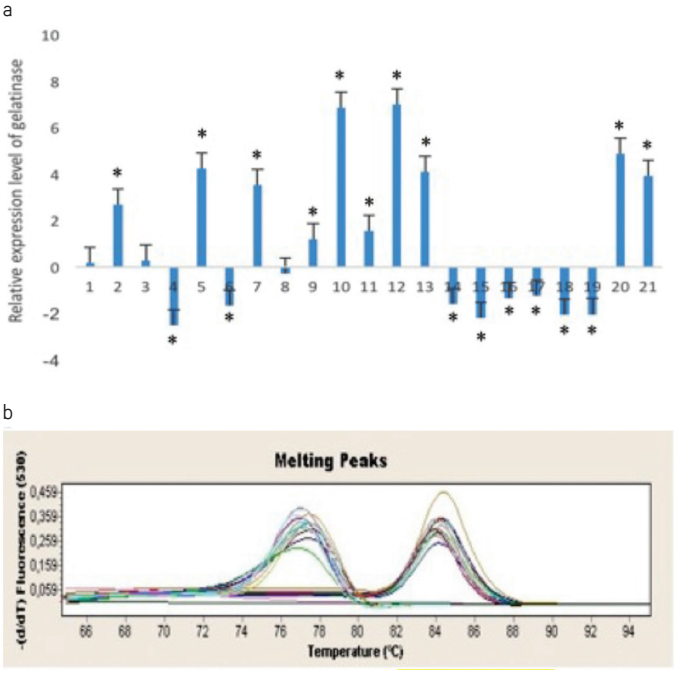

Figure 3. Gelatinase gene relative expression ratios of *Enterococcus faecalis* ATCC 29212 and clinical isolates in planktonic and biofilm cells.

*: Statistically significant (p value<0.05), (a, b) Melting curves of gelE and 16srRNA (housekeeping gene) of the bacteria, respectively

DISCUSSION

Biofilm-related urinary tract infections represent the main cause of nosocomial infections. Enterococci (especially *E. faecalis*) and *S. aureus* are a major challenging problem for treatment of urinary tract infections.[24] It is widely known that the presence of bacterial biofilms on the inner or outer surface of the catheter leads to catheter-associated urinary tract infections (CAUTIs).[15] The occurrence of CAUTIs, as the most common hospital-acquired infection, has an important economic and clinical impact and is directly related to the majority of uropathogens such as *E. faecalis* and *S. aureus* that may form biofilms. In the current study, we assessed the ability of biofilm formation of clinical *E. faecalis* isolates in alone and co-culture with *S. aureus in vitro.* Our results indicated that all isolates from inpatients with and without urinary catheters were biofilm positive with regard to the plate counting and crystal violet staining methods (Figures 1 and 2). The starting bacteria concentration was normalized as 6 $\log_{10}$ (10^6 CFU/mL). However, after the incubation period, the lowest bacteria number in the well plates was found to be 8.7 $\log_{10}$. This result showed that all the mono-species biofilm isolates of *E. faecalis* attached and grew on the walls of the wells in microtiter plates (Figure 2).

Interspecies interactions in polyspecies biofilm usually provide various advantages for the inhabitant species such as increased tolerance against several antimicrobials and increased virulence in infections.[25] Pastar et al.[26] showed that the presence of *Pseudomonas* inhibited the growth of *S. aureus in vitro* and induced expression of *S. aureus* virulence factors in polymicrobial wound infection. In another study, the effect of *Streptococcus mutans* on *E. faecalis* biofilm formation was investigated and an increase in biofilm formation of *E. faecalis* by *S. mutans* was obtained.[27] It has been previously shown that the combined effect of *C. albicans* and *E. faecalis* in a mouse model resulted in increased growth of enterococci in the animals when *C. albicans* had been introduced.[28] In a *P. aeruginosa* and *C. albicans* dual biofilm model, it was observed that *P. aeruginosa* formed biofilms on the fungal filaments of *C. albicans* and this close contact caused the killing of the fungal filaments.[29] In our study, the number of sessile cells of *E. faecalis* in dual-species biofilms with *S. aureus* was significantly higher than in their mono-species biofilm. We concluded that the growth and biofilm formation of the *E. faecalis* isolates were increased by *S. aureus* sessile cells. According to the biofilm cell counts between the urine and urinary catheter samples, the counts of *E. faecalis* isolates from the urinary catheters were greater than those of the isolates from urine.

Many virulence factors have significant roles in the pathogenesis of enterococcal infections such as adhesion, colonization, and invasion. Although it has been indicated that some of the major virulence genes were related to biofilm formation on abiotic surfaces in hospital environments, research on the virulence mechanism and related genes in biofilm formation is still needed.[30-32] A high amount of gelE gene expression in *E. faecalis* biofilm cells was shown in some studies, whereas others were in contradiction with this finding.[33-35] Arciola et al.[15] showed the importance of gelE in biofilm formation in implant infections. In a recent study, the prevalence of the gelE gene was determined as 64.3% among 510 clinical *Enterococcus* spp. isolates from UTI and wound infections.[30] However, Kafil and Mobarez[24] did not find a significant effect of the presence or absence of gelE on biofilm production by *Enterococcus* species. We examined the gelE mRNA levels of both planktonic and sessile cells of *E. faecalis* ATCC 29212 and 20 *E. faecalis* isolates by RT-qPCR. Our results showed that the gelE expression levels of ten isolates were significantly enhanced, but eight of the isolates were significantly decreased in biofilms when compared to their planktonic forms ($p\leq0.05$) (Figure 3). Based on this result, we concluded that gelE expression had no effect on biofilm formation of the isolates collected from urinary tract infections ($p>0.05$) (Figure 3). The comparison of gelE mRNA levels of the isolates from the two different samples showed no significant difference either.

CONCLUSIONS

There was no statistically significance between the isolates from catheters and not from catheters in terms of biofilm-forming capability. *E. faecalis* sessile cell counts were increased in the presence of *S. aureus*. Expression of the gelE gene was not affected by *E. faecalis* biofilm formation of the isolates collected from the patients with urinary tract infections.

ACKNOWLEDGEMENTS

We gratefully acknowledge Prof. Dr. Gülşen Hasçelik and Dr. Dolunay Gülmez from Hacettepe University, Faculty of Medicine, Department of Medical Microbiology, for providing the *E. faecalis* clinical strains.

Conflict of Interest: No conflict of interest was declared by the authors.

REFERENCES

1. Van Acker H, Van Dijck P, Coenye T. Molecular mechanisms of antimicrobial tolerance and resistance in bacterial and fungal biofilms. Trends Microbiol. 2014;22:326-333.
2. Bjarnsholt T, Alhede M, Alhede M, Eickhardt-Sørensen SR, Moser C, Kühl M, Jensen PØ, Høiby N. The *in vivo* biofilm. Trends Microbiol. 2013;21:466-474.
3. Hall-Stoodley L, Costerton JW, Stoodley P. Bacterial biofilms: from the natural environment to infectious diseases. Nat Rev Microbiol. 2004;2:95-108.
4. Tay WH, Chong KK, Kline KA. Polymicrobial-Host Interactions during Infection. J Mol Biol. 2016;428:3355-3371.
5. Roberts FA, Darveau RP. Microbial protection and virulence in periodontal tissue as a function of polymicrobial communities: symbiosis and dysbiosis. Periodontol. 2015;69:18-27.
6. Hajishengallis G. Periodontitis: from microbial immune subversion to systemic inflammation. Nat Rev Immunol. 2015;15:30-44.
7. Darveau RP. Periodontitis: a polymicrobial disruption of host homeostasis. Nat Rev Microbiol. 2010;8:481-490.
8. Marom T, Nokso-Koivisto J, Chonmaitree T. Viral-bacterial interactions in acute otitis media. Curr Allergy Asthma Rep. 2012;12:551-558.
9. Wolcott R, Costerton JW, Raoult D, Cutler SJ. The polymicrobial nature of biofilm infection. Clin Microbiol Infect. 2013;19:107-112.
10. Weimer KE, Juneau RA, Murrah KA, Pang B, Armbruster CE, Richardson SH, Swords WE. Divergent mechanisms for passive pneumococcal resistance to beta-lactam antibiotics in the presence of *Haemophilus influenzae.* J Infect Dis. 2011;203:549-555.
11. Elias S, Banin E. Multi-species biofilms: living with friendly neighbors, FEMS Microbiol Rev. 2012;36:990-1004.
12. Madsen JS, Burmolle M, Hansen, LH, Sorensen SJ. The interconnection between biofilm formation and horizontal gene transfer. FEMS Immunol Med Microbiol. 2012;65:183-195.
13. Ruoff KL, De La Maza L, Murtagh Mj, Spargo JD, Ferraro MJ. Species identities of Enterococci isolated from clinical specimen. J Clin Microbiol. 1990;28:435-437.
14. Bulacio Mde L, Galván LR, Gaudioso C, Cangemi R, Erimbaue MI. *Enterococcus faecalis* biofilm formation and development *in vitro* observed by scanning electron microscopy. Acta Odontol Latinoam. 2015;28:210-214.
15. Arciola CR, Baldassarri L, Campoccia D, Creti R, Prini V, Huebner J, Montanaro L. Strong biofilm production, antibiotic multi-resistance and high gelE expression in epidemic clones of *Enterococcus faecalis* from orthopaedic implant infections. Biomaterials. 2008;29:580-586.
16. Pérez-Laguna V, García-Luque I, Ballesta S, Pérez-Artiaga L, Lampaya-Pérez V, Samper S, Soria-Lozano P, Rezusta A, Gilaberte Y. Antimicrobial photodynamic activity of Rose Bengal, alone or in combination with Gentamicin, against planktonic and biofilm *Staphylococcus aureus*. Photodiagnosis Photodyn Ther. 2018;21:211-216.
17. Otto M. Staphylococcal Biofilms. Curr Top Microbiol Immunol. 2008;322:207-228.
18. Archer NK, Mazaitis MJ, Costerton JW, Leid JG, Powers ME, Shirtliff ME. *Staphylococcus aureus* biofilms: properties, regulation and roles in human disease. Virulence. 2011;2:445-459.
19. Stickler DJ. Bacterial biofilms in patients with indwelling urinary catheters. Nat Clin Pract Urol. 2008;5:598-608.
20. Crémet L, Corvec S, Batard E, Auger M, Lopez I, Pagniez F, Dauvergne S, Caroff N. Comparison of three methods to study biofilm formation by clinical strains of *Escherichia coli*. Diagn Microbiol Infect Dis. 2013;75:252-255.
21. Chavant P, Gaillard-Martinie B, Talon R, Hébraud M, Bernardi T. A new device for rapid evaluation of biofilm formation potential by bacteria. J Microbiol Methods. 2007;68:605-612.
22. Naves P, del Prado G, Huelves L, Gracia M, Ruiz V, Blanco J, Dahbi G, Blanco M, Ponte Mdel C, Soriano F. Correlation between virulence factors and *in vitro* biofilm formation by *Escherichia coli* strains. Microb Pathog. 2008;45:86-91.
23. Livak KJ, Schmittgen TD. Analysis of relative gene expression data using real-time quantitative PCR and the 2(-Delta Delta C (T)) method. Methods. 2001;25:402-408.
24. Kafil HS, Mobarez AM. Assessment of biofilm formation by enterococci isolates from urinary tract infections with different virulence profiles. Journal of King Saud University Science. 2015;27:312-317.
25. Henriette LR, Søren JS, Mette B. Studying Bacterial Multispecies Biofilms: Where to Start? Trends Microbiol. 2016;24:503-513.
26. Pastar I, Nusbaum AG, Gil J, Patel SB, Chen J, Valdes J, Stojadinovic O, Plano LR, Tomic-Canic M, Davis SC. Interactions of methicillin resistant *Staphylococcus aureus* USA300 and *Pseudomonas aeruginosa* in polymicrobial wound infection. PLoS ONE. 2013;8:e56846.
27. Deng DM, Hoogenkamp MA, Exterkate RA, Jiang LM, van der Sluis LW, Ten Cate JM, Crielaard W. Influence of *S. mutans* on *E. faecalis* Biofilm Formation. J Endod. 2009;35:1249-1252.
28. Mason KL, Downward JR, Falkowski NR, Young VB, Kao JY, Huffnagle GB. Interplay between the gastric bacterial microbiota and *Candida albicans* during postantibiotic recolonization and gastritis. Infect Immun. 2012;80:150-158.
29. Harriott MM, Noverr MC. Importance of Candida-bacterial polymicrobial biofilms in disease. Trends Microbiol. 2011;19:557-563.
30. Stratevaa T, Atanasova D, Savov E, Petrovac G, Mitov I. Incidence of virulence determinants in clinical *Enterococcus faecalis* and *Enterococcus faecium* isolates collected in Bulgaria. Braz J Infect Dis. 2016;20:127-133.
31. Oli AK, Raju S, Rajeshwari Nagaveni S, Kelmani CR. Biofilm formation by Multidrug resistant *Enterococcus faecalis* (MREF) originated from clinical samples. J Microbiol Biotechnol Res. 2012;2:284-288.

32. Biswas PP, Dey S, Adhikari L, Sen A. Virulence markers of vancomycin resistant enterococci isolated from infected and colonized patients. J Glob Infect Dis. 2014;6:157-163.

33. Wang L, Dong M, Zheng J, Song Q, Yin W, Li J, Niu W. Relationship of biofilm formation and gelE gene expression in *Enterococcus faecalis* recovered from root canals in patients requiring endodontic retreatment. J Endod. 2011;37:631-636.

34. Di Rosa R, Creti R, Venditti M, D'Amelio R, Arciola CR, Montanaro L, Baldassarri L. Relationship between biofilm formation, the enterococcal surface protein (Esp) and gelatinase in clinical isolates of *Enterococcus faecalis* and *Enterococcus faecium*. FEMS Microbiol Lett. 2006;256:145-150.

35. Seno Y, Kariyama R, Mitsuhata R, Monden K, Kumon H. Clinical implications of biofilm formation by *Enterococcus faecalis* in the urinary tract. Acta Med Okayama. 2005;59:7987.

Turk J Pharm Sci 2019;16(3):362-365
DOI: 10.4274/tjps.galenos.2018.52244

ORIGINAL ARTICLE

In Vitro Macrophage Nitric Oxide and Interleukin-1 Beta Suppression by *Moringa peregrina* Seed

Moringa peregrina Tohumlarıyla *İn Vitro* Makrofaj Nitrik Oksit ve İnterlökin-1 Beta Baskılanması

Shaymaa Fadhel Abbas ALBAAYIT*[1,2], Ahmed Salim Kadhim AL-KHAFAJI[1], Hiba Sarmed ALNAIMY[1]

[1]University of Baghdad, Faculty of Science, Department of Biology, Baghdad, Iraq
[2]University of Malaya, Faculty of Science, Institute of Biological Sciences, Kuala Lumpur, Malaysia

ABSTRACT

Objectives: *Moringa peregrina* has long been used in folk medicine to treat diseases including fever, headache, burns, constipation, gut pains, and inflammation. Nitric oxide (NO) and interleukin-1β (IL-1β) play an important role in the pathophysiology of inflammation. The objectives of this study were to determine the effect of *M. peregrina* seed ethanolic extract (MPSE) on the viability of and NO and IL-1β production by lipopolysaccharide (LPS)-activated macrophage (J774A.1) cell line.

Materials and Methods: The 3-(4,5-dimethylthiazol-2-yl)-2,5 diphenyltetrazolium bromide assay was used to determine the cytotoxic effect of MPSE treatment at concentrations ranging from 31.15 to 1000 µg/mL. The NO concentration was determined by Griess assay and IL-1β proinflammatory cytokine concentration by enzyme-linked immunosorbent assay in the supernatant of MPSE-treated LPS-activated J774A.1 cell culture.

Results: The results show that the MPSE was not cytotoxic at 1000 µg/mL but significantly ($p<0.001$) inhibited NO and IL-1β production by the LPS-activated macrophage J774A.1 cells.

Conclusion: These findings suggest that *M. peregrina* seed extract can be used to treat and prevent inflammatory diseases through the inhibition of inflammatory mediators.

Key words: *Moringa peregrina*, nitric oxide, interleukin-1β, inflammation

ÖZ

Amaç: *Moringa peregrina* geleneksel tıpta uzun yıllardan beri ateş, baş ağrısı, yanık, kabızlık, gut ağrıları ve inflamasyonların tedavisinde kullanılmaktadır. Nitrik oksit (NO) ve interlökin-1β (IL-1β) inflamasyonun patofizyolojisinde önemli rol oynamaktadır. Bu çalışmada, *M. peregrina* tohumları etanol ekstresinin (MPSE) sitotoksik ve lipopolisakkarit (LPS) ile aktive edilmiş makrofaj hücre hattının (J774A1) NO ve IL-1β üretimini baskılayıcı etkileri araştırılmıştır.

Gereç ve Yöntemler: Ekstrenin sitotoksik etkilerini tayin etmek için 3-(4,5-dimetiltiyazol-2-il)-2,5-difeniltetrazolyum bromür yöntemi kullanılmıştır. İndüklenmiş makrofaj kültür süpernatantında NO düzeyleri Griess yöntemi ile, IL-1β proinflamatuvar sitokin düzeyleri enzim aracılı immünosorbent yöntemi ile tayin edilmiştir.

Bulgular: Sonuçlar, MPSE'nin J774A1 hücrelerine toksik olmadığını göstermiştir. Ayrıca, ekstre LPS ile aktive edilmiş J774A1 hücre makrofajlarında NO ve IL-1β üretimini önemli ölçüde baskılamıştır.

Sonuç: Bu bulgular, *M. peregrina* tohum ekstrelerinin, inflamatuvar mediyatörlerin aşırı üretiminin eşlik ettiği inflamatuvar hastalıklardan korunma ve bu hastalıkların tedavisinde yararlı olabileceğini göstermektedir.

Anahtar kelimeler: *Moringa peregrina*, nitrik oksit, interlökin-1β, inflamasyon

***Correspondence: E-mail:** shaymaa_albaayit@yahoo.com, **Phone:** +9647808430086 **ORCID-ID:** orcid.org/0000-0002-8168-7048
Received: 03.04.2018, **Accepted:** 21.06.2018

INTRODUCTION

The inflammatory process plays a key role in the development of various conditions, such as gastritis, diabetes, atherosclerosis, and cancer.[1] Macrophages have critical roles in inflammatory response by phagocytosis or producing inflammatory mediators such as nitric oxide (NO) and pro-inflammatory cytokines such as interleukin (IL)-1β, IL-6, and tumor necrosis factor-α (TNF-α). These inflammatory molecules can be induced by certain stimulants, such as lipopolysaccharide (LPS), which can stimulate and activate macrophages.[2,3] NO is a signaling protein synthesized by NO synthase (NOS) from L-arginine. It is a short-lived intercellular biomolecule that performs key roles in the regulation of a variety of inflammatory diseases. It has also important antitumor and antiviral properties.[4-6] IL-1β is considered a key inflammatory cytokine responsible for the induction of inflammatory reactions and the production of reactive oxygen species.[6,7] Although cytokines and NO play special roles in mediating immune function, the same molecules have been involved in enhanced expression, which might cause chronic inflammatory diseases and tissue injury.[8,9]

Moringa peregrina (Forssk.) Fiori can be found in Africa and countries bordering the Red Sea.[10] In folk medicine, all parts of this plant are used for the treatment of abdominal pains, diabetes, headache, fever, and burns. It is also administered to pregnant women to facilitate fetus delivery.[11] Pharmacological studies have reported the validation of this plant for anti-inflammatory, antimicrobial, antiulcer, and antioxidant use.[10,12] *M. peregrina* seed oil contains high amounts of oleic acid, linoleic acid, tocopherols, and phenolic compounds, which help to reduce inflammation.[13,14] Thus, the present study was undertaken to investigate the effect of *M. peregrina* seed extract, which might be used as a natural drug for treatment of inflammatory-related disease, on NO and pro-inflammatory cytokine IL-1β production in lipopolysaccharide (LPS)-induced macrophage cell line J774A.1.

MATERIALS AND METHODS

Plant material and extraction

The *M. peregrina* seeds were authenticated by Dr. Maha Kordofani (Resident Botanist) at the Botany Department, Faculty of Science, University of Khartoum. Fresh seeds were dried at room temperature, powdered, and macerated in 1:5 dried plant weight to solvent (ethanol) volume ratio for 3 days. The filtrate was collected and the residues were subjected to further macerating with ethanol. The filtrates were combined and concentrated to dryness under reduced pressure using a rotary evaporator at 45°C to 50°C in order to obtain the crude extracts.[15]

5(3-(4, 5-Dimethylthiazol-2-yl)-2.5-diphenyl tetrazolium bromide) MTT assay

The extract used in all cell culture assays was diluted in the growth media of the J774A.1 cell line. The vehicle for initial stock of the drug was 0.1% dimethyl sulfoxide (DMSO).

Effects of MPSE on the viability of macrophages were detected using the MTT assay. The J774A.1 cells were seeded at a density of 5.0×10^3 cells/mL in a 96-well plate, treated with MPSE at concentrations ranging from 31.25 to 1000 µg/mL, or left untreated as a control and incubated for 24 h under 5% CO_2 at 37°C. Then 20 µL of MTT solution was added to each well and the plate was incubated for 3 h, after which the purple formazan was dissolved with DMSO. Absorbance was determined at 570 nm with the reference at 630 nm using a microplate reader (Tecan, Austria). Each experiment was repeated three times with triplicate wells for each concentration.[16]

NO assay

Nitrite concentration was detected using the Griess reaction. Pretreatment of macrophage cells was performed with MPSE at concentrations ranging from 31.25 to 200 µg/mL, or 0.5 µg/mL dexamethasone (DXM) as a positive control, followed by incubation for 1 h. To trigger the inflammatory response, LPS was added to the treatment wells of the 96-well plate at a concentration of 1 µg/mL per well. Nitrite in the cell culture supernatants was quantified according to methods described previously.[17]

IL-1β cytokine determination via ELISA

The macrophage cell suspensions with concentrations adjusted to 3×10^5 cells/mL were seeded into 24-well plates and cultured for 24 h. The cells were pretreated with MPSE at concentrations ranging from 31.25 to 200 µg/mL, or 0.5 µg/mL DXM as a positive control, and then incubated for 1 h under the same culture conditions. Then 1 µL of 1 mg/mL LPS was added to the treatment cells to activate the macrophages. ELISA kits (Cusabio Biotech Co. Ltd, USA) were used for interleukin IL-1β determinations in the supernatants, using spectrophotometric measurement according to the manufacturer's instructions. The cytokine concentrations were calculated as percentage to the LPS-induced control, which was set to 100% IL-1β production.

Statistical analysis

All data were expressed as mean ± standard error, and statistical significance was determined by one-way ANOVA with Tukey's *post-hoc* test using GraphPad Prism 6.0 statistical software with significant differences set at $p<0.01$ and $p<0.001$.

RESULTS

Cytotoxicity assay

Detection of suitable concentration ranges, which are not toxic, can be used for further *in vitro* anti-inflammatory screening assays of MPSE. The colorimetric assay results showed that increasing concentrations of MPSE caused reduction in macrophage cell viability. On the other hand, MPSE was not toxic to macrophages at concentrations ranging from 31.25 to 125 µg/mL when compared to culture media without seed extract acting as the control (Figure 1).

Inhibition effects of M. peregrina on NO production

To assess the potential of MPSE to modulate NO release in macrophages, nitrite concentrations were detected in the

culture supernatants of LPS-induced macrophages in the absence or presence of MPSE. The results shown in Figure 2 demonstrated that the treated LPS group activated nitrite production by the macrophage cells. On the other hand, treatment with different concentrations of MPSE as well as DXM significantly ($p<0.001$) inhibited nitrite generation from the LPS-induced macrophages. The MPSE suppressed nitrite production to 64.2%, 43.1%, 34.9%, and 30.1% of the LPS-stimulated control at concentrations of 25, 50, 100, and 200 µg/mL, respectively.

Effects of M. peregrina on LPS-induced IL-1β expression in J774A.1 macrophages

IL-1β is a potent activator that may stimulate NO production in macrophages. The activation of macrophages with LPS trigged the expression of proinflammatory cytokines IL-1β in a concentration-dependent manner as shown in Figure 3. The MPSE significantly suppressed LPS-induced IL-1β expression in a concentration-dependent manner with values of 54.4%, 49.7%, 24.6%, and 21.9% of the LPS-stimulated control at concentrations of 25, 50, 100, and 200 µg/mL, respectively. Moreover, pretreatment of stimulated cells with MPSE significantly ($p<0.001$) decreased the expression of IL-1β in comparison to untreated control cells with MPSE.

DISCUSSION

Many traditional plants have been shown to possess excellent medicinal properties against various diseases. Although *M. peregrina* seeds have been reported to be widely used in traditional medicine, only a few scientific studies exist on its therapeutic efficacy and mechanism of action.[11,14,18,19] As a follow-up to those studies, our aim was to investigate the effects of MPSE, which may be considered a potential anti-inflammatory drug, on NO and IL-1β in LPS-induced J774A.1 macrophage cells. Macrophages are the predominant cells in immunologic responses. In the laboratory, the J774A.1 macrophage cell line is one of the most common types of cells used for screening anti-inflammatory drugs *in vitro*, because these cells share phenotypic and functional features with normal macrophages.[20-22] In the present study, the cytotoxicity assay of MPSE on J774A.1 cells showed that MPSE did not have a toxic effect on macrophage cells since cell viability was more than 80%. Concentrations ranging from 31.25 to 200 µg/mL were chosen for anti-inflammatory screening of MPSE on J774A.1 cells.

The secretion of NO and IL-1β can be stimulated by a variety of compounds including LPS, a macrophage activator. Thus, one of the phenomena in inflammation is massive production of these molecules by activated macrophages, causing intense inflammatory reactions.[23]

In the present study, it was found that MPSE caused dose-dependent suppression of nitrite levels in LPS -induced macrophages. Nevertheless, the generation of pro inflammatory cytokines, such as IL-1β, and TNF-α is important for the induction of NO production in LPS-induced macrophages through NF-αB activation.[7,23,24] The present study also determined that MPSE can modulate IL-1β expression in inflammatory cells. The inhibited level of NO synthesis observed in the macrophage culture might be related to the antioxidant capacity and suppression of pro-inflammatory cytokine release provided by MPSE.

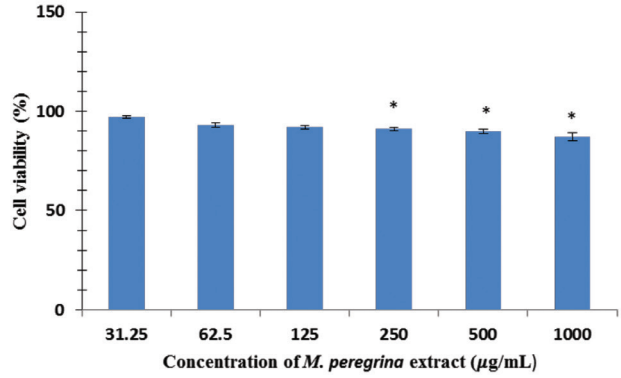

Figure 1. Viability of J774A.1 macrophage via MTT assay after treatment with MPSE. Values are mean ± standard deviation. $p<0.01$ versus control

MPSE: *Moringa peregrina* seed ethanolic extract

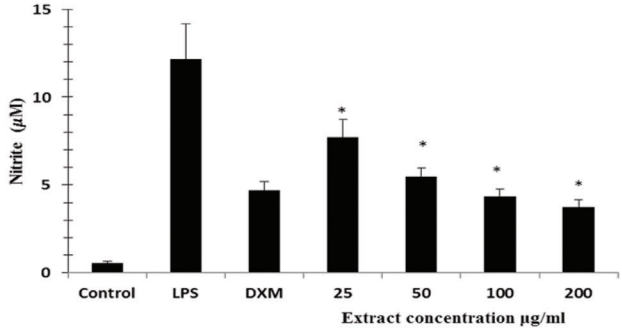

Figure 2. Effects of MPSE, and DXM on nitric oxide production by LPS-induced macrophage J774A.1 cells. Values are mean ± standard deviation. * Indicates significantly different from those of untreated lipopolysaccharide-activated J774A.1 cells (LPS) at $p<0.001$

MPSE: *Moringa peregrina* seed ethanolic extract, DXM: Dexamethasone, LPS: Lipopolysaccharide

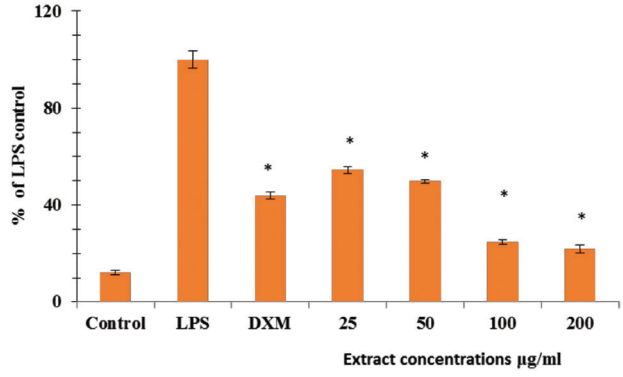

Figure 3. Effects of MPSE and DXM on IL-1β generation by LPS-induced J774A.1 macrophage cells. Values are mean ± standard deviation. * Indicates significantly different from those of untreated lipopolysaccharide-activated J774A.1 cells (LPS) at $p<0.001$

MPSE: *Moringa peregrina* seed ethanolic extract, DXM: Dexamethasone, LPS: Lipopolysaccharide, IL: Interleukin

MPSE has been reported to contain high amounts of oleic acid, linoleic acid, tocopherols, and phenolic compounds, which are attributed to the NO radical scavenging and anti-inflammatory properties of extract.[1,3,14,24-26] Our outcome is in agreement with findings reported by Fard et al.,[26] who stated that *M. oleifera* has a significant inhibitory effect on the secretion of NO and IL-1β.

CONCLUSIONS

M. peregrina seeds, which act as inhibitors of NO and IL-1β production in LPS-activated macrophage cells, may be suggested as good anti-inflammatory agents that could normalize the conditions created by inflammation. This study has supported the traditional use of seeds of *M. peregrina* in the treatment of inflammatory-related conditions.

ACKNOWLEDGEMENTS

This study was financially supported by the University of Malaya PPP Grant no. PG059-2013A.

Conflict of Interest: No conflict of interest was declared by the authors.

REFERENCES

1. Cheenpracha S, Park E, Rostama B, Pezzuto J, Chang L. Inhibition of nitric oxide (NO) production in lipopolysaccharide (LPS)-activated murine macrophage RAW 264.7 cells by the norsesterterpene peroxide, epimuqubilin A. Mar Drugs. 2010;8:429-437.
2. Arteaga Figueroa L, Barbosa Navarro L, Patiño Vera M, Petricevich VL. Preliminary studies of the immunomodulator effect of the *Bougainvillea xbuttiana* extract in a mouse mode. Evid Based Complement Alternat Med. 2015;2015:479412.
3. Liu Y, Song M, Che T, Bravo D, Pettigrew J. Anti-inflammatory effects of several plant extracts on porcine alveolar macrophages *in vitro*. J Anim Sci. 2012;90:2774-2783.
4. Azadmehr A, Afshari A, Baradaran B, Hajiaghaee R, Rezazadeh S, Monsef-Esfahani H. Suppression of nitric oxide production in activated murine peritoneal macrophages *in vitro* and *ex vivo* by *Scrophularia striata* ethanolic extract. J Ethnopharmacol. 2009;124:166-169.
5. Yang EJ, Yim EY, Song G, Kim GO, Hyun CG. Inhibition of nitric oxide production in lipopolysaccharide-activated RAW 264.7 macrophages by Jeju plant extracts. Interdiscip Toxicol. 2009;2:245-249.
6. Blonska M, Czuba ZP, Krol W. Effect of Flavone Derivatives on Interleukin-1β (IL-1β) mRNA Expression and IL-1β Protein Synthesis in Stimulated RAW 264.7 Macrophages. Scand J Immunol. 2003;57:162-167.
7. Amirghofran Z, Malek-Hosseini S, Golmoghaddam H, Kalantar F, Shabani M. Inhibition of nitric oxide production and proinflammatory cytokines by several medicinal plants. Iran J Immunol. 2011;8:159-169.
8. Bogdan C. Nitric oxide and the immune response. Nat Immunol. 2001;210:907-916.
9. Lee D, Lau A. Effects of *Panax ginseng* on tumor necrosis factor-α-mediated inflammation: a mini-review. Molecules. 2011;16:2802-2816.
10. Al-Majali IS, Al-Oran SA, Hassuneh MR, Al-Qaralleh HN, Rayyan WA, Al-Thunibat OY, Mallah E, Abu-Rayyan A, Salem S. Immunomodulatory effect of *Moringa peregrina* leaves, *ex vivo* and *in vivo* study. Cent Eur J Immunol. 2017;42:231-238.
11. El-Hak HNG, Moustafa ARA, Mansour SR. Toxic effect of *Moringa peregrina* seeds on histological and biochemical analyses of adult male Albino rats. Toxicol Rep. 2017;12:38-45.
12. Koheil M, Hussein M, Othman M, El-Haddad A. Anti-inflammatory and antioxidant activities of *Moringa peregrina* seeds. Free Rad Antiox. 2011;1:49-61.
13. Selvakumar D, Natarajan P. Hepato-protective activity of *Moringa oleifera* Lam leaves in carbon tetrachloride induced hepato-toxicity in albino rats. Phcog Mag. 2008;4:97-98.
14. Abd El Baky H, El-Baroty S. Biological activity of the Egyptian *Moringa peregrina* seed oil, Paper presented at International Conference of Agricultural Engineering; 2012:8-12.
15. Albaayit SF, Abba Y, Abdullah R, Abdullah N. Evaluation of antioxidant activity and acute toxicity of *Clausena excavata* leaves extract. Evid Based Complement Alternat Med. 2014;2014:975450.
16. Albaayit S, Abba Y, Abdullah R, Abdullah N. Effect of *Clausena excavata* Burm. F. (Rutaceae) leaf extract on wound healing and antioxidant activity in rats. Drug Des Devel Ther. 2015;9:3507-3518.
17. Adewoyin M, Mohsin S, Arulselvan P, Hussein M, Fakurazi S. Enhanced anti-inflammatory potential of cinnamate-zinc layered hydroxide in lipopolysaccharide-stimulated RAW 264.7 macrophages. Drug Des Devel Ther. 2015;9:2475-2484.
18. Lalas S, Gortzi O, Athanasiadis V, Tsaknis J, Chinou I. Determination of antimicrobial activity and resistance to oxidation of *Moringa peregrina* seed oil. Molecules. 2012;17:2330-2334.
19. Padayache B, Baijnath H. An overview of the medicinal importance of Moringaceae. J Med Plant Res. 2012;6:5831-5839.
20. Sommella E, Pepe G, Pagano F, Tenore G, Marzocco C, Manfra S, Campiglia P. UHPLC profiling and effects on LPS-stimulated J774A.1 macrophages of flavonoids from bergamot (*Citrus bergamia*) juice, an underestimated waste product with high antiinflammatory potential. J Funct Foods. 2014;71:641-649.
21. Xu Y, Liu L. Curcumin alleviates macrophage activation and lung inflammation induced by influenza virus infection through inhibiting the NF-κB signaling pathway. Influenza Other Respi Viruse. 2017;11:457-463.
22. Rabe SZ, Ghazanfari T, Siadat Z, Rastin M, Rabe SZ, Mahmoudi M. Anti-inflammatory effect of garlic 14-kDa protein on LPS-stimulated-J774A.1 macrophages. Immunopharmacol Immunotoxicol. 2015;37:158-164.
23. Tan WS, Arulselvan P, Karthivashan G, Fakurazi S. *Moringa oleifera* flower extract suppresses the activation of inflammatory mediators in lipopolysaccharide-stimulated RAW 264.7 macrophages via NF-κB pathway. Mediators Inflamm. 2015;2015:720171.
24. Kim J, Kim H, Choi H, Jo A, Kang H, Yun H, Im S, Choi C. Anti-Inflammatory Effects of *Stauntonia hexaphylla* Fruit Extract in Lipopolysaccharide-Activated RAW-264.7 Macrophages and Rats by Carrageenan-Induced Hind Paw Swelling. Nutrients. 2018;10:110.
25. El-Alfy TS, Ezzat SM, Hegazy AK, Amer AM, Kamel GM. Isolation of biologically active constituents from *Moringa peregrina* (Forssk.) Fiori. (family: Moringaceae) growing in Egypt. Phcog Mag. 2011;7:109-115.
26. Fard MT, Arulselvan P, Karthivashan G, Adam SK, Fakurazi S. Bioactive Extract from *Moringa oleifera* Inhibits the Proinflammatory Mediators in Lipopolysaccharide Stimulated Macrophages. Phcog Mag. 2015;11:556-563.

Turk J Pharm Sci 2019;16(3):366-370
DOI: 10.4274/tjps.galenos.2018.50103

ORIGINAL ARTICLE

The Influence of Piperine on the Radioprotective Effect of Curcumin in Irradiated Human Lymphocytes

Piperinin Işınlanmış İnsan Lenfositlerinde Kurkuminin Radyoprotektif Etkilerine Etkisi

Noora GHELISHLI[1,2], Arash GHASEMI[3], Seyed Jalal HOSSEINIMEHR[1]*

[1]Mazandaran University of Medical Sciences, Faculty of Pharmacy and Pharmaceutical Sciences Research Center, Department of Radiopharmacy, Sari, Iran
[2]Mazandaran University of Medical Sciences, Student Research Committee, Sari, Iran
[3]Mazandaran University of Medical Sciences, Faculty of Medicine, Department of Radiology and Radiation Oncology, Sari, Iran

ABSTRACT

Objectives: Ionizing radiation (IR) induces DNA damage in normal cells, leading to genotoxicity. The radioprotective effects of co-treatment with curcumin and piperine were investigated against genotoxicity induced by IR in human normal lymphocytes.

Materials and Methods: Human blood samples were pretreated with curcumin at different concentrations (5, 10, and 25 µg/mL) and/or piperine (2.5 µg/mL) and then were exposed to IR at a dose 1.5 Gy. The radioprotective effects of curcumin and piperine were assessed by micronucleus (MN) assay.

Results: Curcumin and piperine reduced the percentage of MN induced by IR in lymphocytes. Piperine alone significantly reduced genotoxicity induced by IR as compared to curcumin alone at all concentrations. An additive radioprotective effect was observed with combination of piperine and curcumin at the low concentration of 5 µg/mL, while this synergistic effect was not observed with curcumin at the higher concentrations of 10 and 25 µg/mL.

Conclusion: Piperine has a potent radioprotective effect at low concentration as compare to curcumin. However, an additive radioprotective effect was observed with co-treatment with piperine and curcumin at low concentration, while piperine increased the percentage of MN in normal lymphocytes when co-treated with curcumin at higher concentration.

Key words: Curcumin, piperine, radioprotective genotoxicity, ionizing radiation

ÖZ

Amaç: İyonize radyasyon (IR) normal hücrelerde DNA hasarına neden olarak genotoksisiteye neden olur. Curcumin ve piperin ile ortak tedavinin insan normal lenfositlerinde iyonlaştırıcı radyasyonun neden olduğu genotoksisiteye karşı koruyucu etkileri araştırıldı.

Gereç ve Yöntemler: İnsan kan numuneleri, farklı konsantrasyonlarda (5, 10 ve 25 µg/mL) kurkumin ve/veya (2.5 µg/mL) piperin içerisinde ile ön muamele edildi ve daha sonra 1.5 Gy'lik bir dozda IR'ye maruz bırakıldı. Curcumin ve piperinin radyo-koruyucu etkileri mikronükleus (MN) testi ile değerlendirildi.

Bulgular: Kurkumin ve piperin, lenfositlerde IR tarafından indüklenen MN yüzdesini azaltmıştır. Sadece piperin, tüm konsantrasyonlarda tek başına uygulanan kurkumin ile karşılaştırıldığında, IR tarafından indüklenen genotoksisiteyi önemli ölçüde azaltmıştır. Düşük konsantrasyonda 5 µg/mL'de piperin ve kurkumin kombinasyonu ile ilave bir radyo-koruyucu etki gözlenirken, bu sinerjistik etki 10 ila 25 µg/mL'lik yüksek konsantrasyonlarda kurkuminle gözlenmedi.

Sonuç: Piperin, kurkuminle karşılaştırıldığında düşük konsantrasyonda güçlü bir radyo-koruyucu etkiye sahiptir. Bununla birlikte, düşük konsantrasyonda piperin ve kurkumin ile birlikte yapılan muamele ile ilave bir radyo-koruyucu etki gözlenirken, piperin yüksek konsantrasyonda kurkumin ile birlikte muamele edildiğinde normal lenfositlerde MN oranını artırmıştır.

Anahtar kelimeler: Kurkumin, piperin, radyo-koruyucu genotoksisite, iyonize radyasyon

*Correspondence: **E-mail:** sjhosseinim@yahoo.com, **Phone:** 989113210663 **ORCID-ID:** orcid.org/0000-0001-8055-8036
Received: 27.05.2018, **Accepted:** 21.06.2018

INTRODUCTION

Ionizing radiation (IR) is widely used for cancer treatment in patients. In this strategy, IR produces free radicals and reactive oxygen species (ROS) when passing through cells. These toxic substances react with critical macromolecules such as DNA, resulting in genotoxicity and cell death. While IR is focused on cancerous cells, unwanted exposure to normal cells results in damage to normal tissue. The side effects induced by IR limit the use of radiotherapy in patients. Radioprotective agents protect normal cells against genotoxicity and death induced by IR.[1,2] Several protection mechanisms are proposed for radioprotective agents such as free radical scavenging and increasing endogenous cellular antioxidants enzymes.[2] Curcumin is a natural component that is prepared from *Curcuma longa* and widely used as an additive for flavoring in foods. This compound has several beneficial biological properties such as antioxidant, anti-inflammatory, and anticancer.[3,4] Curcumin protects cells from genotoxicity and death induced by IR.[5,6] Poor bioavailability in oral consumption is the main disadvantage of curcumin for clinical application.[7] It is interesting that some natural compounds act as an enhancer of curcumin through oral absorption. Piperine is a natural product prepared from black pepper (*Piper nigrum* L.). This natural product is consumed with *C. longa* as a spice in food. Piperine is used as an anticancer agent as well as a natural bioenhancer for curcumin.[8] Piperine enhances the protective effects of curcumin against oxidative stress-related diseases in animal models.[9,10] Moreover, synergistic effects of curcumin and piperine were observed in the suppression of tumor proliferation in animals.[11,12] With respect to the beneficial effects of piperine and curcumin on oxidative stress and prevention of cancer, the aim of the present study was to investigate the influence of piperine on the radioprotective effect of curcumin against genotoxicity induced by IR on normal human lymphocytes.

MATERIALS AND METHODS

Materials

Curcumin was prepared from Sami Labs (India) and piperine was from Qingado BNP Co. (China). Phytohemagglutinin M (PHA-M), Roswell Park Memorial Institute (RPMI-1640) medium, fetal bovine serum (FBS), penicillin, and streptomycin-L-glutamine were purchased from Gibco (USA). Cytochalasin-B was purchased from Sigma Chemicals Co. (St. Louis, MO, USA). Giemsa stain, methanol, and acetic acid were obtained from Merck (Germany).

Blood treatment

After obtaining permission from the research and ethical committees of Mazandaran University of Medical Sciences, this study was performed. Four healthy, nonsmoking male volunteers, aged from 22 to 28 years were enrolled. Twelve milliliters of whole blood was collected in heparinized tubes and divided among centrifuge tubes with 0.9 mL in each. Blood samples were pretreated with 100 µL of solution of curcumin at a concentration of 5, 10, or 25 µg/mL and/or piperine (2.5 µg/mL). These samples were incubated for 3 h at 37°C. Curcumin (CUR) and piperine (P) were dissolved in DMSO and diluted in RPMI cultural medium. The 12 samples groups were as follows: control, ionizing radiation (IR), 5 µg/mL CUR+IR, 10 µg/mL CUR+IR, 25 µg/mL CUR+IR, 5 µg/mL CUR+2.5 µg/mL (P)+IR, 10 µg/mL CUR+2.5 µg/mL (P)+IR, 25 µg/mL CUR+2.5 µg/mL (P)+IR, 2.5 µg/mL (P)+IR, 25 µg/mL CUR, 2.5 µg/mL (P), 5 µg/mL CUR+2.5 µg/mL (P). The curcumin concentrations were selected based on previous studies.[5,13] Piperine concentration was selected based on previous studies that showed P has a IC_{50} of 61 µg/mL on the HeLa cell line[14] and it did not exhibit any genotoxicity or cellular toxicity up to 60 µM (17 µg/mL).[15] Control samples were treated with diluted DMSO in RPMI at the same concentration as the other curcumin and/or piperine samples.

Ionizing radiation and micronucleus test

Whole blood samples in microtubes were kept on a plastic box containing water as a phantom and then were irradiated with a 6 MV X-ray beam produced by a linear accelerator (Siemens, Primus, Germany) at a dose of 1.5 Gy with a dose rate of 1.9 Gy/min. Samples from four volunteers were allocated as controls (nonirradiated samples). After irradiation, subsequently, 0.5 mL of each sample (control and irradiated samples in duplicate) was added to 4.4 mL of RPMI 1640 culture medium, which contained a mixture of 10% FBS and 100 µL of PHA. All cultures were incubated at 37°C. Cytochalasin B (100 µL at final concentration: 6 µL/mL) was added after 44 h of culture. Following 72 h of incubation, the cells were collected by centrifugation and resuspended in cold 0.75 M potassium chloride. The cells were immediately fixed in a fixative solution of methanol:acetic acid (6:1 V:V) two times. The fixed cells were dropped onto clean microscopic slides, air dried, and stained with 10% Giemsa solution. All slides were evaluated at 1000× magnification in order to determine the frequency of micronuclei in the cytokinesis-blocked binucleated cells with a well-preserved cytoplasm.[16] For each treated group from each volunteer, a total of 1000 binucleate cells (in the duplicate cultures) were examined to record the frequency of micronuclei-containing cells. All slides were evaluated by an expert using a light microscope. A total of 4000 binucleated lymphocytes were blindly counted in each treated group from three volunteers, and totally 48,000 binucleated lymphocytes were counted for the 12 treated groups in this study. The criteria for scoring micronuclei were a diameter between 1/16 and 1/3 of the main nuclei, nonrefractile, not linked to the main nuclei, and not overlapping the main nuclei.[16]

Statistical analysis

The data values are presented as mean ± standard deviation. The statistical analysis was performed using one-way ANOVA, as well as *post hoc* Tukey multiple comparison tests. A p value <0.05 was considered significant and highly significant (Prism 7 Software, 2016, USA).

RESULTS

A typical binucleated lymphocyte with a micronucleus is shown in Figure 1. The mean percentage of micronuclei in the irradiated samples was 8.57±0.09, while it was 0.71±0.06 in

the nonirradiated control samples. It showed a statistically significant increase (12-fold rise) in the frequency of micronuclei in irradiated samples at a dose of 1.5 Gy (Table 1, Figure 2) ($p<0.001$). In irradiated samples with CUR pretreatment, the frequency of micronuclei at the concentrations of 5, 10, or 25 µg/mL was 6.10±0.14%, 4.47±0.09%, and 4.35±0.19% (Table 1). The data demonstrate that samples pretreated with CUR at concentrations of 5, 10, or 25 µg/mL exhibited a significant decrease in the frequency of micronuclei as compared to irradiated samples without CUR addition ($p<0.001$). Total micronuclei frequencies were reduced by 1.40-, 1.92-, and 1.97-fold in irradiated samples with CUR treatment at concentrations of 5, 10, or 25 µg/mL, respectively, as compared to just irradiated samples (Table 1). The maximum protection of lymphocytes was observed with CUR treatment at a concentration of 25 µg/mL. A dose-manner protective effect was observed with CUR at concentrations of 5, 10, and 25 µg/mL ($p<0.01$). However, the nonirradiated sample with CUR treatment at a concentration of 25 µg/mL did not show any increased genotoxicity as compared to the control group.

In irradiated samples with CUR+P pretreatment, the frequency of micronuclei at the concentrations of 5 µg/mL CUR+2.5 µg/mL (P)+IR, 10 µg/mL CUR+2.5 µg/mL (P)+IR, and 25 µg/mL CUR+2.5 µg/mL (P)+IR was 3.07±0.24%, 4.87±0.26%, and 5.25±0.29%, respectively (Table 1). The data demonstrate that pretreated samples with CUR (5 µg/mL) and P (2.5 µg/mL) exhibited significant decreases in the frequency of micronuclei as compared to irradiated samples with CUR alone at all concentrations (5, 10 and 25 µg/mL). It is interesting to see increased frequencies of micronuclei in human lymphocytes treated with CUR+P+IR as compared to CUR (10 µg/mL)+IR or CUR (25 µg/mL)+IR ($p<0.05$). Piperine significantly reduced the frequency of micronuclei in irradiated lymphocytes as compared to irradiation alone. The frequency of micronucleus lymphocytes with P at a concentration of 2.5 µg/mL was insignificant as compared to control samples, while the combination of CUR (25 µg/mL) and P (2.5 µg/mL) increased significantly the frequency of micronuclei in binucleated lymphocytes as compared to control samples (Table 1, Figure 2).

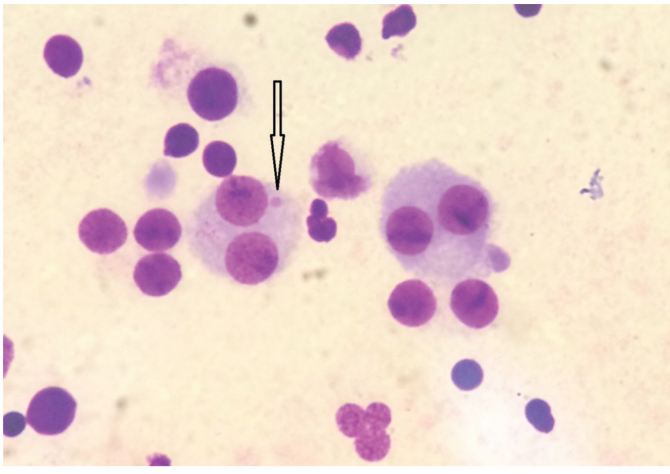

Figure 1. A typical binucleated lymphocyte with a micronucleus in our study

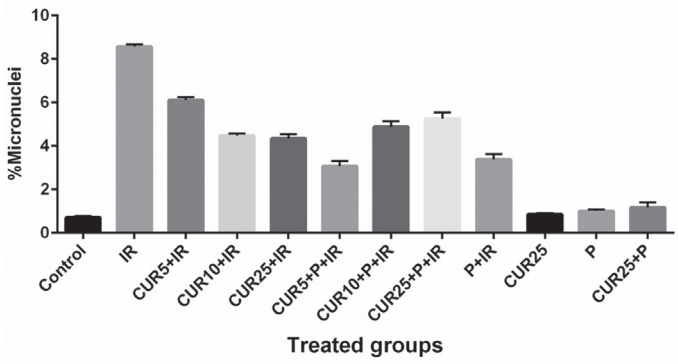

Figure 2. The effect of curcumin (CUR) and piperine (P) on frequency of micronuclei induced by 1.5 Gy X-ray radiation (IR) in cultured blood lymphocytes (n=4)

DISCUSSION

Curcumin, a natural product, is widely used in food and drug compositions and has several biological and pharmacological properties. Curcumin exhibits anticancer, anti-inflammatory, and antioxidant effects.[3,4] Curcumin scavenges free radicals and ROS[17] generated by toxic substances such as IR. The anti-inflammatory effect was reported for curcumin through diminishing cytokines and interleukins involved in the inflammation process.[18] Oxidative stress and inflammation are two suggested main mechanisms involved in cellular toxicity induced by IR. Curcumin acts as a radioprotective agent through

Table 1. The frequency of micronuclei induced *in vitro* by 1.5 Gy X-ray radiation (IR) in cultured blood lymphocytes at different concentrations of curcumin and/or piperine (P) (n=4)[a]

Volunteer treated group	% Micronuclei in binucleated lymphocytes				
	I	II	III	V	Mean ± standard deviation
Control	0.8	0.66	0.7	0.7	0.71±0.06
IR	8.6	8.5	8.7	8.5	8.57±0.09[b]
CUR5+IR	6	6.1	6.3	6	6.10±0.14[c]
CUR10+IR	4.6	4.5	4.4	4.4	4.47±0.09[c]
CUR25+IR	4.6	4.4	4.2	4.2	4.35±0.19[c]
CUR5+P+IR	2.9	3.1	2.9	3.4	3.07±0.24[c,d]
CUR10+P+IR	5	5.1	4.5	4.9	4.87±0.26[c]
CUR25+P+IR	5	5.5	5.5	5	5.25±0.29[c]
P+IR	3.5	3.5	3	3.5	3.37±0.25[c]
CUR25	0.8	0.9	0.8	0.9	0.85±0.06[e]
P	1	1.1	0.9	1	1.00±0.08[e]
CUR25+P	1.00	1.5	1.2	1	1.17±0.24[f]

[a]1000 binucleated lymphocytes were examined in each sample, and 4000 binucleated lymphocytes from four volunteers in each group, [b]$p<0.001$ compared to control, [c]$p<0.001$ compared to IR, [##]$p<0.01$ compared to control group, [d]$p<0.01$ compared to CUR5+IR, CUR10+IR, CUR25+IR, [e]Nonsignificant compared to control, [f]$p<0.05$ compared to control,
C: Control, IR: Ionizing radiation, CUR5: Curcumin 5 µg/mL, CUR10: Curcumin 10 µg/mL, CUR25: Curcumin 25 µg/mL, P: Piperine 2.5 µg/mL

the two mentioned mechanisms. Recently we showed that curcumin had a protective effect against genotoxicity induced by radioactive iodine in human lymphocytes.[5] Curcumin could selectively sensitize thyroid cancer cells to death induced by radioactive iodine without any toxicity on nonmalignant fibroblast cells.[13] In the present study, we showed that curcumin significantly protected human healthy lymphocytes from genotoxicity induced by external IR. These results showed curcumin has a radioprotective effect on normal cells and a radiosensitizing effect on cancer cells, and so is promising for use as a natural agent in cancer therapy.

The highest radioprotection of lymphocytes with curcumin alone treatment was observed at a concentration of 25 µg/mL. Although this maximum protection is interesting, this concentration should be achieved *in vivo* by oral administration of curcumin. Curcumin could not achieve its expected therapeutic outcome *in vivo* due to its low solubility and poor bioavailability. The poor oral bioavailability of curcumin is due to its limited intestinal uptake and rapid metabolism and this is the biggest limitation of this natural product for human usage.[7] Several strategies have been applied for enhancement of the oral bioavailability of curcumin such as improvement of its formulation[19,20] and bioavailability enhancement.[21] Piperine, as a major plant alkaloid, is widely used as a condiment and flavoring agent for many types of dishes. Piperine acts as an enhancer of the bioavailability and pharmacological activity of curcumin.[11,22] There are two suggested mechanisms for piperine as a bioenhancer: promoting rapid absorption of drugs and nutrients and inhibiting enzymes involved in the biotransformation of drugs. Piperine is a potent inhibitor of the P-gp efflux transporter present in the gastrointestinal wall.[21,23] Although the enhancing effect of piperine has been extensively studied *in vivo* for improvement of oral bioavailability, there are limited *in vitro* studies on the co-treatment of curcumin with piperine for cytoprotective effect or cytotoxicity. The uptake of curcumin was evaluated with curcumin–piperine mixture emulsion in Caco-2 cell cultures as a model for intestinal uptake. The extent of curcumin uptake was improved markedly by piperine addition.[24] The combined effect of curcumin and piperine was studied on human osteogenic sarcoma cells. Curcumin combined with piperine suppressed osteoclastogenesis *in vitro* without causing any cytotoxic effects in periodontal ligament cells.[25] Our study showed that piperine alone significantly reduced genotoxicity induced by IR in lymphocytes at a concentration of 2.5 µg/mL (8.7 µM) and was more potent than CUR at a concentration of 25 µg/mL (68 µM). Piperine exhibited a 1.3-fold decrease in the frequency of micronuclei as compared to CUR, while the molar concentration of piperine was 8-fold lower than that of CUR. In the present study, piperine was used at a concentration of 2.5 µg/mL which was lower than that in other reports of the protective effects of piperine *in vitro*.[26,27] For the first time, the present study showed that piperine exhibited a radioprotective effect *in vitro* on normal cells that was more potent than the effect of CUR. Recently the comparative efficacy of piperine and curcumin in deltamethrin (DLM) (DLM; a potent immunotoxicant)-induced splenic apoptosis and altered immune functions was evaluated. That study strongly demonstrated that piperine displayed more anti-oxidative, anti-apoptotic, and chemoprotective properties in the DLM-induced splenic apoptosis as compared to curcumin.[28] Other studies have shown the protective effect of piperine against cellular toxicity induced by oxidative stress in cellular and animal models. The mechanisms of the protective effect of piperine are antioxidant, reduction of intracellular ROS level, reduction of levels of pro-inflammatory mediators, and anti-apoptotic.[29,30] Piperine has a synergistic effect with CUR in reduction of micronucleus frequency in lymphocytes at a low concentration of CUR (5 µg/mL). In the present study, co-treatment with CUR (5 µg/mL) and piperine (2.5 µg/mL) showed the highest radioprotective effect against genotoxicity induced by IR on human lymphocytes, while no additive protective effects were observed with CUR at concentrations of 10 and 25 µg/mL with piperine. It is interesting that addition of piperine to CUR at concentrations of 10 and 25 µg/mL resulted in a reduction in protective efficacy as compared to CUR alone at these concentrations. On the other hand, CUR alone at concentrations of 10 and 25 µg/mL is more potent than addition of piperine to CUR (10 and 25 µg/mL) for radioprotection. It is clear that the synergistic effect of CUR and piperine is concentration dependent and a diminishing radioprotective effect was observed with increasing concentration of CUR with piperine. Increased genotoxicity was observed in co-treatment with CUR and piperine at concentrations of 25 µg/mL and 2.5 µg/mL, respectively, on human normal lymphocytes. The exact mechanism of the cellular toxicity of piperine and CUR at high concentrations is unclear and future studies are needed for finding the exact mechanism.

CONCLUSIONS

In the present study, piperine exhibited a potential radioprotective effect at a low concentration of 2.5 µg/mL that was more potent than the effect of curcumin at a concentration up to 25 µg/mL. The addition of piperine to curcumin at a low concentration of 5 µg/mL caused a synergistic effect as compared to curcumin alone in the radioprotective effect, while additional protection was not observed at higher concentrations of curcumin with piperine.

ACKNOWLEDGEMENT

This study was supported by a grant from Mazandaran University of Medical Sciences (grant number 2773).

Conflict of Interest: No conflict of interest was declared by the authors.

REFERENCES

1. Hosseinimehr SJ, Ahmadi A, Beiki D, Habibi E, Mahmoudzadeh A. Protective effects of hesperidin against genotoxicity induced by (99m)Tc-MIBI in human cultured lymphocyte cells. Nucl Med Biol. 2009;36:863-867.
2. Hosseinimehr SJ. Trends in the development of radioprotective agents.

Drug Discov Today. 2007;12:794-805.

3. Hosseinimehr SJ. A review of preventive and therapeutic effects of curcumin in patients with cancer. Journal of Clinical Excellence. 2014;2:13.
4. Agrawal DK, Mishra PK. Curcumin and its analogues: potential anticancer agents. Med Res Rev. 2010;30:818-860.
5. Shafaghati N, Hedayati M, Hosseinimehr SJ. Protective effects of curcumin against genotoxicity induced by 131-iodine in human cultured lymphocyte cells. Pharmacogn Mag. 2014;10:106-110.
6. Sebastia N, Montoro A, Montoro A, Almonacid M, Villaescusa JI, Cervera J, Such E, Silla A, Soriano JM. Assessment *in vitro* of radioprotective efficacy of curcumin and resveratrol. Radiation Measurements. 2011;46:962-966.
7. Liu W, Zhai Y, Heng X, Che FY, Chen W, Sun D, Zhai G. Oral bioavailability of curcumin: problems and advancements. J Drug Target. 2016;24:694-702.
8. Shoba G, Joy D, Joseph T, Majeed M, Rajendran R, Srinivas PS. Influence of piperine on the pharmacokinetics of curcumin in animals and human volunteers. Planta Med. 1998;64:353-356.
9. Rinwa P, Kumar A. Piperine potentiates the protective effects of curcumin against chronic unpredictable stress-induced cognitive impairment and oxidative damage in mice. Brain Res. 2012;1488:38-50.
10. Singh S, Jamwal S, Kumar P. Piperine Enhances the Protective Effect of Curcumin Against 3-NP Induced Neurotoxicity: Possible Neurotransmitters Modulation Mechanism. Neurochem Res. 2015;40:1758-1766.
11. Patial V, S M, Sharma S, Pratap K, Singh D, Padwad YS. Synergistic effect of curcumin and piperine in suppression of DENA-induced hepatocellular carcinoma in rats. Environ Toxicol Pharmacol. 2015;40:445-452.
12. Sehgal A, Kumar M, Jain M, Dhawan DK. Modulatory effects of curcumin in conjunction with piperine on benzo(a)pyrene-mediated DNA adducts and biotransformation enzymes. Nutr Cancer. 2013;65:885-890.
13. Hosseinimehr SJ, Hosseini SA. Radiosensitive effect of curcumin on thyroid cancer cell death induced by radioiodine-131. Interdiscip Toxicol. 2014;7:85-88.
14. Paarakh PM, Sreeram DC, D SS, Ganapathy SP. *In vitro* cytotoxic and *in silico* activity of piperine isolated from *Piper nigrum* fruits Linn. In Silico Pharmacol. 2015;3:9.
15. Thiel A, Buskens C, Woehrle T, Etheve S, Schoenmakers A, Fehr M, Beilstein P. Black pepper constituent piperine: genotoxicity studies *in vitro* and *in vivo*. Food Chem Toxicol. 2014;66:350-357.
16. Fenech M. The *in vitro* micronucleus technique. Mutat Res. 2000;455:81-95.
17. Aftab N, Vieira A. Antioxidant activities of curcumin and combinations of this curcuminoid with other phytochemicals. Phytother Res. 2010;24:500-502.
18. Okunieff P, Xu J, Hu D, Liu W, Zhang L, Morrow G, Pentland A, Ryan JL, Ding I. Curcumin protects against radiation-induced acute and chronic cutaneous toxicity in mice and decreases mRNA expression of inflammatory and fibrogenic cytokines. Int J Radiat Oncol Biol Phy. 2006;65:890-898.
19. Schiborr C, Kocher A, Behnam D, Jandasek J, Toelstede S, Frank J. The oral bioavailability of curcumin from micronized powder and liquid micelles is significantly increased in healthy humans and differs between sexes. Mol Nutr Food Res. 2014;58:516-527.
20. Sasaki H, Sunagawa Y, Takahashi K, Imaizumi A, Fukuda H, Hashimoto T, Wada H, Katanasaka Y, Kakeya H, Fujita M, Hasegawa K, Morimoto T. Innovative preparation of curcumin for improved oral bioavailability. Biol Pharm Bull. 2011;34:660-665.
21. Ajazuddin, Alexander A, Qureshi A, Kumari L, Vaishnav P, Sharma M, Saraf S, Saraf S. Role of herbal bioactives as a potential bioavailability enhancer for Active Pharmaceutical Ingredients. Fitoterapia. 2014;97:1-14.
22. Tu YS, Fu JW, Sun DM, Zhang JJ, Yao N, Huang DE, Shi ZQ. Preparation, characterisation and evaluation of curcumin with piperine-loaded cubosome nanoparticles. J Microencapsul. 2014;31:551-559.
23. Singh DV, Godbole MM, Misra K. A plausible explanation for enhanced bioavailability of P-gp substrates in presence of piperine: simulation for next generation of P-gp inhibitors. J Mol Model. 2013;19:227-238.
24. Gülseren İ, Guri A, Corredig M. Effect of interfacial composition on uptake of curcumin-piperine mixtures in oil in water emulsions by Caco-2 cells. Food Funct. 2014;5:1218-1223.
25. Martins CA, Leyhausen G, Volk J, Geurtsen W. Curcumin in Combination with Piperine Suppresses Osteoclastogenesis In Vitro. J Endod. 2015;41:1638-1645.
26. Fu M, Sun ZH, Zuo HC. Neuroprotective effect of piperine on primarily cultured hippocampal neurons. Biol Pharm Bull. 2010;33:598-603.
27. Pathak N, Khandelwal S. Cytoprotective and immunomodulating properties of piperine on murine splenocytes: an *in vitro* study. Eur J Pharmacol. 2007;576:160-170.
28. Kumar A, Sharma N. Comparative efficacy of piperine and curcumin in deltamethrin induced splenic apoptosis and altered immune functions. Pestic Biochem Physiol. 2015;119:16-27.
29. Ma Y, Tian M, Liu P, Wang Z, Guan Y, Liu Y, Wang Y, Shan Z. Piperine effectively protects primary cultured atrial myocytes from oxidative damage in the infant rabbit model. Mol Med Rep. 2014;10:2627-2632.
30. Mao QQ, Huang Z, Ip SP, Xian YF, Che CT. Protective effects of piperine against corticosterone-induced neurotoxicity in PC12 cells. Cell Mol Neurobiol. 2012;32:531-537.

Turk J Pharm Sci 2019;16(3):371-374
DOI: 10.4274/tjps.galenos.2018.79095

REVIEW

An Overview of iQOS® as a New Heat-Not-Burn Tobacco Product and Its Potential Effects on Human Health and the Environment

Isıtmalı Tütün Ürünü iQOS® Hakkında Değerlendirme, İnsan ve Çevre Sağlığı Üzerindeki Etkileri

Rahman BAŞARAN[1], Naile Merve GÜVEN[2], Benay Can EKE[2]*

[1]School of Chemistry, University of Leeds, Leeds, United Kingdom
[2]Ankara University, Faculty of Pharmacy, Department of Pharmaceutical Toxicology, Ankara, Turkey

ABSTRACT

Tobacco smoke from regular cigarettes contains a number of harmful chemicals such as nicotine, arsenic, benzene, carbon monoxide, heavy metals, and tobacco-derived nitrosamines. About 1% of over 7000 chemical substances formed by burning tobacco are identified as the leading causes or possible risk factors of smoking-related diseases such as lung cancer, cardiovascular diseases, and emphysema. The concept of heating tobacco without combustion and smoke has been designed for more than two decades. The products developed with this idea, known as "Heat-Not-Burn" tobacco cigarettes, were first introduced in the late 1980s but did not achieve commercial success. However, the tobacco giants have been trying to remarket tobacco heating systems with new technological and modified features for over 10 years. I-Quit-Ordinary-Smoking (iQOS®) is one of the latest heat-not-burn tobacco products, first launched in Japan and Italy. The company then made a submission to the Food and Drug Administration as a modified-risk tobacco product application to sell its own tobacco-heating device iQOS® under its Marlboro® brand in the USA with reduced-risk claims in 2016, but it was rejected. This device is, however, now sold in more than four dozen countries. There are some striking claims that iQOS®, which is described as a novel hybrid product between traditional cigarettes and electronic cigarettes, offers an alternative way to substantially reduce the amount of harmful components compared with traditional cigarettes by its new technology in which tobacco is heated up to 350˚C instead of being burnt. It is claimed to produce vapour containing nearly 90% less toxic substances than cigarette smoke and not be a source of second-hand smoking negatively affecting indoor air quality. The purpose of this article is to objectively review the potential effects of iQOS® on human health and the environment by searching and integrating the published research findings.

Key words: iQOS®, heat-not-burn tobacco products, cigarette, nicotine, smoking

ÖZ

Geleneksel sigaraların yanması sonucunda ortaya çıkan tütün dumanı nikotin, arsenik, benzen, karbonmonoksit, ağır metaller ve tütüne özgü nitrozaminler gibi birçok zararlı kimyasalı içermektedir. Tütünün yanmasıyla oluşan 7000'den fazla kimyasalın yaklaşık %1'i akciğer kanseri, kardiyovasküler hastalıklar ve amfizem gibi sigara içimine bağlı hastalıkların nedeni veya potansiyel nedeni olduğu bilinmektedir. Sigara içiminde tütünün yanması yerine ısıtıldığı sistemler, yirmi yıldan fazla süredir tasarlanmaktadır. "Heat-Not-Burn" tütün ürünleri olarak bilinen bu ürünler, ilk kez 1988'de piyasaya çıkmış ancak ticari bir başarı sağlayamamıştır. Son 10 yılda, pek çok sigara firması tarafından yeni tasarımlı ısıtmalı tütün ürünleri yeniden piyasaya sürülmektedir. İlk kez Japonya ve İtalya'da tanıtılan I-Quit-Ordinary-Smoking (iQOS®) için modifiye edilmiş risk tütün ürünü olarak Amerikan Gıda ve İlaç Dairesi'ne başvurusu yapılmış fakat bu başvuru reddedilmiştir. Ancak günümüzde 41 ülkede halen satışı devam etmektedir. Geleneksel sigara ve elektronik sigara arasında melez bir ürün olarak kabul edilen iQOS®, tütünün yanmadığı ve 350˚C'ye kadar ısıtıldığı yeni teknolojisi ile geleneksel sigaralara kıyasla zararlı bileşenlerin seviyesinde önemli derecede azalma vadetmektedir. Tamamen iQOS®'ye geçiş yapan sigara içicilerinde birden fazla zararlı bileşene maruz kalma oranının azaldığı, iQOS® tarafından üretilen buharın sigara dumanından çok daha az toksik olduğu, iQOS® kullanımının iç hava kalitesini olumsuz yönde etkilemediği ve iQOS®'nin pasif içicilik için bir duman kaynağı olmadığı konusunda bazı görüşler mevcuttur. Bu çalışmanın amacı, iQOS® üzerine yapılan bilimsel araştırmaların incelenerek, iQOS®'nin insan sağlığı ve çevre üzerine etkilerini objektif bir şekilde ortaya koymaktır.

Anahtar kelimeler: iQOS®, ısıtmalı tütün ürünleri, nikotin, tütün, sigara

***Correspondence: E-mail:** eke@pharmacy.ankara.edu.tr, **Phone:** +90 312 203 31 15 **ORCID-ID:** orcid.org/0000-0001-9817-9034
Received: 01.02.2019 , **Accepted:** 28.02.2019

INTRODUCTION

The combustion of tobacco generates inhalable toxic chemicals that cause some deadly diseases, notably cancer. Tobacco companies have long been developing products such as e-cigarettes and nicotine replacement therapy to prevent burning. In response to the scientifically proven harmful effects of traditional smoking, heat-not-burn tobacco products as a new attack by the tobacco industry are gaining popularity and taking over the markets. While hot debates still continue over the use of such devices, Philip Morris International (PMI) has embarked upon marketing a new generation heat-not-burn tobacco product, called I-Quit-Ordinary-Smoking (iQOS®), which is claimed to have revolutionary technology that heats tobacco instead of burning it. PMI claims that this product gives the real taste of tobacco with no fire, no ash, and less smoke as well as eliminating the undesirable effects related to smoking by reducing the levels of toxic chemicals.[1] iQOS® consists of three main components: a tobacco stick (called a HeatStick), a battery-powered tobacco heating holder, and a charger. It is used by inserting the disposable tobacco stick into a slot and then heating it at temperatures below 350˚C. The holder provides heat to the tobacco unit for about 6 min or 12-14 puffs. The most important difference between iQOS® and traditional cigarettes is that while tobacco in a regular cigarette is burned at above 600˚C, iQOS® just heats tobacco up to 350˚C. It has long been said that iQOS® does not release smoke containing unhealthy components due to not burning tobacco at high temperatures, and it prevents users from being exposed to the same levels of carcinogens and toxic chemicals found in a conventional cigarette.[2,3]

More than $3 billion has been spent over a 10-year period in research and development to design and produce new devices like iQOS® according to PMI's statements, and pilot schemes for iQOS® began in Italy and Japan during late 2014.[2] However, Food and Drug Administration (FDA) approval was required to market the device in America as a less harmful product than continuing to smoke cigarettes in accordance with its commercial purposes. PMI filed modified risk tobacco products (MRTP) applications MRTP for three different iQOS® cartridges (Marlboro HeatSticks, Marlboro Smooth Menthol HeatSticks, and Marlboro Fresh Menthol HeatSticks) with the US FDA on 5th December 2016. PMI's claims in this application are as follows: completely switching from cigarettes to iQOS® considerably reduces the risk of tobacco-related diseases and would cause less harm than regular smoking by significantly preventing exposure to harmful or potentially harmful chemicals.[4,5] The FDA's Tobacco Products Scientific Advisory Committee discussed the MRTP applications in January 2018 and rejected the proposal that iQOS® should be marketed as healthier than traditional cigarettes in the US,[6,7] but the product is currently being sold in more than 40 countries.[2]

There is no legal regulation in respect of using iQOS® in this country. Smoking accounts for 27% of deaths[8] and 120.000 people (one person every 5 min) die every year in Turkey due to tobacco and tobacco-related diseases. Therefore, all kinds of legislation of practice that this country will put into place regarding cigarettes and tobacco products are of utmost importance. Turkey has been fighting a running battle against tobacco since 2008. As smoking-related regulatory efforts have been correctly addressed to achieve sustainable progress, Turkey has become the first country to achieve the highest level of implementation for all six World Health Organization (WHO) tobacco control policy measures (Monitor, Protect, Offer, Warn, Enforce, Raise). After the implementation of comprehensive laws in 2009, the overall rate of smoking, which was 31.2% in 2008, decreased to 27% in 2012[9] and 23.8% in 2015, and it is estimated that this rate will drop to 19% in 2025 in Turkey.[10] In addition to these advances, the exposure prevalence in workplaces and restaurants decreased considerably from 37% and 56% in 2008 to 16% and 13% in 2012, respectively. Despite the smoking ban in enclosed public spaces in Turkey, the rate of passive smoking is still over 50% in total because exposure to smoke in homes is quite high (38.3%).[11] Cigarette smoke, also called passive smoke or environmental tobacco smoke, contains 72 fully characterized carcinogens[12] as well as at least six toxic substances that are toxic to reproduction. Second-hand smokers inhale the combination of the smoke exhaled by an active smoker and the smoke from the burning cigarette, and they are more exposed to these toxic chemicals than regular smokers. Furthermore, there is no known safe level of exposure to passive smoking.[13] Legal regulation is therefore necessary for iQOS®, which does not have a risk assessment in this country.

As iQOS® has a short (4-year) history, there are not enough studies on its effects on human and environmental health. As investigations on iQOS® were carried out only by the producing company and its competitors in those years and this has driven the need for more independent scientific data about its safety, the number of studies on this product has been increasing considerably in recent years. Given the discouraging laws that are enforced in many countries to protect people from passive smoke of tobacco products, the claims that iQOS® does not release harmful fumes makes it an attractive device to smokers, and the adverse health effects will be reduced if the tobacco is consumed only by heating without burning. The hazardous constituents of tobacco smoke are related to the intake of a large number of chemical substances resulting from the completed combustion (pyrolysis) and heat decomposition (thermogenic degradation) of tobacco. Eight volatile organic compounds and 13 polycyclic aromatic hydrocarbons (PAHs) are released by iQOS®. Although almost all of them are present in moderately to greatly lower amounts than in conventional cigarettes, a number of cancer-causing chemicals are still present in iQOS® emissions. The levels of nicotine, benzaldehyde, and formaldehyde were 84%, 50%, and 74% of those from a typical cigarette, respectively. However, acenaphthene was found at levels 295% of that released from a regular cigarette and its effects on human health are not known. Based on the fact that the idea that there should be a threshold value for the toxic effects of passive smoking should be rejected, according to Principle 1 for implementing article 8 of the WHO convention on tobacco control, it is argued that iQOS® cannot be considered

as a different product from traditional cigarettes and this device should fall under the same smoking bans for regular cigarettes.[14]

Based on the claim that iQOS® can prevent passive smoking, Protano et al.[15], in 2016, compared the profiles of passive smoking exposure by measuring the submicron particles (SMPs) generated by the use of traditional cigarettes, iQOS®, and electronic cigarettes. SMPs emitted from traditional and hand-rolled cigarettes during smoking and also accumulated in the respiratory system of passive smokers were observed four times higher than those released from electronic cigarettes and iQOS®. These particles produced by conventional and hand-rolled cigarettes have been found to remain for a long time in the environment after smoking. It has been reported that the concentrations of these particles, which are emitted from electronic devices and iQOS®, rapidly return to their previous state and their mean diameter increases by combining with each other, and therefore they precipitate immediately. In addition, SMPs produced as a result of combustion have been observed to maintain their dimensions and therefore they have been suspended in the air for a long time. It was also stated that about half of these accumulated particles were small enough to reach the alveoli of passive smokers.[15] Contrary to this research showing that iQOS® smoke can be less harmful than traditional cigarettes, Bekki et al.[1] found different findings for iQOS® in 2017. In that study, the harmful compounds such as nicotine, carbon monoxide, tar, and tobacco-specific nitrosamines in iQOS® tobacco and smoke were explored and their concentrations were compared with those in reference cigarettes such as 1R5F and 3R4F. The nicotine concentration in iQOS® tobacco and smoke was almost the same as that of traditional cigarettes, and nitrosamine and carbon monoxide were found at levels of one-fifth and 1% that of regular cigarettes, respectively. Toxic compounds have been reported to be present in iQOS® vapour, even though at low levels.[1] Farsalinos et al.[16] demonstrated that the nicotine concentrations in iQOS® tobacco sticks are roughly similar to those of traditional cigarettes and are higher than those of electronic cigarettes when the puff time is short.[16] On the other hand, the size and volatility characterization of the particles were also calculated by measuring their concentration and distribution in iQOS® aerosol. The particle concentration in iQOS® smoke was less than 1×10^8 particles/cm^3, but their size distribution was found about 100 nm. However, it has been shown that as the temperature rises, the particle size distribution drops roughly to 20 nm (300˚C) and the volatility of particles increases. The amount of nonvolatile particles breathed by iQOS® users was calculated as 1-2 mm^2 per puff in regard to the surface area of the particles. This was 4-fold higher than the amount inhaled by electronic cigarette users.[17]

It is predicted that there may be a positive correlation between the use of this product and the occurrence of respiratory diseases. A study evaluating the relationship between iQOS® and the expression of nasal platelet activating factor receptor (PAFR), which affects the adhesion of bacteria causing respiratory tract infection, observed that PAFR expression significantly increased in nasal epithelial cells after iQOS® exposure and bacterial adhesion to nasal epithelial cells thus increased.[18] In particular, that study also provided evidence that the use of iQOS® increased the vulnerability to respiratory tract infections and infection-induced asthma attacks. Sohal et al.[19] investigated the effect of e-cigarettes, tobacco smoke, and iQOS® on human lungs *in vitro*. The data obtained from their study show that mitochondrial respiration function alters in consequence of iQOS® exposure, as in e-cigarette and traditional cigarette exposure. Mitochondrial dysfunction may further lead to respiratory infections, airway remodelling, and lung cancer by stimulating epithelial mesenchymal transition, as seen in chronic lung diseases. iQOS® is also thought to enhance infections by increasing microbial adhesion to the airway. Their study highlighted for the first time that exposure to iQOS® smoke is as harmful as that to cigarette and electronic cigarette smoke for human lung cells.[19]

There are also very limited scientific data about the potential effects of iQOS® on the environment. Given the fact that air pollution caused by cigarette smoke is ten times higher than that created by a diesel engine,[20] it is of great importance to identify the possible harmful effects of iQOS® on the environment. In this regard, when the emission factors of many air pollutants were calculated to quantify harmful compounds released to the atmosphere, the metal emission values for iQOS® were relatively low compared to traditional and electronic cigarettes. However, some *n*-alkanes and organic acids have been emitted in significant amounts, whereas PAH compounds could not be detected in iQOS® smoke. Even though the emission of these toxic compounds is lower than that of traditional cigarettes, this product is not without risk to the environment.[3]

According to the results of a survey on awareness and use of this new tobacco product offered for sale under striking advertising slogans such as Heat-Not-Burn, approximately 20% of the 3086 participants aged 15 and over had knowledge about iQOS®. While the number of nonsmokers among the people who had previously tested iQOS® was similar to that of active smokers, the number of nonsmokers who wanted to try this product was higher than that of the current users.[21]

Since iQOS® is a new device, it is assumed that there will be some risks related to its use. When the possible risks of the filter and its cleaning on human health are examined, the polymer film filter in the tobacco unit is observed to easily melt during use (90˚C), and even though in low amounts formaldehyde cyanohydrin, which is a very toxic substance, is formed. Researchers have highlighted that iQOS® is not just a product that only heats tobacco because iQOS® tobacco appears charred, and this toxic compound also increased when it was not cleaned after each use. The product has also been reported to have limitations that would affect the application of ISO 3308 standard smoking protocols.[22]

CONCLUSIONS

In order to make a general conclusion about iQOS®, which is described as a device that combines technology with tobacco, there are not enough research-based findings yet. Especially taking into account that it is a youth-appealing product with its

technological design, there are big concerns owing to the fact that there is no universally accepted risk assessment behind it. In contrast to the company's claims, the presence of PAHs in iQOS® aerosol can be a sign of burning tobacco. Although it is still unclear what the exact harmful effects of this device are, there is a small consensus that it is less risky than continuing to smoke cigarettes. However, it is also underlined that toxic chemicals are still present in iQOS® smoke and the product could lead to people taking up smoking cigarettes. Therefore, more scientific research data are needed to reach an objective conclusion about the effects of iQOS® on human health and the environment. The best way to protect people from passive smoke is to encourage active users to quit smoking completely.

Conflict of Interest: No conflict of interest was declared by the authors.

REFERENCES

1. Bekki K, Inaba Y, Uchiyama S, Kunugita N. Comparison of chemicals in mainstream smoke in heat-not-burn tobacco and combustion cigarettes. J UOEH. 2017;39:201-207.
2. https://www.pmi.com/smoke-free-products/iqos-our-tobacco-heating-system (Accessed January 12, 2019)
3. Ruprecht AA, De Marco C, Saffari A, Pozzi P, Mazza R, Veronese C, Angellotti G, Munarini E, Ogliari AC, Westerdahl D, Hasheminassab S, Shafer MM, Schauer JJ, Repace J, Sioutas C, Boffi R. Environmental pollution and emission factors of electronic cigarettes, heat-not-burn tobacco products, and conventional cigarettes. Aerosol Sci Technol. 2017;51:674-684.
4. https://www.fda.gov/downloads/TobaccoProducts/Labeling/MarketingandAdvertising/UCM560044.pdf (Accessed January 12, 2019)
5. https://www.fda.gov/TobaccoProducts/Labeling/MarketingandAdvertising/ucm546281.htm (Accessed January 12, 2019)
6. https://www.fda.gov/AdvisoryCommittees/Calendar/ucm584231.html(Accessed January 12, 2019)
7. https://www.nytimes.com/2018/01/25/health/fda-tobacco-philip-morris.html(Accessed January 12, 2019)
8. Turkey Statistical Institute, Cause of Death Statistics, 2017, Issue: 27620, April 26, 2018.
9. Ministry of Health Official Website, Updated on: 24/10/2016 https://www.saglik.gov.tr/ TR,3881/turkiyenin-dumansiz-hava-sahasi-dunyaya-resmen-ornek-oldu.html
10. WHO global reports on trends in prevalence of tobacco smoking 2000-2025, second edition. Genova: World Health Organization; 2018.
11. Drope J, Schluger N, Cahn Z, Drope J, Hamill S, Islami F, Liber A, Nargis N, Stoklosa M. The Tobacco Atlas (6th ed). Atlanta; American Cancer Society and Vital Strategies; 2018:22-23.
12. Hecht S, Park SL, Carmella S, Stram D, Haiman C, Marchand L, Murphy S, Yuan JM. Tobacco Carcinogens and Lung Cancer Susceptibility. Journal of Thoracic Oncology. 2017;12:19-20.
13. Repace J, Kawachi I, Glantz S. Fact sheet on secondhand smoke. 2nd European Conference on Tobacco or Health, 1999.
14. Auer R, Concha-Lozano N, Jacot-Sadowski I, Cornuz J, Berthet A. Heat-not-burn tobacco cigarettes: smoke by any other name. JAMA Intern Med. 2017;177:1050-1052.
15. Protano C, Manigrasso M, Avino P, Sernia S, Vitali M. Second-hand smoke exposure generated by new electronic devices (IQOS® and e-cigs) and traditional cigarettes: submicron particle behaviour in human respiratory system. Ann Ig. 2016;28:109-112.
16. Farsalinos KE, Yannovits N, Sarri T, Voudris V, Poulas K. Nicotine delivery to the aerosol of a heat-not-burn tobacco product: comparison with a tobacco cigarette and e-cigarettes. Nicotine Tob Res. 2018;20:1004-1009.
17. Pacitto A, Stabile L, Scungio M, Rizza V, Buonanno G. Characterization of airborne particles emitted by an electrically heated tobacco smoking system. Environ Pollut. 2018;240:248-254.
18. Miyashita L, Grigg J. Effect of the iQOS electronic cigarette device on susceptibility to *S. pneumoniae* infection. J Allergy Clin Immunol. 2018;141:AB28.
19. Sohal SS, Eapen MS, Naidu VGM, Sharma P. IQOS exposure impairs human airway cell homeostasis: direct comparison with traditional cigarette and e-cigarette. ERJ Open Res. 2019;5:00159-2018.
20. WHO Protection from exposure to second-hand tobacco smoke. Policy recommen-dations. Genova, World Health Organization, 2007.
21. Liu X, Lugo A, Spizzichino L, Tabuchi T, Pacifici R, Gallus S. Heat-not-burn tobacco products: concerns from the Italian experience. Tob Control. 2018;28:113-114.
22. Davis B, Williams M, Talbot P. iQOS: evidence of pyrolysis and release of a toxicant from plastic. Tob Control. 2018;28:34-41.